UNIVERSITÀ DEGLI STUDI DI PISA

Corso di laurea Magistrale in Ingegneria Energetica

TESI DI LAUREA MAGISTRALE

Study on a Dielectric Elastomer Power Take-Off for Wave Surge Energy Converters

Relatori:

Prof. Ing. Alessandro FRANCO

Ing. Marco FONTANA

Ing. Rocco VERTECHY

Candidato:

Giacomo MORETTI

ANNO ACCADEMICO 2012/2013

Contents

Preface

The topic of Wave Energy Conversion has a history spanning four decades: the origin of the subject is usually attributed to an article by Stephen Salter, from Edinburgh University, edited in 1974 on the prestigious magazine 'Nature' [1].
Forty years of research and prototyping have generated a relevant number of technical solutions, patented prototypes, demonstrative installations and an outstanding number of scientific works.
Nonetheless, Wave Energy is still far from the identification of a technical standard and from the definitive comprehension of which technology, which power size, which operative conditions are those indicated for a feasible and effective implementation of this principle on a full-scale commercial perspective.
It could be stated that the regular development course of each new renewable energy follows a series of phases. The first phase could be designate as the 'spot' phase, since a series of particularistic technical solutions emerge, basing on a physical principle or on a technical intuition, but no clarity is brought on the pragmatic engineering limitations and constraints that obstruct the factual spread of the technology. In a second phase, a systematic and applied research on the limiting factors allows the identification of a power size for the converters, a technical standard and an operative framework that is optimal for the investigated resource, allowing its feasibility. That has happened, i.e., for photovoltaic and wind energy: among a series of spotted differentiated prototypes, the technology has experimented a great spread in correspondence of particular modular solutions (100 m-tall generators of about 1 MW rated power in the case of wind energy; 1-2 m^2 modules with rated power of few hundred Watts for photovoltaic) that have supplanted the other solutions, going through a much greater development. A third hypothetic and mature phase would promote the equilibrate diffusion of the reference renewable resource in an integrated context, aware of the environmental constraints even in relation with the electric grid limits and the particular energetic framework.
Wave Energy is still at the 'spot' level: a number of devices and converters exist on paper, but a series of criticalities and limits have not been overcome yet.

The present thesis originates within the PolyWEC project, a multidisciplinary program carried out by a consortium of European institutions, leading by Scuola Superiore Sant'Anna (Pisa) and including

- 'Petru Poni' Institute of Macromolecular chemistry, Romania

- Selmar S.r.l., Italy
- University of Edinburgh, UK
- Wave Energy Center, Portugal

The project bases on the presupposition that one of the most crucial limiting factors that have hindered the diffusion of Wave Energy Converters is the presence of heavy, corrosive, shocking-sensitive and mechanically complicated components within the traditional power take-off systems adopted to convert the mechanical energy harvested by the main body to electric energy. The aim of the program is, thus, investigating the possibility of exploiting new types of conversion mechanisms based on dielectric elastomers and electroactive polymers, that, exploiting relatively simple mechanisms and layout, allow a simplification and improvement of the existing technology.

Dielectric Elastomer generators are promising thank to their adaptability to devices performing oscillating and reciprocating motion, to their good efficiency at low frequencies, to their simple manufacturing and low cost. On the other hand, the employment of these materials and solution would put the technology in front of a rather different scenario, with a series of technical criticalities and unknowns (like the adaptability of the materials to the sea environment, the fatigue lifetime, the aging effects) that must be resolved by mean of scientific research and experimental investigation.

The work has been carried out in cooperation with PERCRO SEES laboratory of Scuola Sant'Anna, and focuses on the study of a lozenge-shaped dielectric elastomer generator and on the simulation of a pitch oscillating wave energy converter, consisting in a flap vertically hinged to the sea bed in shallow water, exploiting the mentioned generator as power take-off.

The work comprises both an experimental and a theoretical numerical part.

Experimental work has been addressed to the mechanical characterization of an acrylic elastomer, used as reference material for the subsequent simulations. Experiments have been entirely carried out at PERCRO laboratory (Pisa), during the period February-March 2013.

The work is structured into three chapters.

Chapter one presents a review of sea waves physics and an examination of the state of the art of the technology, with particular care to the sensitive engineering parameters describing the different wave energy converters and their operation limits. Some mathematical models describing the principal converters are also presented.

Chapter two presents an overview on dielectric elastomer transducers, and introduce a model for a novel concept lozenge-shaped dielectric elastomer generator. Results from the experimental mechanical characterization are described, and a mathematical model for the mentioned generator is described. At the end of the chapter, an introduction on the application of polymeric generators to wave energy conversion is given.

Chapter three considers the simulation of an oscillating wave surge energy converter. The analysis takes into exam the operation of the system with an electric linear power take-off and with a polymeric lozenge-shaped generator. The energetic and dynamic behavior of the

system is examined, and a preliminary assessment of the performances of the new technology, even in comparison with traditional systems, is carried out.
In conclusion, a series of possible improvements and future work hints is presented.

The work presented herein must not be is far from being a complete and definitive design of a new concept of wave energy converter; it is rather an introductive study on a novel concept, with the aim of providing a solid comprehension on the order of magnitudes and on the points of interest (as long as on the weak aspects) within the considered technology.

Pisa, 22nd September 2013
G.M.

Chapter 1

Overview on Wave Energy Conversion

1-1 Generalities

1-1.1 Introduction

Wave Energy Conversion has a relatively recent history. Although the enormous potential of ocean waves is known from centuries, it is only from the seventies that efforts have been spent in order to achieve the conversion of wave energy to electric energy [1] [2] [3], and first patents concerning Wave Energy Converters (WECs) hail from those years [4] [5].

Several natural sources causing ocean waves may be identified. The most common ones can be summarized in [6]:

- Bodies moving near or riding the surface, causing low-energy waves
- Winds generating swells
- Seismic phenomena, such as tsunamis
- Lunar and Solar gravitational interaction with Earth, resulting in tides.

In most of the works of literature, tides are considered as a different and separate phenomenon with respect to ocean waves [6] [7], and also their exploitation is carried out with different systems [8].

In the present work, wind-wave energy only is considered, and the technical solutions presented and proposed here are referred specifically to wind generated sea waves rather than to sea currents (induced, in most cases, by tidal phenomena).

As known, wind energy descends from solar energy: solar radiation is absorbed by both ground and water of the oceans, causing the air above those surfaces to warm due to convective heat exchange. Winds originate from temperature gradients (and, thus, pressure gradients) of the air in adjacent regions. The interaction of the winds with the surface of the oceans generates the waves. Sea waves formation occurs in a region called ‘fetch’, within which a phenomenon occurs (i.e. a storm) that provokes a strong interaction between the two phases (water and air) on the interface [9].

After their formation in the fetch, waves continue to travel in the direction of their formation even if wind is no longer acting on them. To distances far from the fetch, sea waves have a regular shape and the phenomenon is called ‘swell’.

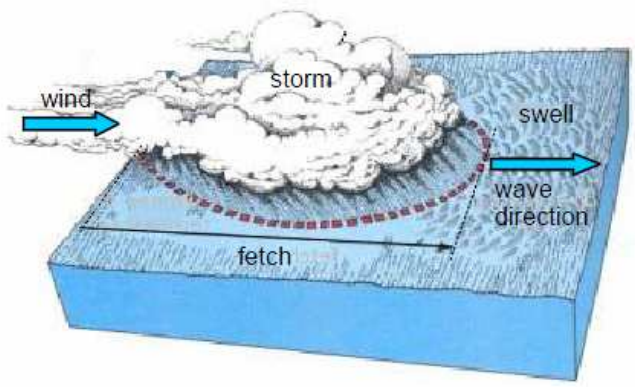

Figure 1-1 - Waves formation within a fetch region

It is then immediate to understand that wave energy is a product of solar energy, that undergoes a series of transformations. An important aspect, that makes wave energy an interesting source in the panorama of renewable energies, is that in each transformation the power intensity increases.

McCormick [6] reports that, for a location with latitude of 15° N with mean solar radiation of 170 W/m^2, the average power per unit surface of wind currents is estimated in 580 W/m^2.

Since the power P per unit surface A (perpendicular to the flow direction) for a fluid current is given by

$$P/A = 1/2\rho U^3,$$

the corresponding average wind-speed U is about 10 m/s (assuming a density ρ of ~10 m/s).

In the successive passage, energy from the wind is transferred to sea waves, with an increased intensity of about 8500 W/m^2.

Many studies exist that try to estimate numerically the potential, in terms of power, coming from the waves [3] [10] [11].

Since the height of the waves tends to decrease approaching the coastline, it is immediate to understand that the most 'energetic' waves are met in open ocean, at distances from the shoreline of hundreds of meters.

The wave energy potential is usually characterized referring to a specific quantity that is the power per unit crest-width carried by the wave: this approach descends from a description of the wave as a bi-dimensional phenomenon (linear sinusoidal waves, that will be discussed in the following), that is the simplest and most common description used for the physical study of ocean waves.

We refer here to the data spread by the Norvegian company Frugo OCEANOR (www.oceanor.no), specialist in the design, manufacture, technological development, installation and support of private and public sector environmental monitoring, ocean observing and forecasting systems [3]. Fugro OCEANOR has developed the WorldWaves global database, a global collection of wind and wave time series data. The data are derived from the European Centre for Medium-range Weather Forecasts' (ECMWF) operational

models and are calibrated by Fugro OCEANOR against satellite data, and, where available, in-situ buoy data. Data are available on a 0.5° grid at 6-hourly intervals for the period December 1996 to present.

In Figure 1-2, a map of the yearly average power (per unit crest–width) of the waves at different locations is shown.

As expected, the major potential is met in open oceans. The coastal regions that present the maximum resource potential are

- South shores of America (Land of Fire), Africa and Australia.
- North European coasts and, more generally, the Atlantic patch between Northern Europe and Greenland

Of course, high wave power potential is also present in regions far from the coastlines, that therefore are not of interest for wave energy conversion.

The average global gross theoretical resource is estimated in 3.7 TW: excluding those regions where the power per unit crest length is lower than 5 kW/m (and, thus, not of interest for wave energy conversion) and the regions covered by ice, the net resource amounts to about 3 TW.

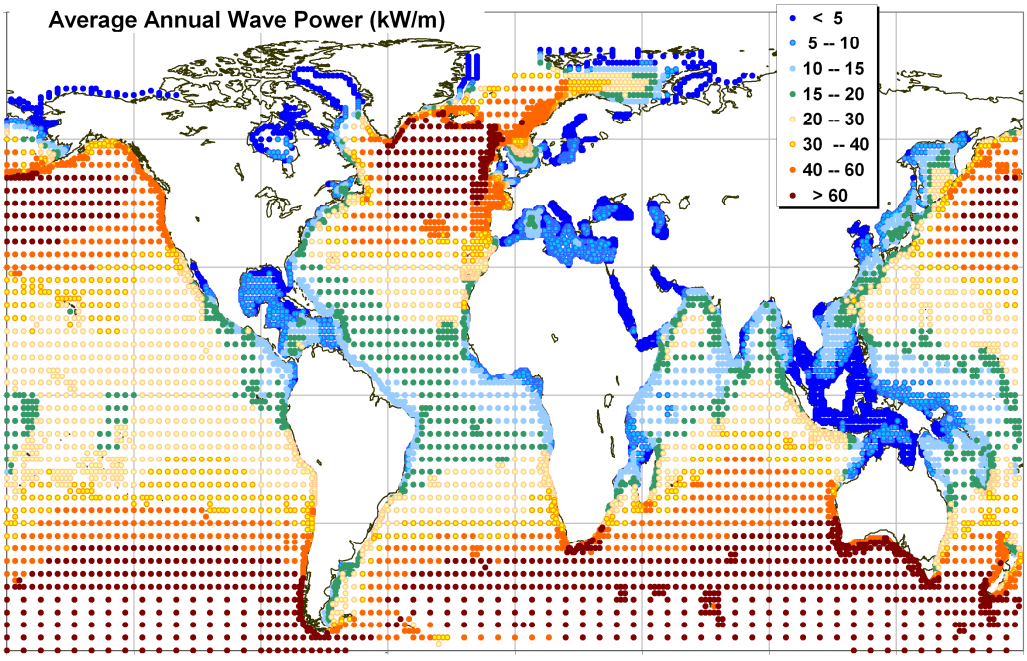

Figure 1-2 – Map of wave power per unit crest-length [kW/m]

Another example of wave energy potential estimation is presented by Vicinanza et al. [12], with reference to the Mediterranean Sea. Figure 1-3 shows the power per unit crest length, in kW/m, detected in various location around the Italian coasts, where buoys are placed. It is possible to notice that the gross power does not overtake the value of 15 kW/m, that is far from the typical values actually employed in wave energy conversion (50-75 kW/m).

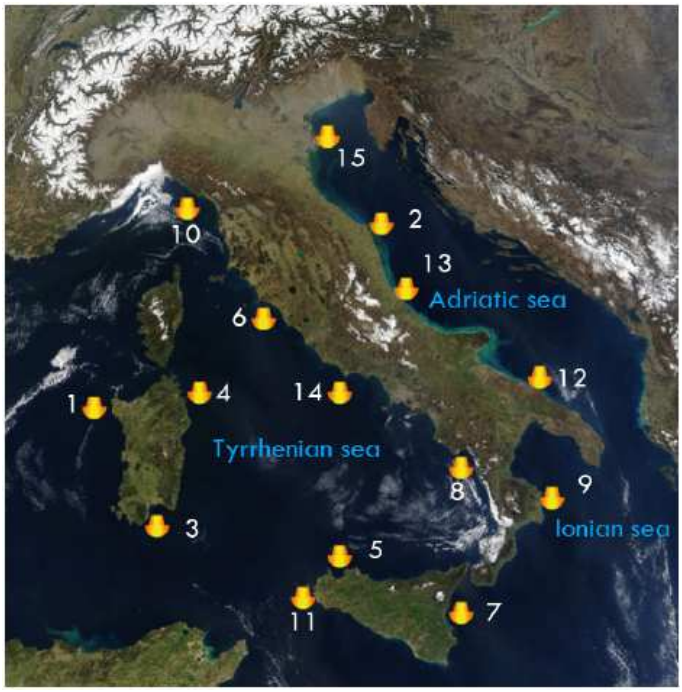

Figure 1-3 - Estimation of the wave energy in the Italian offshore

A complete understanding of the presented data and of how they can be drawn requires a review of the mathematical models describing sea waves.

1-1.2 Wave mechanics

Oscillatory phenomena are described by specific forms of wave equation. In general, the wave equation and the boundary conditions may be either linear or non-linear.

In the specific case of sea waves, the linear theory is used to describe waves featured by height to wavelength ratio lower than 1/50, in other words, for swells. The swell is the most frequently observed wave and, for this reason, is of primary importance in wave energy conversion.

A complete overview on ocean wave physics is presented by McCormick [6] [13].

A quick review of the main results is here presented. Let refer to Figure 1-4; the descriptive features of a linear wave can be listed as:

- Wavelength λ: is the distance between two successive crests
- Height H of the wave, measured from the trough to the crest of the wave. The half-height is usually indicated with a: $H = 2a$.
- Water depth h under the still-water level (SWL) that is the undisturbed position of the water surface.
- Wave phase velocity c.

The origin of the Cartesian coordinates system lies on the SWL, with z axis perpendicular to the SWL itself (see Figure 1-4).

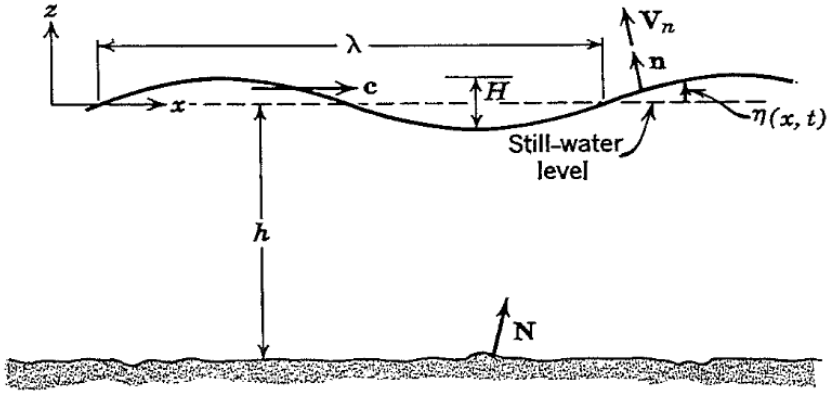

Figure 1-4 - Schematic drawing of linear wave

The displacement of the free surface from the SWL at any position (*x*,*z*) and time *t* is indicated with η. The wave is supposed bi-dimensional, thus, no dependence on *y* coordinate (perpendicular to the page surface) is be present.

According to the linear wave theory, the equation for the free-surface displacement can be written as

$$\eta = \frac{H}{2}\cos\left(\frac{2\pi x}{\lambda} - \frac{2\pi t}{T}\right)$$

Indicating with *T* the wave period, reciprocal of the frequency *f*, the following relationship between wavelength and period can be proved:

$$\lambda = \frac{gT^2}{2\pi}\tanh\left(\frac{2\pi h}{\lambda}\right)$$

In order to simplify the equation, that is implicit in λ, two limit cases are usually identified

- *Deep water*. For engineering purposes deep water is defined where $h/\lambda \geq 1/2$

$$\lambda \simeq \frac{gT^2}{2\pi}$$

- *Shallow water*, where $h/\lambda \leq 1/20$

$$\lambda \simeq \sqrt{gh}T$$

The cases with $1/2 < \lambda < 1/20$ are considered intermediate.

In most engineering applications, deep water only is considered, since WECs installation are often positioned offshore where the wave intensities are significant.

It is useful to introduce the wave number *k* and the circular frequency ω:

$$k = \frac{2\pi}{\lambda} \quad ; \quad \omega = \frac{2\pi}{T}$$

The wave phase velocity is described by the equation

$$c = \frac{\lambda}{T} = \frac{gT}{2\pi}\tanh(kh)$$

with the limit approximations

- Deep water: $c = \frac{gT}{2\pi}$
- Shallow water: $c = \sqrt{gh}$

Attention is now focused on the motion of fluid particles within the wave. In the hypothesis of potential flow (that means inviscid and incompressible flow), a velocity potential function φ is introduced.

Considering that the gauge pressure (using as reference value the atmospheric pressure) on the free surface is 0, Bernoulli's theorem takes the form

$$\frac{\partial \varphi}{\partial t} + g\eta + \frac{V^2}{2} = 0$$

where V is the module of the fluid particle velocity in the considered position.

With reference to Figure 1-4, considering a right-running wave, the velocity potential is expressed by

$$\varphi = \frac{Hg}{2\omega} \frac{\cosh\big(k(z+h)\big)}{\cosh(kh)} \sin(kx - \omega t)$$

The velocity components of the particles are calculated as $(u, w) = \nabla\varphi$:

$$u = \frac{Hgk}{2\omega} \frac{\cosh\big(k(z+h)\big)}{\cosh(kh)} \cos(kx - \omega t)$$

$$w = \frac{Hgk}{2\omega} \frac{\sinh\big(k(z+h)\big)}{\cosh(kh)} \sin(kx - \omega t)$$

Again, approximated expressions can be written for the extreme cases:

- Deep water: $u = \frac{Hgk}{2\omega} \mathrm{e}^{kz} \cos(kx - \omega t)$; $w = \frac{Hgk}{2\omega} \mathrm{e}^{kz} \sin(kx - \omega t)$
- Shallow water: $u = \frac{H}{2}\sqrt{\frac{g}{h}} \cos(kx - \omega t)$; $w = \frac{H}{2}\sqrt{\frac{g}{h}} \sin(kx - \omega t)$

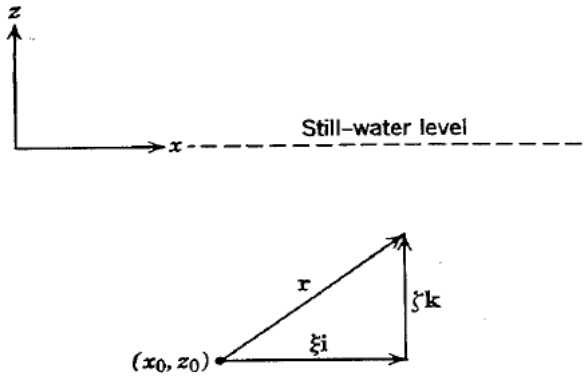

Figure 1-5 - Definition of (ξ,ζ) coordinates

Considering the general equations, it can be shown that the particles follow a close trajectory, that, at first order approximation, is an ellipse [13].

Let consider a fixed point (x_0, y_0) in the wave: choosing a new reference system with Cartesian axes with center in (x_0, y_0), two new coordinates ξ and ζ can be introduced (Figure 1-5).

Integrating the general equations for the velocity components, it is possible to get the expressions for the displacement components:

$$\xi = -\frac{Hgk}{2\omega^2}\frac{\cosh\big(k(z_0+h)\big)}{\cosh(kh)}\sin(kx_0-\omega t)$$

$$\zeta = \frac{Hgk}{2\omega^2}\frac{\sinh\big(k(z_0+h)\big)}{\cosh(kh)}\cos(kx_0-\omega t)$$

From the equations above, it is immediate to check that

$$\frac{\xi^2}{\frac{H^2g^2k^2}{4\omega^4}\frac{\cosh^2\big(k(z_0+h)\big)}{\cosh^2(kh)}}+\frac{\zeta^2}{\frac{H^2g^2k^2}{4\omega^4}\frac{\sinh^2\big(k(z_0+h)\big)}{\cosh^2(kh)}}=1$$

that is the equation of an ellipse with the center in the origin of the new reference system, thus in point (x_0, y_0).

Notice that in *deep water* ($h \gg 1$) the trajectory takes the form

$$\frac{\xi^2}{\frac{H^2g^2k^2}{4\omega^4}\mathrm{e}^{2kz_0}}+\frac{\zeta^2}{\frac{H^2g^2k^2}{4\omega^4}\mathrm{e}^{2kz_0}}=1$$

And, remembering the equation that links period T and wavelength λ in deep water, the expression simplifies to

$$\frac{\xi^2}{\frac{H^2}{4}\mathrm{e}^{2kz_0}}+\frac{\zeta^2}{\frac{H^2}{4}\mathrm{e}^{2kz_0}}=1$$

Since z_0 is negative below the SWL, the equation describes a circular path the radius of which decreases exponentially with depth: when $z_0 < \lambda/2$, $\mathrm{e}^{2kz_0} < 5\%$, thus, at that depth, fluid particles motion is practically inexistent.

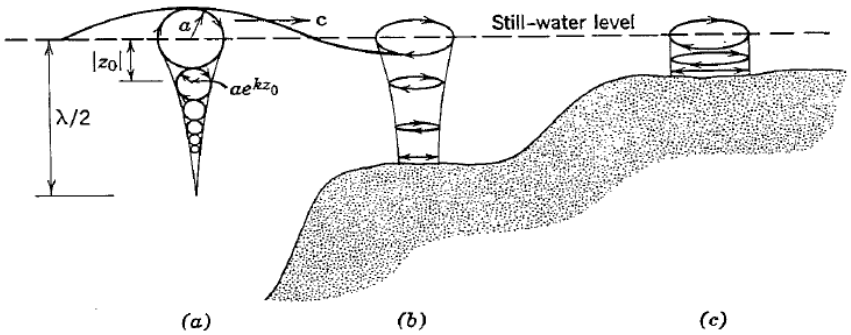

Figure 1-6 - Particle paths at different water depth a) Deep water b) Intermediate water depth c) Shallow water

1-1.2.1 Wave Energy and Power

Sea and ocean waves are kinds of "material waves". This means that, being the fluid particles oscillating around a fixed position, there is no net movement of water mass from a point to another of the system. Particles simply moves in the neighborhood of their equilibrium

position. The only physical quantity that propagates and is transmitted from a point to another is, thus, Energy.

Effectively, water waves are simply the result of energy transmission to the water from an external source (usually wind, but also any other kind of moving source, like ships or earthquakes).

The overall energy contained in a defined water control volume, interested by the presence of waves, is the sum of two contributions:

- Kinetic energy, associated to the movement of the fluid particles within the volume and, thus, to their velocity
- Potential energy, associated to the vertical position of waves particles with respect to a reference level (i.e. SWL)

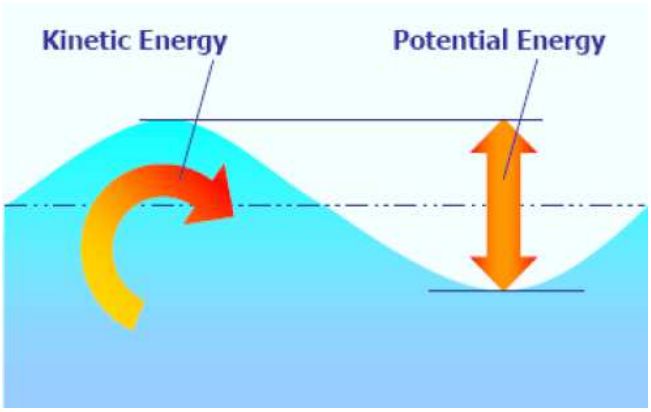

Figure 1-7 - Wave energy components

Referring to the previously described reference system, let consider a control volume with unitary width in *y* direction, length equal to the wavelength λ in *x* direction and containing the whole amount of water (below the air-water interface and above the ground level) present in *z* direction. It is possible to calculate the energy within the described water volume considering an infinitesimal water particle with dimensions *dx* and *dz* in *x* and *z* direction respectively and unitary width (Figure 1-8).

For the energy calculation, we refer to a situation of deep water, and use the consequent approximations.

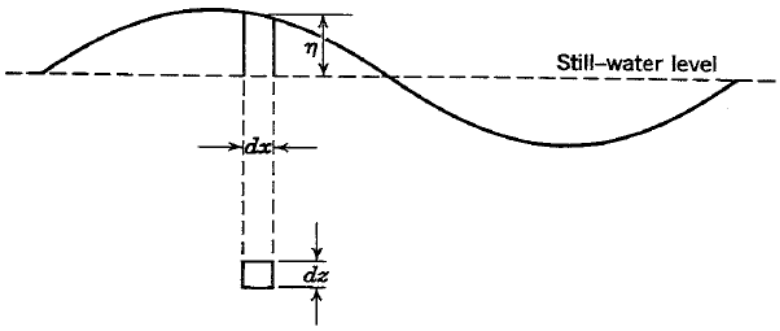

Figure 1-8 - Fluid particles definition

The particle in exam has kinetic energy of $dE_k = 1/2\,\rho(u^2 + w^2)\,dx\,dz$.
The total Kinetic Energy over the control volume is

$$E_k = \frac{1}{2}\rho \int_{-h}^{0}\int_{0}^{\lambda} (u^2 + w^2)\,dx\,dz = \frac{\rho g H^2 \lambda}{16}$$

Let then consider a water element with length *dx* and height η above the SWL. The element has potential energy $dE_p = \rho\eta dx\; g\,\eta/2$.
Recalling the equation for the free-surface displacement and integrating over a wavelength, the overall Potential Energy is obtained.

$$E_p = \frac{\rho g}{2}\int_{0}^{\lambda} \eta^2 dx = \frac{\rho g H^2 \lambda}{16}$$

One important result of the linear theory is thus that the energy of the wave is equally composed by potential and kinetic energy.

$$E = E_k + E_p = \frac{\rho g H^2 \lambda}{8}$$

Referring now to the general case (whatever water depth), the wave power *P* (per unit crest width) can be calculated.
The wave power is defined as the average energy flux that in a time range equal to the wave period *T* flows through a surface normal to the flow direction, and is simply calculated as

$$\vec{P}_w = \frac{1}{T}\int_{-h}^{0}\int_{0}^{T} \rho \frac{\partial \varphi}{\partial t}\vec{V} dt\,dz = \frac{\rho g H^2 c}{16}\left[\frac{2kh}{\sinh(2kh)} + 1\right]\vec{\imath}$$

Notice that, in general, the energy flux represents a vector quantity. In this case, the resulting flux is directed in *x* direction (featured by the unit vector $\vec{\imath}$), that the wave propagation direction. Therefore, in the following, we will refer to *P* as a scalar quantity, given as an assumption that the energy flux moves in the same propagation direction of the wave.
It is convenient to introduce the group velocity c_g

$$c_g = \frac{c}{2}\left[\frac{2kh}{\sinh(2kh)} + 1\right]$$

In a calm sea, waves generated by wind, or boats, appear to travel in group, forming a patch. This patch of waves moves at a speed that is, indeed, the group velocity c_g [13].
The power per unit crest length in a wave is given by:

$$P_w = \frac{\rho g H^2 c_g}{8}$$

Considering the sub-cases of deep and shallow water

- Deep water: $c_g = c/2$; $P_w = \frac{\rho g^2 H^2 T}{32\pi}$
- Shallow water: $c_g = c$; $P_w = \frac{\rho g H^2 \sqrt{gh}}{8}$

In conclusion of this overview on sea waves physics, a remark is necessary: linear wave theory is the most commonly used in literature for its mathematical simplicity, but it is not

appropriate to describe all the sea conditions. Particularly, it is satisfactory mainly to describe deep-water swells, the profile of which can be considered sinusoidal (McCormick, 2007).
As the wave begins to shoal, that is, to be affected by the seafloor, the wave profile tends to assume a different shape, with narrow crest and broad through.
Different non-linear theories exist, that try to approximate the described behavior with better approximation with respect to the linear theory; examples are [6]:

- Stoke's wave: starting from the linear theory, waves can be modeled as a sum of harmonics. Thus, higher order models can be considered.
  As an example, the shallow water wave profile predicted by Stoke's second order theory is
  $$\eta = \frac{H}{2}\cos(kx - \omega t) + \frac{3}{16}\frac{H^2}{k^2 h^3}\cos\big(2(kx - \omega t)\big)$$
- Solitary Wave theory: the theory starts from the consideration that a relatively long swell in shallow water can be approximated as an isolated phenomenon, and that when the swell approaches the surf zone the free surface of the wave can be completely above the SWL.

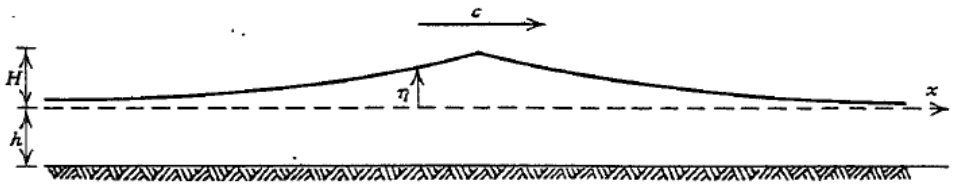

Figure 1-9 - Example of profile of solitary Wave

Although the existence of these advanced models, the linear theory is adopted in most of the literature concerning wave energy conversion for historical and for simplicity reasons, also in the description of shallow water conditions.

1-1.3 Real Seas

In this paragraph, we present an overview on the tools used to describe real random seas and the most common parameters present in literature for the their description and for the estimation of the wave energy potential in a site.
Observing a real sea in a windy day, it is possible to understand that different waves, with random height, period and direction are present.
The description is usually carried out in the frequency domain [12].
In a first analysis, a random sea can be considered composed by numerous linear waves [6]. For the *i*-th wave, the energy is written as
$$E_i = 1/8\,\rho g {H_i}^2 \lambda_i$$
The wave height term is expressed using the wave spectrum $S(f)$:
$${H_i}^2/8 = S(f_i)df_i$$

with *f* indicating the frequency.

In general, in a random sea, the waves behavior depends on the direction, thus, a dependence on the direction θ has to be accounted in the spectrum: $S = S(f, \theta)$.

The wave spectrum induces a series of moments, computed as [3]

$$m_n = \int_0^{2\pi} \int_0^{\infty} f^n S(f, \theta) df d\theta$$

Wave data are normally presented in terms of 'mean significant wave height', H_{m0}

$$H_{m0} = 4\sqrt{m_0}$$

The significant wave height is defined with reference to the wave spectrum, anyway, a historical (not equivalent) definition is sometimes present in literature [6], according to which the significant wave height is defined as the mean wave height of the highest third of the waves.

Another significant parameter is the mean period T_{-10}, defined as

$$T_{-10} = \frac{m_{-1}}{m_0}$$

The wave power per unit crest length is obtained as

$$P_w = \rho g \int_0^{2\pi} \int_0^{\infty} S(f, \theta) c_g(f, \theta) df d\theta$$

where c_g is the group velocity.

It is possible to demonstrate that in deep water *P* is computed as [12]

$$P_w = \frac{\rho g^2 {H_{m0}}^2 T_{-10}}{64\pi}$$

Wave potential estimations, like the one in Figure 1-2, are based on such a type of analysis. Wave significant height and period can be calculated by direct measurements based on altimeters, buoys and satellites.

1-1.4 Waves modification

Breaking waves. The surface particle velocity increases as the depth decreases. Considering the equations for the wave velocity *c* and for the fluid particles velocity in *x* direction, *u*, it is possible to demonstrate that, at a certain depth, the maximum value of *u* (obtained putting $\cos(kx - \omega t) = 1$) calculated on the crest of the wave (at $z = H/2$) equals the value of *c* [6]. At that depth level, the velocity of the water particles equals that of the wave itself. There can be no greater forward speed of the water of that one, because the water would then plunge forward out of the wave: in other words, the wave would 'break' [14].

This condition is called 'breaking'. As the water approaches the shore, the breaking condition is met, therefore the water spills and wave energy is lost to turbulence and friction.

Refraction, Reflection and Diffraction. Water waves, like other material waves, interact with physical obstacles being subjected to different phenomena: refraction, reflection and diffraction.

Refraction is due to transitions in water depth. When a wave moves through a region with variable water depth, if the wave front is not parallel to the iso-depth contours, the portion of wave in deeper water moves faster than the part in shallow water. This difference of velocity among different points of the wave front provokes a turning of the wave front: the wave front changes its profile and tends to align with the depth contours. Generally, any change in the wave speed, for instance due to gradients of surface currents, may bring to refraction, irrespective of the water depth [14].

Reflection occurs when the wave strikes a barrier. When a wave hits an obstacle perpendicular to its propagation direction (a seawall, or an object within the water), wave energy can be partially absorbed by the body: the amount of energy that is not absorbed is reflected. In a limit case of vertical, flat, rigid, impermeable, smooth barrier, the whole amount of incident energy gets reflected [6].

The phenomenon of diffraction occurs in the lee of an obstruction, where a calm water region exists (shadow zone). In the shadow zone, waves are still present, with reduced height and propagating in circular fronts [6] [14].

As emerging from the following of the thesis, considering the waves modification in the neighborhood of WECs devices is necessary to gain a correct modeling of the hydrodynamic of the systems and thus to carry out a correct study of the energy conversion systems.

1-2 Wave Energy Conversion Technology

1-2.1 Introduction

Up to date, it is possible to assert that wave energy conversion is in its pre-commercial phase: a large amount of technical solutions has been proposed [6] [15] , but a technological standard has not been found yet.

There are several reasons that make Wave Energy a source of interest in the panorama of renewable energies. Schematically [16]:

- Wave Energy can count on large potentialities (as demonstrated above) and represents, de facto, an unlimited source of power.
- Population is mostly concentrated on the coastlines, therefore power grid is more readily accessible for coupling to wave energy devices.
- It is implementable as part of harbors development projects and requalification
- It can be exploited for in-site applications like the desalination of sea water
- A technical background exists from the oil industry, since offshore platforms have been operated successfully in rough sea environments. Technological solutions in terms of mooring and platform operations can be ‘borrowed’ from the oil industry.

- Undersea cables have known a technical development and a cost reduction thanks to their application to offshore platforms for oil and wind energy, paving the way for the transmission of energy from offshore WECs.
- Advances in industrial control are creating tools that can be applied to the electronics of WEC systems.
- Technologies that are being taken into account are usually modularized: many devices can be woven together into an integrated power systems with a certain flexibility in the choice of the total size of the single installation.

As a counterpart, some nodal criticalities still make the installation of WECs an unresolved issue, in particular:

- The resource presents good intensities far from the shores, thus the devices require complex mooring systems and, in any case, underwater cables are needed.
- Ocean and sea waves are very variable in terms of height, period and wavelength: devices operating in a large range off the nominal operative conditions are required, moreover, survivability in extreme sea conditions has to be somehow guaranteed [15].
- Sea water is an aggressive environment due to its salinity, moreover many electrical components composing the electric energy extraction system of the device are not suitable to work in water.
- Ocean waves have time period around 10 s (frequency of 0.1 Hz), while electric grids require frequencies of 50 or 60 Hz: appropriate power take-off (PTO) systems and electric layouts must be adopted to exploit the produced electrical energy. These PTOs have to be adapt to operate at different time scales, due to the variability of the sea conditions.

Up to date, pilot scale plants and few demonstrative experimental full-scale WECs exist (like the Pelamis wavefarm at Aguçadoura, Portugal).

1-2.2 Capture Width

The capture width is the classical parameter used to measure the efficiency of a three dimensional isolated device [17] [18]. It is defined as the ratio between the power (electric) output of the WEC, P_{dev}, and the power per unit crest width of the incident wave, P_w, and is, thus, calculated with reference to a monochromatic wave:

$$L_{cap} = \frac{P_{dev}}{P_w}$$

Notice that, having P_{dev} the dimensions of a power [W] and P_w the dimensions of a power per unit length [W/m], the capture width L_{cap} has the dimensions of a length [m], and physically represents the width of wave front from which all the energy is virtually extracted.

In general, it is useful to refer to a non-dimensional measure of the efficiency, indicated as 'capture width ratio', or 'relative capture width', ϵ [18] [19]:

$$\epsilon = \frac{L_{cap}}{b}$$

where *b* indicates the width of the device (parallel to the wave front).

For two-dimensional devices, the capture width ratio ϵ is often referred to as 'efficiency' [18], anyway, in the present work, we indifferently refer to 'capture width ratio' for two-dimensional devices also.

An important remark is necessary: two-dimensional devices are intrinsically able to absorb power from only a unit width of the incident wave front, having a maximum allowed capture width ratio (or efficiency) of 1. For three-dimensional devices, three-dimensional effect makes possible to absorb power from the total wave front incident upon the device and not restricted to a wave front possessing just the same width as the device, therefore the capture width ratio can be effectively greater than unity [18].

1-2.3 WECs classification

Many possible classifications have been proposed for the different WECs concepts. The most common classification bases on the relative dimensions of the WEC with respect to the wavelength and on its orientation with respect to the wave propagation direction [18]. We consider two significant dimensions for the bodies, identified by sectioning the devices with a plane parallel to the SWL.

In particular, the following categories of devices can be identified (Figure 1-10).

- Point Absorbers: they have both the significant dimensions much smaller than the wavelength. These devices are often axi-symmetric about a vertical axis. For these type of devices, the scattered wave field is usually neglected, thus, the forces due to the direct waves only can be considered for design purposes. These devices can capture energy from a wave front that is larger than their dimensions, exploiting three-dimensional effects.
- Attenuators: they have one dimension much larger than the other one (and comparable with the wavelength λ), parallel to the wave propagation direction; It is usual for attenuators to be compliant or articulated structures [16].
- Terminators: these devices have the dominant dimension (comparable with λ) perpendicular to the wave propagation direction. They can either be compliant or rigid. An efficient terminator will create waves that are exactly in antiphase with the incident wave.

  Both terminator and attenuator devices have directionally dependent efficiency. Since attenuators have smaller area perpendicular to the wave direction, they are subjected to lower stresses than terminators [16].

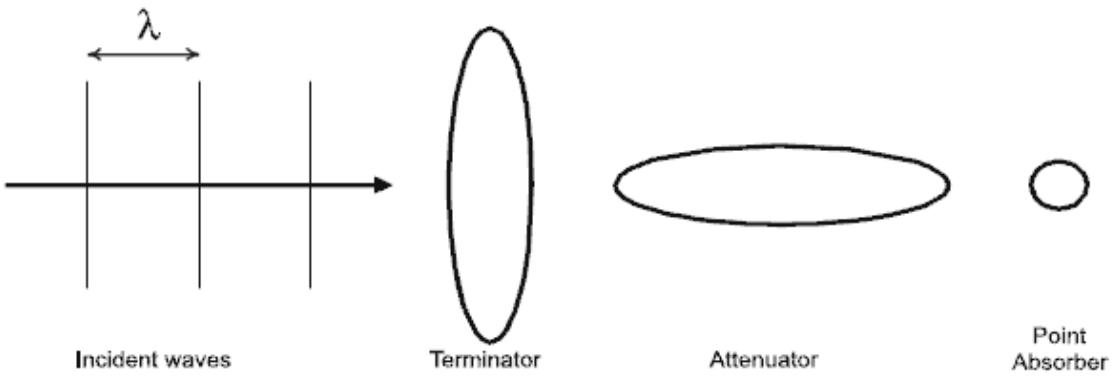

Figure 1-10 - WECs classification

Other possible classifications can concern the location (offshore, onshore, nearshore), the operating principle (Oscillating Water Columns, Overtopping Devices, Wave Activated Bodies) and the energy component (kinetic, potential or both) that they are able to capture [16].

We now focus on this last classification, proposed by Carter (2005) [16]:

- Up-down motion bodies: Many WECs use a float, that possesses up and down heave motion, capturing the potential energy of the wave. The efficiency of the device depends on its relative size with respect to the incident wavelength. Typical examples of this type of devices are wave buoys, that exploit heaving motion to transfer energy to a fluid or to a linear generator. Other devices that may be considered part within this category are Oscillating Water Columns (OWCs), that will be described further in the following: in this case no heaving floats are exploited, but an up-down moving water column is exploited to transfer energy to a volume of compressible fluid (air) that is forced to pass through a turbine.
- Roll devices: Devices that roll with the waves extract both the kinetic and potential energy of the wave. The maximum efficiency condition is usually reached by these devices when operating in phase with the wave and with same amplitude of oscillation. The roll movement is usually exploited to pressurize a fluid (that can be subsequently fed to a Pelton-like turbine). Examples of such devices are the Pelamis and the Salter Nodding Duck, described later on.
- Impact: Waves impacting on a fixed or flexible structure capture the kinetic and potential energy of a narrow band of wave energy spectrum. Examples of such applications are hinged flaps (like the one that is the subject of the last chapter of this thesis) or fixed bodies (like inflating bodies).
- Flush Up and Flush In: Many shore-line devices exploit the flush-up concept to store the wave potential energy. Usually, a ramp is present that allows the wave (when a crest approaches the device) to overtop the device and to spill over into a basin where

the water is stored. The resulting hydraulic head is used to generate electricity with a turbine.

The described concepts are schematically resumed in Figure 1-11.

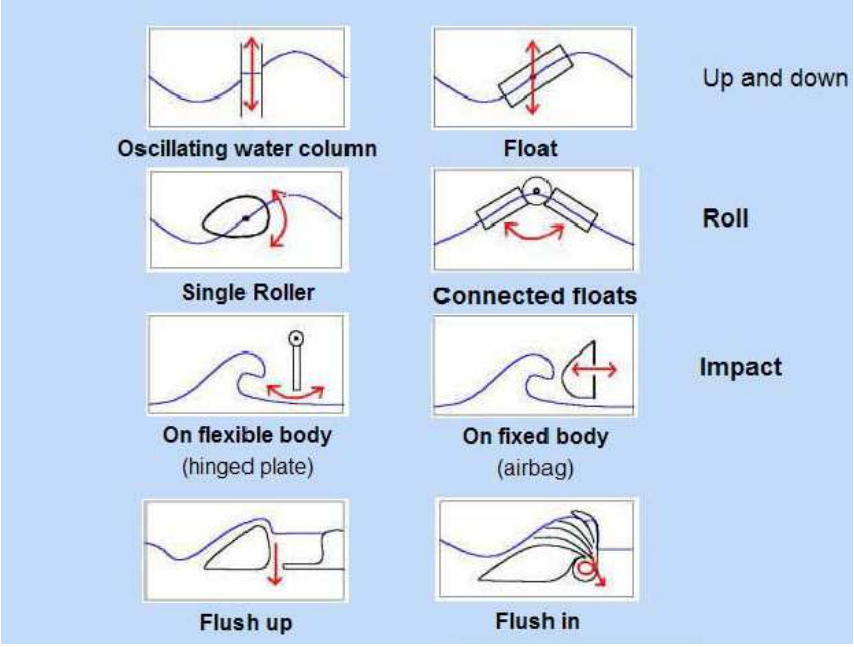

Figure 1-11 - WECs classification based on Energy conversion mechanism

In this section, starting from the just discussed classification of the WECs, some standard concepts and the corresponding real installations are described. Moreover, for some selected devices, simple mathematical analytic models are presented with the aim of explaining how the study of the hydrodynamics and energetic of WECs is carried out.

A final remark is necessary: the classifications above include wave energy converters only, that are the object of interest of the present dissertation. It is necessary to discern Wave Energy from Ocean Currents Energy. Ocean Current Energy converters are a mature technology compared to WECs. Two types of Ocean currents exist [20]: marine currents and tidal currents. The first ones are originated from differences in water temperature within the Ocean; tidal currents are the result of the gravitational interaction between Earth and Moon. Depending on the location, tides have periodicity of half-day, 1 day, 14 days: tidal currents do not have constant flow in one direction but reverse their direction at the end of the cycle. The technology is based on horizontal and vertical axis hydro-turbines; the plant typology is essentially based on two concepts of energy generation from tidal currents: building a tidal barrier across an estuary or a bay, or extracting energy from free flowing water [21].

1-2.3.1 Up-down motion bodies

These generators are the most common example of WECs, since they include floating bodies like heaving buoys.

Heaving Pitching Bodies

Let refer to Figure 1-12 [6]: the body in figure a) is allowed to heave only, moving up-down in vertical direction. Figure b) shows the effect of relative lengths of the body *L* and of the wave λ.

It is immediate to understand that no heaving motion will occur if a crest and a through occur simultaneously on the float, conversely, a net vertical force is present when

$$L = N\,\lambda/2 \qquad \text{with} \qquad N = 1,3,5\ldots$$

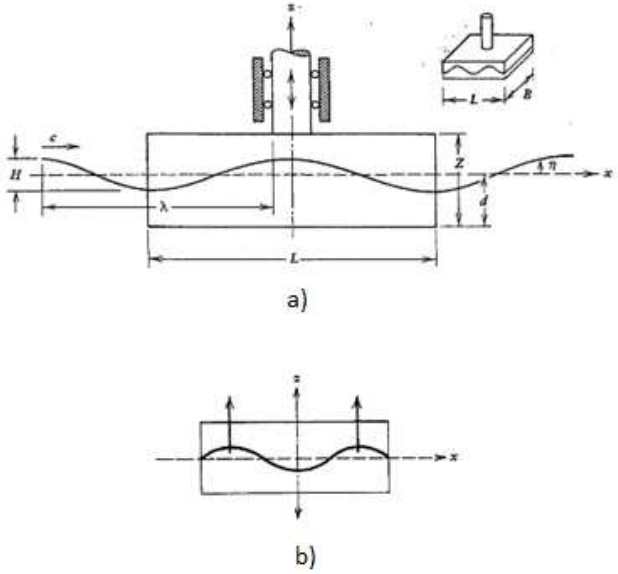

Figure 1-12- Floating bodies: a) purely heaving float; b) pure heaving condition

In a random sea, the above mentioned condition is seldom encountered. Anyway, far from the fetch where the waves are generated (i.e. due to a storm), dispersion has taken place and low period waves have overtaken high period waves. The encountered waves are swell and are nearly monochromatic [6].

A number of experimental buoy prototypes have been installed. The energy extraction and the conversion to electric energy has been usually carried out using hydraulic systems or linear electric generators.

Falcao (2010) [15] presents a review of the technology of heaving buoys with relative installations.

One of the first attempt was a device named G-1T, consisting of a wedge-shaped buoy with rectangular section (1.8 m x 1.2 m at SWL); the PTO was a hydraulic ram in a circuit including a gas accumulator [22].

Another example of installation was tested in Denmark and consists in a buoy connected to a bottom-fixed structure [23].

An example of buoy exploiting a linear-generator system was tested at Upsala University, Sweden. The generator is placed on the sea floor [24].

The concept of a single heaving body moored to the sea bed brings some difficulty due to the relatively high distance between SWL and sea bed plane and to the variations in water depth induced by tidal effect. Two-body systems may be an alternative, in which the energy is converted from the relative motion between two bodies oscillating differently.

One of the most interesting two-body point absorbers for wave energy conversion is the IPS buoy [15], developed in Sweden by the company Interproject Service (IPS). It consists of a buoy rigidly connected to a fully submerged vertical tube open at both ends. The tube houses a piston whose motion relative to the tube (motion originated by wave action on the floater) drives a PTO mechanism.

Another interesting example of two-body heaving device is represented by the Archimede's Wave Swing (Figure 1-13), a fully submerged heaving device, developed in Holland consisting on an oscillating upper part and a bottom-fixed basement. The wave induced motion of the moving part drives a linear electric generator, with the interior air pressure acting like a spring. A prototype was built and tested off Portugal coasts in 2004 [15] [18]. The maximum peak power of the prototype was 2 MW, rated stroke and velocity were 7 m and 2.2 m/s respectively. The overall mass of the device was 7000 tons (primarily due to the sand ballast tanks), of which 400 tons was the mass of the moving part.

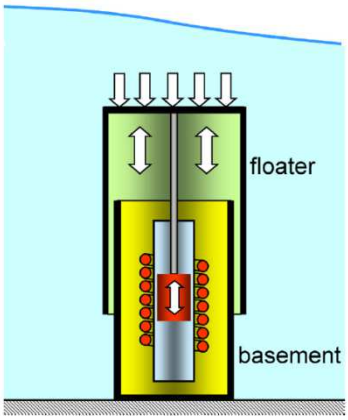

Figure 1-13 - Archimede's Wave Swing schematic

Mathematical model of a heaving buoy

In the following, an extremely simplified analytical mathematic model of a heaving buoy is presented. A complete and comprehensive analysis requires numerical and computational tools that will be explained and applied later on in the thesis.

Let consider a single buoy that drives an electric generator (or any type of PTO system). Generally speaking, the equation of motion for the buoy can be written as [25]

$$M_{eff}\frac{d^2 z_b}{dt^2} = F_w + F_v - F_d$$

Where M_{eff} is the effective mass of the buoy, given by the sum of the inertial buoy mass and of the added mass (at infinite frequency): $M_{eff} = M + M_\infty$ and z_b is the buoy displacement from the equilibrium position. The forces acting on the body can be resumed in

- F_w is the wave induced force that, in a very preliminary analysis can be written as

$$F_w = \rho g A(\eta - z_b)$$

with ρ equal to the sea water density, A equal to the buoy cross section and η equal to the free surface displacement.

In a first approximation, the buoy can be considered small with respect to the wavelength (point-absorber approximation): the equation presented above for η can be used replacing a specific value of the coordinate x (0, for simplicity), obtaining

$$\eta = \frac{H}{2}\cos(\omega t)$$

Where H is the wave amplitude and ω is the wave angular frequency.

- F_v is a force acting on the buoy due to radiated waves: it is indeed necessary to remember that, due to the buoy motion, a radiated wave is produced on the water: the resulting fluid particles velocity field is the result of the superimposition of the wave induced field and of the body induced field. Therefore, together with the incident wave induced force, the float is subjected to a radiated wave induced force, that, in an extremely simplified model, can be written in the form

$$F_v = C_1 S\left(\frac{d\eta}{dt} - \frac{dz_b}{dt}\right)$$

Where C_1 is a proper coefficient and S is an effective buoy water surface area (in general, different from A).

- F_d is a damping force that takes into account both the effect of the viscous drag (that, for point absorbers is usually negligible) and of the PTO system that, in most of the literature, is modeled as a viscous damper [17] [26]

$$F_d = \alpha \frac{dz_b}{dt}$$

With the hypotheses above, the differential equation describing the system dynamics becomes

$$M_{eff}\frac{d^2 z_b}{dt^2} + (\alpha + C_1 S)\frac{dz_b}{dt} + \rho g A\, z_b = \rho g A \eta + C_1 S \frac{d\eta}{dt}$$

With the mentioned expression for $\eta(t)$.

The ordinary differential equation above has a solution that can be written as a sum of two terms:

- An addendum representing the solution of the homogeneous associated equation: this part of the solution influences the transient phase only of the buoy motion, and tends to disappear during time due to the coefficient $(\alpha + C_1 S)$, that represent a dissipative effect. Since we are interested in the regime behavior of the solution only, we do not care of this term.
- Another addendum that is a particular solution of the non-homogeneous equation and represents also the steady-state oscillating response of the system.

We concentrate on the second term only. For simplicity, we use a formalism that makes use of complex numbers, and we write

$$\eta = \frac{H}{2} e^{i\omega t}$$

Since the effective expression for the water surface displacement is given by the real part only of the previous expression, we remember that the real part only of the final solution has to be considered.

A solution in the form

$$z_b = Z e^{i\omega t}$$

with $M \in \mathbb{C}$ has to be found.

Indicating with

$$K_1 = M_{eff} \quad ; \quad K_2 = \alpha + C_1 S \quad ; \quad K_3 = \rho g A$$

An easy calculation brings to the following result for *M*:

$$Z = \frac{\left[\rho g A \frac{H}{2}(K_3 - K_1\omega^2) + K_2 C_1 S \omega^2 \frac{H}{2}\right] + i\left[C_1 S \omega \frac{H}{2}(K_3 - K_1\omega^2) - K_2 \omega \rho g A \frac{H}{2}\right]}{(K_3 - K_1\omega^2)^2 + {K_2}^2\omega^2}$$

Once the oscillating motion of the float is known, the extracted power can be calculated.

Instantaneously, $P(t) = F_d(t)\frac{dz_b}{dt}$.

As a consequence, the time-averaged power extracted is [27]

$$P_{dev} = \frac{\alpha}{2}\omega^2 |Z|^2$$

An analysis of the result shows immediately that, in order to maximize the average extracted power, it is necessary that

- $K_3 - K_1\omega^2 = 0$, that corresponds to $\omega = \sqrt{\frac{\rho g A}{M_{eff}}}$. This condition is known as 'resonance' and is of fundamental importance in wave energy conversion.

  The resonance condition requires that the natural frequency of the float, given by $\omega_z = \sqrt{\frac{\rho g A}{M_{eff}}}$, is equal to the wave frequency ω.

  In general, almost all the WECs operate in resonance condition and are designed to resonate with a significant monochromatic wave [6].

- $\frac{dP}{d\alpha} = 0$, this brings, after some algebra, to the condition

  $$\alpha = C_1 S$$

  that is, the energy extraction rate must equal the radiation damping rate. This result too is well known and can be generalized to other WECs using a similar PTO system [27].

After this optimization, the expression for the averaged produced power gets simplified:

$$P_{dev} = \frac{H^2}{32}\frac{{C_1}^2 S^2 \omega^2 + (\rho g A)^2}{C_1 S}$$

The estimation of the parameter C_1 is a non-trivial hydrodynamic problem, that requires the employment of specific computational tools (i.e. WAMIT) and, in a detailed analysis, should keep into account three-dimensional effects (that for point-absorber WECs are non-negligible).

Oscillating Water Column (OWC)

The OWC system consists on a chamber built in the shoreline coast or mounted on a floating structure.

The motion of sea waves pushes an air pocket up and down behind a breakwater. When a wave crest approaches the column, the water level within the chamber rises, generating a compression of the on-top air volume: the air is pushed through an air turbine. Successively, when the wave returns to the sea, an air depression will occur: the air flow through the turbine reverses its direction; however, the turbine (usually consisting in a Well's turbine) is designed in such a way that, even without reversing its rotating direction, it is able to produce power with opposite air flows [6] [9].

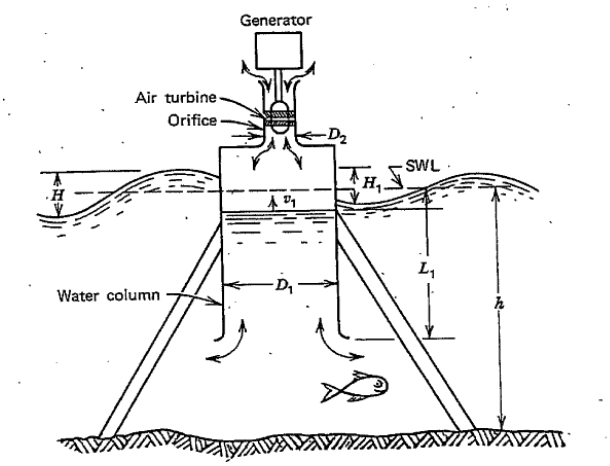

Figure 1-14 - Sketch of OWC system.

The OWC technology, like the major part of WECs, exploit the principle of resonance: the natural angular frequency of the device can be approximated as

$$\omega_z = \sqrt{\frac{g}{L_1 + L_1'}}$$

where L_1 is the depth of the column below the SWL (Figure 1-14) and L_1' is an 'effective' length due to the added mass excited by the water column [6]: this angular frequency must equal the angular frequency ω of the wave in order to achieve resonance.

Fixed structure OWCs comprise a partly submerged concrete or steel structure, open below the water surface, inside which air is trapped above the water free surface.

Among the fixed-structure OWC prototypes, we remember the LIMPET and Pico projects [18].

LIMPET (Land Installed Marine Power Energy Transmitter) prototype was built by Wavegen company in Islay Island, Scotland, in 2000. The installation exploited, as PTO system, a pair of Well's turbine, of 250 kW each and with blades diameter of 2.6 m.

Another relevant installation is that of the Pico plant, off the Azores [18] [28]: this is a 400 kW rated plant, equipped with a 2.3 m diameter Wells turbine coupled to an asynchronous generator. The turbine includes two fixed guide-vane stators, one at each side of the rotor.

Figure 1-15 - Backview of the Pico plant

Floating-structure OWCs also have been prototyped. The functional principle is shown in Figure 1-16: if the system is properly designed, it can take advantage not only of the cavity resonance but also of the heaving motion of the associated float [6].

Floating-OWC structures were the first to be investigated; the most ancient prototype comes from the seventies and is known as Backward Bent Duct Buoy (BBDB) [6].

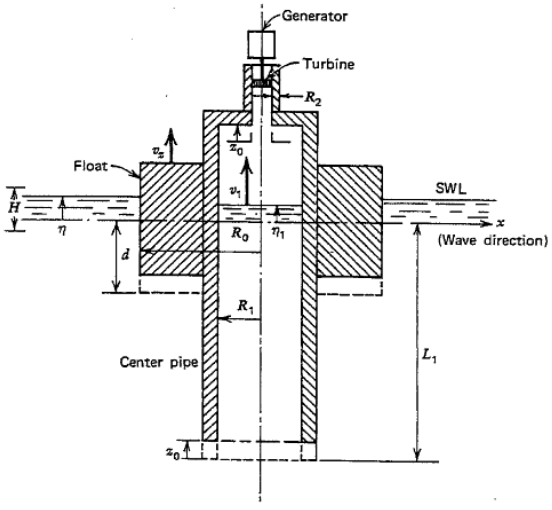

Figure 1-16 - Floating-structure OWC

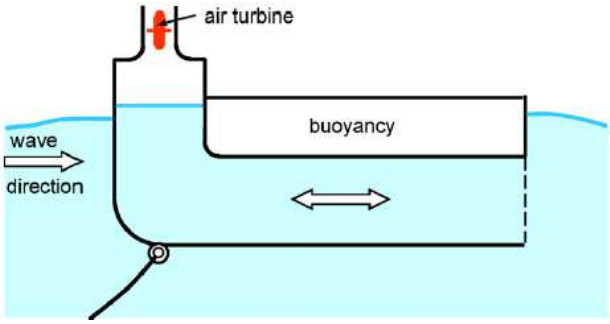

Figure 1-17 - Schematic representation of BBDB

In the BBDB, the OWC duct is bent backward from the incident wave direction (Figure 1-17), in this way, the length of the water column could be made sufficiently large for resonance to be achieved, while keeping the draught of the floating structure within acceptable limits.
Another, more recent example of floating-OWC is the Mighty Wale, developed by the Japan Marine Science and Technology Center. The device consists of a floating structure (length 50 m, breadth 30 m, draught 12 m) which has three air chambers and buoyancy tanks. Each air chamber is connected to a Wells air turbine that drives an electric generator. The total rated power is 110 kW. The device was deployed near the Gokasho Bay, Japan, in 1998 and tested for several years [15].

1-2.3.2 Roll devices

We examine two examples of roll devices: as an example of single rolling device we consider Sater's Duck prototype, as an example of hinged connected floats we consider the Pelamis device.

Salter's Duck

One of the first methods to extract energy from the waves was invented in 1974 by Professor Stephen Salter of the University of Edinburgh, Scotland, in response to the Oil Crisis [5] [9] [18].
The device is essentially constituted by a cam that is free to rotate about a pivot.

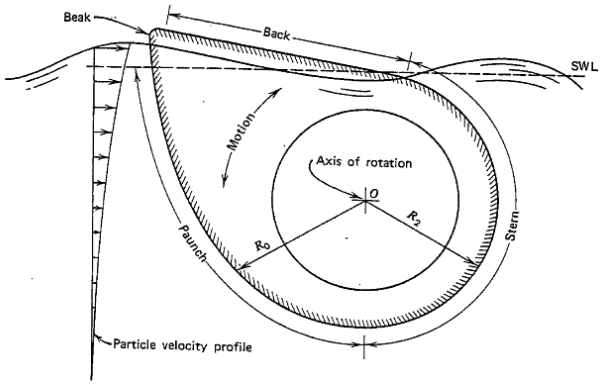

Figure 1-18- Salter's duck schematic

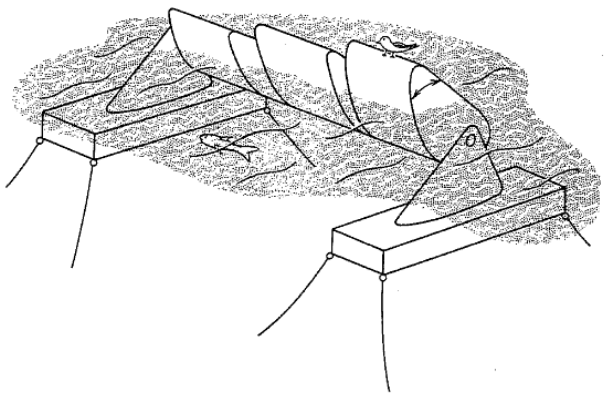

Figure 1-19 - Moored three-duck system

The 'paunch' of the duck is shaped in such a way that the dynamic pressure induced to particle motions forces the duck to rotate through the axis O (Figure 1-18), capturing part of the kinetic energy within the wave. Moreover, the changing hydrostatic pressure contributes to the rotation by causing the buoyant forebody near the 'beak' to rise up and fall down. In order to emphasize the buoyancy effect (improving the capture of the potential energy component of the incident wave power), buoyancy tanks are positioned by the 'beak'.
Salter's duck prototypes were first built and tested at Edinburgh University, then, a prototype was constructed in 1976 off Dores Beach (Scotland).

Significant experiments were carried out by Carmichael (1978) [29] on a small-scale model: capture width ratios up to 150% were detected. This high efficiency values are explained by McCormcik [6] as the result of a three-dimensional antenna effect (similar to that occurring on point-absorber converters) or, most probably, as the effect of reflections from the wave tank walls of the experimental setup.
Even if it has been experimentally proved that Salter's Duck is one of the most efficient WECs, no real installations have been produced, primarily because of its complex hydraulic PTO system, that is not well suited to incremental implementation and because of the high costs and risks of a full-scale prototype [9].

Pelamis Wave Energy Converter

The Pelamis WEC, developed by the Scottish company "Pelamis Wave Power" is a semi-submerged articulated structure composed by 4 cylindrical sections linked by hinged joints and held on station by a compliant mooring system that allows the machine to auto-align with the incoming wave [18].
The energy conversion depends on the relative angular motion of the cylindrical sections pairs: the wave induced motion of the joints is resisted by hydraulic rams, which pump high-pressure oil through hydraulic motors driving three electrical generators. Gas accumulators are present with the aim of providing some energy storage capacity [15].

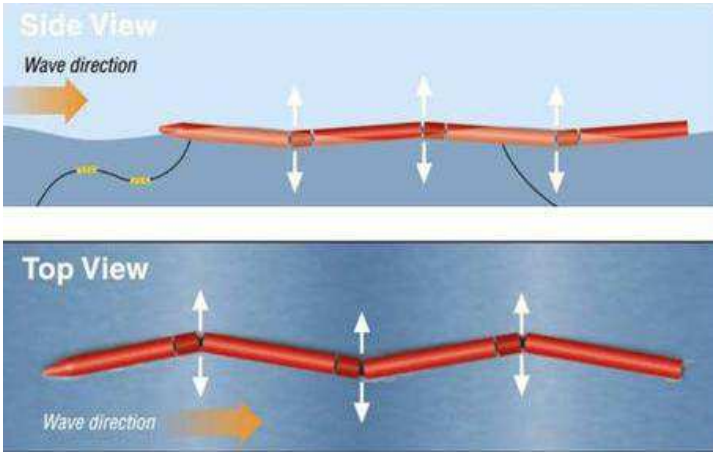

Figure 1-20 - Pelamis schematic views

In their first version, the cylinders have 3.5 m diameter and 30 m length, the power modules have 3.5 m diameter and 5 m about length, for a total length of the machine of 140 m. The device is placed 2/3 semi-submerged offshore in deep-water. The nominal power output of the machine is 750 kW, a 10 kV three phase power transformer is situated in the front floater and send the electric energy across underwater power cables to a substation in land [9].
The Pelamis has been the first commercial scale wave energy converter to generate electricity to a national grid from offshore waves: in 2004, a full scale prototype machine was installed at EMEC (European Marine Energy Center) in the Orkney Islands (UK).

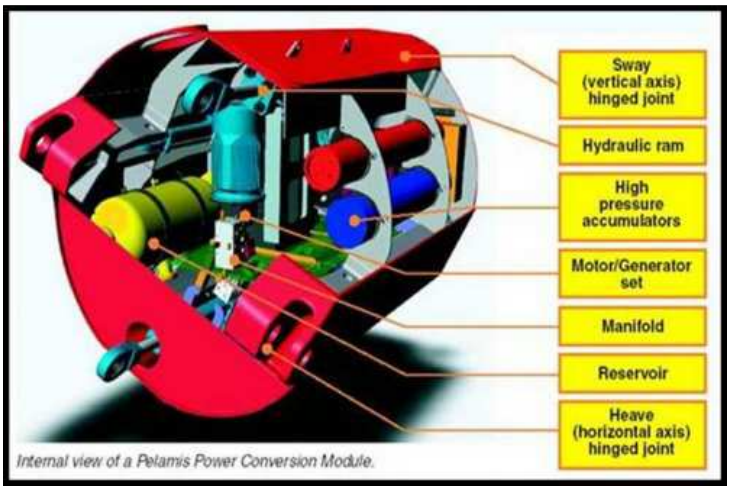

Figure 1-21 - Details of the Pelamis PTO system

In 2008 the first wave farm was built at Aguçadoura, off the northwest coast of Portugal, under commission of the Portuguese electricity company Enersis. The wave farm was constituted by three first generation Pelamis machines (P1), for a nominal power of 2.25 MW. The farm started generating in July 2008 but was put off in November 2008 due to the financial difficulties of Enersis's parent company, Babcock & Brown (www.pelamiswave.com).

Figure 1-22 - Aguçadoura Pelamis wave farm

Rodrigues [9] asses that a single Pelamis machine, placed on a sea with 55 kW/m of power per unit crest width, produces $2.2 \cdot 10^6$ kWh per year. Considering a nominal power of 750 kW, this brings to a load factor *LF* of

$$LF = \frac{2.2 \cdot 10^6 \text{ kWh}}{750 \text{ kW} \cdot 365 \text{ days} \cdot 24 \text{ hr/day}} \approx 0.34$$

That is considered a good value if compared to the corresponding average value for other WECs (in the order of 0.25).

According to the data provided by Pelamis Wave Power, the power output of the device is a function of the significant wave height as shown in Figure 1-23.

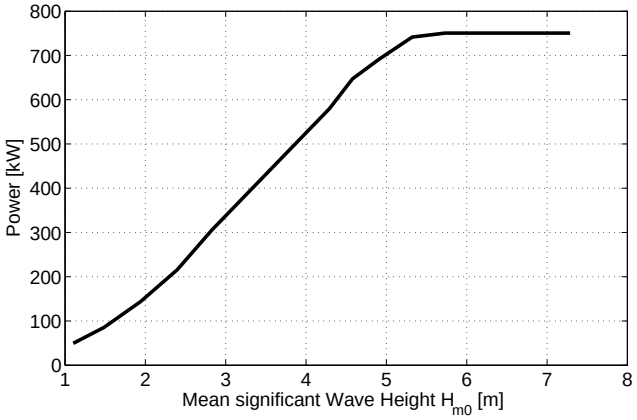

Figure 1-23 - Pelamis power limiting

In 2010, Pelamis Wave Power began tests of the second generation Pelamis machine (P2) at EMEC: among the modification with respect to the P1 design we remember:

- The cylindrical sections diameter has been increased to 4m, and the total length has been brought to 180 m;
- An extra tubular section (and, thus, an extra power module) has been added;
- Rather than the separate sections of the P1, power modules are now integrated into the main tube sections. A universal joint allowing two-degrees of freedom replaces the single degree hinged joints.

The historical antecedent of the Pelamis is a device proposed by Sir Christopher Cockerell in the seventies and known as Cockerell's raft: the devices is made by a series of rafts or pontoons linked by hinges, that follow the wave contour and have PTO systems at the hinges [6] [15].

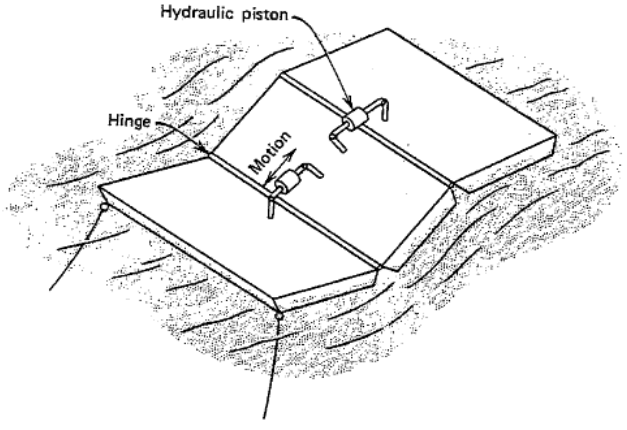

Figure 1-24 - Sketch of a Cockerell's raft system

The main difference between the Cockerell's raft system and the Pelamis is that, while the first system is in good approximation a bi-dimensional system, the Pelamis, thanks to its three-dimensional geometry (the different cylindrical sections are not homogeneously aligned parallel to the wave propagation direction) can experiment capture width greater than its

longitudinal dimension. According to Pelamis Wave Power website, the device has capture widths up to 20 m in small seas (even though the Pelamis is only 4 m wide).

Mathematical model of a single raft hinged to a sea wall

In the present paragraph, an illustrative analytical model of roll device is presented. A single raft hinged to a vertical wall is modeled. The simple model presented is the premise to any study of more detailed systems, like trains of hinged rafts or the Pelamis WEC itself.

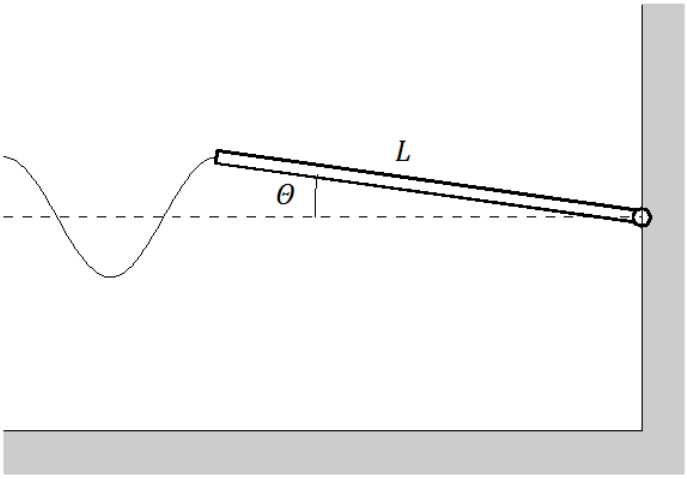

Figure 1-25 - Single raft hinged to a sea wall

The study is extremely similar, for what concerns both the procedure and the results, to the one carried out on a single heaving buoy. Anyway, starting from a work carried out by Haren (1979) [27], a deeper analysis of the hydrodynamics of the system is achieved. In the reference article, moreover, a detailed procedure for the optimization of a train of rafts also is described.

Let indicate with L the raft length and with D its draft in the equilibrium position (Figure 1-26).

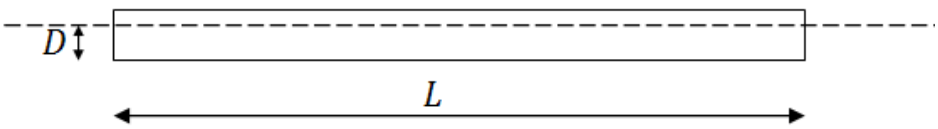

Figure 1-26 - Dimensions definition

Let suppose that an energy absorber (PTO), modeled as a viscous damper (with constant α), is connected to the hinge.

The following analysis is valid in the hypothesis of shallow water conditions, that is, when $k \cdot h \ll 1$ where k is the wave number and h is the water depth, in accordance with the symbols used in the previous sections.

We remember that, in shallow water, $\omega = k\sqrt{gh}$.

Let ω be the incident wave frequency; the generic physical quantity describing the hydrodynamics of the system and the motion of the flap, can be written (using the complex numbers formalism adopted also in the heaving buoy example) in the form

$$\xi = \Xi\, \mathrm{e}^{-i\omega t}$$

with $\Xi \in \mathbb{C}$ in general. So, for example, the velocity potential φ is written as

$$\varphi = \Phi\, \mathrm{e}^{-i\omega t}$$

The equation governing the potential under the free surface (at the side of the raft) is

$$\Phi_{xx} - k^2\Phi = 0$$

this is valid in shallow water only, where the dependence on the z coordinate (perpendicular to the SWL) is negligible.

Remembering that, from Bernoulli's equation, the dynamic pressure is $p = -\rho\frac{\partial\varphi}{\partial t}$, thus

$$P = i\rho\omega\Phi$$

The equation for the velocity potential in the region under the raft can be derived using the following procedure.

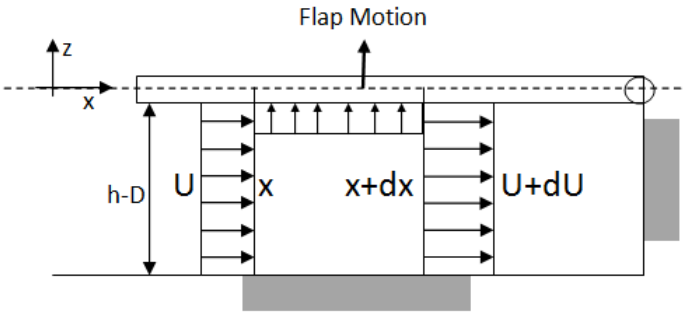

Figure 1-27 - Mass balance on a fluid volume

With reference to Figure 1-27, let consider the water volume contained between *x* and *x+dx* below the raft. Indicating with $z = Z\, \mathrm{e}^{-i\omega t}$ the displacement of the flap in correspondence of the longitudinal position *x*, the mass balance over the described volume has the form

$$\rho(h-D)u = \rho(h-D)(u+du) + \rho\, dx\frac{dz}{dt}$$

that brings to equation for the velocity potential under the raft:

$$i\omega Z = (h-D)\Phi_{xx}$$

The total pressure at the bottom of the raft is the sum of the dynamic pressure of the added hydrostatic pressure (due to the raft displacement) and of the static pressure:

$$P_{TOT} = i\rho\omega\Phi - \rho g Z + \rho g D$$

Under the free surface, in accordance to the described theory for shallow water conditions, the solution of the hydrodynamic fields is (omitting, as usual, the time-dependent factor $\mathrm{e}^{-i\omega t}$):

Free surface displacement: $\eta = \frac{H}{2}\left(\mathrm{e}^{ikx} + r\,\mathrm{e}^{ikx}\right)$

Velocity potential: $\Phi = -\frac{igH}{2\omega}\left(\mathrm{e}^{ikx} + r\,\mathrm{e}^{ikx}\right)$

Particles horizontal velocity: $U = \frac{gHk}{2\omega}\left(\mathrm{e}^{ikx} - r\,\mathrm{e}^{ikx}\right)$

where H is the wave height and r is a reflection coefficient that keeps into account the reflection due to the presence of the raft.

Let suppose that the origin of the reference system ($X=0$) is on the SWL, in correspondence of the non-hinged edge of the raft (when it is in horizontal equilibrium position), so that the hinge lies at $X=L$, and let suppose that the angle Θ formed by the flap with the SWL is positive for counterclockwise rotations.

Thus, the vertical displacement Z of the raft at the generic longitudinal position X is

$$Z = \Theta(X - L)$$

where Θ is not a function of X (and is thus constant since the dependence from the time has been simplified).

Using the equation for the velocity potential under the raft, with the condition $U(L) = \Phi_x|_L = 0$, under the raft the fluid field result

Velocity potential: $\Phi = \frac{i\omega}{(h-D)}\left[\frac{\Theta}{6}(X-L)^3 + C\right]$

Particles horizontal velocity: $U = \frac{i\omega}{(h-D)}\frac{\Theta}{2}(X-L)^2$

Summarizing:

<u>Free surface</u>:

$$\Phi = -\frac{igH}{2\omega}\left(\mathrm{e}^{ikx} + r\,\mathrm{e}^{ikx}\right)$$

$$U = \frac{gHk}{2\omega}\left(\mathrm{e}^{ikx} - r\,\mathrm{e}^{ikx}\right)$$

<u>Under-raft</u>:

$$\Phi = \frac{i\omega}{(h-D)}\left[\frac{\Theta}{6}(X-L)^3 + C\right]$$

$$U = \frac{i\omega}{(h-D)}\frac{\Theta}{2}(X-L)^2$$

In this set of equations, three unknowns are present: r, Θ and C.

For $X=0$, continuity in the values of Φ and U must be verified then two conditions are obtained:

$$ik\frac{H}{2}(1-r) = -\frac{1}{2}(kL)^2\Theta\left(\frac{h}{h-D}\right)$$

$$-k\frac{H}{2}(1+r) = \left[-\frac{1}{6}(kL)^3\Theta + k^3C\right]\left(\frac{h}{h-D}\right)$$

The third condition is the equation describing the dynamics of the raft, the is derived in the following.

The wave induced torque on the raft has to be calculated. Disregarding the own weight of the body (supposed to be balanced by the buoyancy force), let consider the dynamic pressure acting on the raft:

$$P = i\rho\omega\Phi - \rho gZ$$

Notice that respect to the expression for P_{TOT} the last addendum $\rho g D$ is not present, since it represents the contribution of the hydrostatic pressure, that is supposed to be balanced by the own weight of the body.

The dynamic torque about the hinge (per unit width of the raft) is

$$T = -\int_0^L P(X)(L-X)dX = -\Theta\left(\frac{\rho\omega^2 L^5}{30(h-D)} + \frac{1}{3}\rho g L^3\right) + \frac{C\rho\omega^2 L^2}{2(h-D)}$$

Assuming a moment of inertia (per unit width) for the raft of I and considering the viscous damping due to the PTO, the equation for the system dynamics is

$$-\omega^2 I\Theta = i\omega\alpha\Theta + T$$

Using this equation, together with the two conditions derived above, r, Θ and C can be found. In particular, the solution for r and Θ results in

$$r = 1 - \frac{ik}{2}\left[\left(\frac{I(h-D)}{\rho L^3} + \frac{1}{20}\right)k^2 - \frac{1}{3}\frac{h-D}{h} + ik\left(\alpha\frac{h-D}{h} + \frac{1}{4}\right)\right]$$

$$\Theta = \left(\rho g\frac{H}{2}L^2\right)\left[\left(I + \frac{\rho L^5}{20(h-D)}\right)\omega^2 - \frac{1}{3}\rho g L^3 + i\omega\left(\alpha + \frac{h\rho L^4}{4(h-D)}\sqrt{\frac{g}{h}}\right)\right]^{-1}$$

Using this result, the time-averaged power extracted from the wave is

$$P_{dev} = \frac{\alpha}{2}\omega^2|\Theta|^2$$

that is

$$P_{dev} = \frac{\omega^2}{8}\frac{(\rho g H L^2)^2\alpha}{\left[\left(I + \frac{\rho L^5}{20(h-D)}\right)\omega^2 - \frac{1}{3}\rho g L^3\right]^2 + \omega^2\left(\alpha + \frac{h\rho L^4}{4(h-D)}\sqrt{\frac{g}{h}}\right)^2}$$

In order to maximize the extracted power the following conditions must be imposed:

- $\left(I + \frac{\rho L^5}{20(h-D)}\right)\omega^2 - \frac{1}{3}\rho g L^3 = 0$ that is the resonance condition. Noticing that $\frac{\rho L^5}{20(h-D)} = I_h$ is the hydrostatic added moment of inertia, the condition of resonance requires the wave frequency to equal the body natural frequency $\omega_z = \sqrt{\frac{1/3\rho g L^3}{I+I_h}}$.
- $\frac{dP_{dev}}{d\alpha} = 0$, that brings to the resulting optimal value for α: $\alpha = \frac{h\rho L^4}{4(h-D)}\sqrt{\frac{g}{h}}$. The energy extraction rate must then equal the radiation damping rate, that is the same condition found for the heaving buoy of the previous example.

Notice also that, when the optimal conditions above are respected, the resulting reflection coefficient r is 0.

Remembering that the power per unit crest width carried by a wave in shallow water is given by

$$P_w = \frac{\rho g H^2 \sqrt{gH}}{8}$$

the expression for the capture width ratio (in the optimal conditions hypothesis) reduces to a simple form:

$$\epsilon = \frac{P_{dev}}{P_w} = \frac{h - D}{h}$$

1-2.3.3 Impact WECs

Impact devices can be essentially divided into two main sub-categories: rigid undeformable WECs and flexible (or inflatable) WECs. We consider the first category only and discuss here the example of the Oscillating Wave Surge Converter (OWSEC), that is the object of a following chapter of the present thesis.

Oscillating Wave Surge Energy Converter (OWSEC)

The OWSEC is a concept of shoreline or near-shore WEC. Many studies have been recently addressed to the investigation and energy performance assessment of this device [26] [30] [31] [32] and the modeling of a novel concept of OWSEC exploiting Dielectric Elastomer generators as PTO system is also the object of part of the present work.

The OWSEC consists of a hinged flap (or paddle) rotating about a horizontal axis and perpendicular to the direction of wave propagation.

Two main conceptual prototypes exist: one having the pivot axis above the SWL and the other with the axis underwater in the vicinity of the seabed (Figure 1-28).

Since the fluid particles velocity is larger near the SWL, hinging the flap at the bottom generally represents a better solution, since this produces higher wave induced torques on the device. However in shallow water the horizontal water particles motion is still significant at the sea bed, whilst the horizontal motion of the flap would be zero at the hinge.

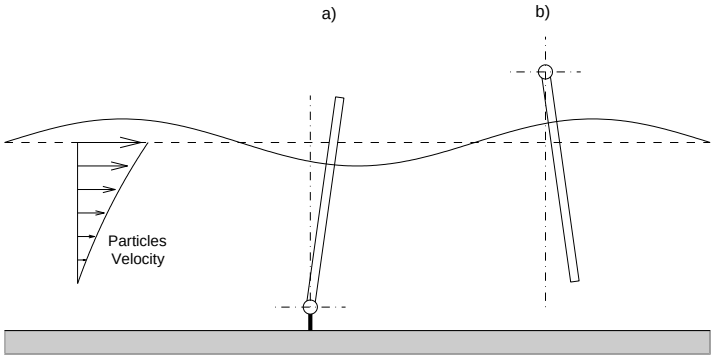

Figure 1-28 - Wave Surged hinged a) at the bottom b) at the top

Hinging the paddle above the SWL provides two benefits: first, the PTO system is easily accessible, secondly, the top hinged paddle suffers no end-stop problems and could feasibly swing through a full 360° angle [30].

A prototype of top hinged flap (known as PENDULOR) was built and tested during the eighties in Japan by the Muroran Institute of Technology [33]. The prototype was 2.5 tons of weight and 7 m long from the top hinge to the bottom end and had a PTO system based on a reciprocated cylinder located atop the flap with the aim of pumping oil through a hydraulic circuit. The experimental measured value of the capture width ratio was up to 80%.

Up to date, four OWSEC prototypes, in a pre-commercial stage, can be identified; all al them are hinged from the bottom to a pivot that lies in the vicinity of the sea-bed. A description of the devices can be found in [26].

EB Frond

EB Frond has been developed by Lancaster University and from the company Engineering Business Ltd.

EB Frond is constituted by an oscillating arm pivoted near the seabed having a collector vane at its top. The device is provided with hydraulic cylinders connected between the arm and the structure which deliver high-pressure oil to a hydraulic motor driving an electric generator [34].

Figure 1-29 - EB Frond WEC

Wave Roller

Wave Roller has been developed by AW-Energy OY. It is a bottom hinged plate connected to a hydraulic piston pump [26].

The system is fully submerged and is thus invisible from the surface. The machine operates in near shore areas (approximately 0.3-2 km from the shore) at depths between 8 and 20 m. A single WaveRoller unit (one panel) is rated at between 500 kW and 1000 kW.

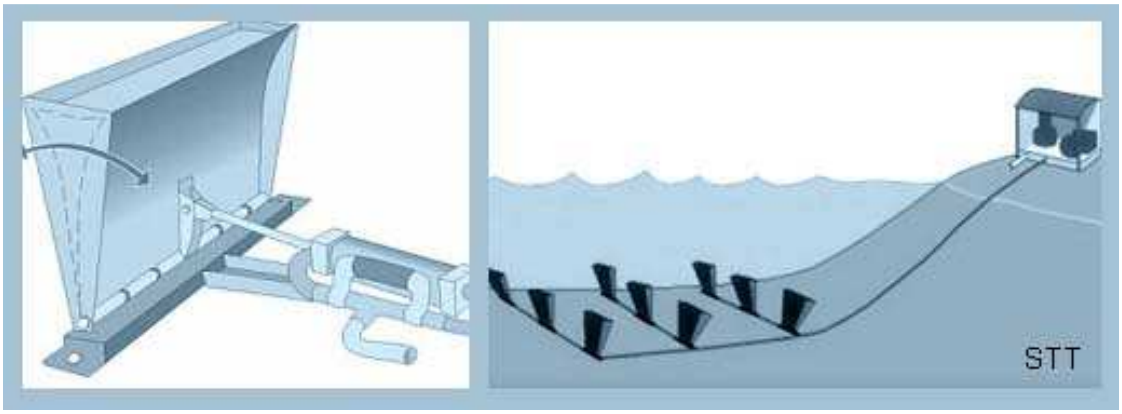

Figure 1-30 - Wave Roller (on the left) and Wave Roller farm schematic (right)

Open sea tests of a semi-scale device have been conducted during 2007 and 2008 in Peniche (Portugal) (aw-energy.com).

BioWave

BioWave has been developed by the University of Sidney and BioPower Systems Pty. Ltd. The systems takes inspiration from the swaying motion of sea plants in presence of ocean waves [26].

The device is mounted on the seafloor and brings an array of buoyant floats at its top. The PTO system is, like for the other devices, hydraulic. The bioWAVET prototype currently under development will operate at a depth of 30m, while the planned 1 MW commercial model will operate where the depth is 40-45m (www.biopowersystems.com).

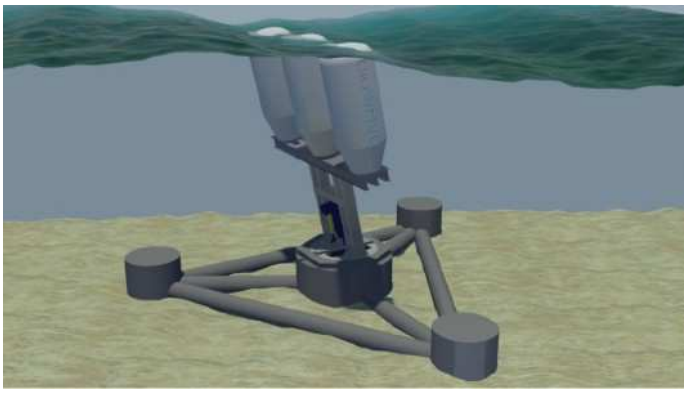

Figure 1-31 - The BioWave WEC

Oyster

The Oyster WEC is probably the most famous example of OWSC. It has been developed by Queen's University Belfast and by the company Acquamarine Power LTd.

In its present configuration, Oyster is located at a nominal water depth of 12 m (which in many locations is close to the shoreline). The system consists in a buoyant flap 18 m wide and 10 m high, hinged at its base to a sub-frame which is pinned to the sea bed using tensioned anchors. The flap oscillates compressing and extending in turn two hydraulic cylinders mounted between the flap and the sub-frame which pumps water at high pressure through a

pipeline back to the beach. On the shore, there is a small hydro-electric plant consisting of a Pelton wheel turbine driving a variable speed electrical generator coupled to a flywheel. The nominal power output of the device is 350 kW [35].

The first Oyster device was installed (and grid connected) in 2009 off Orkney (Scotland), at EMEC and operated for a period over 6000 hours during two winters (www.aquamarinepower.com).

Wave tank experiments carried out at Queen's University Belfast have brought to an estimation of an average yearly capture width ratio up to 70% [36].

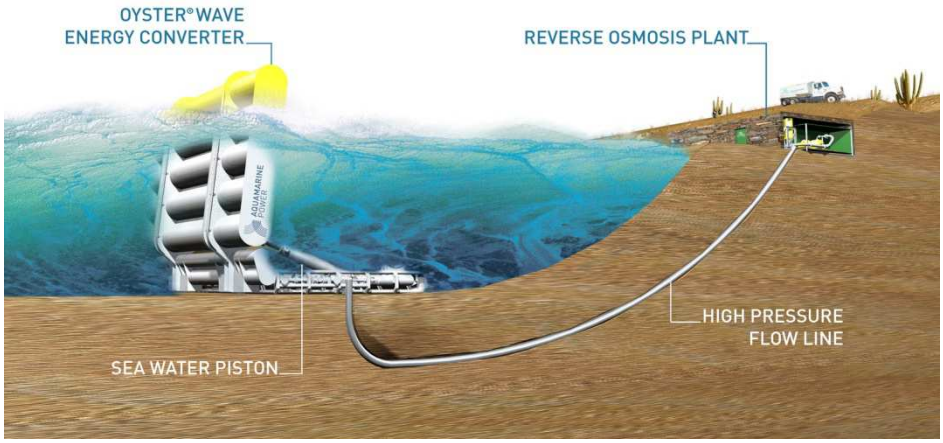

Figure 1-32 - Oyster device with its power extraction circuit

1-2.3.4 Flush Up and Flush In WECs

These devices are more often designed with the name of "overtopping devices". In their usual most common form, they are provided with a reservoir tank where water, collected exploiting an overtopping mechanism thanks to a ramp, forms with the SWL a head that can be usefully exploited in a hydraulic turbine. The hydrodynamic of overtopping devices is strongly non-linear: a different mathematical approach has to be followed with respect to the cases examined until now, and the use of statistical and experimental correlations is necessary (Falcao).

We consider here two classes of devices: onshore devices (with the reservoir located on the shoreline) and offshore devices. For the first category, the TAPCHAN prototype is considered; for the second category, we mathematically examine the Wave Dragon prototype.

TAPCHAN

TAPCHAN stands for Tapered Channel device. The device was developed in Norway during the eighties.

The TAPCHAN comprises a gradually narrowing channel with wall heights typically of 3 to 5 m above SWL. Waves enter the wide end of the channel; as they propagate through the narrowing channel, the wave height is amplified until the wave crests spill over the walls to the reservoir, which is raised above sea level.

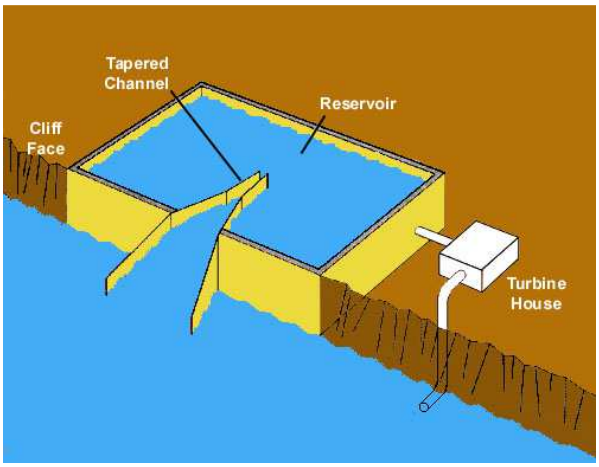

Figure 1-33 - Schematic of the TAPCHAN WEC

The water in the reservoir returns to the sea passing through a conventional low head Kaplan turbine, which works in quite stable conditions due to the storage capacity of the reservoir.
A prototype with rated power 350 kW, 40 m wide, was built in 1985 at Toftestallen, Norway, and operated for several years, until the early 1990s, when modification works destroyed the tapered channel [37].
Planning of a larger TAPCHAN project in Indonesian Island of Java was also undertaken. The plant was designed for an output power of 1.1 MW. The construction was scheduled to start in 1998, but due to general financial problems, it was not realized [38].

Wave Dragon

The Wave Dragon is a floating offshore overtopping WEC, developed in Denmark by the Wave Dragon Aps company; it has been the world's first near-shore WEC producing power for the grid [9].
It basically consists of two arms, behaving as wave reflectors, focusing the waves towards a ramp. Behind the ramp is the reservoir where the water that runs up the ramp is collected and temporarily stored. The PTO consists of several variable speed low-head hydro-turbines directly coupled to permanent magnet generators. The turbines are of axial type with fixed propeller blades and guide vanes. The rotational speed of the turbines is controlled in accordance with the available pressure head [39].

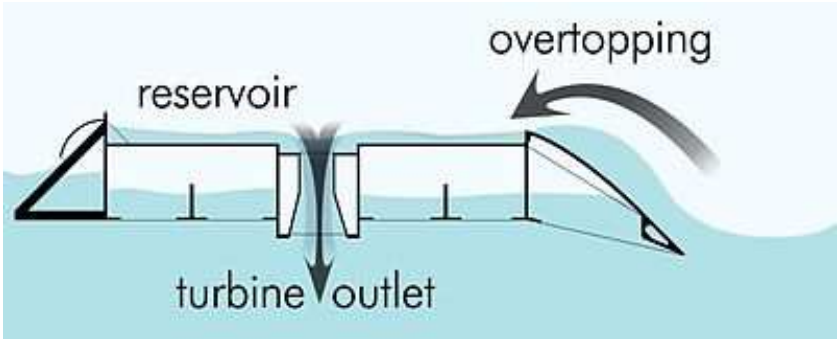

Figure 1-34 - Wave Dragon conceptual scheme

Comparing to the other WECs, one point of interest is that Wave Dragon is a relatively simple and reliable device, since the only moving parts are the hydro-turbines: this is essential for a device operating in near-shore conditions, where the extreme forces seriously affect any moving part [9].

A 57 m-wide, 237 t (including ballast) prototype of the Wave Dragon has been deployed in Nissum Bredning, Denmark; such a prototype was constructed to match a wave climate with estimated power per unit crest length of 0.4 kW/m only and had a rated power output of 20 kW. The prototype was grid connected in May 2003 and has been tested 3 years and a half.

The Nissum Bredning prototype is a traditional (ship-like) steel plate construction, primarily made by 8 mm steel plates. The total steel weight of the main body plus the ramp is 150 t. To obtain the desired 237 tonnes total weight, 87 tons of primarily water ballast are added (www.wavedragon.net).

Figure 1-35 - Wave Dragon prototype at Nissum Bredning (DK)

With respect to a typical North Sea condition, the tested prototype represent a 1/4.5 scale model: indeed, referring to a yearly average power per unit crest width of 24 kW/m, a 22000 tons reinforced concrete structure is required, occupying an area of about 150 m x 260 m, having rated power of 4 MW [39], however, according to the site of the company, the dimensions can be scaled differently in order to adapt the device to stronger wave climates also.

Table 1 reports a range of features for some hypothetical scaled commercial versions of the device (www.wavedragon.net).

The tests performed at Nissum Bredning allowed to investigate many aspects which cannot be successfully modeled in the laboratory, like the low head hydro turbines controlled by variable speed Permanent Magnet Generators, and the hydraulic response of the platform with its open buoyancy compartments, and have produced a series of scientific works [39] [40] [41].

Rated wave power per unit crest width:	Nissum Bredning prototype	24 kW/m	36 kW/m	48 kW/m
Total weight	237 t	22,000 t	33,000 t	54,000 t
Total width and length	58 x 33 m	260 x 150 m	300 x 170 m	390 x 220 m
Wave reflector length	28 m	126 m	145 m	190 m
Height	3.6 m	16 m	17.5 m	19 m
Reservoir Volume	55 m^3	5,000 m^3	8,000 m^3	14,000 m^3
Number of Kaplan turbines	7	16	16 - 20	16 - 24
Permanent magnet generators	7 x 2.3 kW	16 x 250 kW	16/20 x 350 - 440 kW	16/24 x 460 - 700 kW
Rated power/unit	20 kW	4 MW	7 MW	11 MW
Annual power production/unit	-	12 GWh/y	20 GWh/y	35 GWh/y
Water depth	6 m	> 20 m	> 25 m	> 30 m

Table 1 - Wave Dragon scaling

Mathematical model o fan overtopping device

Mathematical models for overtopping devices are substantially different from those of the other WECs, due to the high non-linearity of their hydrodynamic behavior and, thus, to the impossibility of applying the linear wave theory. Predictions are then based on empirical methods, mainly derived from experimental tests of reduced-scale models.

The empirical equations employed in the design of overtopping devices like the Wave Dragon derive mainly from studies carried out on dykes and breakwaters.

The results presented in the following are based on some studies made by Kofoed [38] and Parmeggiani [39], and refer to a floating overtopping device.

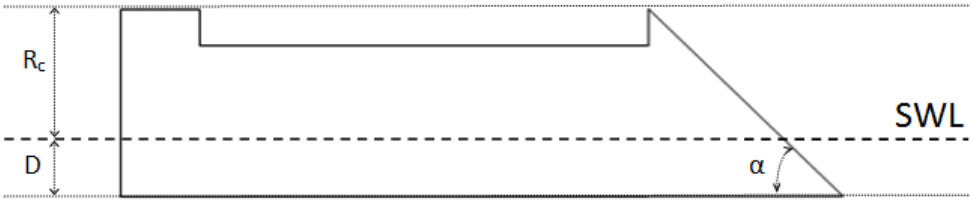

Figure 1-36- Overtopping device sketch

In Figure 1-36, some geometric parameters are defined:

R_c is the device crest level (above the SWL);

D is the draft of the device;

α is the slope angle of the ramp.

The power produced by the hydro-turbine can be simply written as

$$P_{dev} = \eta_t \, q \, \rho \, g \, H_t$$

where η_t is the turbine efficiency, q is the mean overtopping discharge [m^3/s], that is the mean volume flow rate through the turbine, H_t is the difference between the mean water level

in the reservoir and the SWL. As H_t is necessarily lower than R_c, the water stored in the reservoir has less potential energy than when overtopping the ramp, the excess being progressively dissipated by cross-waves within the reservoir itself.

The principal issue of the analysis is the determination of the discharge rate q.

The overtopping flow, in its non-dimensional form q^*, is usually fitted to experimental data in the following form:

$$q^* = \frac{q}{b\sqrt{gH_{m0}{}^3}} = A \cdot \exp\left(-B\frac{R_c}{H_{m0}}\right)$$

where b is the device width, H_{m0} is the significant wave height (according to the previous definition) for the reference sea and the ratio R_c/H_{m0} is indicated with R (non-dimensional crest level).

For $0.58 \leq \cot(\alpha) \leq 2.75$ and $0.15 \leq R \leq 2$, Parmeggiani et al. report the following fitting results (valid for a generic floating overtopping WEC):

$$A = 0.2\lambda_{dr}\lambda_s \quad ; \quad B = 2.6$$

where

- λ_{dr} represents the proportion of energy the device is able to intercept due to its limited draft (lower than the water depth). It can be calculated as the ratio of the mean energy flux included between the SWL and the draft of the device over the mean energy flux over the whole water depth. Introducing a conceptual stretching, this ratio can be calculated referring to the linear theory (that is not followed in the rest of the analysis):

$$\lambda_{dr} = \frac{\int_{-D}^{0}\int_{0}^{T}\rho\frac{\partial\varphi}{\partial t}u\,dt\,dz}{\int_{-h}^{0}\int_{0}^{T}\rho\frac{\partial\varphi}{\partial t}u\,dt\,dz} = 1 - \frac{\sinh\left(2kh\left(1-\frac{D}{h}\right)\right) + 2kh\left(1-\frac{D}{h}\right)}{\sinh(2kh)+2kh}$$

  where k is the wave number and h the water depth.

  Since the linear theory does not apply to this problem, a correction can be introduced in the form

$$\lambda_{dr} = 1 - \kappa\frac{\sinh\left(2kh\left(1-\frac{D}{h}\right)\right) + 2kh\left(1-\frac{D}{h}\right)}{\sinh(2kh)+2kh}$$

  with a proposed value of κ of 0.4.

  Notice that, for a given value of the ratio D/h, λ_{dr} still depends on h, expressing the fact that the percentage of incoming wave energy that the device is able to intercept progressively increases in deeper waters.

- λ_s is an ulterior correction factor given by

$$\lambda_s = 0.4 \sin\left(\frac{2\pi}{3} R\right), \text{ if } R < 0.75$$
$$\lambda_s = 1, \text{ if } R \geq 0.75$$

In order to calculate the capture width factor, the expression for the mean power in a real sea can be used:

$$P_w = \frac{\rho g^2 {H_{m0}}^2 T_p b}{64\pi}$$

where T_p is the peak-period for the reference sea.

The deep-water wavelength referred to the peak period is $\lambda_{0p} = \frac{g{T_p}^2}{2\pi}$, therefore P_w can be re-written as

$$P_w = \frac{\rho g {H_{m0}}^2 b}{32} \sqrt{\frac{g\lambda_{0p}}{2\pi}}$$

The capture width ratio has then the following expression:

$$\epsilon = 32\sqrt{2\pi}\, \eta_t A \frac{H_t}{H_{m0}} \sqrt{\frac{H_{m0}}{\lambda_{0p}}} \exp(-BR)$$

As previously mentioned, H_t is at most equal to R_c: for simplicity, we write $H_t = \nu R_c$, obtaining a new, more expressive, equation for ϵ as a function of R (remember that also A depends on R due to λ_s).

$$\epsilon = 32\sqrt{2\pi}\, \eta_t A \nu \sqrt{\frac{H_{m0}}{\lambda_{0p}}} R \cdot \exp(-BR)$$

By way of illustration, we make some assumptions:

- $D/h \ll 1$, so that $\lambda_{dr} \approx 1 - \kappa = 0.6$
- ν can be estimated using the results presented by Knapp [40] that reports the assessed values of maximum and minimum head for the turbine for different wave heights, basing the calculation on the Wave Dragon prototype. From the data, the mean head H_t can be calculated (using the arithmetic mean) and the ratio ν can be calculated for each case.

H_{m0} [m]	R_c [m]	min. head [m]	max. head [m]	avg. Head H_t [m]	$\nu = H_t/R_c$
1	0.8	0.4	0.6	0.5	0.63
2	1.4	0.9	1.2	1.1	0.75
3	2.2	1.4	1.8	1.6	0.73
4	2.7	2.0	2.4	2.2	0.81
5	3.5	2.4	3.0	2.7	0.77

  A good estimation for ν can therefore be $\nu = 0.75$
- η_t is assumed equal to 1 since we restrict to considerate the power available upstream the turbine itself.

- The ratio H_{m0}/λ_{0p} can be estimated by using the data reported by Parmeggiani [39] (H_{m0} vs T_p) for the Danish part of the North Sea.

T_p [s]	H_{m0} [m]	λ_{0p} [m]	H_{m0}/λ_{0p}
5.6	1	4.90E+01	2.04E-02
7	2	7.65E+01	2.61E-02
8.4	3	1.10E+02	2.72E-02
9.8	4	1.50E+02	2.67E-02
11.2	5	1.96E+02	2.55E-02

Basing on these results, the assumed value for the ratio is 2.5E-02.

With the above mentioned remarks, the capture width as a function of the non-dimensional crest level is shown in Figure 1-37.

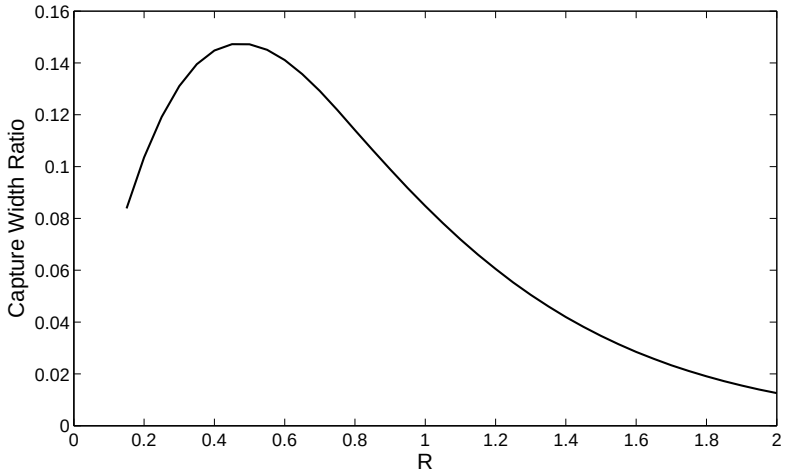

Figure 1-37 - Capture width ratio vs R

The numerical values obtained for ϵ are particularly low, due also to the fact that the concentrating effect of eventual reflector arms (like those of the Wave Dragon) has not been accounted here.

Apart from this, it is interesting to notice that a value of R exists that maximizes the captured energy: this is an aspect to be taken into account when designing an overtopping WEC.

1-2.3.5 Synthesis and main references

Wave Energy conversion is one of the most fast-growing sectors within the panorama of renewable sources. In the last few years an extraordinary spread of technical and scientific works has been observed and in 2013 only hundreds of articles (published in specialized magazines or presented at conferences) have been produced.

The present paragraph has the aim of providing a basic bibliography on wave energy in general and on the specific technologies in particular. Of course, the References of the present thesis themselves have been selected, read and chosen with the aim of providing a complete and up-to-date overview of the subject. Anyway, for the sake of completeness and synthesis,

some of the most relevant works are here listed and briefly commented, in order to furnish a targeted bibliography of the subject.

Review of the technologies

Falnes J.; *A review of Wave-Energy extraction*; Marine Structures (20) 185-201, 2007. [42]

A classic of the literature on Wave Energy. The article is totally methodological, describing the main principles that allow to exploit wave energy rather than the state of the art of the technology. A general mathematical model to describe oscillating WECs is sketched, and some classic considerations about the upper bounds existing to the power output of the devices are here presented.

Falcão A. F. de O.; *Wave energy utilization: A review of the technologies*; Renewable and Sustainable Energy Reviews 14 899–918, 2010. [15]

This is one of the most cited and well-know works about wave energy. The article reports a very synthetic resume of the general mathematical model used to describe WECs motion in frequency domain. Then, it presents an overview of the main technologies, with a particular focus on the existing prototypes and installations: a wide range of numerical data (devices sizes, powers rate etc.) is also present. Finally, a review of some PTO technologies also is present. The article is totally descriptive (the general mathematical model is sketched only) but very complete and critical. Moreover, a large bibliography is reported.

Babarit A., Hals J., Muliawan M. J., Kurniawan A., Moan T., Krokstad J.; *Numerical benchmarking study of a selection of wave energy converters*; Renewable Energy, 41, 44-63, 2012. [19]

This recent article is an example of systematic application of the linear theory, used to model oscillating WEC, to a selection of devices in a set of significant reference seas. The interest of the article lies in the methodological approach and in the description of the general model used to simulate the devices. The result consist in a series of tables that, for each of the selected devices, furnishes the typical dimensions, the simulated power matrix and the resulting productivity in real seas. Of course, some remarks have to be taken into account when considering this work: 1) the linear theory is valid only for small oscillations of the WECs, and extrapolations of the results over a wide range of sea states may bring to strong uncertainties (that, anyway, are here estimated); 2) The dimensioning of the systems should be tailor-made basing on the particular sea-state. Anyway, for commercial devices, also the opposite approach (given the device, calculate the productivity in a certain context) is of interest.

Prototypes

In the present paragraph, attention is focused on some of the full-scale prototypes discussed and described previously.

In order to clarify the operating conditions and the different operating contexts for the different technologies, the devices are collocated in a map reporting typical water depths for the installation and the range of operating significant wave heights. Of course, many other parameters can influence the performances of a prototype in a real sea, i.e.

- **Wave frequency**: this is a crucial parameter, especially for those devices that operate in resonance with the most frequent or energetic sea states. Anyway, the operating

wave period for different categories of devices is always in a relatively small range, around 10 s (that is a typical value for an average sea). In deep water, high-period waves are met, in shallow water, due to the Venturi effect produced by the reduction in water depth, waves tend to acquire higher velocities and their period tends to decrease. Anyway, for given values of water depth and wave height, quite univocal values of the waves frequencies can be identified exploiting available scatter matrices or correlations.

- **Wavelength**: the wavelength is a relevant parameter, since the relative dimensions between the WEC device and the wavelength determine different energy extraction mechanisms. We remember anyway that, if the wave period is assessed, once the depth is know, the wavelength can be easily calculated exploiting the equations presented in a previous paragraph.

Water depth and wave height have been here used as relevant parameters since they provide a quite complete understanding of both the energy intensities present within the corresponding sea states and of the safety range of operation for the devices.

For each of the devices considered in the map, some significant literature references providing relevant information about the design, the modeling, the operating conditions and the manufacturing and installation processes are briefly described.

IPS Buoy

Web site: http://www.ips-ab.com

Falcao A., Candido J., Justino P., Henriques J.; *Hydrodynamics of the IPS buoy wave energy converter including the effect of non-uniform acceleration tube cross section*; Renewable Energy 41, 105-114, 2012. [43]

A theoretical study about the geometric optimization of the IPS buoy design. The study is interesting under the methodological point of view since it reports a frequency-domain analysis of the device in both regular and irregular sea conditions.

Archimedes Wave Swing

Web site: http://www.teamwork.nl

Prado M.; *Archimedes Wave Swing*; in 'Ocean Wave Energy, current state and future perspectives', Springer, 2008. [18]

A general description of the device, with a wide range of numeric data concerning a full-scale prototype installed in Portugal.

Wave Dragon

Pelamis

Pico OWC

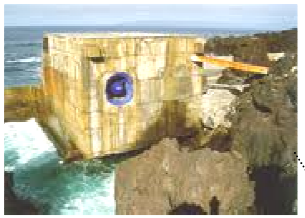

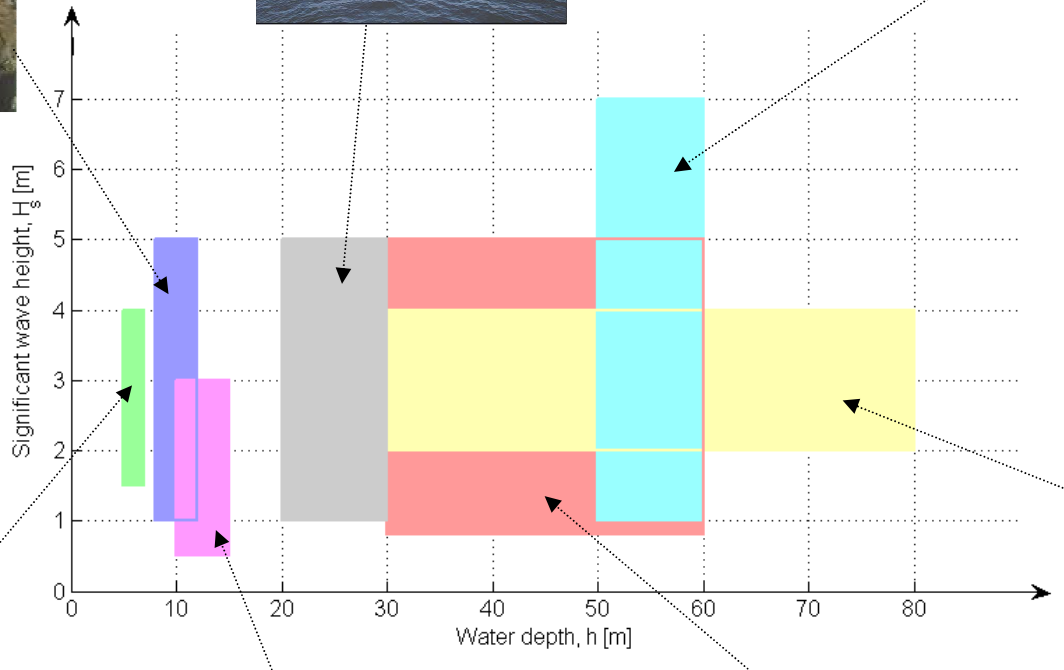

Limpet OWC

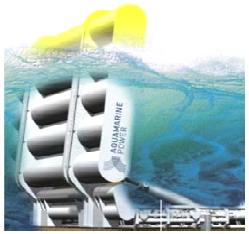

Oyster

Archimede's Wave Swing

IPS buoy

Pico OWC plant

Web site: http://www.pico-owc.net/

Brito-Melo A., Neumann F., Sarmento A.; *Full-scale Data Assessment in OWC Pico Plant*; International Journal of Offshore and Polar Engineering (ISSN 1053-5381), Vol. 18, No. 1, pp. 27–34, 2008. [44]

This article presents an overview of the Pico plant and reports a wide range of data from on-site measurements.

Le Crom I., Cabrera Bermejo H., Pecher A., Brito Azevedo E., Reis F. V.; *Incident wave climate at the OWC Pico plant: Validation of a feed-forward based propagation method (ANN) and a numerical simulation (SWAN) with measured data*; Proceedings of the 9th European Wave and Tidal Energy Conference (EWTEC 2011), Southampton, UK, 05-09 September 2011. [45]

An interesting study about the wave climate of the Pico site, useful to understand the real operative conditions of the plant.

Limpet OWC plant

Boake C., Trevor J., Whittaker T., Folley M.; *Overview and Initial Operational Experience of the LIMPET Wave Energy Plant*; Proceedings of The 12th International Offshore and Polar Engineering Conference; Kitakyushu, Japan, 2002. [46]

A complete overview on the design of the Limpet 500, focused in particular on the power and control equipment of the plant.

Pelamis

Web site: http://www.pelamiswave.com

Cruz J., Henderson R., Yemm R.; *Pelamis*; in 'Ocean Wave Energy, current state and future perspectives', Springer, 2008. [18]

This article focuses on the aspects of manufacturing and assembly of the units and reports result and measurements from the full-scale prototype in Orkney.

Retzler, C. H.; Pizer, D. J.; *The hydrodynamics of the PELAMIS wave energy device: experimental and numerical results*; Proceedings of OMAE'01 20th International Conference on Offshore Mechanics and Arctic Engineering, 2001. [47]

A technical article focused on the hydrodynamic study (theoretical and experimental) of the Pelamis.

Oyster

Web site: http://www.aquamarinepower.com/

Henry A., Doherty K., Cameron L., Whittaker T., Doherty R.; *Advances in the Design of Oyster Wave Energy Convetrter*; In RINA Marine and Offshore Renewable Energy. London, UK., 2010. [36]

Collier D., Whittaker T., Crowley M.; *The Construction of Oyster – A Nearshore Surging Wave Energy Converter*; Aquamarine Power, 2008. [48]

Whittaker T., Collier D., Folley M., Osterried M., Henry A., & Crowley M.; *The development of Oyster–A shallow water surging wave energy converter*; Proceedings of the 7th European Wave and Tidal Energy Conference, Porto, Portugal, 2007. [35]

Cameron, L., Doherty, R., Henry, A., Doherty, K., Hoff, J. V., Kaye, D., Whittaker, T.; *Design of the next generation of the Oyster wave energy converter*; Proceedings of the 3rd international conference on ocean energy (Vol. 6), 2010. [49]

This series of articles is written by the members of the Aquamarine Power std. (the company that developed the Oyster) and by the Queen's University Belfast staff. This works provide a quite complete overview on the operation principle, the assembly process and the working conditions of the Oyster. The articles are quite generic and descriptive, and many details within the design and the operation of the devices remain silenced.

Wave Dragon

Web site: http://www.wavedragon.net

Parmeggiani S., Kofoed J. P., Friis-Madsen, E.; *Experimental Update of the Overtopping Model Used for the Wave Dragon Wave Energy Converter*; Energies, 6(4), 1961-1992; 2013. [39]

This article presents an overview on the Wave Dragon device, introduces a classical semi-empiric model for the study of overtopping devices and applies the results from experiments on a scale model to generate a tailor-made model based on correlations that are specifically valid for the Wave Dragon.

1-2.4 Traditional Power Take-Off Systems

In this section, a review of traditional PTO systems for WECs is presented. Some significant examples are here described. Wider descriptions of PTO systems are presented by Cruz [18] and Falcão [15].

1-2.4.1 Air turbines for OWC

Two types of air turbines are generally associated to the idea of OWC prototypes: the Well's turbine and the Impulse turbine.

Generally speaking, the key design parameter to be considered in terms of the impact on the turbine performance is the speed, which operationally will be determined by the required torque/speed characteristic and the generator power rating [18].

Two matching principles have to be followed when designing a turbine for an OWC system:

- The turbine must provide a damping effect (that, among other, limits the air flow exiting the system) that maximizes the conversion from wave energy to air flow kinetic energy.
- The turbine must also maximize the conversion from air kinetic energy to mechanical energy (transferred to the generator) over the range of effective flow rates. Notice that, in any case, this conversion is upper bounded by the Betz limit (no more than 16/27 of the kinetic energy of air can be converted to mechanical energy for the generator).

Wells Turbine

The Wells turbine was invented during the seventies by Allan Wells of Queen's University Belfast. It is a self-rectifying air turbine, that means that its torque is not sensitive to the air flow direction. This is an essential feature since the operating principle of OWC provokes air moving in a certain direction while the water level in the column is raising, and in the opposite direction when the water level drops. Several versions have been studied: single rotor with or without guide vanes (used in Pico prototype), twin rotors in series, two counter-rotating rotors (like in LIMPET). The Wells turbine is the most frequently proposed PTO for OWC systems [15].

The turbine is based on a symmetric airfoil; the operating principle of the turbine is shown in Figure 1-38.

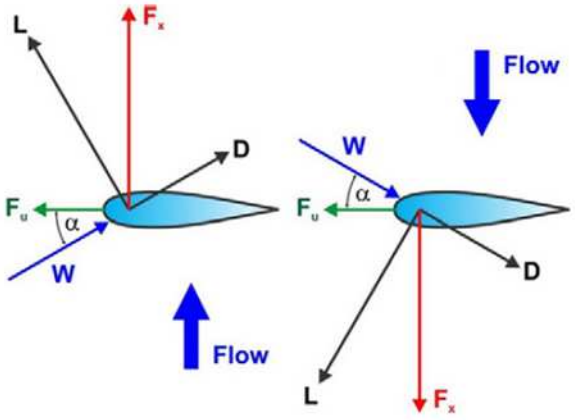

Figure 1-38 - Wells turbine operating principle

Impulse Turbine

The most popular alternative to the Wells turbine seems to be the self-rectifying impulse turbine. It has a rotor that is identical to the one of a conventional single-stage steam turbine (with symmetric blades). Since the turbine is required to be self-rectifying, instead of a single row of guide vanes there are two specular rows, one at each side of the rotor [43].

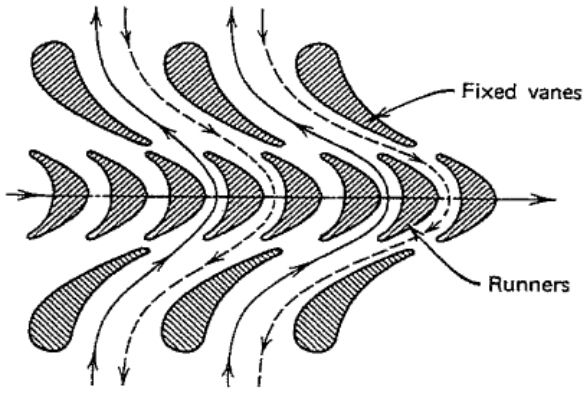

Figure 1-39 - Impulse turbine blades

.

1-2.4.2 Hydraulic systems

Hydraulic systems are generally based on an oil high-pressure circuit, that usually includes a gas accumulator system (with time energy storage capacity of few wave periods) with the aim of smoothing the power output of the connected WEC, making it as constant as possible [15].
Other components are

- An hydraulic cylinder or ram with the aim of converting the mechanical energy acquired by the WEC to hydraulic potential energy
- A fast hydraulic motor used to run an electric generator. Usually, in Wave Energy Conversion, axial-piston bent-axis variable-displacement motors are adopted: these machines are available from manufacturers in a rated power range between few kW from 1 MW, with operating oil pressure up to 350 bar [15].

The schematic of a typical hydraulic circuit for the extraction of energy from a heaving WEC is shown in Figure 1-40.
Notice that, in the example of the figure, in order to guarantee a better smoothing effect for the produced power, gas accumulators upstream and downstream the motor have been decoupled.
Beyond the well known criticalities carried around by a hydraulic circuits (high number of components, heaviness, sensitivity to damages), these systems are probably the most suited to handle relevant forces like those acting on the WECs. The net force generated by an oil circuit with a typical pressure of 350 bar is at least one order of magnitude higher than those allowed by an electrical machine [18].
For this reason, high-pressure oil circuits have been tested as PTO system both in translational heaving WECs (mainly buoys) and rotational devices (like Pelamis or Oyster).

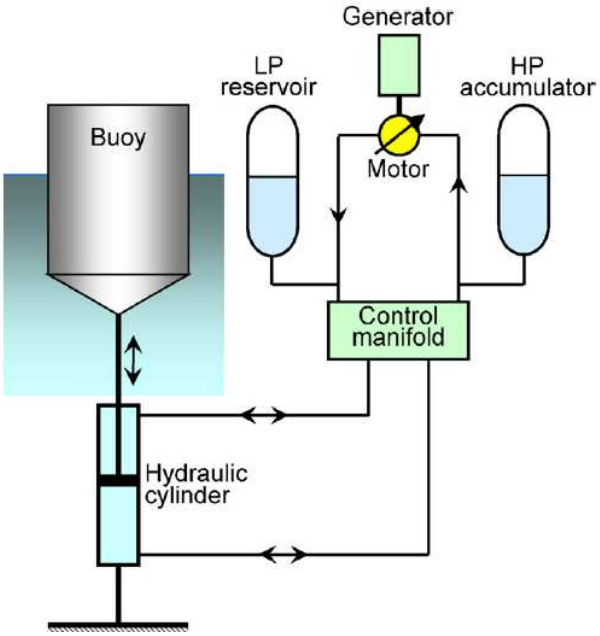

Figure 1-40 - Hydraulic PTO of a heaving WEC

1-2.4.3 Linear Generators

The use of linear electric generators may represent an advantage for application that involve linear or reciprocating motion since they bring a simplification in the design and in the mechanical interface (gears and shafts).

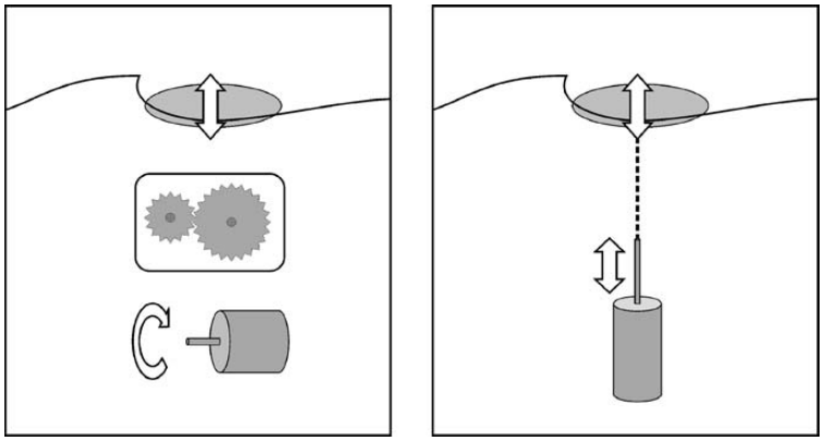

Figure 1-41 - Comparison between rotary and linear generator

In Figure 1-41 a comparison is shown between the operation of a rotary generator (on the left) and a linear generator (right) coupled with a heaving WEC: to convert the slow reciprocal motion of the ocean wave into a fast rotating motion, required by conventional high speed rotating generators, some kind of intermediate conversion step is necessary, that has to be provided by gears or shafts.

A low speed linear generator can be directly connected to the heaving WEC and no intermediate system is needed [18].

A linear generator consists of a moving part (translator), on which magnets are mounted with alternating polarity. The translator plays the same role of the rotor in rotating generators. It moves linearly next to a stationary stator that contains windings of conductors, the armature windings.

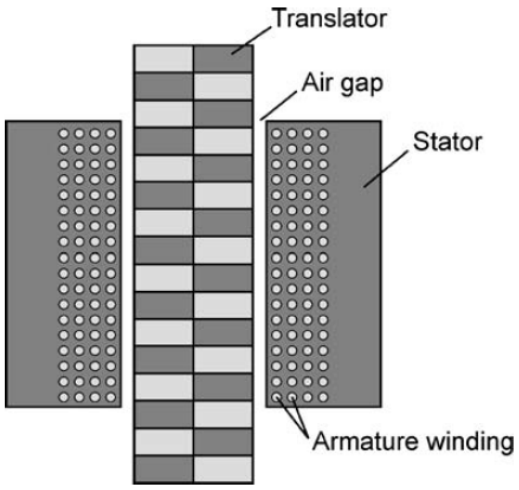

Figure 1-42 - Operating principle of linear generator

An air gap is present between the translator and the stator. The translation of the moving part generates time dependent variations in the magnetic field that induce a voltage in the windings.

In wave energy applications the translator reciprocating motion matches the motion of the actual device, at speeds two orders of magnitude lower than the typical velocities of rotary generators. At such low speed, the forces are very large, which requires a physically large machine.

The advantages in terms of simplicity of this technology with respect to the rotary generators is partly counterbalanced by the large number of engineering requirements on the generator [15].

1-2.5 WECs modeling: general procedure

Beyond the simple models presented in the previous paragraphs, a general procedure can be identified to model almost all of the WECs (different from overtopping devices), based on the linear wave theory.

A complete and deepened description of the methodology is presented by Alves [17], in a recent PhD thesis work.

One of the milestones of the methodology lies in the following consideration: a body moving in a wavy sea is subjected to the effect of the external waves (described by the linear theory) that induce on it forces and moments. At the same time, it is a source of ulterior waves that are generated as a result of the body motion itself. Thus, the coupled hydrodynamics of the problem (external wind-generated waves plus body-motion generated waves) presents a certain complexity. The base fundamental assumption of the linear theory is that the hydrodynamics can be decomposed into two separate problems that are then summed using the principle of linear superimposition.

Under the assumption of linearity, it is possible to consider the resultant wave as a superposition of an incident wave, a diffracted wave and a radiated wave. The incident wave is a propagating wave in the absence of the body. The diffracted wave results from the interaction between the incident wave and the body when it is fixed. Finally, the radiation wave results from the body motions in the absence of incident waves.

In other words, indicating with φ the velocity potential representing the whole hydrodynamics of the problem (motion of a WEC in a wavy sea), φ can be written as

$$\varphi = \varphi_D + \varphi_r$$

in which $\varphi_r$is the radiation potential and φ_D is given by

$$\varphi_D = \varphi_0 + \varphi_d$$

being φ_0 and φ_d the incident and diffracted (scattered) potential respectively. All these potentials need to satisfy the Laplace equation in the fluid domain and the free surface and ocean bottom boundary conditions.

We remember that the potential theory (under the hypotheses of which a velocity potential can be defined) is valid for inviscid incompressible flows. This represent quite a strong assumption for WECs, anyway, a complete modeling, that also keeps into account turbulence and viscous effects by the mean of CFD simulation would be exceedingly complicated (since also with the linear theory assumption the problem is numerically time-consuming) and would be of poor handling for the purpose of designing WEC devices.

The problem of a WEC motion is faced by simply applying the second Newton's law: the entire force must be decomposed into hydrodynamic and external sources. The hydrodynamic source comprises the excitation force, inflicted by the incident waves assuming that the body is fixed, the buoyancy force, which comes out due to the submergence variation caused by the oscillatory motions under hydrostatic pressure distribution, and the radiation force, related to the pressure, over the submerged surface, impinged by the fluid displaced due to the device oscillations. Moreover, the device motion might also be constrained by external forces induced by the PTO equipment and the mooring system.

A schematic representation of the chain of interactions is shown in Figure 1-43; the scheme is also the base and sketch for any simulation carried out in computational environments like Simulink.

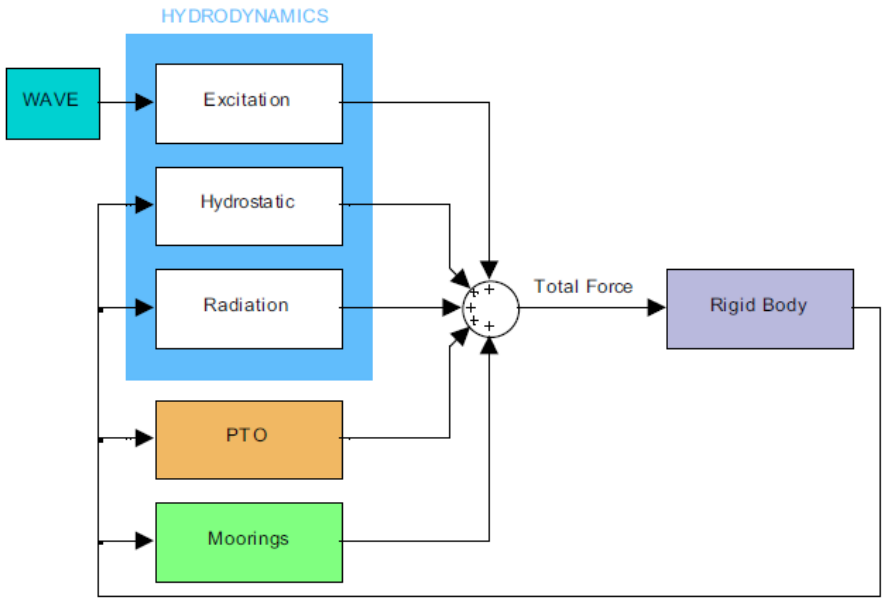

Figure 1-43 - Generic WEC model

In case of low amplitude waves and device oscillations the hydrodynamic of the problem can be described by mean of an entirely linear approach: this requires, in addition to the exploitation of the linear wave theory and of the described superimposition principle, the linearization of the PTO and eventual mooring systems behavior and of the buoyancy of the body constituting the WEC. Under this hypothesis, the analysis is usually carried out in the frequency domain. As a result, all the physical quantities vary sinusoidally with time, according to the frequency of the incident wave. Hence, under these circumstances, the

motion equations become a linear system, that might be solved by means of different approaches.

In many practical cases, anyway, the WEC dynamics has some parts which are strongly non-linear. Therefore, the superposition principle is no longer applicable. Non-linearity is mostly due to the mooring system, to the buoyancy behavior of the converter (for example in the case of high-amplitude oscillations) or to the PTO system. This is also the case of the problem studied in the present thesis, where Dielectric Elastomer PTO systems (which are intrinsically non-linear) are applied to WECs.

For this reason, a correct analysis of the non-linear components of the problem has to be done in the time domain.

One particular difficulty in conducting the time domain analysis is the computation of the radiation effect, as it includes a convolution between the velocity and an impulse response function. Nevertheless, a convenient technique to treat this problem is the state-space method: it is possible to demonstrate that the convolution integral of the radiation hydrodynamic interaction can be well represented by a small number of first order linear constant coefficient differential equations. More details are provided in the following and in the reference work [17].

Finally, a partially non-linear approach is possible, assuming as valid the linear decomposition of the complete problem in a diffraction and radiation problem, but treating the buoyancy and the PTO induced forces as non-linear terms, while keeping the scattering and radiation forces as linear.

1-2.5.1 Problem formalization

We derive here the generic equation of motion of a WEC with *n* degrees of freedom (DoF).

Generally speaking, the equation of motion for a generic PTO is written as

$$\boldsymbol{M}\ddot{\boldsymbol{\xi}}(t) = \boldsymbol{F}_{pe}(t) + \boldsymbol{F}_{PTO}(t) + \boldsymbol{F}_{f}(t) + \boldsymbol{F}_{m}(t)$$

where bold letters denote matrices and vectors .

$\boldsymbol{M}$ is the inertia matrix, $\boldsymbol{\xi}$ is the displacement vector and $\boldsymbol{F_i}$ represent the generic *i*-th force vector. In particular,

- $\boldsymbol{F}_{pe}$ is the external pressure forces vector
- $\boldsymbol{F}_{PTO}$ is the vector of the loads due to the PTO
- $\boldsymbol{F}_{f}$ is the friction force vector
- $\boldsymbol{F}_{m}$ is the mooring-force vector. We do not examine here this term, since it is not of interest for the case-study described in the following chapters.

Notice that, beyond the mathematic symbols, the vectors $\boldsymbol{F_i}$ are made of elements that do not have necessarily the dimensions of forces, but can also be torques (when $\boldsymbol{\xi}$ can represent an angular displacement). At the same way, $\boldsymbol{M}$ is a matrix of masses and/or moments of inertia depending on the corresponding DoF.

In particular, considering the most generic case with 6 DoF (displacement in *x*, *y*, *z* direction and rotation about the same axes), the inertia matrix takes the form

$$M = \begin{bmatrix} m & 0 & 0 & 0 & mz_g & -my_g \\ 0 & m & 0 & -mz_g & 0 & mx_g \\ 0 & 0 & m & my_g & -mx_g & 0 \\ 0 & -mz_g & my_g & I_{11} & I_{12} & I_{13} \\ mz_g & 0 & -mx_g & I_{21} & I_{22} & I_{23} \\ -my_g & mx_g & 0 & I_{31} & I_{32} & I_{33} \end{bmatrix}$$

where m is the mass of the body, (x_g, y_g, z_g) are the coordinates of the center of mass and I_{ij} are the moments of inertia.

In the hypothesis of fully-linear theory, the vector $\boldsymbol{\xi}$ is written as

$$\boldsymbol{\xi}(t) = Re\{\hat{\boldsymbol{\xi}}(\omega)\mathrm{e}^{i\omega t}\}$$

Thus, in a frequency-domain analysis, attention is focused on the quantity $\hat{\boldsymbol{\xi}}(\omega)$.

The forces acting on the body can be generally written in the forms presented below:

External pressure force $\boldsymbol{F}_{pe}$: it can be split into two terms, one concerning static pressure force, the other concerning dynamic pressure force.

$$\boldsymbol{F}_{pe} = \boldsymbol{F}_{hs} + \boldsymbol{F}_{hd}$$

$\boldsymbol{F}_{hs}$ represents the vector of hydrostatic restoring loads due to gravity and buoyancy. In general, this is a non-linear term (especially in presence of large oscillations). In the entirely linear approach, however, this term is simplified and written in the form

$$\boldsymbol{F}_{hs} = -\boldsymbol{G}\boldsymbol{\xi}$$

where $\boldsymbol{G}$ is a symmetric matrix. Details on the calculation of the coefficients G_{ij} are present in the reference [17].

Of course, passing to the frequency domain, the previous expression takes the form

$$\hat{\boldsymbol{F}}_{hs} = -\boldsymbol{G}\hat{\boldsymbol{\xi}}$$

In general, the quantities with the caret are the images in the frequency domain of the corresponding quantities in time domain.

The dynamic term has the form

$$\boldsymbol{F}_{hd} = \rho \int \frac{\partial \varphi}{\partial t}\mathbf{n}\, dS_b$$

where S_b is the total wet surface of the body and $\mathbf{n} = (n_1, \dots, n_k)$ is the unit vector normal to the body surface (in a generic point), with k number of DoF.

We remember that

$$\varphi = \mathrm{Re}\{(\hat{\varphi}_0 + \hat{\varphi}_d + \hat{\varphi}_r)\mathrm{e}^{i\omega t}\}$$

and the radiation term is $\hat{\varphi}_r = i\omega\boldsymbol{\varphi}^T\hat{\boldsymbol{\xi}}$, where $\boldsymbol{\varphi}^T$is the transposed vector of complex radiation potentials due to the body oscillations with unitary velocity amplitude.

Then (in the frequency domain)

$$\widehat{\boldsymbol{F}}_{hd} = i\omega\rho \int (\hat{\varphi}_0 + \hat{\varphi}_d)\mathbf{n}\, dS_b - \omega^2\rho \int \boldsymbol{\varphi}\hat{\boldsymbol{\xi}}\mathbf{n}\, dS_b$$

where the first term corresponds to the excitation force vector

$$\widehat{\boldsymbol{F}}_e = i\omega\rho \int (\hat{\varphi}_0 + \hat{\varphi}_d)\mathbf{n}\, dS_b$$

This term is usually calculated by a 3D Boundary Element Method (BEM) software, like WAMIT.

BEM is a numerical computational method for the solution of linear integral differential equations. The BEM makes use of the given boundary conditions to fit boundary values into the integral equation, rather than values throughout the space domain of the differential equation. Once this is done, the integral equation is used again to calculate the numerical solution at any desired point in the interior of the solution domain.

WAMIT is a BEM radiation/diffraction panel program developed for the linear analysis of the interaction of surface waves with various types of floating and submerged structures [50]. The software bases on the assumption that the flow is ideal and time harmonic; the free surface condition, in last version (V7), is a second order condition.

The second term in the expression of $\widehat{\boldsymbol{F}}_{hd}$ is the vector of complex amplitudes of the radiation force

$$\widehat{\boldsymbol{F}}_r = -\omega^2\rho\hat{\boldsymbol{\xi}} \int \boldsymbol{\varphi}\mathbf{n}\, dS_b$$

that is further written in the form

$$\widehat{\boldsymbol{F}}_r = -i\omega\boldsymbol{Z}\hat{\boldsymbol{\xi}}$$

Where $\boldsymbol{Z} = -i\omega\rho \int \boldsymbol{\varphi}\mathbf{n}\, dS_b = \boldsymbol{B} + i\omega\boldsymbol{A}$ with $\boldsymbol{A}$ and $\boldsymbol{B}$ symmetrical matrices of real numbers.

$$\widehat{\boldsymbol{F}}_r = -i\omega\boldsymbol{B}\hat{\boldsymbol{\xi}} + \omega^2\boldsymbol{A}\hat{\boldsymbol{\xi}}$$

and $\boldsymbol{A}$ and $\boldsymbol{B}$ represent respectively the matrices of added mass and damping coefficients.

The added mass coefficients include a frequency dependent term plus a positive constant component that represents the added inertia at infinite frequency (when there are no waves radiated), i.e. $\boldsymbol{A}_\infty = \lim_{\boldsymbol{\omega}\to\infty} \boldsymbol{A}$.

The damping and added mass matrices, as well as the limiting added mass matrix at infinite frequency, may be straightforward computed with a 3D BEM numerical code.

In conclusion, the $\boldsymbol{F}_{pe}$ term becomes

$$\widehat{\boldsymbol{F}}_{pe} = \widehat{\boldsymbol{F}}_e - \boldsymbol{G}\hat{\boldsymbol{\xi}} - i\omega\boldsymbol{B}\hat{\boldsymbol{\xi}} + \omega^2\boldsymbol{A}\hat{\boldsymbol{\xi}}$$

PTO induced load $\boldsymbol{F}_{PTO}$: In general, this load is non-linear due to the operation of the PTO (and of its complex control strategy). Under the hypothesis of regular waves, a linear form can be used for simplification purposes:

$$\boldsymbol{F}_{PTO} = -\boldsymbol{K}_{PTO}\boldsymbol{\xi} - \boldsymbol{B}_{PTO}\dot{\boldsymbol{\xi}}$$

with $\boldsymbol{K}_{PTO}$ and $\boldsymbol{B}_{PTO}$ matrices of mechanical spring and damping coefficients respectively.

Of course, in the frequency domain

$$\widehat{\boldsymbol{F}}_{PTO} = -\boldsymbol{K}_{PTO}\hat{\boldsymbol{\xi}} - i\omega\boldsymbol{B}_{PTO}\hat{\boldsymbol{\xi}}$$

For what concerns the energy absorption, due to the PTO, it is only the mechanical damper of the PTO that contributes to the power absorption, as the term related with the spring effect is a reactive term, and so, its average value over a wave period is zero.

Assuming for simplicity one DoF (B_{PTO} is 1x1 matrix),

$$P_{dev} = \frac{1}{T}\int_0^T B_{PTO}\dot{\xi}^2 dt = \frac{B_{PTO}}{T}\int_0^T \left[\mathrm{Re}\left(i\omega\hat{\xi}\mathrm{e}^{i\omega t}\right)\right]^2 dt = \frac{1}{2}\omega^2 B_{PTO}\left|\hat{\xi}\right|^2$$

It could be demonstrated in a general way (Alves) that the optimal choice for the mechanical spring is such that the device is resonating. So, for example, for the heave mode

$$-\omega^2(m_3 + A_{33}) + G_{33} + K_{PTO} = 0$$

Notice that the resonance condition does not depend on the mechanical damping.

It can be also shown that the optimality for the mechanical damping is reached when the mechanical damping equals the hydrodynamic damping, thus (for pure heave)

$$B_{PTO,33} = B_{33}$$

Basically, this condition highlights the principle, apparently paradoxical, which sets that to absorb energy from the incident waves it is necessary to generate waves, too.

Friction force $\boldsymbol{F}_f$: it is often described by a quadratic dependence on the velocity (that will be deepened in the following), in the form

$$\boldsymbol{F}_f = -\boldsymbol{B}_{f,q}\left|\dot{\boldsymbol{\xi}}\right|\dot{\boldsymbol{\xi}}$$

but, in a linearized form, it is

$$\boldsymbol{F}_f = -\boldsymbol{B}_f\dot{\boldsymbol{\xi}}$$

then, in the frequency domain,

$$\widehat{\boldsymbol{F}}_f = -i\omega\boldsymbol{B}_f\hat{\boldsymbol{\xi}}$$

1-2.5.2 Frequency domain analysis

The mathematical formalisms behind the entirely linear formalization of the WEC motion and, thus, to its description in the domain of frequency, has been briefly summarized in the previous paragraph.

A frequency domain model solves, essentially, the linear system of motion equations described above.

As anticipated, the application of a 3D radiation-diffraction model is generally necessary.

The model computes the complex amplitudes of the hydrodynamic forces (excitation, radiation) and the hydrostatic force by means of the WAMIT outcome. Therefore, after identifying the hydrodynamic forces, it is straightforward to simulate the device free floating motions.

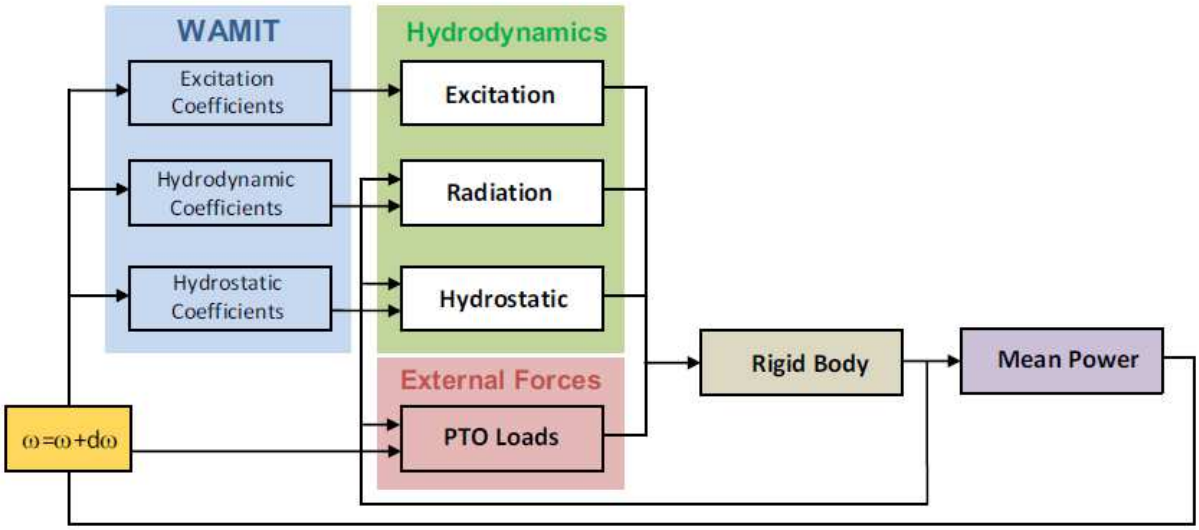

Figure 1-44 – Schematic example of frequency domain model implementation. Friction and mooring are neglected

In the scheme of Figure 1-44, the only external force taken into account is that of the PTO. Notice that the PTO features have to be tuned in order to achieve resonance and maximum power output condition. The block-diagram model sketched in Figure 1-44 is suited to be applied in a block-diagram environment such as Simulink.

1-2.5.3 Time domain analysis

When non-linearities are present or, anyway, the linearization of the problem would bring to excessive deviations with respect to the real behavior, frequency domain analysis is not practicable, and a time dependent approach is necessary.

The main difficulty of operating in the time domain lies in the representation of the radiation force. A convenient technique to characterize that force in time domain is the state-space method, which consists of representing the convolution integral of the radiation hydrodynamic interaction by a small number of first order differential equations with constant coefficients.

As explained above, and under the hypothesis of single-degree of freedom WEC, the equation of motion for the PTO in time domain is

$$M\ddot{\xi}(t) = F_{pe}(t) + F_{PTO}(t) + F_f(t) + F_m(t)$$

As already mentioned, the pressure induced term F_{pe} is written as

$$F_{pe}(t) = F_e(t) + F_r(t) + F_{hs}(t)$$

When operating in time domain, even in presence on non-linearity in the PTO or buoyancy, anyway, the linear theory can be used for incident and radiated waves. Under the linear wave approximation, the radiation force (for one-degree of freedom bodies) can be rearranged:

$$\hat{F}_r(\omega) = -\left[B(\omega) + i\omega\left(A_\infty + A(\omega)\right)\right]i\omega\hat{\xi} = \omega^2 A_\infty\hat{\xi} - [B(\omega) + i\omega A(\omega)]i\omega\hat{\xi}$$

Introducing, in the frequency domain, the so-called radiation impedance' $\widehat{K}$ [51] the radiation force is compactly written as

$$\hat{F}_r(\omega) = \omega^2 A_\infty \hat{\xi} - \hat{K}(\omega) i\omega \hat{\xi}$$

thus, passing to the time domain:

$$F_r(t) = A_\infty \ddot{\xi}(t) - \int_0^t K(t-\tau)\dot{\xi}(\tau)d\tau$$

where the first term is an inertial force, and A_∞ is the infinite-frequency added inertia; the second integral term is the convolution between the velocity and the radiation impulse response function $K(t)$, which represents the fluid memory effect and is therefore also called 'memory function'.

Practically, assuming the system to be casual and time invariant, the convolution integral can be approximated by a state-space model. The result only is here presented.

$$y = \int_0^t K(t-\tau)\dot{\xi}(\tau)d\tau \cong \begin{matrix} \dot{x} = Ax + B\dot{\xi} \\ y = Cx \end{matrix}$$

This method has the benefit of summarizing in the state vector, x, all the past information of the system at any time instant.

Notice that, if the system is described by a state vector with dimension *n*, being $\dot{\xi}$ at a given time a scalar, *B* is a *n x 1* vector, *A* is a *n x n* matrix and *C* is a *1 x n* matrix.

With this assumption, the solution of the WEC motion in the time domain must be forerun by the identification of *A, B* and *C*, that can be carried out both in frequency or time domain, by means of the use of the WAMIT software (details discussed in [17]).

Once these parameters has been determined, the problem follows the same conceptual scheme of the frequency-domain.

We remember that, if the non-linearity is due to the PTO system or to the buoyancy load only, the external wave induced force and the radiated wave force can be calculated using WAMIT, and implementing separately (i.e. in Simulink) non linear blocks modeling the PTO and the buoyancy force.

Of course, in any time-dependent analysis, a numerical solver of differential equations is required (i.e. the ode45 tool of Matlab).

1-2.5.4 Application of the methodology to the design problem

The design procedure for any type of WEC must be carried out considering some relevant factors:

- The nominal sea conditions (in terms of wave height and period)
- The desired power output at nominal condition
- The operational performances of the device off the nominal conditions
- The environmental boundary conditions (water depth, distance from the shoreline, visual impact etc.)

In general, the design must be carried out with the aim of maximizing the estimated average yearly energy productivity.

The methodology used to estimate the energy productivity of a certain WEC over a given period is proven and diffusely described in literature. A conceptual scheme is presented by Murray [52], and sketched in Figure 1-45.

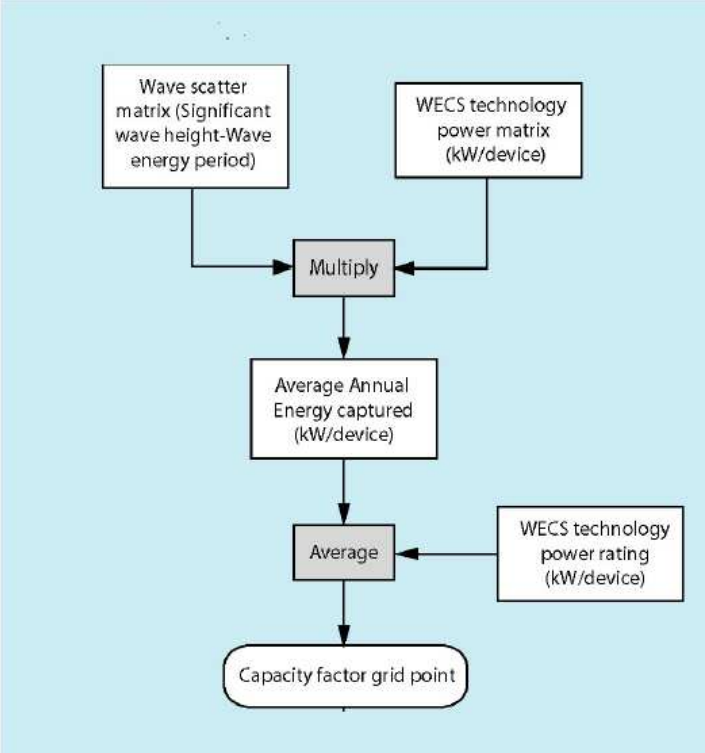

Figure 1-45 - Captured energy and capacity factor assessment

The assessment of the energy productivity requires data about the wave climate of the reference installation location to be available. Thus, a 'wave scatter matrix' must be built: this matrix report the occurrence frequency (or, alternatively, the hours of occurrence over a one-year period) of a certain sea-state, identified, in a specific location (with known average water depth) by a couple of values: significant wave height and wave period.

From the WEC point of view, the behavior of the device has to be predicted for each of the reference sea-states. In other words, the power output of the converter has to be predicted for each of the sea states identified by the points of the wave scatter matrix. This brings to the construction of the so called 'power matrix' of the device, a table that, for any sea-state (period vs. wave height) provides the mean power output of the device. In order to build such a matrix, mathematical models such the one outlined above may be used, or experimental investigations can be carried out.

Once the wave scatter matrix and the power matrix are given, the calculation of the energy productivity over a time horizon is immediate.

Indeed, indicating with the subscripts *ij* the generic sea-state (identified by the *i*-th value of wave height and *j*-th value of time period), the power matrix has generic element P_{ij} (power [kW] in the sea-state *ij*), the scatter matrix has generic element f_{ij} (with *f* indicating the frequency, or probability of the corresponding sea-state).

Significant wave height (H_{sig}, m) \ Power period (T_{pow}, s)	5.0	5.5	6.0	6.5	7.0	7.5	8.0	8.5	9.0	9.5	10.0	10.5	11.0	11.5	12.0	12.5	13.0
0.5	idle	idle	idle	idle	idle	idle	idle	idle	idle	idle	idle	idle	idle	idle	idle	idle	idle
1.0	idle	22	29	34	37	38	38	37	35	32	29	26	23	21	idle	idle	idle
1.5	32	50	65	76	83	86	86	83	78	72	65	59	53	47	42	37	33
2.0	57	88	115	136	148	153	152	147	138	127	116	104	93	83	74	66	59
2.5	89	138	180	212	231	238	238	230	216	199	181	163	146	130	116	103	92
3.0	129	198	260	305	332	340	332	315	292	266	240	219	210	188	167	149	132
3.5	-	270	354	415	438	440	424	404	377	362	326	292	260	230	215	202	180
4.0	-	-	462	502	540	546	530	499	475	429	384	366	339	301	267	237	213
4.5	-	-	544	635	642	648	628	590	562	528	473	432	382	356	338	300	266
5.0	-	-	-	739	726	731	707	687	670	607	557	521	472	417	369	348	328
5.5	-	-	-	750	750	750	750	750	737	667	658	586	530	496	446	395	355
6.0	-	-	-	-	750	750	750	750	750	750	711	633	619	558	512	470	415
6.5	-	-	-	-	750	750	750	750	750	750	750	743	658	621	579	512	481
7.0	-	-	-	-	-	750	750	750	750	750	750	750	750	676	613	584	525
7.5	-	-	-	-	-	-	750	750	750	750	750	750	750	750	686	622	593
8.0	-	-	-	-	-	-	-	750	750	750	750	750	750	750	750	690	625

Figure 1-46 - The Pelamis power matrix

Choosing any reference time period t_{ref} [h] (i.e. 8760 hours if referring to a full-length year), the assessed energy productivity amounts to

$$En = f_{ij} P_{ij} t_{ref} \qquad \text{[kWh]}$$

An interesting parameter than can be calculated is the so called loading factor (or capacity factor), that is the ratio between the mean assessed power output and the device power rating P_{nom}:

$$LF = \frac{f_{ij} P_{ij}}{P_{nom}}$$

One of the objective of the design of a WEC may be identified in the maximization of the energy productivity En.

Once the design parameters (PTO, geometry etc.) have been fixed, the general analysis described in the previous paragraphs can be applied, in order to build the power matrix that allows the assessment of the energy productivity of the device.

An example of numerical application of the presented method with the aim of assessing the productivity of a number of WECs is presented by Babarit [19].

Chapter 2

Dielectric Elastomer Generators

2-1 Overview on Dielectric Elastomers

2-1.1 Introduction

Dielectric Elastomers (DEs) are polymeric materials which can experiment deformations over 500% of their length under the effect of a mechanical load; due to their mechanical compliance and to their non-conductive electric behavior they are exploited as transducers, meaning that they operate as devices that convert energy form one form to another [53].

DEs use a reversible transduction mechanism, therefore, they can both convert electrical energy to mechanical energy (actuator configuration) or, vice versa, mechanical energy to electrical energy (generator configuration): the present study concentrates on this second possibility and takes in exam a particular configuration of DE generator (DEG).

Anyway, an overview on the general functional principle of these materials and on their typical applications is opportune.

The main commercial elastomers are acrylics, silicones and natural rubber: they are usually shaped in thin membranes (films) and distributed in rolls, for usages that can also be different from transduction purposes (i.e. acrylics are often used as adhesive materials).

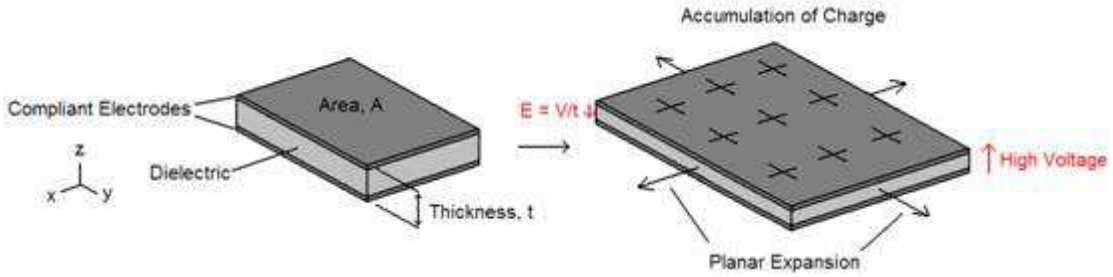

Figure 2-1 - DEs functional principle

Let refer to Figure 2-1: on the right, a membrane of elastomer in the undeformed configuration is shown (light grey film), sandwiched between two compliant conductive electrodes (dark films covering the elastomer, usually made by conductive grease).

If a total charge $+Q$ is deposited on one of the electrodes and an opposite charge $-Q$ is put on the other electrode (or, as an alternative, a voltage V is applied between the electrodes), the mutual interaction among the charges induce an electrostatic pressure p (in z direction) that

causes the material to squeeze in thickness (*z* direction) and stretch in length [54]. This behavior is known as "electrostriction" and is usually distinguished from piezoelectricity since the response is proportional to the square of the applied electric field (as shown in the following), while in piezoelectric materials it results proportional to the field.

Notice that the device obtained by coating the DE with the electrodes is, to all effects, a deformable capacitor. The described mechanical response to an electric charging is the starting principle for all the future considerations about the physics of DEs. Since DEs react to a voltage with a significant stretch (where 'significant' means of the same order of magnitude of the initial dimensions of the sample, due to the extremely compliant nature of the polymers), they are often referred to as "artificial muscles" [53]: the analogy lies in the fact that, like muscles, they change in length in response to input stimulus.

Although the principle shown in Figure 2-1 is quite simple, an appropriate modeling is important in order to both choose the best material for a certain application and to design practical devices.

A way to express the effective electrostatic pressure (acting in z direction) is reported by Pelrine [54] and by Carpi [53].

If *U* is the electrostatic energy of the system of charges, the induced pressure *p* can be written as

$$p = \frac{1}{A}\frac{dU}{dz}$$

where *A* is the area of the membrane corresponding to the thickness *z*.

A very common constraint when considering this type of material is the hypothesis of incompressibility [55]: the material volume is assumed constant and, thus

$$A \cdot z = const.$$

Assuming that a fixed charge *Q* is deposited on the electrodes (+*Q* on one electrode, -*Q* on the other), the stored electrostatic energy results in

$$U = \frac{1}{2}\frac{Q^2}{C} = \frac{1}{2}\frac{Q^2 z}{\varepsilon A}$$

where ε is the dielectric constant of the material, given by the product of the dielectric constant in vacuum ($\varepsilon_0 = 8.85 \cdot 10^{-12}\ F/m$) and of the relative dielectric constant: $\varepsilon = \varepsilon_0 \varepsilon_r$.

Differentiating the equation for *U* the result is

$$dU = (0.5Q^2/\varepsilon A)dz - (0.5Q^2 z/\varepsilon A)\, dA/A$$

but, from the incompressibility constraint, $dA/A = -dz/z$, so $dU = (Q^2/\varepsilon A)dz$

and $p = Q^2/\varepsilon A^2$.

In a generic condenser, the electric field (assumed homogeneous between the electrodes) is calculated as

$$E = \frac{Q}{\varepsilon A}$$

then, the final expression for the induced electrostatic pressure is

$$p = \varepsilon E^2$$

Notice that this is twice the pressure in a common plate capacitor: the difference is explained considering the presence of the term with *-dA* in the expression of *dU*; in fact, differently from a rigid capacitor, the effect of an increase in the area of the capacitor spreads the charges reducing the electrostatic potential of the system, while a reduction of the charges brings an increase in *U* due to the major vicinity of the charges.

Basing on this general considerations, a proper description of the different applications of the DEs can be done [53].

2-1.2 DEs classification

DEs belong to the broader class of Electroactive Polymers (EAPs), representing one of the simplest components of this set.

Beyond DEs, a large range of materials is of interest for actuation and generation purposes. A complete overview on the properties of EAPs is presented by Shankar [56], while the present works examines DEs only.

In DEs the electric field-induced response is initiated by the electrostatic attraction between oppositely charged conductive layers applied to opposite surfaces of a thin elastomeric film, as previously explained.

A wide variety of elastomers derived from chemically cross-linked homopolymers has been investigated as DEs.

Homopolymers are constituted by one type of monomer only and may be classified as “structured polymers” (in contrast with “non-structured” polymers).

The main investigate homopolymers are acrylics, silicones, polyurethanes, fluoroelastomers, ethylene–propylene rubber, polybutadiene and polyisoprene (natural rubber).

We analyze in detail only the first two types and natural rubber.

2-1.2.1 Acrylic Elastomers

This class of EAPs, commercially available as pressure-sensitive adhesives constitutes one of the most extensively investigated DEs.

Acrylate monomers are based on the structure of acrylic acid. Acrylic elastomer is a general term for a type of synthetic rubber whose main component is acrylic acid alkylester (ethyl or butyl ester).

These elastomers, manufactured as double-sided adhesive tapes, are commonly pre-shaped to film thicknesses of 0.5 and 1 mm, in which case they are usually pre-strained before electrical loading.

The elastic modulus of acrylic materials vary considerably, usually as a consequence of material anisotropy or defects.

Shankar et al. [56] report a tensile modulus for a sample of acrylic elastomer of 0.20 MPa and a compressive modulus of 0.26 MPa. Anyway, it is important to consider that, in a wide range of deformation (that can overpass 6 times the initial dimension of the sample), the behavior of the material is strongly non-linear, and a description via hyperelastic models is required.
Acrylic elastomer films are commercialized as adhesives i.e. by 3M.
In the following of the thesis a detailed characterization of the hyperelastic behavior of an acrylic film of VHB 4910 (by 3M) will be carried out.

2-1.2.2 Silicone Elastomers

Silicones, or polysiloxanes, consist on molecular chains in the form $(–Si\text{-}R_1\text{-}R_2–O–)_n$ with the groups R_1 and R_2 covalently attached to Si atom. Commercial silicones are usually featured by groups $R_1=R_2=CH_3$. The polymers are often treated with fillers in order to improve properties or reduce costs.
Silicone rubber is generally non-reactive, stable, and resistant to extreme temperature conditions. Due to these properties and its ease of manufacturing and shaping, silicone rubber can be found in a wide variety of products, other from actuators and generators.
A commercial example of dielectric Electroactive silicone, provided by Danfoss company [57], is the PolyPower DEAP material. This material is specifically thought for actuation and sensing purposes, and is provided with 3D anisotropic corrugated compliant silver electrodes, sinusoidal in shape, with nanometric thickness that allow the elastomer to stretch up to 100% without any permanent damage.

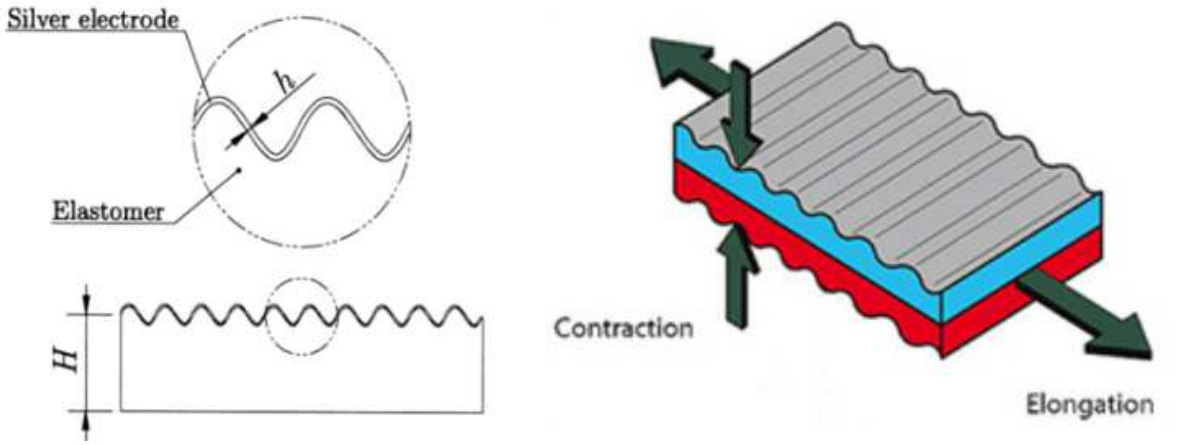

Figure 2-2- PolyPower composite, with electrode detail

2-1.2.3 Natural Rubber

Natural rubber is mainly made by polymers of the organic compound isoprene, with minor impurities of other organic compounds plus water.
In particular, some forms of natural polyisoprene are classified as elastomers.

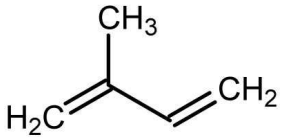

Figure 2-3. Isoprene skeletal formula

Natural rubbers properties are modified by mean of the process of vulcanization, by which the elastomer molecules become chemically cross-linked to form three-dimensional structures having dimensional stability. Sulfur, peroxides, resins and metal oxides are typically used as vulcanizing agents [58].

Natural rubber, in general, presents higher stiffness with respect to silicones or acrylics (according to Kim [59], 1.3 MPa), and presents also higher values of the electric break-down field, resulting, thus, of high interest in the panorama of the DEs for generation usage. Conversely, the application of natural rubber for DEAs is unfavorable because its elevated stiffness allows (with the same applied force) lower actuation displacements with respect to the others DEs.

Natural rubber is publicly traded. The average price in 2012 was 5.1 $/kg.

2-1.3 Dielectric Elastomer Actuators (DEAs)

Actuation purposes are the oldest and original field of application of DEs.

DEs in actuation arrangement are activated by a voltage applied between the electrodes. Basing on the principle described above, the electrical activation induces an area expansion and thus a point displacement that can be used to produce mechanical work.

Therefore, the basic conceptual scheme of a DEA can be described referring to a lozenge-shaped configuration, studied by Vertechy et al. [60] and depicted in Figure 2-4.

This configuration represent the premise and the dual of the generator that is the subject of the present thesis.

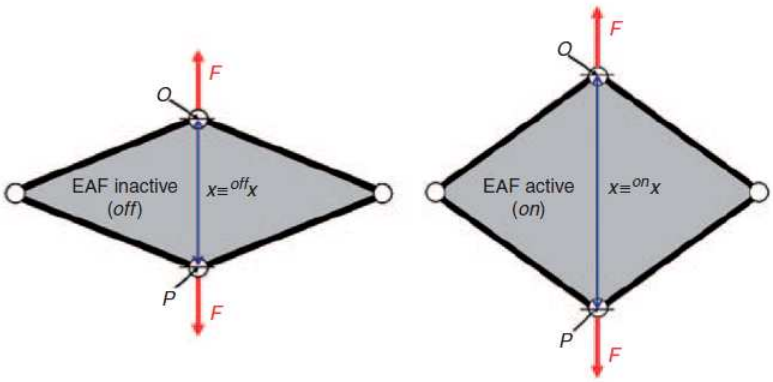

Figure 2-4 - Lozenge-shaped actuator

With reference to Figure 2-4, a constant force *F* (ling in the plane of the membrane) is present on the opposite joints O and P of the device in the inactive configuration (on the right). When

a certain voltage is applied to the electrodes coating the film, the membrane stretches in length (and squeezes in thickness), as shown on the left, thus the points of application of the two forces move in opposite directions: the final result is that a certain amount of electrical energy (given to the material in the activation phase) is converted to mechanical energy, corresponding to a work equal to the product of F and of the length variation of the diagonal x.

In Vertechy's study [60], for a side length of the lozenge of 93 mm, with a 4-layers membrane of 0.8 mm each, a maximum force output of about 3 N is obtained for a voltage of 4.8 kV and stretch up to 300%.

The constructive layout of a DEA typically consists in a membrane that is constituted by a pile of thin elastomer sheets and a flexible supporting frame that can either be an elastic structural element [61] or, most commonly, a compliant mechanism. Depending on the number of composing DE sheets, the membranes can be mono or multi-layered.

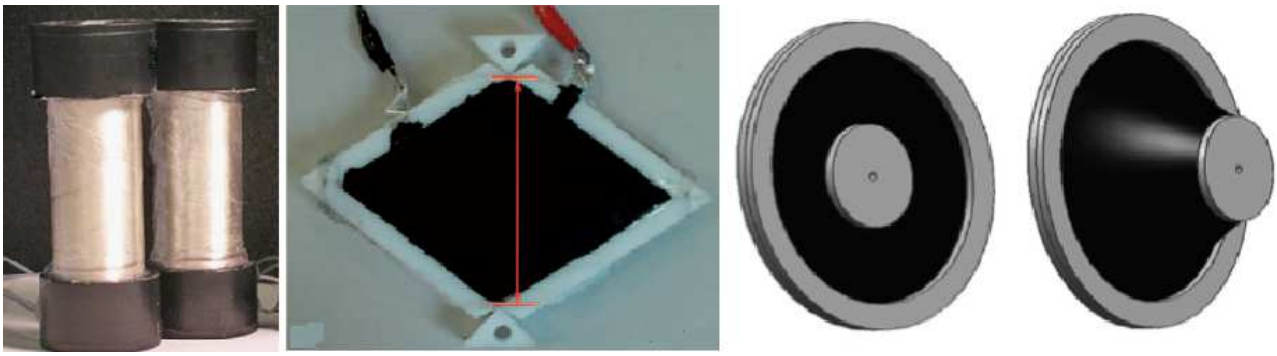

Figure 2-5 - Some examples of DEA

Lozenge-shaped actuators can be classified as "linear planar" actuator, since the force and the strain of the material lie on the plane of the frame and it constitutes one of the simplest design solutions.

Many other actuator configurations exist, for example

- tubular-shaped [62] (Figure 2-6): DE sheets rolled into tubes constitute a bundle of elastomers in parallel that produce an amplification of the produced force. The tubular actuators try to mimic human muscle functionalities providing axial stretch when a voltage is applied.

According to Sarban [62], up to date, there are two main tubular actuator prototypes. The most popular approach comprises a pre-stretched acrylic elastomer (VHB 4910 by 3M) with a compliant electrode.

The membrane is rolled up around a compressed spring core which maintains longitudinal and circumferential pre-stretch even allowing longitudinal actuation. For this prototype, the high stress concentration at the interface between the soft polymer film and the spring core provokes mechanical failure, strongly reducing the device life-time.

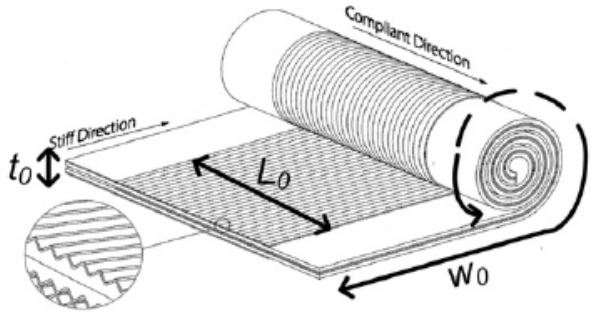

Figure 2-6 - roll actuator

The other prototype (by Danfoss PolyPower A/S) has no-pre-stretch on the DE membrane: this model exploits very small strains (<3%) but have excellent durability (~10^7 cycles).

- conical [63] [64]: These actuators belong to the class of linear actuators (since they exploit linear motion of a frame). They are constituted by a rigid frame that consists in two separate parts: an inner circular dish and an outer circular ring. In the undeformed configuration the frames and the membrane (coated with compliant electrodes) lie on the same plane. During the operation, the frames move relatively to each other in longitudinal direction (parallel to the axis of the device) and the membrane assumes approximately conical shape. The membrane is given a certain pre-stretch through a pre-loading part (i.e. a spring) (Figure 2-7).

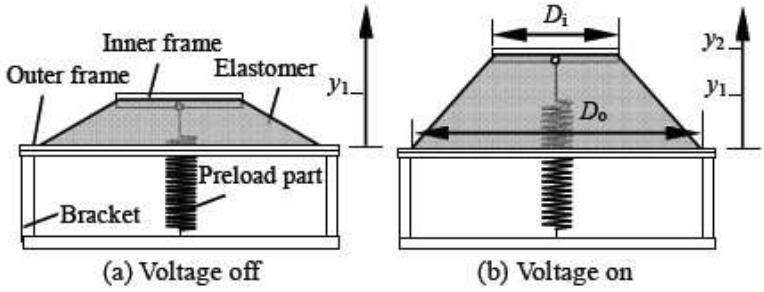

Figure 2-7 - Conical actuator functional principle

When a voltage is applied to the membrane, the lateral surface of the cone expands (and membrane thickness reduces) causing the relative distance between the two frames in longitudinal direction to increase.

In a study by Wang [64] three cones of 100 mm of outer diameter are assembled together in parallel to obtain a maximum force of 5 N with a maximum displacement of 17 mm.

- multiple-degree-of-freedom actuators. In an article presented by Choi et a. [65], an actuator capable to perform motions such as forward, backward, controllable compliance is presented. The actuator contains two films (coated with compliant electrodes) with a pretensioner in the middle. The pretensioner generates pre-stretches on both films.

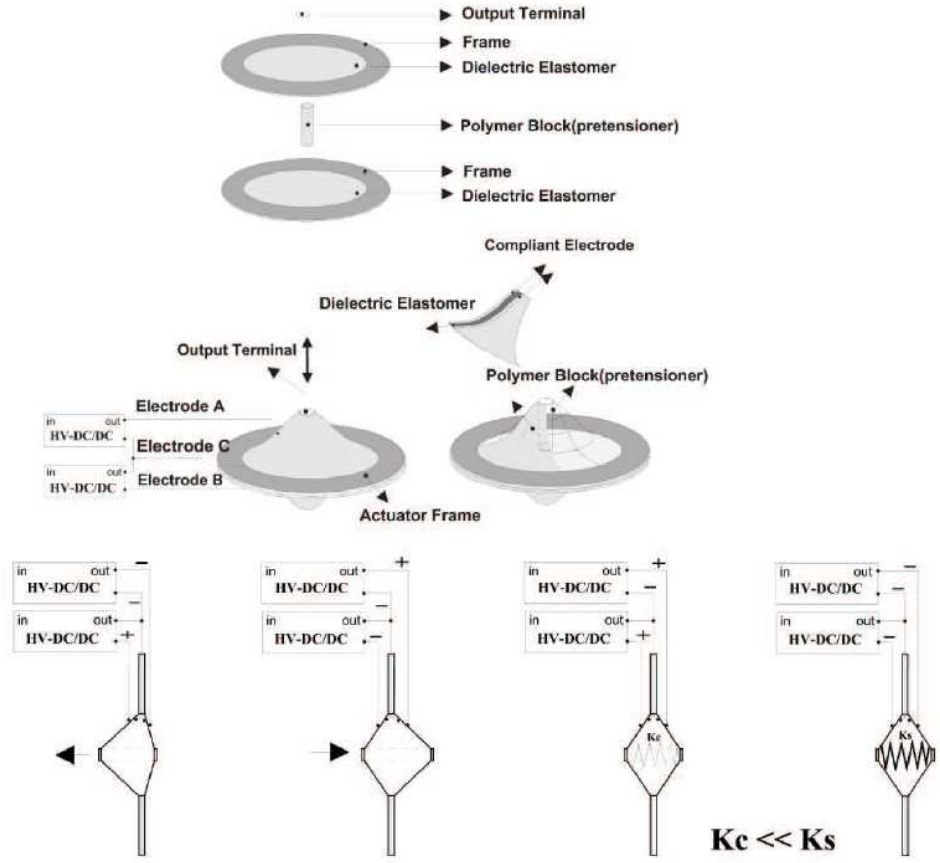

Figure 2-8 - Multiple-degree-of-freedom actuator

With reference to Figure 2-8, bringing, for example, electrode A to a certain voltage, the film connected to that electrode reduces its tension and the output terminal moves perpendicularly to the film membrane towards the side of electrode A, restoring the forces equilibrium.
If the same tension is applied to electrodes A and B (with respect to electrode C) the terminal becomes loose, even maintaining its position.

- Elastic frame generators: some examples of deformable-frames actuators are present in literature. We refer, as an example, to the solution proposed by Kofod et al. [61], consisting in a triangular deformable polymeric frame containing a pre-stretched membrane of dielectric material.

When the material is in the inactive configuration, due to the pre-stretch of the film, the frame results contracted (Figure 2-9.c), but when the membrane is given a certain voltage, the system changes its configuration (Figure 2-9.d). This principle can be exploited, for example, to grip and transport objects (Figure 2-10). The prototype experimented by Kofod had transversal dimension (in the inactive state) of 41 mm, and, with an activation voltage of 3 kV, was able to supply an actuation movement up to 12 mm and to lift up small object of 700 mg of weight.

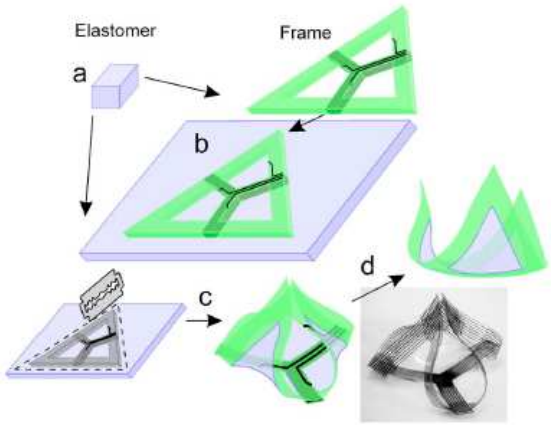

Figure 2-9 - Functional principle

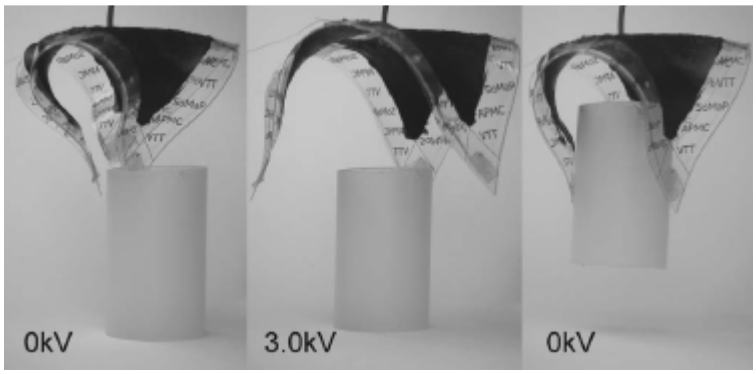

Figure 2-10 - Deformable frame actuator operation

The main advantages of the usage of DEs for actuation purposes is that these materials are more integrated, lightweight, flexible, high strain, economic, silent, resilient than the classical actuation technologies [60] and have relatively low cost; for this reason, they are promising for mechatronic applications.

Artificial muscles

Some configurations of DEAs (i.e. the roll actuator) are often classified as "artificial muscles" [53]. The technology of artificial muscles is of interest in robotic and automation engineering.
Human muscles are quite sophisticated since they exploit a complex mechanism based on the combined motion of different proteins to create force and displacement, are composed of bundles of fibers and present relevant life cycles (~10^9).
Although these features are unlikely to be replicated, DEs are probably the closest technology to human muscles. A complete dissertation about the subject is presented by Bar-Choen [66].
As an evidence, up to date, the main applications of DEs as actuators consist in a range of biomimetic robots [67].

2-1.4 Dielectric Elastomer Sensors (DESs)

DEs can be used as sensors for the measure of the strain [53].

With reference to the previous dissertation and to Figure 2-1, if the material is assumed linear with a constant material modulus *Y*, the strain in *z* direction can be expressed as

$$S_z = -\frac{p}{Y} = -\frac{\varepsilon}{Y}E^2 = \frac{\varepsilon}{Y}\left(\frac{V}{z}\right)^2$$

If the applied voltage is small enough with respect to the thickness and stiffness of the film, the strain in the actuated state is negligible. For example, if 1 kV provokes a strain of 10%, 10 V will produce a strain 4 orders of magnitude lower (according to previous equation) and, thus, negligible. Vice versa, if the film is stretched by an external force the percentage change in the applied voltage is non-negligible.

In fact, being the voltage expressed as (*B* is the volume of the elastomer, assumed constant):

$$V = \frac{Q}{C} = \frac{Q \cdot z}{\varepsilon A} = \frac{B}{\varepsilon}\frac{Q}{A^2}$$

If *Q* is constant, the voltage varies with A^2.

As explained previously, the percentage deformation of a DEs is usually relevant: these sensors may be employed to sense large deformations.

Two main measurement schemes can be followed:

- Direct measurement of the voltage variations. This solution shows criticalities in DC, since leakage and other effects make it difficult to keep a constant charge *Q* in time.
- Measure of the film capacity. Capacity measurements can be achieved by means of several techniques and can be directly correlated to the changes in polymer area:

$$C = \frac{\varepsilon A}{z} = \frac{\varepsilon A^2}{B}$$

2-1.5 Dielectric Elastomer Generators (DEGs)

DEGs are the object of the present thesis. In this paragraph an overview on the functional principle and of the prototypes presented in literature is reported.

Classical generations technologies are based on hydraulic, pneumatic, and electromechanical systems: although these technologies are proven, functioning and reliable, they have their own limits and criticalities [67]. In particular, most of these systems are heavy, bulky, relatively complex and constituted by several moving parts. These aspects may represent an inconvenience for some classes of usages like, indeed, Wave Energy Conversion: the presence of a corrosive and aggressive environment and of frequent solicitations like those provoked by the waves and by the sea-storms makes it necessary robust design generators. It has been proposed that smart materials such as piezoelectric ceramics and electroactive polymers can be used to harness mechanical energy.

The functional principles of DEGs can be explained as in the following.

The DE membrane, coated between two compliant electrodes constitutes a deformable capacitor (the capacitance of which varies with the deformation). Let refer, for simplicity, to Figure 2-11

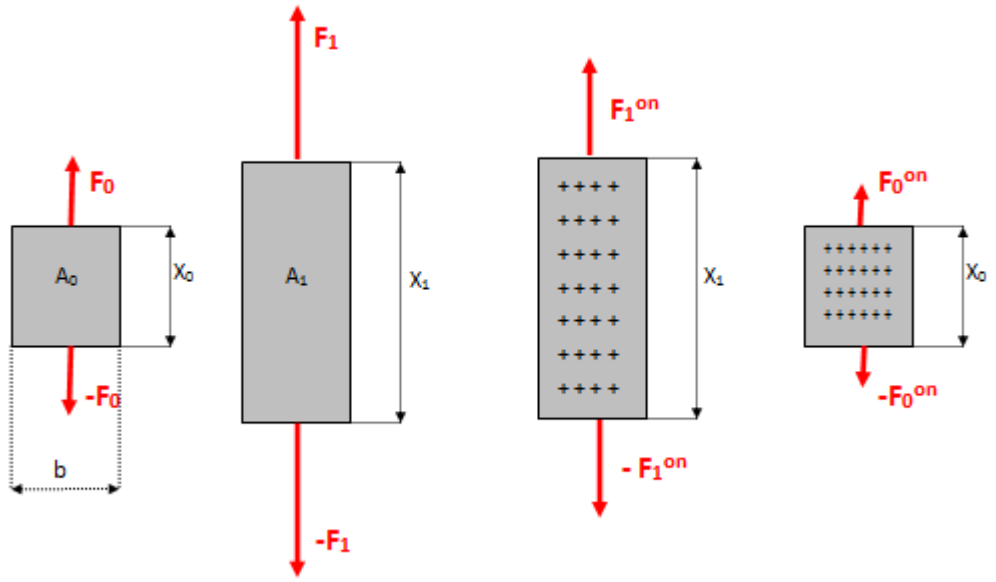

Figure 2-11 - DEG operation principle

An energy conversion cycle is carried out: the material is stretched from the initial position (corresponding to the configuration with minimum surface of the capacitor plates) to the final position (maximum area): in this phase, mechanical energy is stored in the material. Subsequently, a certain charge is deposited on the capacitors plates (+*Q* on one plate –*Q* on the opposite one).

Due to electric activation, and then to the onset of an electrostatic pressure in the film thickness direction, the DE membrane manifests a tendency to stretch in surface. However, if the membrane is kept in its position (for example by a solid frame) without the possibility of varying its shape, the result is that a decrease in the force necessary to maintain the membrane in the stretched position occurs.

For this reason, while the material returns to its initial configuration, the retracting force results lower than the force applied during the stretch phase, thanks to the electric activation; so, the mechanical energy for the material return is lower than the mechanical energy acquired in the loading phase: the difference between these energy amounts is converted to electrical energy.

During the unloading phase, the material returns to its original configuration, thus, the capacitance of the device decreases from C_1 to C_2. If the charge on the plates is kept, for example, constant, the extracted electrical energy results in $\Delta En = \frac{1}{2} Q^2 \left(\frac{1}{C_2} - \frac{1}{C_1}\right)$.

An example of energy conversion cycle is presented by Wang et al. [68]: in this study, a mono-axial deformation is given to the material; then, a charge *Q* is deposited on the electrodes, the material is unloaded at constant charge *Q* and then discharged.

The cycle is represented in the Force-displacement plane (Figure 2-12).

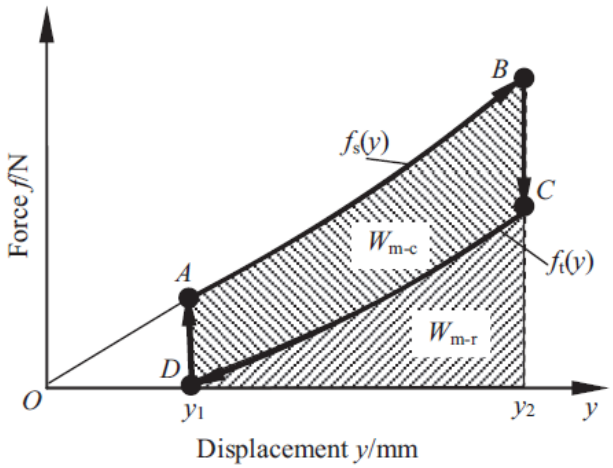

Figure 2-12 - Example of energy conversion cycle.

The following phases are represented:

AB → loading cycle (discharged material)

BC → material charging

CD → unloading cycle (constant charge, *Q*)

DA → material discharging

The two areas $W_{m\text{-}c}$ and $W_{m\text{-}r}$ represent respectively the amount of mechanical energy converted to electrical energy and the mechanical energy for the EAP return.

Notice that gained electrical energy ΔEn, in general, is lower than $W_{m\text{-}c}$ due to electrical losses.

According to Wang [68], a "conversion efficiency" can be defined as

$$\eta_c = \frac{\Delta En}{W_{m-c}}$$

At the same time, "total efficiency" for the generator can be defined as

$$\eta_t = \frac{\Delta En}{W_{m-c} + W_{m-r}}$$

this ratio represents the percentage of mechanical energy stored in the material during the loading phase that is usefully converted to electrical energy.

In order to avoid confusion between the parameters, the second index of merit for energy conversion is named "coupling factor" and is defined in a slightly different way [69]:

$$k = \sqrt{\frac{\Delta En}{W_{m-c} + W_{m-r}}}$$

In order to clarify DEGs functional principle, the following situation can be considered. Let refer to Figure 2-11 and let suppose that the polymer can be extended in *x* direction by maintaining its volume constant. Let also suppose that during the deformation the width b of the membrane keeps constant, while the height *x* and the film thickness *t* change.

Indicating with B the volume of material, $B = x_0 b t_0 = A_0 t_0 = x_1 b t_1 = A_1 t_1$.

In order to generically describe the functional principle of DEGs, let suppose the material perfectly elastic.

If x_{ref} is the height of the sample in the unstretched state, the forces in the inactive state corresponding to maximum and minimum height (x_0 and x_1) that the sample assumes during the cyclic operation are, respectively:

$$F_0 = k(x_0 - x_{ref}) = \frac{k}{b}(A_0 - A_{ref}) \quad ; \quad F_1 = k(x_1 - x_{ref}) = \frac{k}{b}(A_1 - A_{ref})$$

where k is an elastic constitutive constant of the material.

During the stretching phase (in absence of any electric activation), the mechanical elastic energy stored in the material is

$$En_{MEC,1} = \frac{k}{2}\left[(x_1 - x_{ref})^2 - (x_0 - x_{ref})^2\right] = \frac{k}{2b^2}\left[(A_1 - A_{ref})^2 - (A_0 - A_{ref})^2\right]$$

When the material is in the configuration of maximum surface, a charge Q is deposited on the electrodes. The membrane behaves as a condenser, this means that an amount of electrical energy $En_{EL,1}$ has been given to the membrane during the charging phase:

$$En_{EL,1} = \frac{1}{2}QV = \frac{Q^2 B}{2\varepsilon {A_1}^2}$$

The deposition of a charge on the electrodes provokes the onset of an electrostatic pressure p, that has previously been calculated. If the membrane was free to expand, the pressure, acting in thickness direction would cause the membrane to further extend its surface (as for actuator devices). In the generator configuration, anyway, the membrane does not withstand any further extension (when charge is put on the electrodes the material is already at its maximum surface configuration) and the effect of the electrostatic induced pressure is a reduction in the stretching force F_1. It is possible to demonstrate (APPENDIX A) that, due to the hypothesis of incompressibility, the electrostatic induced pressure behaves as an hydrostatic load, acting not only along the thickness direction but also in the direction of the stretching force (Figure 2-13).

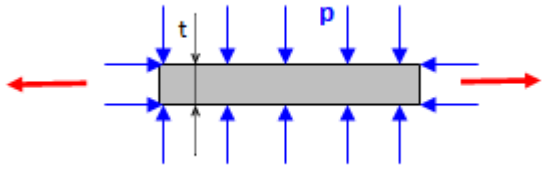

Figure 2-13 - Electrostatic pressure distribution

The stretching force after the electric activation results then in

$$F_1^{on} = F_1 - p \cdot b \cdot t_1 = F_1 - \varepsilon E^2 b \cdot t_1 = F_1 - \frac{Q^2 B b}{\varepsilon {A_1}^3}$$

In general, during the return phase to the initial position x_0, the force is expressed as function of the height x of the sample at a generic position:

$$F(x) = k(x - x_{ref}) - \frac{Q^2 B}{\varepsilon x^3 b^2}$$

Therefore, during its return, the material releases an amount of mechanical energy given by

$$En_{MEC,2} = \int_{x_0}^{x_1} F(x)dx = \frac{k}{2b^2}\left[\left(A_1 - A_{ref}\right)^2 - \left(A_0 - A_{ref}\right)^2\right] + \frac{Q^2B}{2\varepsilon {A_1}^3} - \frac{Q^2B}{2\varepsilon {A_0}^3}$$

Notice now that at the end of the cycle, when the membrane is back to its original position x_0, with a charge Q on its faces, the electrostatic energy stored in the electric field is

$$En_{EL,2} = \frac{Q^2B}{2\varepsilon {A_0}^2}$$

and, being $A_0<A_1$, $En_{EL,2} > En_{EL,1}$. This is clear thinking that when the membrane is brought back to low-surface configuration, the charges present on its faces result somehow more "dense" than in the stretched position.

It is also immediate to notice that $En_{MEC,1} - En_{MEC,2} = En_{EL,2} - En_{EL,1}$ that means that a certain amount of mechanical energy has been converted to electrical energy.

In this simple example only the very basic principle of DEGs functioning is explained: the energy conversion mechanism is fully explained by geometrical considerations regarding the "distance" among the charges, and the elastomers are no required to have any particular property but being dielectric deformable materials.

Since in the example above linear-elasticity was considered and no dissipative forces were present, the whole amount of the difference between mechanical energy in the stretch phase and in the return phase was fully converted to electrical energy.

In a real situation, the main reasons of loss-of-energy will be due to hysteretic material behavior and to electrical losses in the circuitry to which the deformable condenser is connected (leakage currents).

As for the DEAs, many different configurations for DEGs can be envisaged.

Some examples are present in recent literature, anyway, being the DEGs the dual of the actuators, many of the geometrical layouts described for actuation purposes can find an application in the field of electric generation.

Wang et al. [64] [68] studied conical shaped generators, that have the same constructive design of the corresponding generators but act exploiting the described operation principle of generation.

Wang [64] investigated a conical generator with outer diameter of 40 mm subjected to a voltage in the range of 1000-2000 V, measuring conversion efficiencies (in accordance with the previous definition) up to 50%.

We emphasize that one general parameter that is reported in many literature works about the preliminary characterization of DEGs is the energy per unit weight of elastomer that the generator is able to convert. This parameter plays a significant role in the determination of the amount of material necessary in a certain application and, thus, in the determination of the level of compactness that DEGs can offer.

A pioneer study was carried out by Pelrine et al. [70] who measured energy densities of 0.4 J/g and estimated possible densities up to 1.5 J/g.

Koh et al. [71] [72]studied a theoretical prototype of generator based on a square membrane that is subjected to equi-biaxial state of deformation, that means that the membrane is stretched uniformly along the two sides (Figure 2-14).

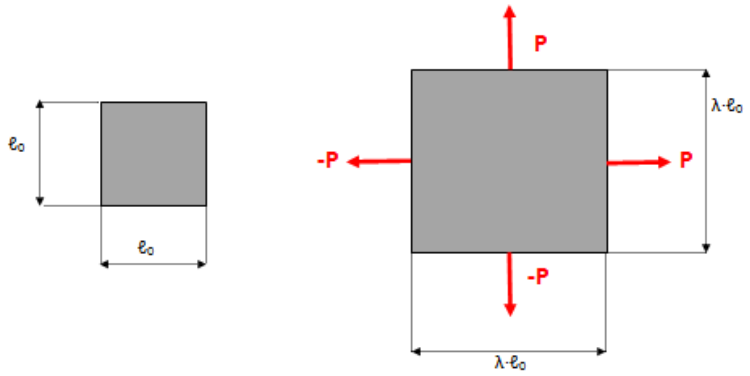

Figure 2-14 - Equi-biaxial state of deformation

For this configuration, a maximum energy density of 3.2 J/g was estimated.
For a similar configuration, Jean-Mistral [73] measured a maximum energy density of 1.7 J/g.
Dielectric elastomers, such as piezoelectric materials, generally need high voltage, typically in the range 1-6 kV [70]: the relative high voltage requires proper design of the electronics of the generators. Inductors and transformers that can handle very high voltage exist, while commercial transistors have still limitations on the maximum allowed voltage. Transistors with 2.5 kV voltage are available, but they are rated at much higher currents and power than those required by DEGs.
From the considerations done so far, it is possible to identify some properties required by DE materials, in particular:

- High dielectric constant ε: the polymeric membrane has to dielectric, avoiding the charge passage from one face to another of the resulting condenser.
- Low stiffness, since high deformations are required (especially for actuators).
- High electric break-down, because, as it will be demonstrated in the following, break-down represents a limitation to the convertible energy per unit material volume.

2-1.6 Characterization of a DEG in the Q-V diagram

In order to elaborate a procedure to calculate the available energy from a DEG (that is the maximum amount of energy that the elastomer can convert to electrical energy), it can be noticed that the state of the elastomer during its operation can be identified by either a point in the stress-stretch plane or in the voltage-charge plane.
Similarly, on each of these planes, transformations that imply the passage from one equilibrium state (described by a single point on a plane) to another are represented by lines. This formalism is analogous to the use of thermodynamics planes representing the state and transformations of thermodynamic systems.
The use of such planes is a useful tool in order to visualise the behavior of DE membranes.

Let consider, i.e., the example of Figure 2-12, concerning a monoaxial deformation of a DE sample that is first stretched and is then given a charge Q (it is assumed that during the charging phase the displacement of the membrane is kept constant) that is then removed at the end of the return phase.

It can be shown that the transformations of the polymers are represented on the two planes according to the plots in Figure 2-15.

Figure 2-15 - Energy conversion cycle on Force-position and Voltage-charge planes

Beyond the procedure needed to report the transformations on the Q-V plane (that is discussed in the following of the paragraph), it is interesting to underline the following aspects:

- Since the DEG is operated in a cyclic way, in order to produce electric energy from a cyclic process, the transformations describing the operation of a generator (in both the planes) describe a cyclic path that is designed henceforth with the name of Energy Conversion Cycle (ECC).
- Purely mechanic transformations (that occur with no charge and voltage present on the membrane) are obviously not represented in the Q-V plane.

In the following of the work, the Q-V plane will be always used and considered.

In order to provide a first exemplification of the formalism and to furnish a prerequisite to the work presented here, we consider a study carried out by Koh et al. [72], who studied the energy available from a square-shaped membrane of dielectric elastomer subjected to an external equal biaxial force.

It is emphasized how the maximum energy conversion is based on some mechanisms of failure: electrical break-down, material loss of tension, rupture.

The limits determined by the mechanisms of failure can be represented as curves on both the presented diagrams. Therefore, since the gathered energy can be expressed as the integral of the mechanical force over the deformation or as the integral of the voltage over the charge, the areas enclosed by the boundary curves on these two planes represent the maximum rate of convertible energy (per cycle).

The analytic results for the equal biaxial case are briefly resumed here.

Symbols:
Q charge
V voltage
$\varepsilon=\varepsilon_r\varepsilon_0$ dielectric constant
t thickness
B volume of the EAP
E electric field
E_{BD} break-down electric field
λ stretch
λ_u stretch at rupture
ℓ side length of the square sample
ℓ_0 side length in the undeformed state
A surface of the electrodes
A_0 surface in undeformed configuration

The capacitance of the device is given by

$$C = \frac{Q}{V} = \frac{\varepsilon A}{t} = \frac{\varepsilon A^2}{B}$$

The material, in literature, is always assumed to be incompressible, so that the volume *B* can be considered constant during the deformation.

The failure conditions, in term of *V* and *Q*, are described as follows.

Electric break-down: the electric field inside a plane capacitor is calculated as

$$E = \frac{V}{t} = \frac{VA}{B}$$

From the first equation, the surface *A* can be expressed in terms of *Q* and *V* and replaced in the expression of the electric field.

For a value of *E* equal to the break-down field (supposed in first approximation to be constant), the condition $E \leq E_{BD}$ takes the form

$$VQ \leq \varepsilon B {E_{BD}}^2$$

That in the Q-V plane identifies a surface bounded by a hyperbola.

Rupture: The rupture condition can be easily expressed referring to the stretch level of the material, by the condition $\lambda \leq \lambda_u$.

Being the deformation equal biaxial, the side length of the deformed square is

$$\ell = \lambda \ell_0$$

thus the area is

$$A = \lambda^2 A_0$$

Using the previous equations, the iso-λ curves result to be straight lines:

$$V = \frac{B}{A_0 \varepsilon \lambda^4} Q$$

therefore, the rupture criterion requires that

$$V \geq \frac{B}{A_0 \varepsilon {\lambda_u}^4} Q$$

Loss of tension: in the reference article [72], this condition is resumed by a inequality in the form $\lambda \geq \lambda_{min}$:

$$V \leq \frac{B}{A_0 \varepsilon {\lambda_{min}}^4} Q$$

The boundary curves are represented on the *Q*-*V* plane:

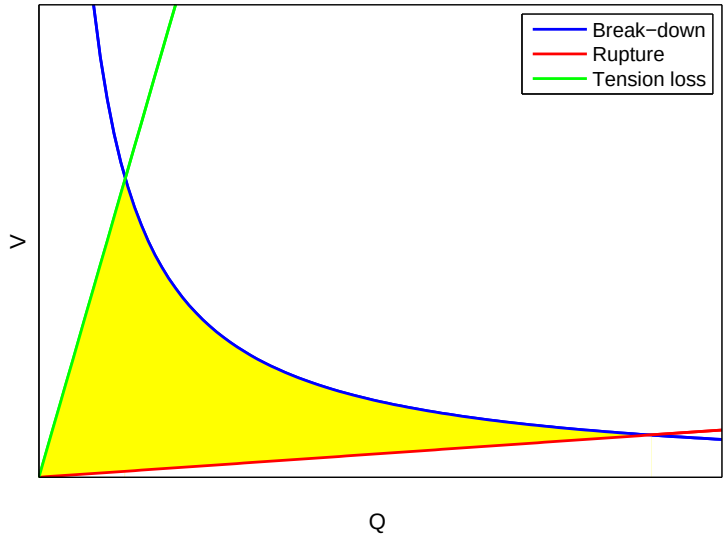

Figure 2-16- Available energy and operation limits for the equal biaxial case

The emphasized area represents the numerical value of the maximum energy that can be converted.

In order to convert the whole amount of energy, the following ECC should be carried out: the EAP must be loaded mechanically from the minimum stretch (corresponding with the loss of tension condition) to the maximum one (given by the rupture condition); susequently, it has to be charged at constant stretch and then discharged progressively following the break-down curve until the loss of tension condition. At this level of stretch, the material must be completely discharged, in order to close the cycle.

The cycle of maximum energy is then identified by the lines corresponding to the various mechanisms of failure.

2-2 Modeling and Optimization of Lozenge-Shaped Dielectric Elastomer Generator

2-2.1 Introduction

In the present section, a Lozenge-Shaped DEG (LS-DEG) is studied via preliminary experiments and theoretical arguments. In particular, the present paragraph: 1) presents a number of hyperelastic models that are fitted to a set of experimental tests conducted on a commercial DE membrane; 2) introduces a model to predict the failure conditions that limit the maximum electrical energy per unit volume that can be converted by LS-DEGs; 3) defines

a procedure for the choice of the optimal design parameters that maximize the electricity generation performances of LS-DEGs; 4) analyzes the influence of the chosen hyperelastic model on the results.

As already mentioned, the operation of the lozenge-shaped DE transducer has been examined by Vertechy et al. [60] who proposed a mathematical procedure that optimizes the behavior of the device when used as actuator. However, the analysis and optimization of the LS-DEG requires a different approach and has not been presented in previous research works.

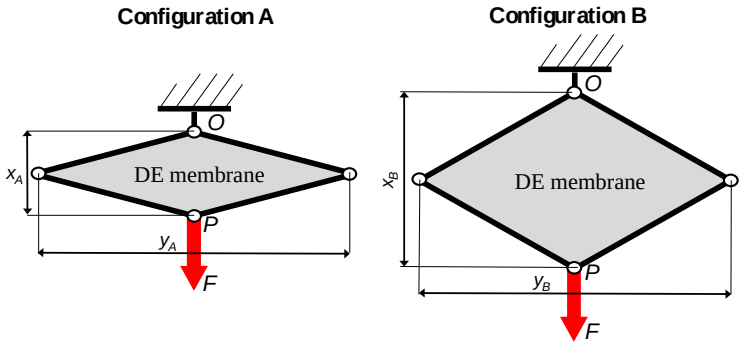

Figure 2-17 - Schematic of a LS-DEG

The LS-DEG consists in a planar incompressible DE membrane that is pre-stretched and clamped to a rigid frame shaped as four-bar mechanism with equal-length links (Figure 2-17). The device position can be uniquely defined by the variable x (hereafter also called 'transducer length' or 'longitudinal length'), with which we indicate the distance between the centers O and P of the two opposite joints of the four-bar mechanism (with reference to Figure 2-17), while the distance between the other two opposite centers of the revolute pairs is indicated with the variable y and is also called 'transversal length'.

With the variation of x, the DE membrane deforms uniformly and the deformation is uniquely identified by the first and second principal stretches, λ_1 (along the x direction) and λ_2 (along the y direction).

The DE membrane has compliant electrodes on both sides (that can be realized using a coductive paste with dispersed metallic particles), forming a deformable parallel-plate capacitor whose capacitance is a function of x.

We consider the loading case in which an external force is applied along the x direction at the joint P and the opposite vertex O is connected through a revolute joint to the ground.

The working principle of the LS-DEG can be briefly described as follows. Let's consider the reciprocating motion of the device while it is opening and closing under the action of an external force, and correspondingly the length x is varying from a value $x = x_A$ to $x = x_B$ (with $x_B > x_A$).

When the transducer length is changed from x_A to x_B (loading phase), elastic energy is stored in the DE membrane. In the position $x = x_B$, the DE membrane is provided with an amount of charge and is electrically activated. During the reverse movement, from the position x_B up to

x_A (unloading phase), the force exerted by the DE membrane to the four-bar mechanism is lower due to the electric load. The difference between the mechanical work performed during the loading and unloading phases represents the amount of electric energy generated by the system.

From the functional point of view, the LS-DEG can be seen as a linear transducer which produces electric energy from the reciprocating motion imposed by an external oscillating force. These generators may be successfully employed as PTO systems for a number of WEC devices, like buoys or flaps.

2-2.2 Electro-mechanical model

The mechanical stress-stretch behavior of a rubber-like isotropic hyperelastic material is described by the strain-energy function ψ (APPENDIX A, [55]).

The calculation of the mechanical stresses acting on a polymeric membrane is carried out basing on the values of the stretches and of the function ψ.

If the membrane is electrically activated, an isotropic hydrostatic pressure $p = -\varepsilon E^2$ acts on the material (where ε is the dielectric constant of the polymer and E the electric field due to activation).

We remember that, for the hypothesis of incompressibility, $\lambda_1\lambda_2\lambda_3 = 1$.

Let refer to the lozenge-shaped membrane sketched in Figure 2-17: λ_1 and λ_2 have already been defined. The third stretch λ_3 is the stretch along the thickness direction, z, and its value is uniquely defined if λ_1 and λ_2 are fixed, so that ψ can be expressed as a function of λ_1 and λ_2 only. Indicating with t_0 the value of the initial thickness of the membrane (in the undeformed configuration), the principal stresses are expressed by (APPENDIX A):

$$\sigma_1 = \lambda_1 \frac{\partial \psi}{\partial \lambda_1} - p$$

$$\sigma_2 = \lambda_2 \frac{\partial \psi}{\partial \lambda_2} - p$$

$$\sigma_3 = -p = -\varepsilon \frac{V^2}{{\lambda_3}^2 {t_0}^2}$$

where V is the voltage between the electrodes of the activated membrane.

In order to prevent material loss of tension, the acrylic film is positioned on the lozenge-shaped mechanism with a certain pre-stretch.

We nominate λ_{1p} the pre-stretch in longitudinal direction, and λ_{1p} that in transversal direction, given at a reference configuration where $x=x_p$.

Once the stresses are known, the equilibrium force F that must be applied to the joints of the membrane to keep it in the equilibrium position (Figure 2-17) can be calculated in both the activate and inactivate configurations.

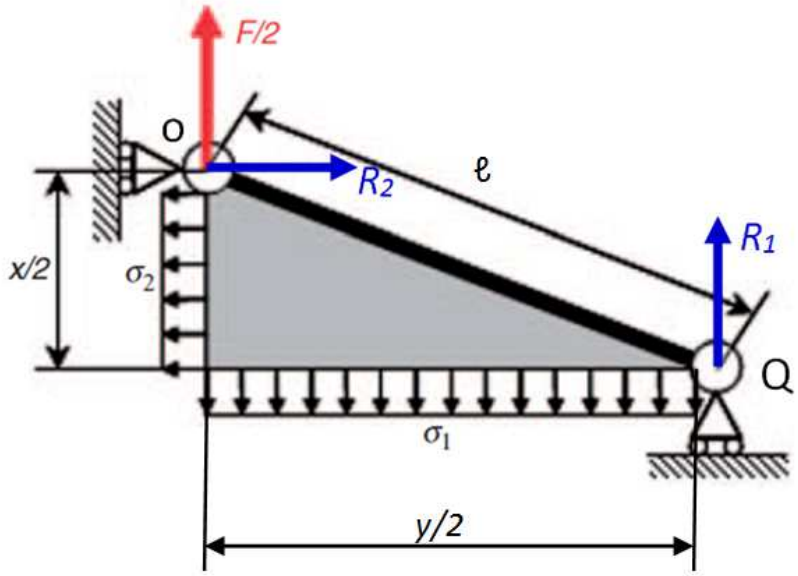

Figure 2-18 - Force equilibrium of LS-DEG

The force *F* acting on the joint O of the lozenge is simply calculated by considering the force balance and the momentum balance (i.e. above joint Q).

From the force balance, the support reactions result in

$$R_1 = \sigma_1\, y\, t/2 - F/2$$

$$R_2 = \sigma_2\, x\, t/2$$

while the momentum balance above Q is

$$\sigma_1 \frac{y^2}{2} t - \sigma_2 \frac{x^2}{2} t - Fy = 0$$

Where the thickness *t* of the membrane is $t = t_0/(\lambda_1\lambda_2)$.

Using this last equation and the expression for the principal stresses, the equation for the equilibrium force of the generator is derived [60].

In particular, in the inactive configuration, $p = 0$ and the force is

$$F_{off}(x) = \frac{t_0}{2}\left(\frac{\sqrt{4\ell^2 - {x_p}^2}}{\lambda_{2p}}\frac{\partial\psi}{\partial\lambda_1} - \frac{x x_p}{\lambda_{1p}\sqrt{4\ell^2 - x^2}}\frac{\partial\psi}{\partial\lambda_2}\right)$$

If otherwise the membrane is activated, $p = -\varepsilon\, V^2/\left({\lambda_3}^2 {t_0}^2\right)$, the equilibrium force is

$$F_{on}(x) = F_{off}(x) + F_{em}(x)$$

where the addendum due to electric activation is

$$F_{em}(x) = -\frac{\varepsilon V^2 \lambda_{1p}\lambda_{2p} x\left(2\ell^2 - x^2\right)}{t_0 x_p \sqrt{4\ell^2 - {x_p}^2}}$$

Notice that, since the system has one degree of freedom, both λ_1 and λ_2 can be expressed as a function of *x* only:

$$\lambda_1 = \lambda_{1p}\frac{x}{x_p}$$

$$\lambda_2 = \lambda_{2p}\frac{\sqrt{4\ell^2 - x^2}}{\sqrt{4\ell^2 - {x_p}^2}}$$

Therefore, the force in the active or inactive configuration can be effectivelly expressed as a function of the variale *x* only.

2-2.3 Mechanical characterization of the material

2-2.3.1 Experimental layout

In order to properly describe the behavior of the system, the theoretical study of the LS-DEG has been preceded by an experimental work of characterization of an elastomeric material, whose mechanical stress-stretch response has been fitted to a number of hyperelastic models.
The DE employed in the present work is the acrylic elastomer VHB-4905 by 3M that is available in thin films with 0.5 mm thickness. The material has been chosen because it is easy to handle and easy to mount on the mechanism frame thanks to its adhesive properties.
Experimental characterization of the material has been carried out at Percro Laboratory (Scuola Sant'Anna, Pisa, Italy).
In order to produce experimental results that are suited to the considered application, mechanical tests have been performed on a test rig (Figure 2-19) which comprises:

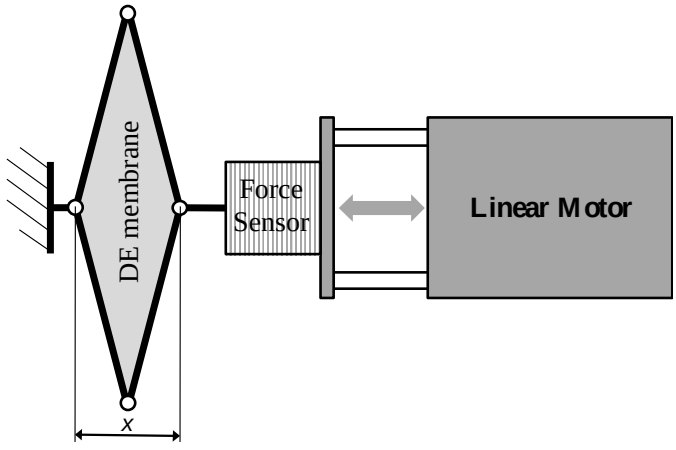

Figure 2-19 - Test rig equipped with linear servomotor and force sensor.

- a lozenge mechanism with side lengths ℓ=80 mm, whose links are designed to easily allow the connection of a DE membrane along its perimeter
- a set of membranes made of three layers of 0.5 mm thick films for a total thickness of 1.5 mm (when unstretched)
- a brushless linear motor (P01-37x120F-HP by LinMot™) with a high resolution linear encoder that is employed to impose the reciprocating force/motion to the LS-DEG

- driving and control electronics in order to regulate the LS-DEG motion according to the desired position profiles
- a single axis load cell and a 13 bits acquisition electronics employed to measure the force of the LS-DEG along the x direction.

Such setup guarantees a force accuracy and resolution better than 25 mN, a position accuracy and resolution better than 0.05 mm and a maximum acquisition rate of 2 kHz.
The setup is controlled by mean of a Simulink model provided by the Laboratory.
During the experiments, the motor is controlled in order to cyclically vary the longitudinal length x of the lozenge membrane from a minimum value of x_A =20 mm to a maximum value of x_B =85 mm with constant speed rate, so that the longitudinal length of the device describes a saw-tooth profile. At the same time, the force F produced by the transducer is acquired and measured with a certain sampling frequency.
Each sample of material has been subjected to several loading-unloading cycles (at least 10 for each measurement).

2-2.3.2 Correction of the offsets in the force measurement

It has been notice that, even when no membrane is present on the four-bar mechanism, the force sensor measures a non-zero force during the cyclic idling motion of the frame.
These loads represent an offset for the force measurement due to the polymeric transducer, that, if not corrected, would introduce a systematic error in the measurements.
The presence of an offset force on the idling system is explained in terms of

- Friction forces, acting on the joints of the four-bar mechanism
- Inertial forces due to the fact that the motion of the frame has not perfectly constant speed: when the system reaches the configuration with minimum or maximum transducer length, it has to reverse its motion, therefore its speed has to change sign. Under ideal conditions, the velocity of the joints of the frame keeps constant and reverses its sign instantaneously in correspondence of the end-stops. This would introduce a discontinuity in the speed, that is physically unfeasible: in the reality, the mechanism will be subjected to a certain acceleration, therefore the force sensor will measure an inertial load due to the dynamic of the system.

Measurements on the unloaded lozenge-mechanism have been taken at a speed rate of 0.5 mm/s (that is the same velocity adopted for the measurements on the acrylic membrane), with sampling frequency of 20 Hz.
It is possible to notice that the offset forces result almost constant. In particular, an offset value can be identified when the transducer length varies from x_A to x_B (elongation phase) and a different value is met when the longitudinal length varies from x_B to x_A (elongation phase).
In Figure 2-20, we report the graphical result for the force offset as a function of the length x.
As already mentioned, two offsets values can be identified for the elongation and the return phase.

The offset for elongation phase can be averaged on the data of Figure 2-20 and amounts to $F_{elong.}$=4.2 N. The offset for the return phase is F_{return}=3.8 N.

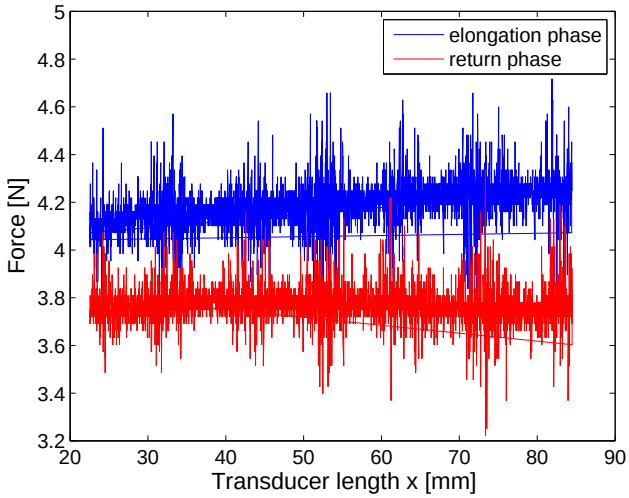

Figure 2-20 - Force offsets

2-2.3.3 Experimental characterization of the acrylic elastomer

Mechanical behavior of polymeric material is visibly affected by viscoelastic hysteresis phenomena. Viscous phenomena within the material, in particular, provoke the dissipation of a rate of mechanical energy. It is known that the rate of dissipated energy due to hysteresis increases with increasing deformation speed [74].

In order to produce a proper mechanical characterization of the material, then, low-speed experiments have been carried out.

Such experiments have been conducted at a deformation speed of 0.5 mm/s, with sampling frequency of 20 Hz.

In order to produce a complete characterization of a material, experiments on different samples subjected to different strain fields must be conducted [75]. The aim of such experiments is the determination of the strain-energy function ψ that describes the mechanical elastic properties of the polymer.

The strain energy function can be in general be expressed as a function of the principal invariants of the strain tensor:

$$\psi = \psi(I_1, I_3)$$

with

$$I_1 = {\lambda_1}^2 + {\lambda_2}^2 + {\lambda_3}^2 \quad ; \quad I_2 = {\lambda_1}^{-2} + {\lambda_2}^{-2} + {\lambda_3}^{-2}$$

while the third invariant, for incompressible materials, is constant: $I_3 = \lambda_1\lambda_2\lambda_3 = 1$.

For a given sample of material, each single type of strain field (i.e. equi-biaxial extension, pure-shear and simple extension) traces out a single line on the free energy surface (Figure 2-21) and does not provide sufficient information for the construction of the surface [75].

In order to obtain a complete characterization of the material, for example, measurements on a same sample, subjected to different strain fields, should be carried out. In the present set of experiments a sort of reversed procedure has been followed.

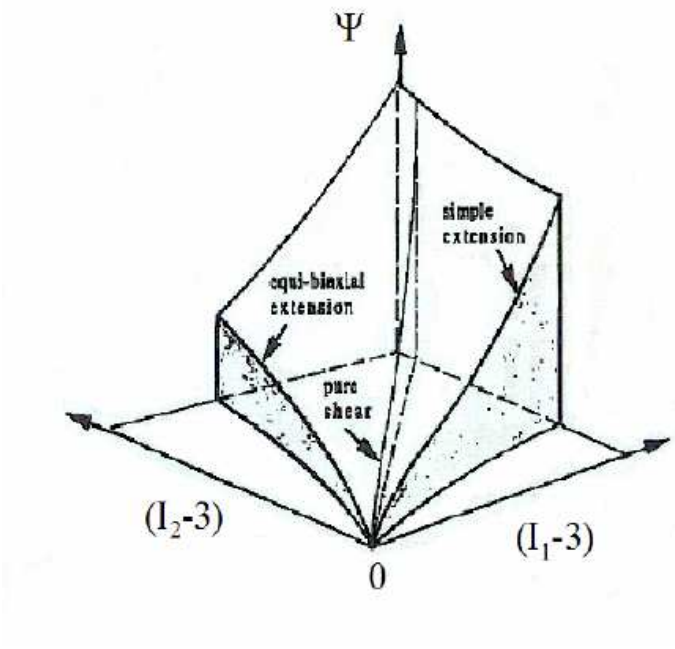

Figure 2-21 - Free energy surface

For the case in exam, experiments are conducted on a test rig: the system has one kinematic degree of freedom only, but different strain fields depending on the arrangement of the polymeric material on the frame.

Instead of using a same polymeric membrane deformed with different mechanisms, the aim of obtaining a complete characterization of the material by mean of producing a set of different strain fields has been here obtained by repeating experiments on different polymeric samples, with different pre-stretches, mounted on the same frame (the features of which have been described above).

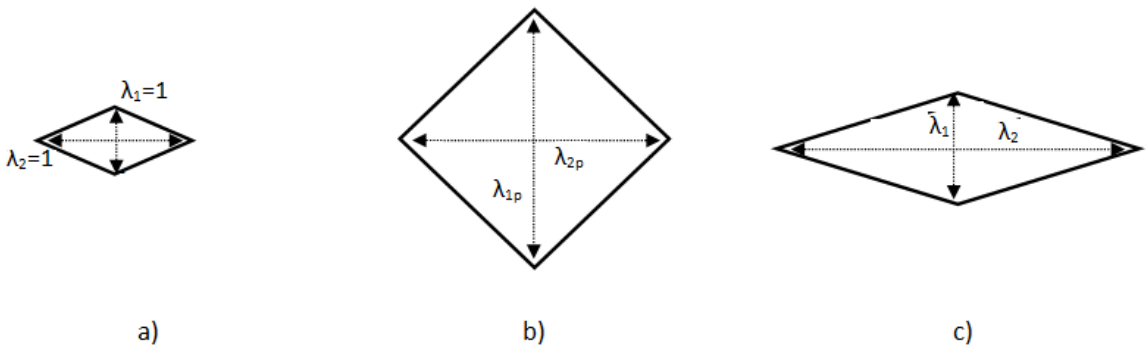

Figure 2-22 - Stetch and stress definition. a) Unstretched sample b) Square configuration (pre-stretches definition) c) Deformed configuration (stretches definition)

Pre-stretches λ_{1p} and λ_{2p} can be given at any arbitrary reference position x_p. In the present work, pre-stretches are referred to the configuration at which the links of the lozenge form right angles, that is $x_p=\ell\sqrt{2}$. It is worth to notice that such a configuration is not necessarily reached during the operation of the device, but it is always possible to mathematically refer the pre-stretches to that configuration.

Five different samples of DE membrane (M1-M5) with different pre-stretches have been tested.

	pre-stretches		*sample dimensions*		*stretches @ $x=x_A$*		*stretches @ $x=x_B$*	
ID	λ_{1p}	λ_{2p}	x_0 **[mm]**	y_0 **[mm]**	λ_1	λ_2	λ_1	λ_2
M1	12.6	3.9	9	29	2.3	5.5	9.4	4.7
M2	11.3	3.9	10	29	2.1	5.5	8.5	4.7
M3	9.4	3.9	12	29	1.7	5.5	7.1	4.7
M4	9.4	3.2	12	35	1.7	4.5	7.1	3.9
M5	11.3	4.7	10	24	2.1	6.6	8.5	5.6

At least ten loading-unloading cycles have been acquired for each measurement (M1-M5); the data have been averaged on the last seven cycles since the response of the material becomes repeatable after some pre-conditioning cycle.

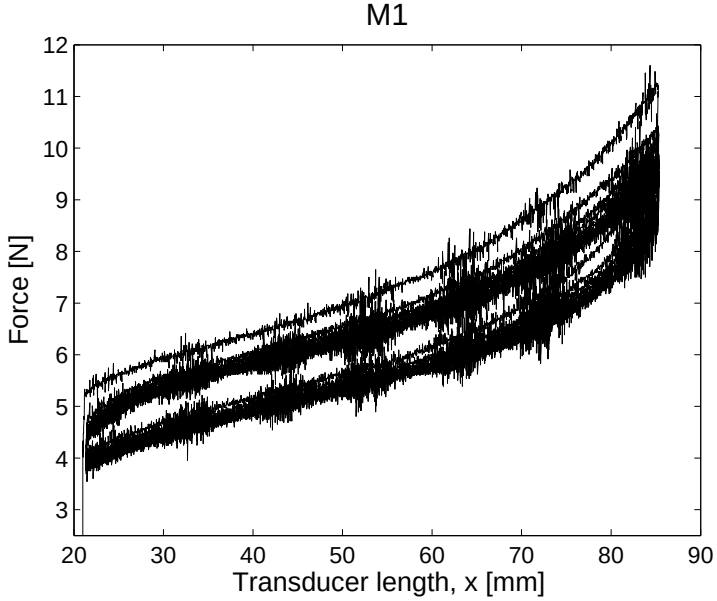

Figure 2-23 - Experimental force displacement curve for membrane 1 (M1)

In Figure 2-23 the measured data for one of the membranes, before the conditioning, are shown: beyond the noise due to the measurement equipment, it is possible to notice that the mechanical response of the material is repeatable only after the first cycles. In the plot of Figure 2-23, the force offset due to friction and inertia are not yet corrected.

Experimental data have been filtered using a moving average filter with span of 41 samples.

Moreover, since the experimental Force-Displacement curves present some remaining hysteresis, an average equilibrium response has been calculated as the average between the loading and unloading curve.

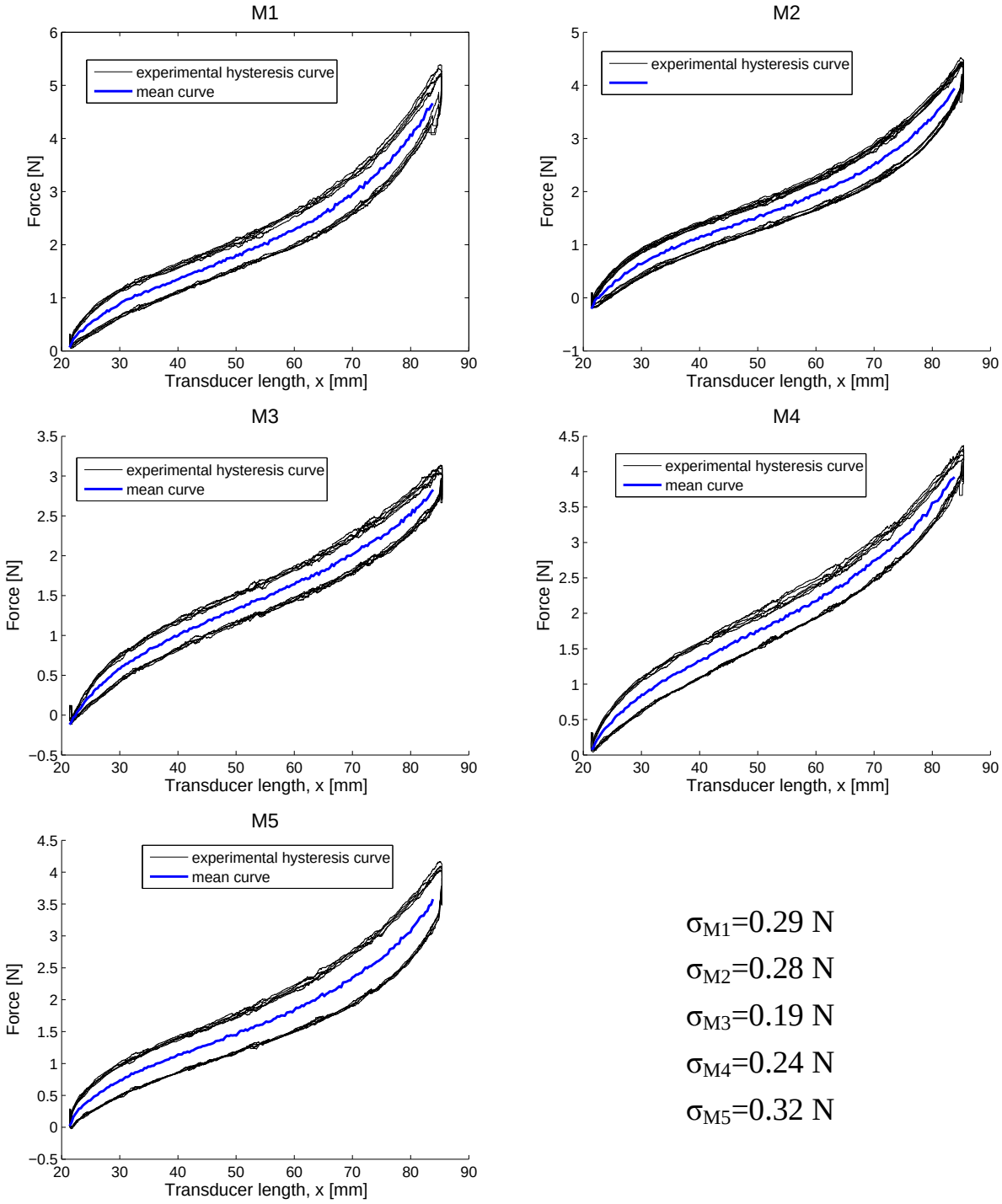

Figure 2-24 - Force-displacement curves for different samples

Results for the 5 films and corresponding mean square root are presented in the plots in Figure 2-24.

The characterization procedure described in the next paragraph is applied to the average equilibrium curves for the various membranes. In the following of the thesis, hysteresis will

be always neglected. This represents quite a strong assumption: the equilibrium curve describes, in fact, the limit behavior of the material corresponding to a deformation velocity which tends to zero. Effectively, when the material is subjected to very small deformations, it can be assumed that the membrane experiments reversible transformations only, moving through a set of equilibrium states.
Making use of the mean equilibrium curve corresponds to take the assumption of quasi-static behavior of the material.
Real applications of DEGs always imply non-negligible velocities, with corresponding hysteresis phenomena that causes part of the energy to be degraded.
Deeper analyses of DEGs should then keep into account the hysteretic phenomena implementing some type of viscoelastic model for the material.

2-2.3.4 Hyperelastic models and fitting results

Until now, it has been stated that the strain-energy function ψ is a function of the principal stretches λ_1, λ_2 and λ_3 (or λ_1 and λ_2 only if incompressibility is assumed). The mathematical form of the strain energy function depends on the constitutive model adopted for the material.
Constitutive models can be divided into phenomenological and micro-mechanical models [76].
Phenomenological models describe the macroscopic nature of materials as continua: they are mainly concerning with fitting mathematical equations to experimental data but are not capable of taking into account the microscopic physical behavior of the material [55].
Micro-mechanical models are intrinsically tied to high computational costs, but they have the advantage of relating material macroscopic mechanical behavior to the causative physical-chemical structure.
In the present work, some traditional phenomenological models only have been considered.
The selected models are briefly described in the following and results of the experimental fittings are presented.
A complete overview on the most well-known hyperelastic models for rubber-like materials is presented by Steinmann et . al. [76], which present a review of the models commonly used in literature and applies them to the fitting of Treolar data [77], a set of measurements on vulcanized rubber that are commonly used in literature to evaluate the performance of new constitutive models.
In most general cases the strain-energy function is formulated in terms of strain invariants I_1, I_2, I_3:

$$\psi = \psi(I_1, I_2, I_3)$$

with

$$I_1 = {\lambda_1}^2 + {\lambda_2}^2 + {\lambda_3}^2$$

$$I_2 = {\lambda_1}^{-2} + {\lambda_2}^{-2} + {\lambda_3}^{-2}$$

$$I_3 = \lambda_1 \lambda_2 \lambda_3$$

For incompressible materials

$$I_1 = {\lambda_1}^2 + {\lambda_2}^2 + {\lambda_1}^{-2}{\lambda_2}^{-2}$$

$$I_2 = {\lambda_1}^{-2} + {\lambda_2}^{-2} + {\lambda_1}^2{\lambda_2}^2$$

$$I_3 = 1$$

And the strain-energy function takes the form $\psi = \psi(I_1, I_2)$.

All the presented models are in this form except for Ogden model, that is a quite sophisticated model in a more general mathematical form.

In its most general form, the strain-energy function for incompressible materials is written as $\psi = \psi(\lambda_1, \lambda_2)$.

Using the considerations mentioned in paragraph 2-2.2, the force on the joint of the transducer can be expressed as a function of λ_1 and λ_2 only in the following form:

$$F = \frac{t_0}{2}\left(\frac{\sqrt{4\ell^2 - {x_p}^2}}{\lambda_{2p}}\frac{\partial\psi}{\partial\lambda_1} - \frac{\lambda_1}{\lambda_2}\cdot\frac{\lambda_{2p}{x_p}^2}{{\lambda_{1p}}^2\sqrt{4\ell^2 - x^2}}\frac{\partial\psi}{\partial\lambda_2}\right)$$

Of course, since the position of the transducer is uniquely described by the variable x, the force may be expresses as a function of λ_1 (or λ_2) only. However, in order to carry out the fitting of hyperelastic materials to experimental data, the form above is used (in order to obtain results that can be extrapolated to strain fields different from those examined in this particular application).

From experimental measurements, the equilibrium force *F* of the device vs. the longitudinal length of the frame *x* is known (Figure 2-24). Since the pre-stretches of the single films are known, each position is directly related to a couple of corresponding values of the stretches $(\lambda_1; \lambda_2)$.

The data for the various films can be collected together and a two-variables fitting can be done using the expression above for the force *F*, being λ_1 and λ_2 the independent variables and the force values the interpolation variable.

The fitting procedure has been carried out in Matlab, using the command *lsqnonlin* from the Optimization Toolbox. This command is used to perform non-linear fitting, given a proper interpolation algorithm. The least-squares algorithm chosen for this particular application, among those supported by the *lsqnonlin* command, was Levenberg-Marquardt algorithm, that is commonly adopted for this type of applications [78].

In the following, we briefly describe the considered hyperelastic models and show the corresponding results.

In order to evaluate the quality of the fitting, the Mean Square Error (MSE) has been used as parameter.

Given a set of n experimental points, indicating with F_e the measured experimental value of the force and with F_{th} the theoretical value obtained applying the fitting parameters of the model in exam, MSE is defined as

$$MSE = \frac{\sum_i^n \left(F_{th,i} - F_{e,i}\right)^2}{n}$$

Ogden model

A sophisticated class of models used for the description of rubber-like materials goes under the name of 'Ogden models'. The free energy function ψ is expressed as a finite sum of powers of the principal stretches λ_i:

$$\psi = \psi(\lambda_1, \lambda_2, \lambda_3) = \sum_{p=1}^{N} \frac{\mu_p}{\alpha_p} \left({\lambda_1}^{\alpha_p} + {\lambda_2}^{\alpha_p} + {\lambda_3}^{\alpha_p} - 3\right)$$

where μ_p are shear moduli and α_p are dimensionless constants, and N is a positive integer which determines the order of the strain-energy function.

In order to obtain a physically plausible solution, a sufficient condition that guarantees stability is given by

$$\mu_p \alpha_p > 0 \qquad \forall\, p$$

For the present work, a second order Ogden model has been selected; the above mentioned sufficient condition has been imposed as constraint for the fitting.

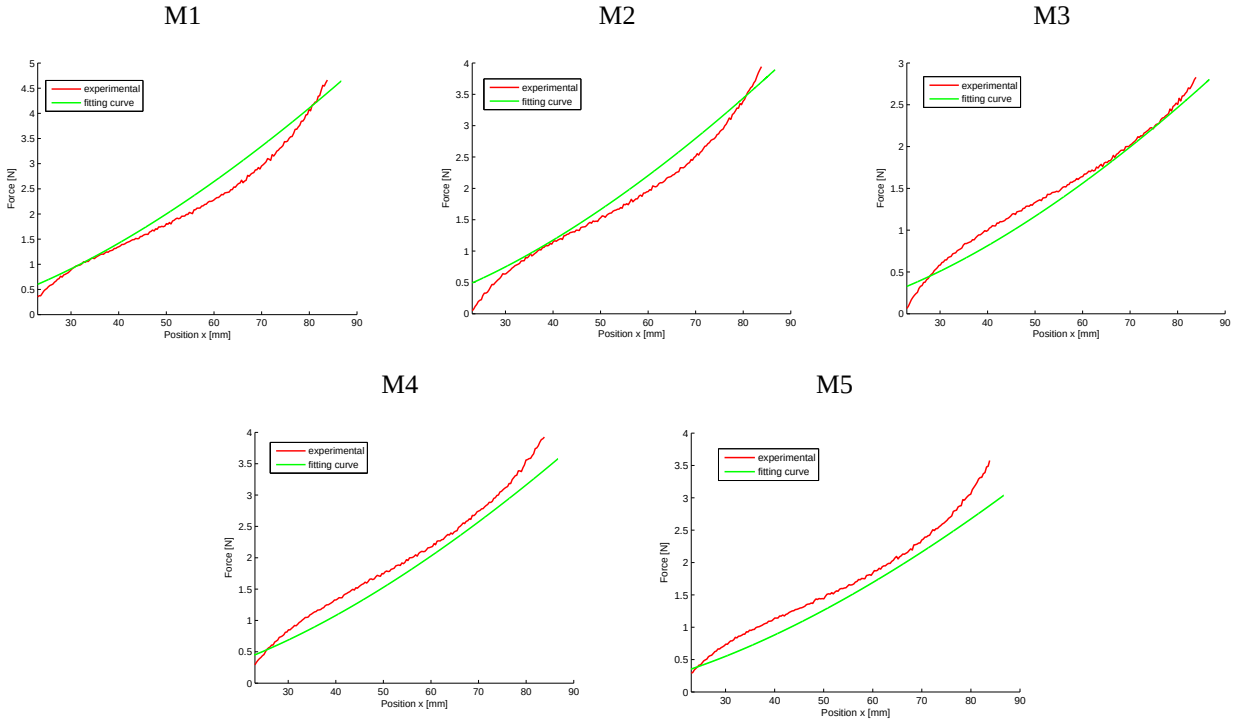

Figure 2-25 - Ogden model fitting

Considering the hypothesis of incompressibility, thus, the final adopted form for ψ results

$$\psi = \psi(\lambda_1, \lambda_2) = \sum_{p=1}^{2} \frac{\mu_p}{\alpha_p} \left({\lambda_1}^{\alpha_p} + {\lambda_2}^{\alpha_p} + {\lambda_1}^{-\alpha_p}{\lambda_2}^{-\alpha_p} - 3\right)$$

The interpolation on the five membranes has produced the following fitting parameters:

$$\mu_1=-1.01\ \text{Pa} \quad ; \quad \mu_2=8.0e3\ \text{Pa} \quad ; \quad \alpha_1=-2.0 \quad ; \quad \alpha_2=2.48$$

with MSE=0.045 N^2.

In the next set of plots (Figure 2-25), for each of the 5 films, we report experimental mean curves, obtained in accordance to the procedure described in paragraph 2-2.3.3, and fitting curves, obtained using the determined parameters and the presented constitutive model.

Ogden model represents somehow exception with respect to the other referenced hyperelastic models, since it relates the function ψ to generic powers of the stretches. All the models presented herein link the free energy function directly to the invariants I_1 and I_2.

Neo-Hooke model

Neo-Hooke is the simplest constitutive hyperelastic model, since it relates the function ψ with the first invariant I_1 postulating a linear link.

$$\psi = \frac{\mu}{2}(I_1 - 3)$$

Beyond its extreme simplicity, Neo-Hooke model presents the disadvantage of providing only an approximate low-accuracy result for the fitting procedure.

The estimated shear modulus results in

$$\mu=1.94e4 \quad \text{Pa}$$

and the corresponding MSE is MSE=0.115 N^2.

As evident from Figure 2-26, the result of the fitting is quite poor.

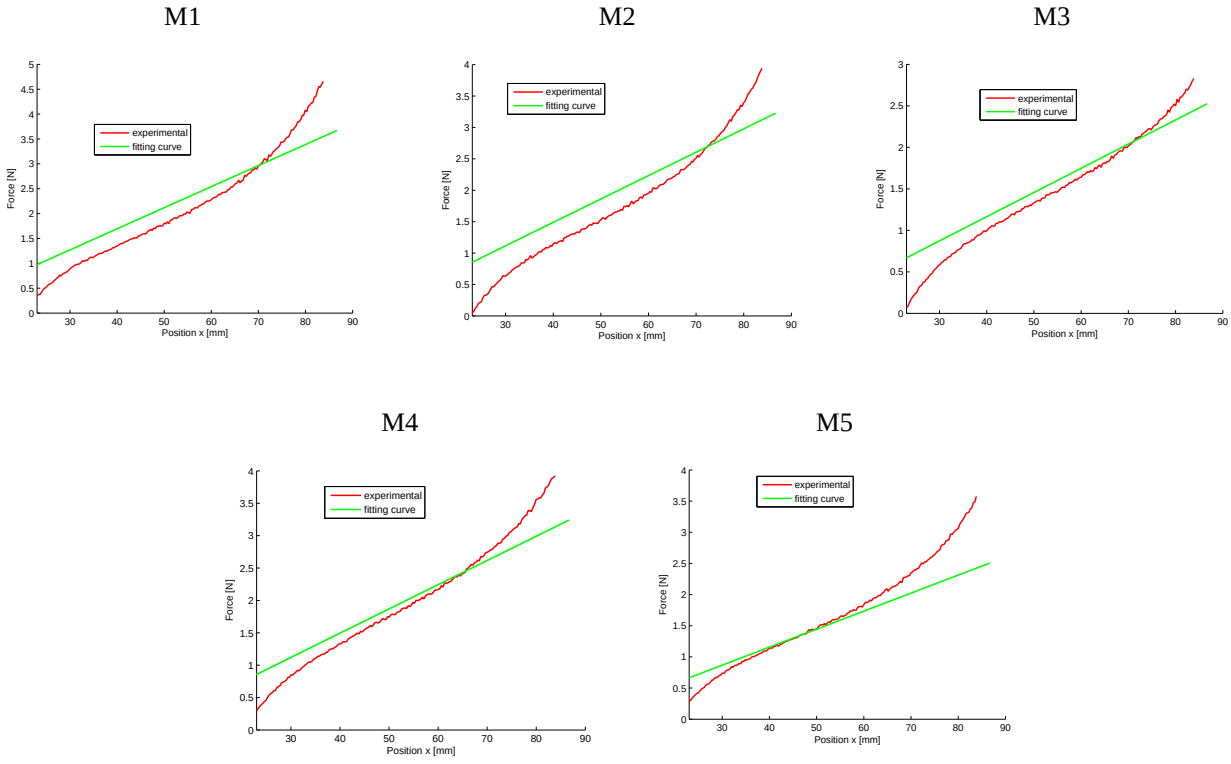

Figure 2-26 - Neo-Hooke model fitting

Mooney-Rivlin model

Mooney-Rivlin model can be considered a particularization of Ogden second order model. Putting N=2, α_1=2 and α_2=-2, the Ogden constitutive equations takes the form

$$\psi = C_1(I_1 - 3) + C_2(I_2 - 3)$$

that is the so-called Mooney-Rivlin model.

Results for the fitting are

$$C_1 = 1.63e4 \text{ Pa} \quad ; \quad C_2 = -3.0e2 \text{ Pa}$$

With MSE=0.096 N^2.

Notice that, referring to the analogy between the Mooney-Rivlin model and the Ogden model under the mentioned conditions, the coefficients C_1 and C_2 are related to the corresponding Ogden parameters by equations

$$C_1 = \mu_1/\alpha_1$$

$$C_2 = \mu_2/\alpha_2$$

and the sufficient stability condition $\mu_p\alpha_p > 0$ corresponds to $C_1 > 0 \ \cap \ C_2 > 0$.

In order to guarantee a better accuracy for the fitting, this condition has not been imposed as constraint for the fitting, and a negative value of C_2 has been obtained. In any case, for the Mooney-Rivlin model, a weaker condition of stability exists, involving the equivalent shear modulus [55]:

$$\mu = 2(C_1 + C_2) > 0$$

The fitting parameters largely meet this condition, so that the model results stable.

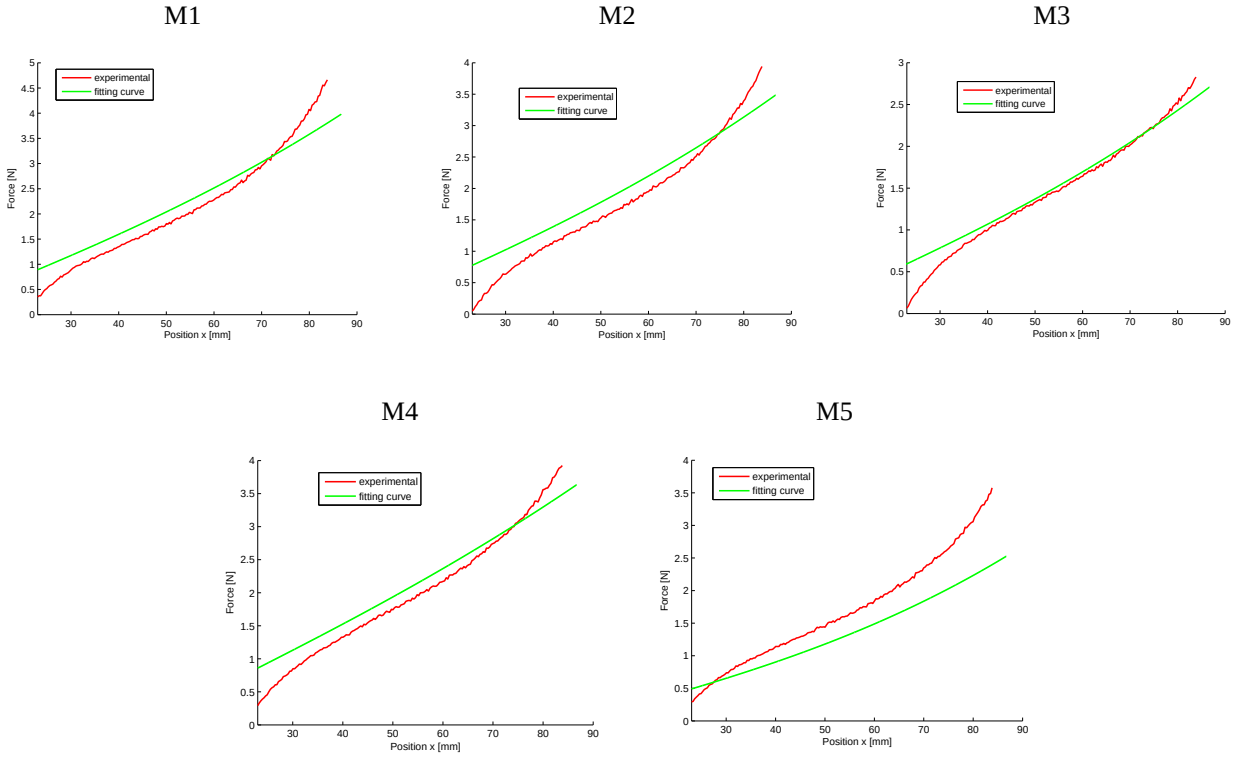

Figure 2-27 - Mooney-Rivlin model fitting

Gent-Thomas model

This two-parameter model is similar to Mooney-Rivlin, but the dependence on the second invariant is expressed in logarithmic form:

$$\psi = C_1(I_1 - 3) + C_2\, ln\left(\frac{I_2}{3}\right)$$

The result for the fitting is

$$C_1\text{=1.09e4 Pa} \quad ; \quad C_2\text{=-3.29e4 Pa}$$

with MSE=0.054 N^2.

Graphical results from Figure 2-28 show that this model, differently from the other considered so far, is particular suitable to describe the non-linear behavior of the material at low stress values, while it is weak in the interpolation of the super-linear part of the response corresponding to high force values.

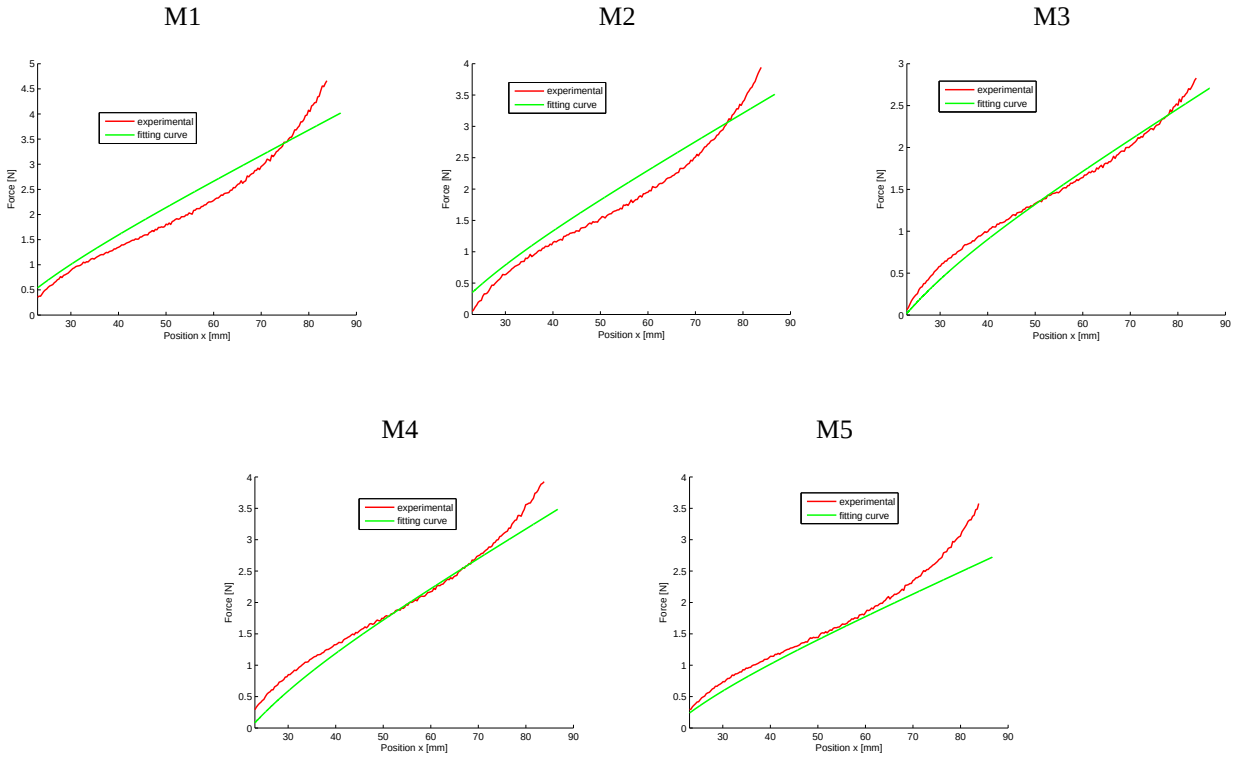

Figure 2-28- Gent-Thomas model fitting

Carroll model

This is a relatively recent model, proposed in 2011 by Caroll [79]. The model has been derived applying Neo-Hooke model to Treolar data. Successively, in order to improve the fitting, a term proportional to ${I_1}^4$ has been added; finally, an addendum proportional to $\sqrt{I_2}$ was introduced.

The resulting strain-energy function has equation

$$\psi = aI_1 + b{I_1}^4 + c\sqrt{I_2}$$

For the reference VHB acrylic, the following data have been obtained:

$$a\text{=1.10e4 Pa} \quad ; \quad b\text{=8.78e-4 Pa} \quad ; \quad c\text{=-4.20e3 Pa}$$

with mean square error MSE=0.041 N^2.

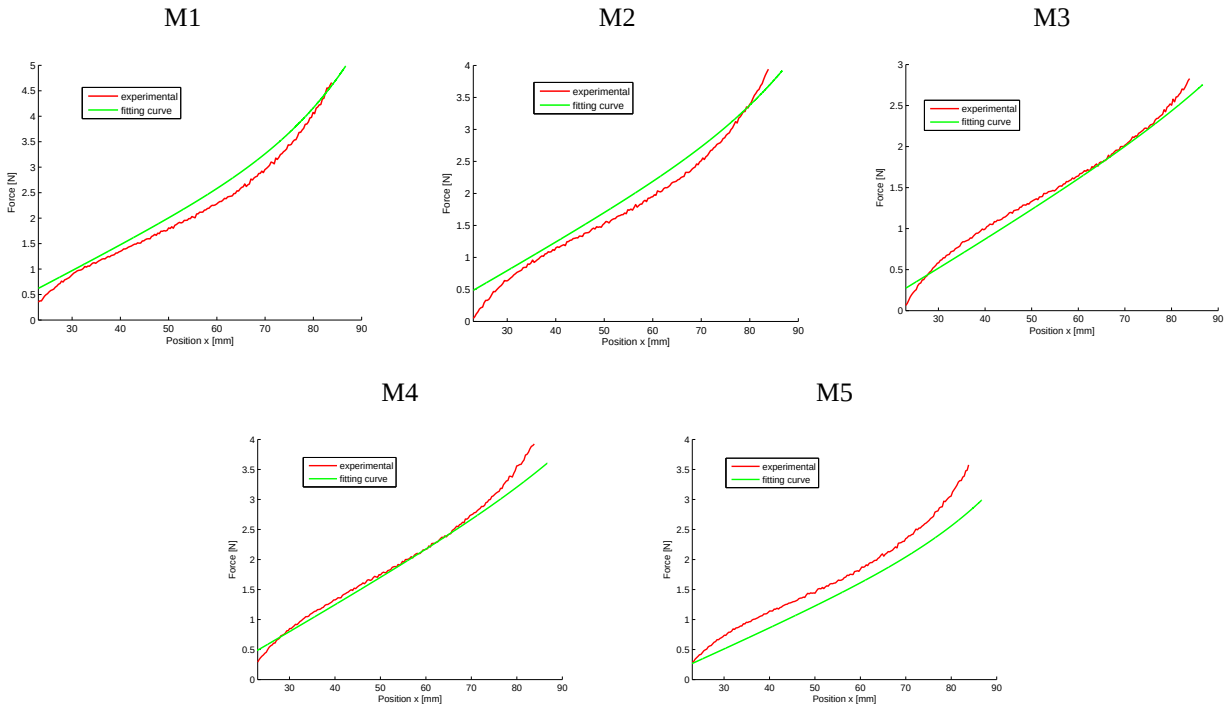

Figure 2-29 - Carroll model fitting

Yeoh model

Many practical engineering elastomers contain reinforcing fillers such as carbon black or silica, with the aim of improving the physical properties (tensile and tear strength) of the material. The resulting stress-strain behavior is highly non-linear [55].

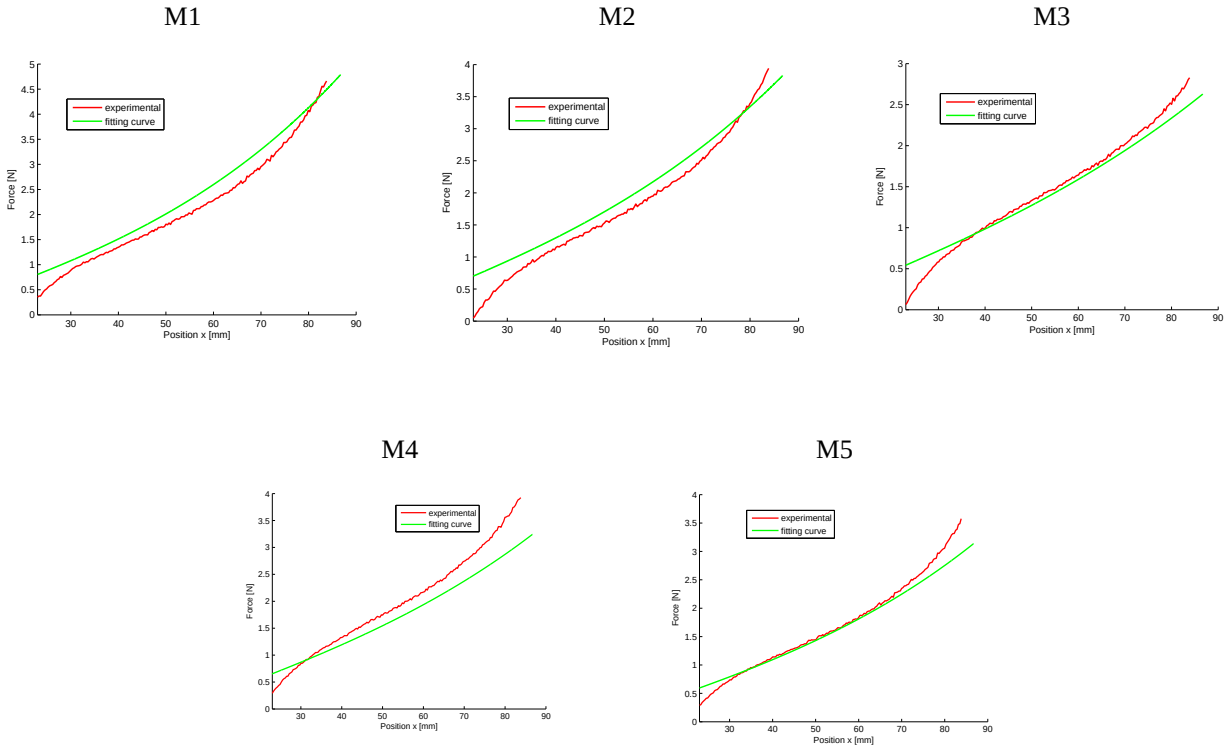

Figure 2-30 - Yeoh model fitting

Yeoh model bases on the experimental evidence that filled elastomers exhibit almost zero values of the term $\partial\psi/\partial\lambda_2$. The result is a three-term free energy function where the second invariant does not appear:

$$\psi = C_1(I_1 - 3) + C_2(I_1 - 3)^2 + C_3(I_1 - 3)^3$$

The result of the fitting on the acrili data is

C_1=6.26e3 Pa ; C_2=22.61 Pa ; C_3=3.13e-2 Pa

with MSE=0.058 N^2.

Gent model

A sophisticated two-parameter model is 'Gent model'. This model is based on the concept of limited chain extensibility, and is thus designed to have a singularity when the first invariant I_1 reaches a limit value I_m.

The model, in its basic formulation, has the following strain-energy function expression:

$$\psi = -a\, ln\left(\frac{I_m - I_1}{I_m - 3}\right)$$

or, alternatively, the mathematical equivalent formulation

$$\psi = -I_m \frac{\mu}{2}\, ln\left(\frac{I_m - I_1}{I_m - 3}\right)$$

where μ is the shear-modulus of the elastomer.

In a more sophisticated formulation, proposed by Caroll [79], a second addendum, depending on the second invariant I_2, has been introduced to improve the fitting with Treolar data.

The 'augmented Gent model' has the following form:

$$\psi = -a\, ln\left(\frac{I_m - I_1}{I_m - 3}\right) + b\sqrt{I_2}$$

We refer to this last form of the Helmoltz free energy function, the resulting fitting parameters are

a=4.09e6 Pa ; b=-3.685e3 Pa ; I_m=430.9

with an error MSE=0.040 N^2.

In Figure 2-31, we report the experimental curves, the fitting curves with the presented parameters and the same curves using the fitted values for a and I_m but assuming the second term $b\sqrt{I_2}$ equal to zero.

It is immediate to notice that the effect of the second term is irrelevant. Therefore, the model can be used in its base formulation, with parameters

a=4.09e6 Pa ; I_m=430.9

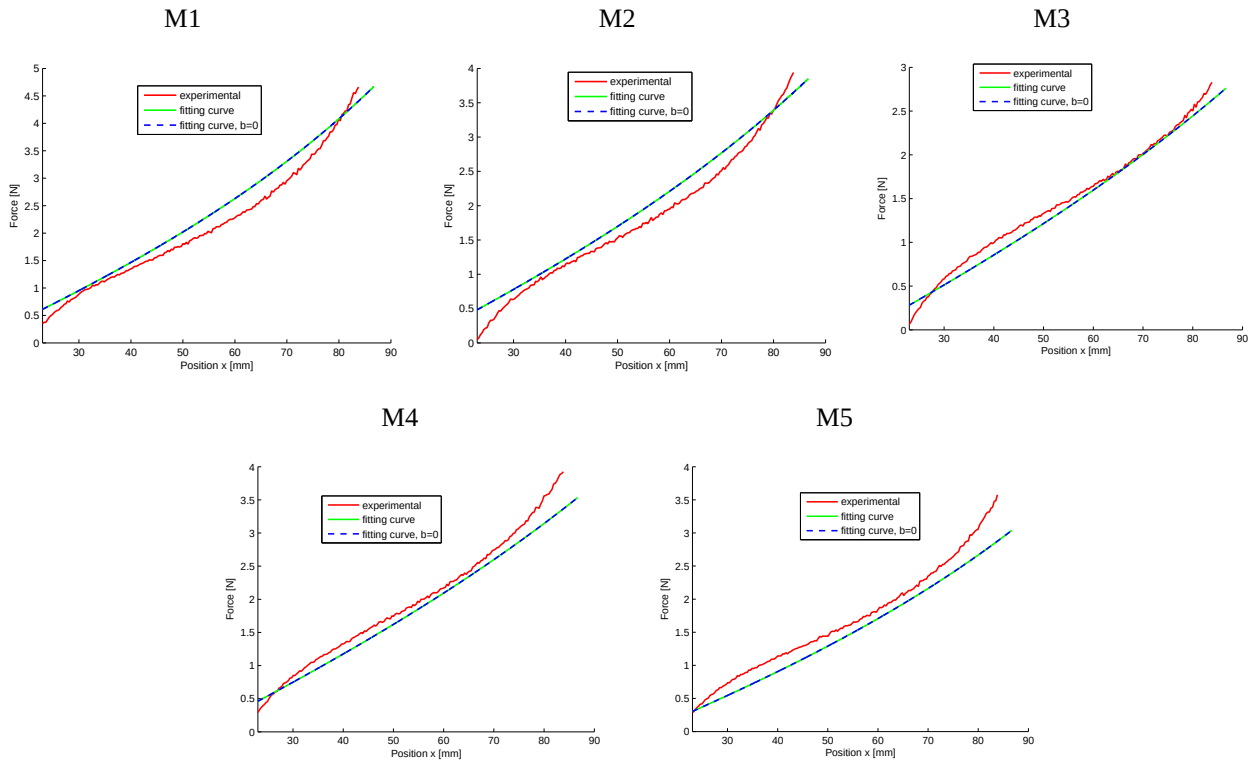

Figure 2-31 - Gent and augmented Gent models fitting

Arruda-Boyce model

A classical hyperelastic model is 'Arruda-Boyce model'. This is a statistical models where the parameters are physically linked to the chain orientations involved in the deformation of the three-dimensional network structure of the material.

The Arruda-Boyce model is generally presented as a series, originated from the Taylor expansion of Langevin function, usually limited to five terms, in the form

$$\psi = \mu \sum_{k=1}^{5} \frac{C_k}{N^{k-1}} \left[{I_1}^k - 3^k \right]$$

with $[C_1, C_2, C_3, C_4, C_5] = \left[\frac{1}{2}, \frac{1}{20}, \frac{11}{1050}, \frac{19}{7000}, \frac{519}{673750}\right]$.

The parameters μ and N represent respectively the shear modulus and the Kuhn number.

The fitting provides an error MSE=0.059 N^2, and the following values for the parameters:

$$\mu = 1.43e4 \quad Pa \quad ; \quad N = 60.52$$

According to the physical meaning of Kuhn number (that is the number of segments in a chain, freely joined together at chemical cross-links), N should be a natural number. For the sake of simplicity, no constraints have been put on the fitting parameters, and the resulting value of N is a real number.

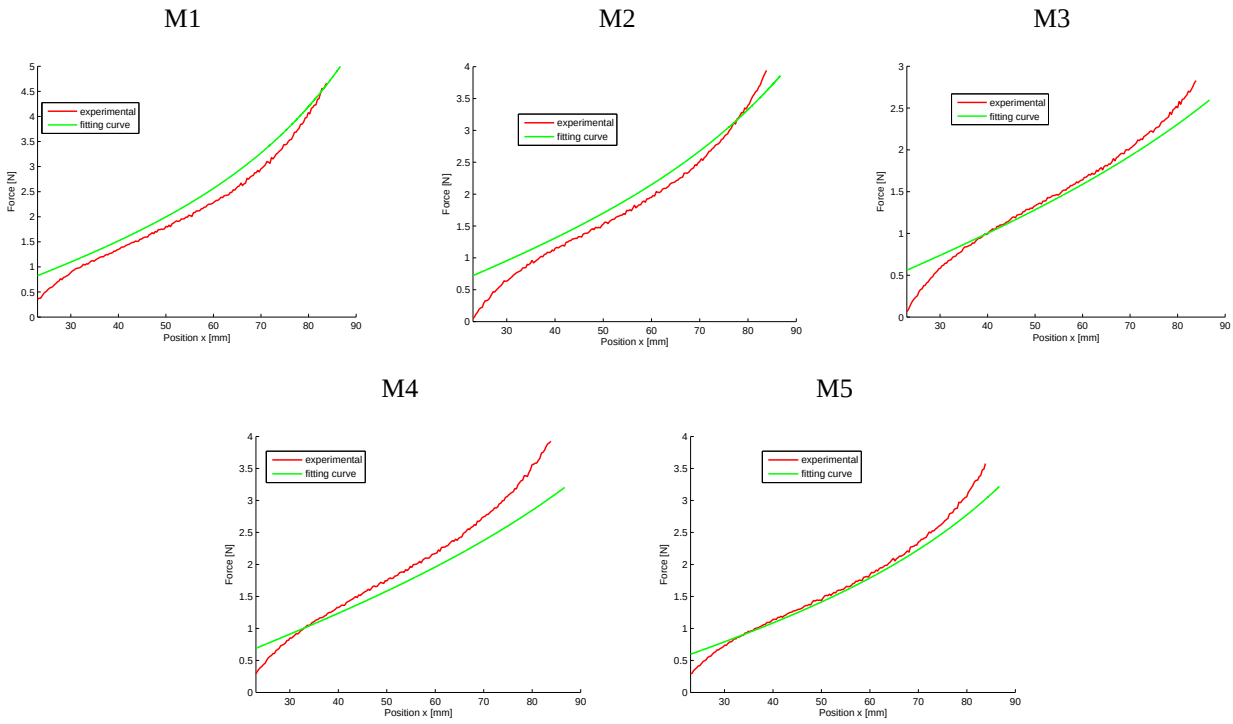

Figure 2-32 - Arruda-Boyce model fitting

Synthesis of the results

In the following, a schematic resume of the fitting results for the different hyperelastic models is presented

Model	*Strain-energy function form*	*Parameters*
Ogden	$\psi = \sum_{p=1}^{2} \frac{\mu_p}{\alpha_p}(\lambda_1{}^{\alpha_p} + \lambda_2{}^{\alpha_p} + \lambda_1{}^{-\alpha_p}\lambda_2{}^{-\alpha_p} - 3)$	$[\mu_1 ; \mu_2]$=[-1.01 ; 8.0e3] Pa $[\alpha_1 ; \alpha_2]$=[-2.0 ; 2.48]
Neo-Hooke	$\psi = \frac{\mu}{2}(I_1 - 3)$	μ=1.94e4 Pa
Mooney-Rivlin	$\psi = C_1(I_1 - 3) + C_2(I_2 - 3)$	C_1=1.63e4 Pa ; C_2=-3.0e2 Pa
Gent-Thomas	$\psi = C_1(I_1 - 3) + C_2\, ln\left(\frac{I_2}{3}\right)$	C_1=1.09e4 Pa ; C_2=-3.29e4 Pa
Carroll	$\psi = aI_1 + bI_1{}^4 + c\sqrt{I_2}$	a=1.10e4 Pa; b=8.78e-4 Pa; c=-4.20e3 Pa
Yeoh	$\psi = C_1(I_1 - 3) + C_2(I_1 - 3)^2 + C_3(I_1 - 3)^3$	C_1=6.26e3 Pa ; C_2=22.6 Pa C_3=3.13e-2 Pa
Gent	$\psi = -a \ln\left(\frac{I_m - I_1}{I_m - 3}\right)$	a=4.09e6 Pa ; I_m=430.9
Arruda-Boyce	$\psi = \mu \sum_{k=1}^{5} \frac{C_k}{N^{k-1}}\left[I_1{}^k - 3^k\right]$ with $[C_1, C_2, C_3, C_4, C_5] = \left[\frac{1}{2}, \frac{1}{20}, \frac{11}{1050}, \frac{19}{7000}, \frac{519}{673750}\right]$	μ=1.43e4 Pa N=60.52

2-2.4 Mathematical model

In the present paragraph, a mathematical model for the LS-DEG is presented. The aim of the model is the construction of the ECC of the generator in the Q-V plane.

In paragraph 2-2.2, a first geometric description of the system has been presented, and a definition for the values of the stretches λ_1 and λ_2 has been given.

The present analysis starts from the presupposition that the generator is, as a matter of fact, a variable surface capacitor.

For this reason, two useful equations are those that express the link between the stretches and the area of the compliant electrodes (in the configuration identified by the values of the stretches). Remembering that the area of the lozenge is $A = xy/2$, the following equations are derived:

$$\lambda_1 = \frac{\lambda_{1p}}{x_p}\sqrt{2\ell^2 - 2\sqrt{\ell^4 - A^2}}$$

$$\lambda_2 = \frac{\lambda_{2p}}{y_p}\sqrt{2\ell^2 + 2\sqrt{\ell^4 - A^2}}$$

$$\lambda_3 = \frac{x_p y_p}{2\lambda_{1p}\lambda_{2p}A}$$

Considering, in addition, the definition of capacitance, $C = \frac{Q}{V} = \frac{\varepsilon A}{t} = \frac{\varepsilon A^2}{B}$, stretches can be also related to charge and voltage, *Q* and *V*:

$$\lambda_1 = \frac{\lambda_{1p}}{x_p}\sqrt{2\ell^2 - 2\sqrt{\ell^4 - \frac{BQ}{\varepsilon V}}}$$

$$\lambda_2 = \frac{\lambda_{2p}}{y_p}\sqrt{2\ell^2 + 2\sqrt{\ell^4 - \frac{BQ}{\varepsilon V}}}$$

$$\lambda_3 = \frac{x_p y_p}{2\lambda_{1p}\lambda_{2p}}\sqrt{\frac{\varepsilon V}{BQ}}$$

where ε is the dielectric constant of the material $\varepsilon = \varepsilon_r\varepsilon_0$and *B* is the employed polymeric volume. For the acrylic polymer, a plausible value of the relative dielectric constant is $\varepsilon_r = 4.5$ [60].

In accordance with the procedure presented by Koh et al. [72], basing on the previous equations, a mathematical expression for the various constraints limiting the producible energy are found. The ECC is bounded by a series of conditions involving both the geometry of the system and the failure conditions that affect the polymer electro-mechanical behavior.

Geometric constraint: in the previous equations, the argument of the square root has to be positive. This yields the limit curve

$$V = \frac{B}{\varepsilon \ell^4} Q$$

The physical meaning of this conditions is that, since the maximum capacitance of the device occurs when $x = \sqrt{2}\ell$, configurations with $x \geq \sqrt{2}\ell$ are not considered, since they bring to a reduction of the capacitance that is equivalently achieved by reducing *x* with respect to the square configuration.

In other words, each configuration with $x \geq \sqrt{2}\ell$ is the dual of a configuration with $x \leq \sqrt{2}\ell$, having the same surface and, thus, the same capacitance. For this reason, the cyclic operation of a LS-DEG can be uniquely described by referring to a stroke included in the interval $x \in [0; \sqrt{2}\ell]$.

Electric break-down: the electric field *E* acting across the LS-DEG cannot exceed the dielectric strength E_{BD} of the considered DE material, namely $E \leq E_{BD}$. Assuming a constant value for the break-down field, by the definition of capacitance, the electric break-down condition yields the following limit curve

$$VQ = \varepsilon B {E_{BD}}^2$$

that represents a hyperbola on the Q-V plane. Notice that this result is the same obtained under the hypothesis of equi-biaxial deformation (paragraph 2-1.6).

Mechanical rupture: the mechanical rupture of DE materials is usually expressed as a limitation on the values of the stretches. For LS-DEGs, there are two rupture conditions: $\lambda_1 \leq \lambda_u$ and $\lambda_2 \leq \lambda_u$.

Since the stretches are related to *Q* and *V* by the previous equations, it is possible to calculate two limit curves, that results in straight lines:

$$V = \frac{\frac{B}{\varepsilon} Q}{\ell^4 - \left(\ell^2 - \frac{{x_p}^2 {\lambda_u}^2}{2{\lambda_{1p}}^2}\right)^2}$$

$$V = \frac{\frac{B}{\varepsilon} Q}{\ell^4 - \left(\ell^2 - \frac{{y_p}^2 {\lambda_u}^2}{2{\lambda_{2p}}^2}\right)^2}$$

With regard to the value of λ_u, according to Vertechy [60] λ_u is equal to 5.5. This is a rather conservative value: experimental tests have been conducted even on larger deformation ranges. Assuming λ_u=5.5 allows both to prevent the material to creep and damage during the cyclic operation and, above all, since the material has been experimentally tested on a wider deformation range, to predict the behavior of the material in a range of deformations that has been completely characterized.

Loss of tension: to function properly, the DE membrane should not wrinkle. This requires the stresses σ_1 and σ_2 to be positive. Manipulating the expression for the electrically induced stress, the following form is obtained:

$$p = \frac{QV}{B}$$

and the loss-of-tension condition for *x* and *y* directions yields the following limit curves:

$$\lambda_1 \frac{\partial \psi}{\partial \lambda_1} = \frac{QV}{B}$$

$$\lambda_2 \frac{\partial \psi}{\partial \lambda_2} = \frac{QV}{B}$$

Among all the failure conditions, loss of tension is the only one that depends on the constitutive equations of the material. Thus, the prediction of loss of tension is generally related to the specific form of the free energy function that is chosen to describe the elastic behavior of the LS-DEG.

Three models have been selected among those presented in the previous paragraph: Ogden, Yeoh and Gent model.
Most of the calculations presented in the following are referred to these three different models, in order to make a comparison of the different results obtained by simply building the model on different hyperelastic models.

The set of limit curves presented above defines the operation domain of the LS-DEG in the *Q*-*V* plane.
In order to generalize the dissertation, making it fit to any possible choice of the lozenge dimensions and the material volume, we express in dimensionless terms the equations above.
We introduce the following dimensionless parameters:

$$x_p{}^* = \frac{x_p}{\ell} \quad ; \quad y_p{}^* = \frac{y_p}{\ell} = \sqrt{4 - x_p{}^{*2}}$$

$$Q^* = \frac{Q}{\varepsilon E_{BD} \ell^2}$$

$$V^* = \frac{V}{E_{BD} \frac{B}{\ell^2}}$$

Referring to the new variables, the limit curves assume the expressions below:

Dimensionless Geometric Constraint (GC): $V^* = Q^*$

Dimensionless electric break-down condition (BD): $Q^* V^* = 1$

Dimensionless mechanical rupture condition (MR):

$$V^* = \frac{Q^*}{1 - \left(1 - \frac{x_p{}^{*2} \lambda_u{}^2}{2 \lambda_1 p^2}\right)^2} \quad ; \quad V^* = \frac{Q^*}{1 - \left(1 - \frac{y_p{}^{*2} \lambda_u{}^2}{2 \lambda_2 p^2}\right)^2}$$

Dimensionless Loss of Tension Condition (LoT):

$$\lambda_1 \frac{\partial \psi}{\partial \lambda_1} = \varepsilon E_{BD}{}^2 Q^* V^* \quad ; \quad \lambda_2 \frac{\partial \psi}{\partial \lambda_2} = \varepsilon E_{BD}{}^2 Q^* V^*$$

Notice that the normalization process involves the geometry of the device only, not the material properties; thus, these equations make it possible to compare different devices with different dimensions but using the same polymeric material.

The limits determined by the introduced electromechanical failure conditions identify an area in the *Q**-*V** plane that represents the usable working space where the LS-DEG can operate safely.

Practical ECCs must lie within the maximal area cycle, the bounds of which are identified by the above mentioned constraints.

In the following, we will always refer to ECC with reference to maximal area cycles, made by a sequence of transformations representing the failure condition described so far.

The energy conversion cycle can now be represented in the *Q**-*V** plane. Any area on this diagram has the dimensions of the product *Q***V**, and represents then a dimensionless energy:

$$En^* = \frac{En}{\varepsilon {E_{BD}}^2 B}$$

2-2.5 Cycles optimization

2-2.5.1 ECCs on the *Q**-*V** plane

In the present section, the mathematical model (with some eventual integration or correction, specified each time) described in paragraph 2-2.4 is applied with the aim of assessing the maximal convertible energy from LS-DEGs operating in different modes.

The optimization described herein focuses on a precise parameter, that is the convertible energy per unit polymeric volume, *En*.

This is out of doubt a crucial quantity, since it allows to understand in which conditions a fixed amount of polymer produces the maximum amount of energy per cycle.

Of course, many possible different optimization approaches may be followed: instead of fixing the polymeric volume, constraint may be present on the maximum allowed thickness of the film, or on some other geometrical dimension. Some alternative cases are discussed and taken into account in the following.

As a matter of fact, the optimization of the producible energy per unit volume of DE material is recognized as the crucial parameter in a large part of the literature concerning DEGs [70] [71] [73].

Another aim of the present dissertation is the comparison of the effect on the ECCs of the different selected hyperelastic models (Ogden, Yeoh, Gent). The specific hyperelastic model influences the shape of LoT curves on the *Q**-*V** plane. As a consequence, using different mechanical models, different forecasts of the producible energy will be generated.

In the following, an example is reported that clarifies both the appearance of ECCs on the *Q**-*V** plane and the effect of the single hyperelastic models, once the other conditions and physical quantities are given.

First of all, a set of reference values (adopted for the present example and for any future calculation in this thesis) is established.

The reference physical quantities are:

- Rupture stretch for the VHB acrylic: λ_u=5.5.
- Dielectric constant: $\varepsilon = \varepsilon_r \varepsilon_0$ with ε_r=4.5 and ε_0=8.85e-12 F/m.
- Break-down field: different assumptions on the break-down field of the acrylic are done, and the adopted value is specified in each case. Vertechy et al. [60] propose a value E_{BD}=70 MV/m. Koh et al. [72] present a stretch-dependent form for the break-down field. In the example of Figure 2-33, a value E_{BD}=50 MV/m is considered.
- Pre-stretches represent the control variables. The optimum of the energy productivity is investigated using pre-stretches as independent variables. As already mentioned, the values of the pre-stretches are referred to the square configuration with $x^* = y^* = \sqrt{2}\ell$.

In Figure 2-33 the ECCs obtained with the different models are shown. The values of the pre-stretches are λ_{1p}=6 and λ_{2p}=2.

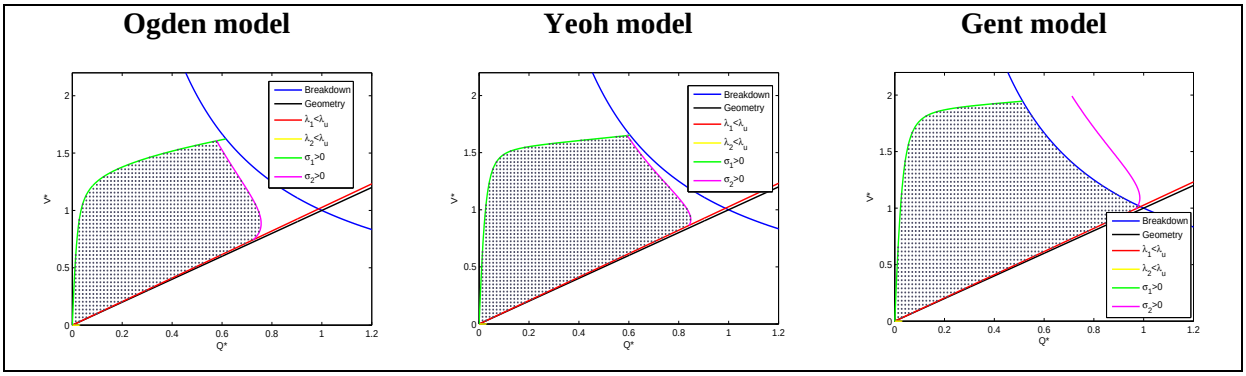

Figure 2-33 - Comparison of predicted energy density by three different hyperelastic models

In the examples of Figure 2-33, the ECC is identified by the curves representing the MR in *x* direction, the BD condition and the LoT conditions.

The condition $\lambda_2 \leq \lambda_u$ is met within the entire operating range, so that the corresponding line is out of the bounds of the figure.

Notice that any straight line passing through the origin of the axis represents an iso-stretch line, that corresponds to a precise configuration of the generator and, thus, to a specific value of capacitance. These lines can be regarded as iso-capacitance lines.

Since $\lambda_{1p} \geq \lambda_u$, the red lines represent the maximum length *x* allowed for the lozenge: exceeding this value, the pre-stretch in *x* direction would overpass the rupture value.

If we had $\lambda_{1p} \leq \lambda_u$, the energy extraction domain in the *Q**-*V** plane would be bounded by the black line, and not by the rupture line, meaning that the maximum transducer length corresponds with the maximum area configuration (square shape).

Notice how the three plots highlight that different hyperelastic models predict different values of producible electrical energy (that is the enclosed area of the cycle).

In the following, we consider some significant cases, based on different assumptions on the break-down field or on the operating configuration. For each examined case, an optimization of the producible energy density as a function of the pre-stretches λ_{1p} and λ_{2p} is carried out.

2-2.5.2 Constant Electric Break-down Condition

For the constant dielectric strength case, two different limit values have been considered: E_{BD} = 50 MV/m and E_{BD} = 70 MV/m. In Figure 2-34, the value of the convertible energy per unit volume as a function of λ_{1p}, for a set of values of λ_{2p}, is plotted.

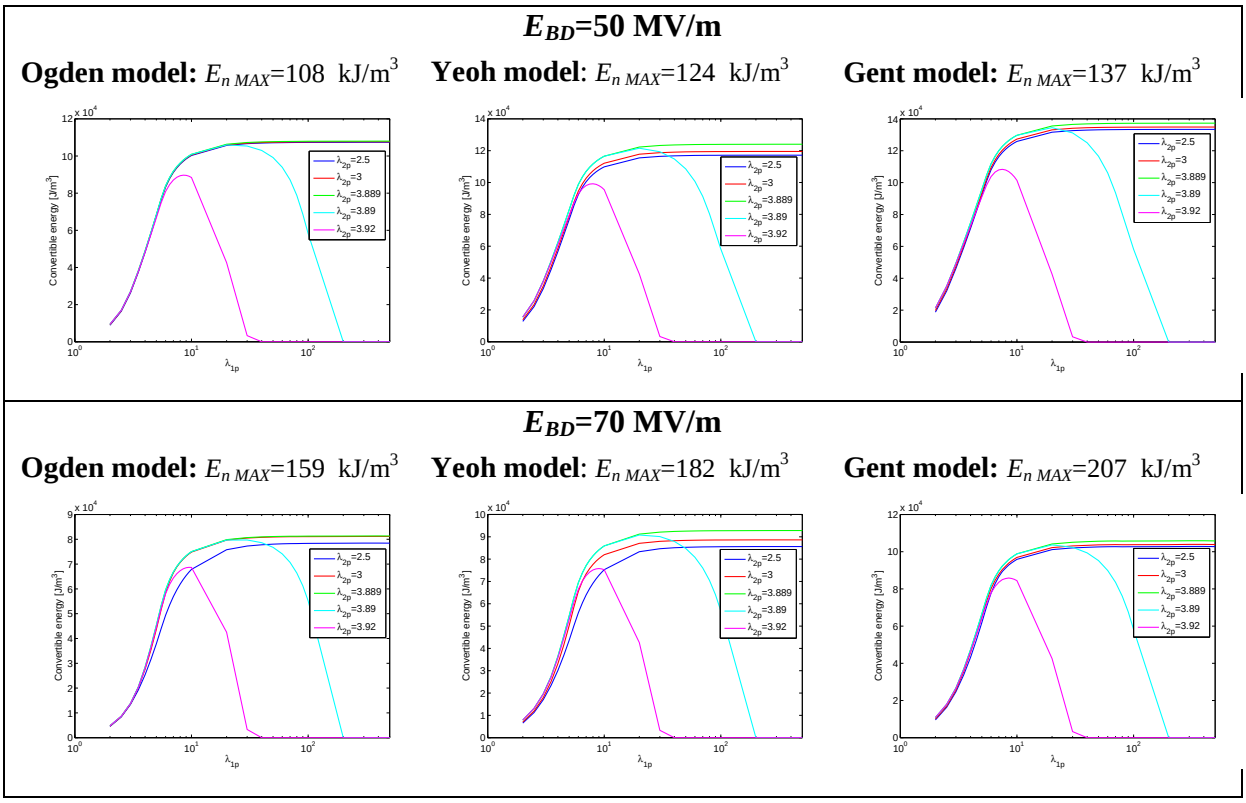

Figure 2-34 - Estimation of the maximum energy per unit volume for two different values of dielectric strength.

As shown, for an appropriate choice of λ_{2p}, the producible energy increases monotonically with λ_{1p}, reaching an asymptotic value (that is specified on the top of the graphs).

Since the maximum pre-stretch in *y* direction is reached for small apertures values of *x*, it is clear that a value of λ_{2p} exists that makes $\lambda_2=\lambda_u$ for $x^*=0$ (that implies $y^*=2$). With the reference value of λ_u=5.5, it is easy to see that the 'critical' value is

$$\lambda_{2p}^{c} = \frac{\sqrt{2}}{2}\lambda_u \cong 3.889$$

It is expectable that, for $\lambda_{2p} \geq \lambda_{2p}^{c}$, high values of λ_{1p} bring the convertible energy to 0. This is because the smallest reachable values of the variable *x*, for which λ_2 reaches the rupture value, becomes larger than the highest value of *x* permitted by the rupture condition on λ_1. Thus, for high values of both pre-stretches, there are no possible operative configurations for the LS-

DEG. Conversely, for $\lambda_{2p} \leq \lambda_{2p}^{c}$, the condition $\lambda_2 < \lambda_u$ is always satisfied and the producible energy increases with λ_{1p}.

Notice that, if λ_{1p} increases, x_A progressively tends to 0, and the stroke of the device tends to decrease, since, due to the high value of λ_{1p}, the rupture condition along x direction is met for small values of x_B. It is possible to conclude that a nearly optimal LS-DEG operates small strokes in the neighborhood of the configuration $x^*=0$.

Comparing the results of Figure 2-34, it is possible to notice that

- the dependence of the converted energy on the pre-stretch λ_{2p} (when lower than λ_{2p}^{c}) is weak (especially for the Ogden model); anyway, for all hyperelastic models, the optimal condition is met when $\lambda_{2p}=\lambda_{2p}^{c}$;
- the three hyperelastic models give significantly different predictions in term of maximum producible energy per unit volume;
- as expected, the producible energy increases as the dielectric strength of the DE material raises.

Since the optimal energy density is reached asymptotically, practical LS-DEGs should be designed keeping into account some feasibility criterion: for example, a LS-DEG can be designed to convert 95% of the maximum asymptotic energy density.

With reference to the case with E_{BD} = 50 MV/m, in Figure 2-35 we report the ECCs (in the Q^*-V^* plane) that result from a choice of λ_{1p} that guarantees the 95% of the asymptotic value of the energy density (assuming $\lambda_{2p} = \lambda_{2p}^{c}$).

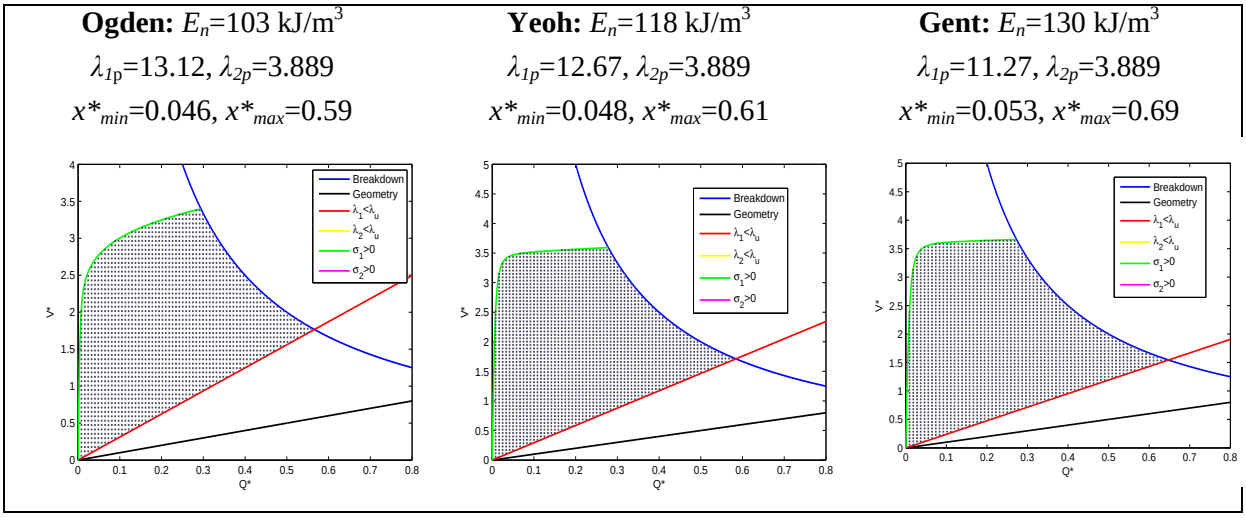

Figure 2-35 - Q*-V* plots of ECCs converting 95% of the asymptotic energy value

For such ECCs, the geometric displacement range is an interval $[x_A^*; x_B^*]$. The maximum value of the LS-DEG length, x_B^*, is given by the rupture limit on λ_1, thus

$$x_B^* = \frac{\lambda_u}{\lambda_{1p}} x_p{}^* = \sqrt{2}\frac{\lambda_u}{\lambda_{1p}}$$

The minimum value x_A^* depends on the LoT limit that is close to the end of the unloading phase and that is represented by the tangent to the curve $\{\sigma_1 = 0\}$ from the origin of the axes. Specifically,

$$x_A^* = \frac{\lambda_{1,min}}{\lambda_{1p}} x_p{}^* = \sqrt{2}\frac{\lambda_{1,min}}{\lambda_{1p}}$$

where $\lambda_{1,min}$ is obtained by solving equation

$$\lambda_1 \frac{\partial \psi(\lambda_1, \lambda_2(\lambda_1))}{\partial \lambda_1} = 0$$

The analysis described above does not consider the presence of specific design constraints such as mechanical end-stops of realistic mechanisms, and thickness limitations of commercial DE membranes. Inclusion of constraints of this kind could yield different results as it is shown below.

With respect to the considerations done so far, the polymeric membrane may be unable to reach the configuration $x^*=0$ due to the presence of mechanical ends, or of any type of geometric obstacle, like the housing of the joints of the lozenge mechanism. A mechanical end introduces a limitation on the minimum value $x_A{}^* = x_{min}{}^*$.

With reference to the experimental lozenge-shaped frame used for the mechanical experiments described in 2-2.3, a value of $x_{min}{}^*=0.26$ has been identified. For the electric break-down, a value of E_{BD}=50 MV/m has been hypothesized.

Results for the energy density are shown in Figure 2-36.

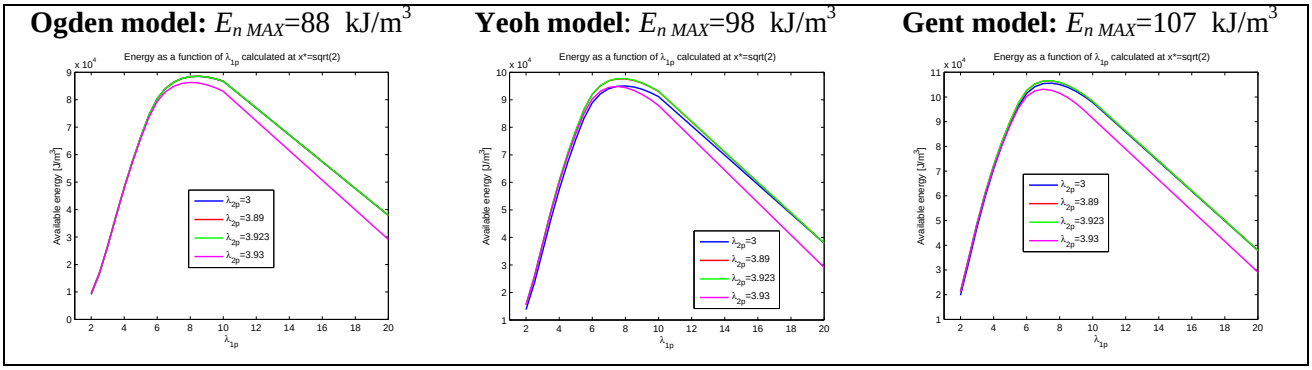

Figure 2-36 - Energy density vs. pre-stretches including the effect of mechanical end

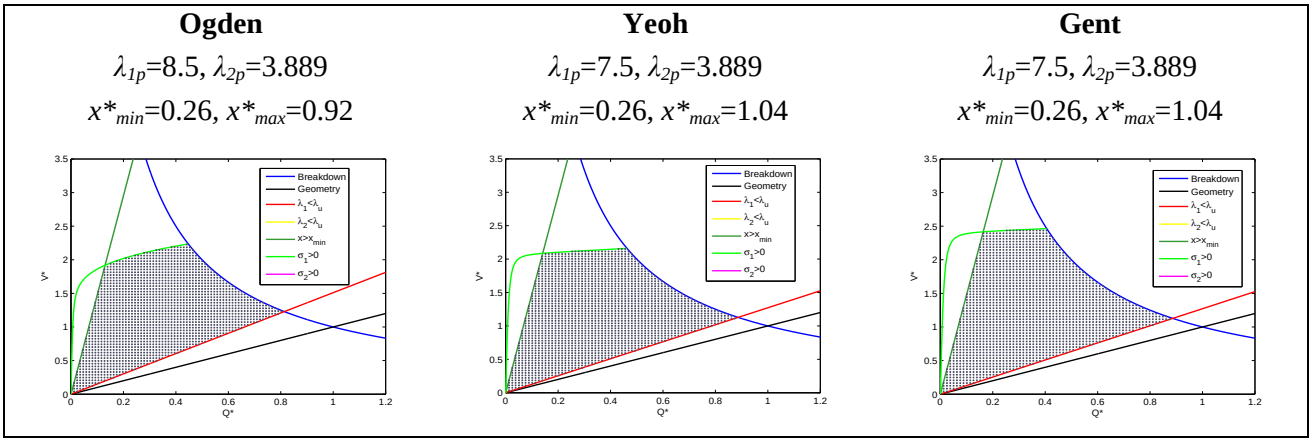

Figure 2-37 - *Q*-V plots of ECCs including the effect of a mechanical end**

Figure 2-36 provides the following insights:

- A critical value for λ_{2p} is identified by the condition

$$\lambda_{2p}^{c} = \frac{x_p^*}{x_{min}^*}\lambda_u$$

that is the value that brings to rupture ($\lambda_2 = \lambda_u$) when $x^* = x^*_{min}$. In this case, $\lambda_{2p}{}^{c}$ = 3.923. The optimal choice for λ_{2p} is $\lambda_{2p} = \lambda_{2p}{}^{c}$.

- A value of λ_{1p} exists that maximizes the producible energy per unit volume.

The optimal ECCs that result from the inclusion of the constraint $x^*_{min} = 0.26$ are shown in Figure 2-37 for the three considered hyperelastic models.

Finally, a constraint may be present on the thickness of the polymeric membrane present in a single frame.

It has been previously stated that, in absence of further constraints, an optimized LS-DEG is designed to operate with small stroke in the neighbourhood of the configuration $x^*=0$.
In such a configuration, if the required volume of polymer is fixed, the single LS-DEG device should house a very thick DE membrane, in order to compensate the low values of the surface of the electrodes to realize the desired volume.
Thick membranes may be obtained by superimpositions of several layers of DE commercial films (usually supplied with 0.5 or 1 mm thickness). Of course, technical limits exist, determined by the thickness of the rigid frame itself or by the available space in the specific assembly.
If a given volume of polymer is required for a certain application, a good solution for the implementation of a nearly optimal ECC (based on small strokes of the lozenge, and on small values of the transducer length x) is the modularization of the system: instead of using a single lozenge frame, housing the whole amount of DE material, the system may be split into several independent generators, each housing a given portion of material. This solution represents a complication in terms of electric control of the system, but offers some relevant advantage, like the possibility of activating a given fraction only of the overall material and a simplification in the maintenance operations (each membrane may be maintained separately, keeping the rest of the system in function).
The analysis of a limited thickness case is carried out introducing the energy per unit surface

$$En^s = En/\ell^2 = \frac{En \cdot x_0^* y_0^* t_0}{2B}$$

We consider here the case with E_{BD}=50 MV/m and t_0 = 1.5 mm.
Results of the optimization procedures are shown in Figure 2-38 that show the energy density as a function of the pre-stretches.
As shown, in case of thickness constraint, optimal values exist for both pre-stretches. Specifically, for a fixed surface of the initial sample, excessive values of λ_{1p} and λ_{2p} bring to very small volume of the DEG sample and, thus, to a significant reduction in the amount of energy that can be converted.

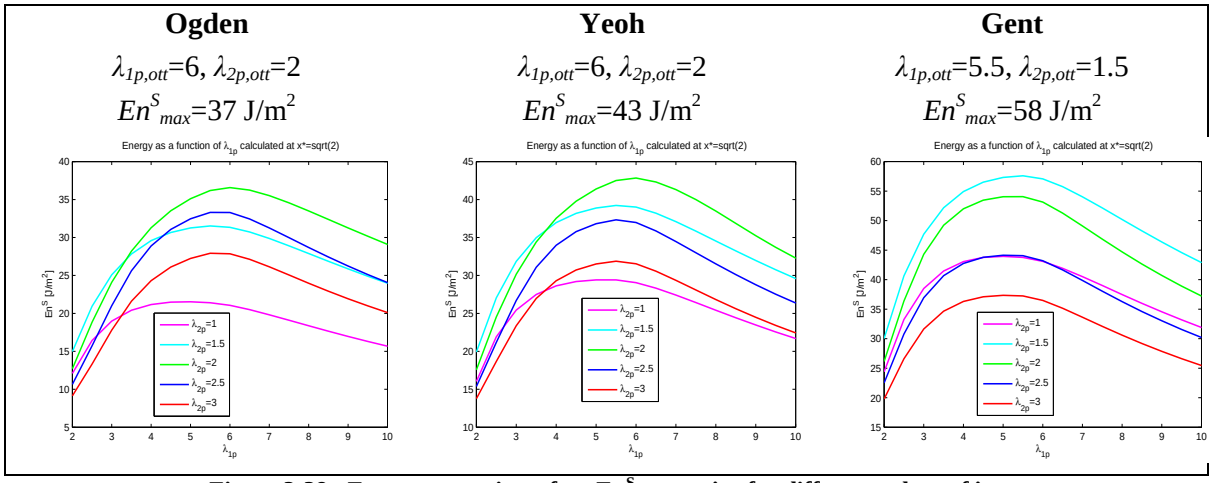

Figure 2-38 - Energy per unit surface En^S versus λ_{1p} for different values of λ_{2p}

2-2.5.3 Constant Electric Break-down Condition

In the previous sub-section, the hypothesis of constant dielectric strength for the considered DE material has been used. However, the dielectric strength may depend on stretch.

According to Koh et al. [72], in case of equi-biaxial deformation, the VHB acrylic has break-down field varying according to the relationship

$$E_{BD}(\lambda) = \bar{E}_{BD}\lambda^R$$

where λ is the stretch, $\bar{E}_{BD}$=30.6 MV/m and R=1.13.

For the lozenge-shaped generator, since the stretches λ_1 and λ_2 are generally different, a new formulation is here proposed.

In a study by Kofod et al. [80], for a film of polyacrilate subjected to biaxial deformation, the break-down field is related to the inverse of the thickness *t* after stretch. Since the volume *B* is constant (for the incompressibility hypothesis), *B=At*, so the inverse of the thickness is proportional to the surface of the film after deformation, and previous equation can be generalized to the form

$$E_{BD} = f\left(\frac{A}{A_0}\right)$$

For an equi-biaxial solicitation, $A/A_0=\lambda^2$, thus, if E_{BD} is thought as a function of the surface instead of the stretch, the above mentioned dependence of the break-down field on the deformation becomes

$$E_{BD}(A/A_0) = \bar{E}_{BD}(A/A_0)^{\frac{R}{2}}$$

For the LS-DEG,

$$\frac{A}{A_0} = \frac{xy}{x_0y_0} = \lambda_1\lambda_2$$

thus it is possible to conclude that

$$E_{BD}(\lambda) = \bar{E}_{BD}(\lambda_1\lambda_2)^{\frac{R}{2}}$$

With this assumption, the BD condition is represented by a different curve in the *Q*-*V* plane, represented by the equation

$$QV = \varepsilon B E_{BD}(1)^2(\lambda_1\lambda_2)^R$$

where λ_1 and λ_2 are a function of Q and V as shown in paragraph 2-2.4.

A slightly different definition of the dimensionless parameters (*Q**, *V** etc.) is used, with E_{BD} simply replaced by $\bar{E}_{BD}$.

Manipulating the previous equation, the break-down condition in dimensionless coordinates takes the form

$$Q^{*(1-R/2)}V^{*(1+R/2)} = \left(\frac{2\lambda_{1p}\lambda_{2p}}{x_p{}^* y_p{}^*}\right)^R$$

Results are presented in Figure 2-39 in terms of energy density vs. pre-stretches. Figure 2-40 reports the corresponding ECCs that exploit 95% of the asymptotic value of the energy density.

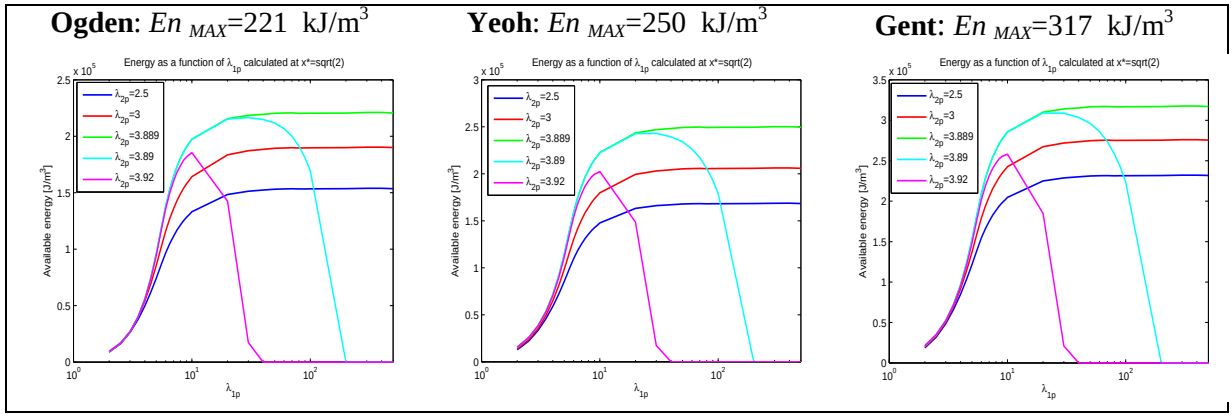

Figure 2-39 - Energy density versus λ_{1p} for different values of λ_{2p} with variable E_{BD}

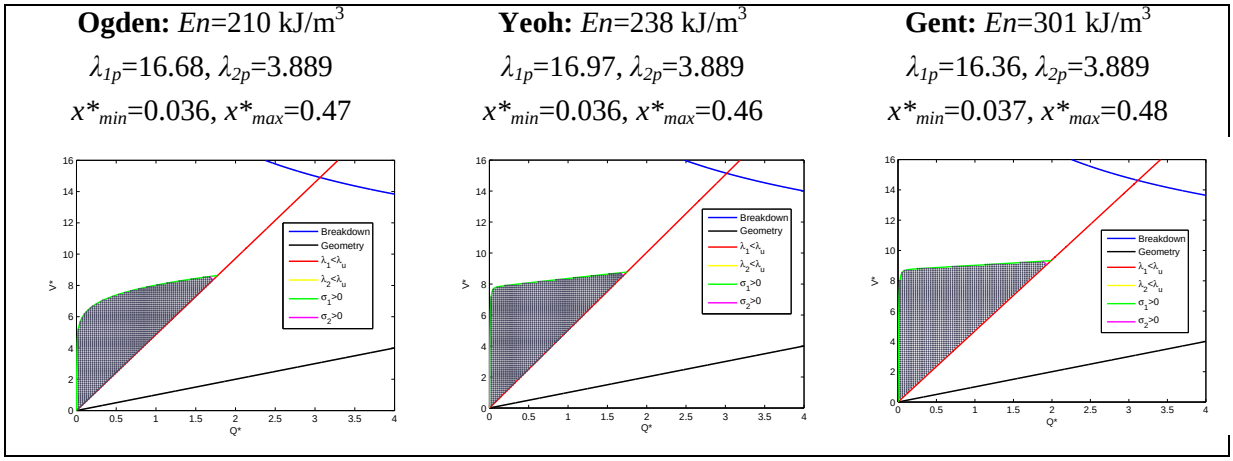

Figure 2-40 - *Q-*V** plots of ECCs converting 95% of the asymptotic energy value - variable E_{BD}**

Differently from the case of constant E_{BD}, the plots show that the resulting ECCs are not bounded by the break-down (BD) curve, but only by the rupture (RC) and loss-of-tension (LoT) conditions. In this particular case, the value of the dielectric strength does not represent

a limitation to the maximum amount of energy that the LS-DEG can convert; thus, these values of the energy density can be considered as “upper limits” to the amount of energy that this type of device can convert.

2-2.6 Synthesis and outcomes

The producible energy per unit volume of DE material that a LS-DEG can convert has been assessed under different hypothesis.

In the table below, a resume of the results is shown.

	Max. Producible Energy per cycle [kJ/m^3]		
	Ogden model	Yeoh model	Gent model
E_{BD}=50 MV/m	108	124	137
E_{BD}=70 MV/m	159	182	207
E_{BD}=50MV/m + end stop	88	98	107
variable E_{BD}	221	250	317

From the listed values, it appears clear that although the results of the fitting procedures are alike, the different hyperelastic models yield appreciable differences in term of energy conversion estimates. Further experimental work is therefore required in order to establish which model, in presence of electric activation, guarantees the best accuracy in the prediction of the shape of the LoT curve on the *Q*-*V* plane.

With a mass density of 1000 kg/m^3 [70] for the considered DE material, the maximum amount of energy per unit volume that can be converted by LS-DEGs results in 0.3 J/g. This value is obtained in the hypothesis of variable dielectric strength and using a hyperelastic model in the Gent’s form.

As already mentioned, previous works investigating equi-biaxial state of deformation based DEGs assessed a producibility per cycle up to 3.2 J/g [72].

It has to be underlined that the strain field produced by a lozenge-shaped mechanism is extremely different from a equi-biaxial deformation, since an increase of the stretch in one direction produces a decreasing stretch in the perpendicular direction.

As a result, the crucial limiting factor for the maximal energy density of LS-DEGs is the LoT condition, which severely affects the feasible working space of the generator.

Nonetheless, LS-DEGs are of great interest for practical applications thanks to their simplicity and easy adaptation in existing energy conversion devices featuring one degree of freedom and reciprocating motion.

As a further remark, we remember that the cases examined in the present work, and the theoretical maximum energy conversion cycles shown above, represent an abstract and ideal estimation of the maximum amount of energy that the material can convert in the LS-DEG configuration, and do not consider the following aspects:

- The effective energy conversion rate depends on the real sequence of electrical and mechanical transformations that approximates the ideal ECC (delimited by the discussed boundary curves). Due to their complex shapes, the curves representing the different failure mechanisms should be approximated as a sequence of elementary iso-voltage and iso-charge transformations, in order to realize a feasible control system for the generator.

  Moreover, appropriate security coefficients should be chosen in order to safeguard the material from the failure conditions.
- In the practice, the effective operation range of the device, $x^* \in [x_A^*; x_B^*]$, is mainly determined by the physical coupling between the device itself and the energy recipient (i.e. the WEC, in case of wave energy harvesting). The operation ranges considered in here are instead determined by the failure conditions bounding the ECC and are, for a given choice of the pre-stretches, the widest allowed ranges.

2-3 Dielectric Elastomer Generators for Wave Energy Conversion

2-3.1 Benefits and Criticalities

In chapter one, WECs and relative PTO systems have been investigated and the state of the art has been present.

The present paragraph approaches the problem of the application of the concepts analyzed in this chapter, about DEGs, to Wave Energy Conversion. In chapter three, finally, the LS-DEG modeled in this chapter is applied to a concept of WEC.

A traditional WEC comprises several rigid components, which are made of stiff, heavy, shock-sensitive, corrosion-sensitive and costly metallic materials, and include wave-interacting bodies, mechanical/hydraulic transmissions, electromagnetic generators, step-up transformers and eventually frequency changers or rectifiers.

In a first simple approach, the employment of DEGs may concern the replacement of traditional electric and hydraulic PTO systems with new-concept polymeric generators.

In a more ambitious perspective, it could be thought to integrate all of the above mentioned components of a traditional WEC into a single soft electroactive elastomeric body, which undergoes liquid-like deformations under the action of sea waves.

The points of interest concerning the application of DEGs to Wave Energy Conversion can be summarized in the following points.

- DEs are soft, resilient, lightweight. Thanks to their high deformability, they are suited to be directly coupled with moving oscillating WECs that undergo large displacements without the necessity of any intermediate mechanic transmission.

- Polymeric materials are corrosion-resistant and, thus, they appear particularly suitable for applications in aggressive environments (like sea water).
- Many common polymeric materials are already widely spread and largely used, thus they are available at relatively low price. Natural rubber, for example, is mainly used in the transportation sector (pneumatic tires, automotive belts) and in the clothing sector (gloves, footwear), and is publicly traded at relative low cost (see 2-1.2.3).
- Traditional electric and mechanic generators are not suitable to operate within the sea environment, since they are made by a series of sensitive moving parts that have to be kept isolated from the water. DEGs application would significantly reduce the amount of mechanical moving parts. Moreover, due to the simplicity of their mechanical layout (that essentially includes an articulated frame and a deformable membrane), permit a drastic reduction in the number of parts that can potentially meet mechanical failure.
- As already mentioned, a large variety of DEGs can be designed, each exploiting a particular motion condition (angular pitch oscillation, reciprocating motion etc.), therefore, for a particular design of a WEC device, a proper design for the corresponding polymeric PTO can be investigated and identified.
- DEGs are suitable to work at low frequencies, like those encountered in sea waves (in the neighborhood of 1 Hz), therefore their application would allow to suppress the troublesome problem of using frequency changers to interface a natural low frequency system (the WEC moving within the waves) and a system that requires high frequency (the traditional electric apparatus, since traditional electric generators usually have high nominal frequency). DEGs convert the energy from the waves into high-voltage direct-current electricity, that is immediately ready to be delivered to the coast via long underwater transmission lines.

Of course, as a counterpart, some criticalities have to be underlined.

- The polymer may be subjected to material aging and performance losses during the lifecycle.

  Woo et al. [81] carried out fatigue tests on natural rubber samples, subjected to loading cycles with frequency of 5 Hz, at different strain levels, at ambient temperature: it was shown that the material experimented visible loss of tension or mechanical failure after 10^6-10^7 loading cycles. For the specific application of DEGs, anyway, specific fatigue tests should be carried out at loading frequency and stretch levels comparable to those employed in elastomeric generators.
- Elastomeric materials present both electric and mechanic hysteretic behavior during loading-unloading cycles, therefore, part of the energy absorbed by the generator is dissipated due to viscous phenomena. A proper analysis of the limitations to the amount of convertible energy due to dissipative phenomena has to be carried out, and a targeted choice of the materials has to be done.

- As already mentioned, since DEs use voltages in the order of some kV, to now, a lack of proper electronic components may be encountered: transistors with rating of 2.5 kV are commercially available, but they are typically rated at much higher currents and power than those needed for the current state of DE technology. High-voltage low-current transistors appear to be more a market than a technology limitation, thus, the commercial development of DEGs would require a parallel development of proper electronic components [70].
- In order to avoid the rupture of the polymeric material, DEGs must be subjected to limited displacements (in order to keep the strain on the elastomeric membranes below the rupture value). WECs operating in real sea are subjected to storms and gales that tends to provoke very large oscillation amplitudes of the converter moving body. DEGs for WECs should be designed in a way that the material is kept below the stretch safety value in a certain (possibly wide) range of conditions; when the sea conditions exceed the safety limit, the oscillating body must be halted or, anyway, the polymeric generator must be disconnected from the moving body. In order to achieve this result, proper safety devices (like controlled clutches, brakes etc.) must be designed.

  In any case, this particular problem can be faced referring to the existing technology, since, also for WECs equipped with traditional generators, safety devices are provided.
- DEGs are a relatively new concept, in fact their study and application is limited to experimental laboratory scale applications. Many of the weak points of this technology have not yet been identified because of leakage of sufficient analysis in a real operating contest.

2-3.2 DE WECs concepts

Two types of DEGs-based WEC concepts, namely first- and second-generation, are considered [82]. The difference between the concepts concerns the mode of interaction between the polymeric energy conversion unit (PECU) and the fluid.

First generation: these devices are characterized by indirect interaction between PECUs and fluid. In this case, the DE deformations are not directly generated by the fluid pressures but by a mechanical interface ((a) and (b) in Figure 2-41). Thus, in these cases, two distinct bodies are identified: a WEC, that is the body mechanically excited by the waves and a polymeric PTO that converts kinetic and potential energy from the WEC to electric energy.

Examples of first generation DE WECs are heaving or pitching bodies (buoys, flaps etc) that activate a deformable DEGs provided with a rigid frame that is partially in-built with the WEC.

Due to the absence of direct fluid-PECU interaction, the modeling and design of first-generation polymeric devices is simplified and consequently the level of uncertainty and risk is reduced.

Second generation: these devices are characterized by direct interaction between PECUs and fluid, which occurs over wide contact surfaces.

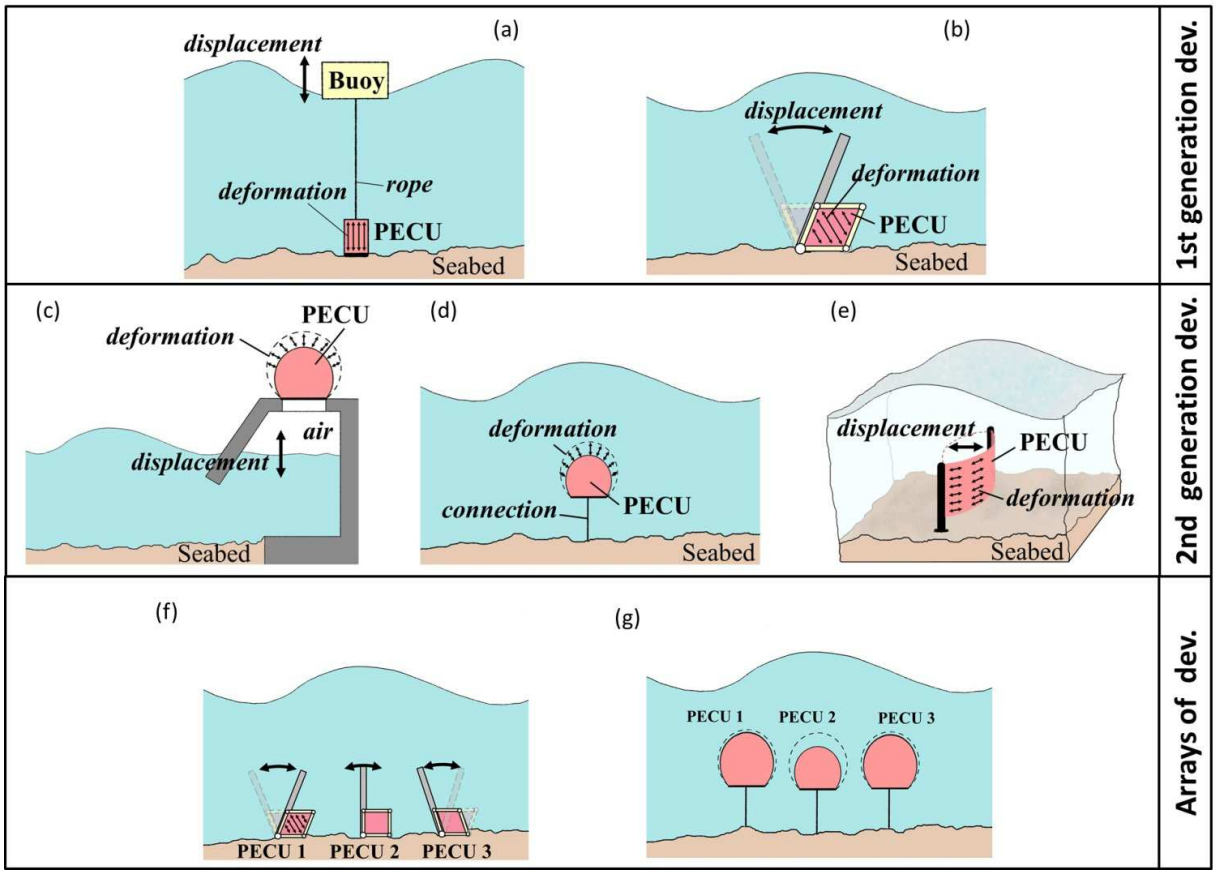

Figure 2-41 - Examples of first and second generations DE-WECs and of arrays of devices

In this case, fluid-PECU interaction is not mediated by any mechanical means, and DE membrane deformation is directly generated by wave-induced fluid pressures ((c), (d) and (e) in Figure 2-41).

As a result, second-generation devices are highly-integrated wave-energy converters that feature the minimal number of mechanical and electrical components beside the PECU. Moreover, thanks to their intrinsic and tunable compliance, such devices make it possible to optimize and control their radiation impedance in order to achieve maximal wave-energy extraction.

Examples of second generation converters are close-chamber oscillating water-columns exploiting a deformable membrane instead of an air turbine [83] [84] and inflatable bodies.

This second type of WECs is however much more difficult to model and design, and its development is rather risky.

For both first and second generation devices, arrays and farms of WECs can be investigate and designed, taking into account the influence of mutual interaction and couple hydrodynamic due to the presence of multiple bodies.

2-3.3 Current Research

SRI

The first working prototype of Wave Energy Converter (WEC) based on DEs has been developed by Chiba et al. [85]. The system is based on a floating buoy that oscillates under the hydrodynamic forces of waves. The scavenging of electrical energy is obtained by employing inertial oscillating masses connected to linear DE transducers. A prototype has been tested in sea waves demonstrating the feasibility of such a concept.

SBM

An innovative DE-based WEC (called S3) has been developed by the company SBM Offshore [86]. The proposed device features a tubular DE membrane sandwiched between deformable electrodes. Its multi-resonant response allows to optimize the harvesting of energy over a large frequency range. SBM, in collaboration with Bayer Material Science and Danfoss Polypower, has intensively worked on the development and on the wave tank testing of a prototype of such a device, and is planning to test a real scale version of it within 2014-2015.

Bosch and Wacker

Bosch has recently patented an Oscillating Water Column (OWC) WEC that employs a DE generator as power take-off system [87], but no analysis has been reported in scientific literature to date.

A similar system has been mathematically examined by Vertechy [83] and Rosati-Papini [84] within PolyWEC project.

PolyWEC

PolyWEC is a FET-Energy project that is partially funded by the 7th Framework Programme of European Community, with the aim of investigating on new concepts and mechanisms for wave energy harvesting that are based on EAPs through a multidisciplinary approach that includes competencies on WEC design/tests, fluid dynamics simulation/test, control/mechatronics and material science (www.polywec.org). The aim of the Project is to develop new knowledge and new technologies aiming at:

- optimizing electroactive materials for WEC applications,
- conceiving new electro-mechanical configurations for DE WECs,
- studying the fluid-elastomer interaction through numerical simulations,
- performing wave-tank tests of small scale prototypes,
- providing economic and environmental assessment.

The partners of the PolyWEC project are

- PERCRO SEES, Istituto TeCIP, Scuola Superiore Sant'Anna (Italy). The laboratory operates in the field of applied mechanics, robotic and mechatronics, and has past experience in the field of Electroactive polymers for robotic application purposes.

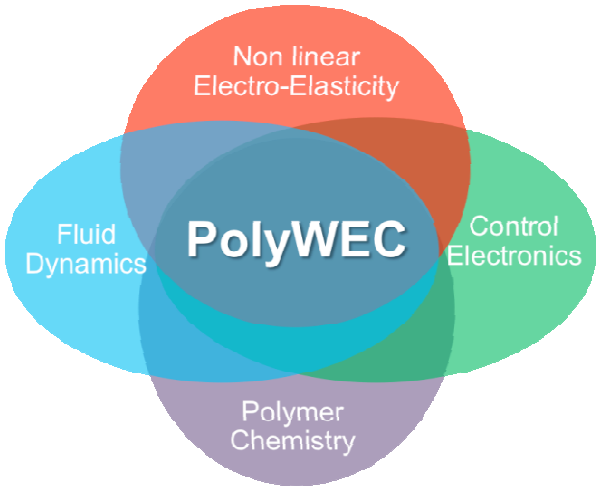

Figure 2-42 - Multidisciplinary approach within the PolyWEC project

- 'Petru Poni' Institute of Macromolecular Chemistry (Romania), an institution for applied research in the field of organic and inorganic chemistry, included polymers synthesis.
- Selmar SrL (Italy), a company operating in design, manufacturing and supplying of mechanical systems and material solutions for vessels in the ship-building industry.
- University of Edinburgh (UK). Wave Power Group of University of Edinburgh leads, from the seventies, the research in the field of Wave Energy Conversion.
- Wave Energy Center (Portugal). This center is involved in several projects concerning Wave Energy installations (like the OWC Pico plant).

PolyWEC is organized in 6 Work Packages (WP).

WP1-"Concept and modelling" concerns with the study of basic wave-energy-conversion principles and concepts based on EAPs, as well as theoretical models and numerical tools needed for the development and assessment of PolyWEC devices. Multi-physics hydrodynamic-electro-mechanical models have to be conceived to provide reliable numerical simulations of the dynamic interaction between polymeric materials and water waves.

WP2-"New materials and transducers" aims at the development of innovative materials and assemblies of energy conversion units for wave-energy harvesting. This WP requires a joint of cometences on electroactive elastomers and on systems integration and control, for the development of innovative nano-structured EAP materials and for the design of EAP-based transducers that are optimised for the wave-electricity conversion principles/concepts that are conceived in WP1.

WP3-"Design and control" deals with the integrated design and implementation of the innovative PolyWEC devices, along with the development of their controllers.

WP4-"Wave tank testing" is a demonstration WP that carries out experimental testing and evaluation of scaled PolyWEC devices (those constructed in WP3) within a wave-tank basin.
WP5-"Assessment, Exploitation and Dissemination" deals with a first economic-environmental assessment of PolyWEC technology, as well as with the dissemination and exploitation of Project results.
WP6-"Management and coordination" focuses on the management and coordination of the Project.

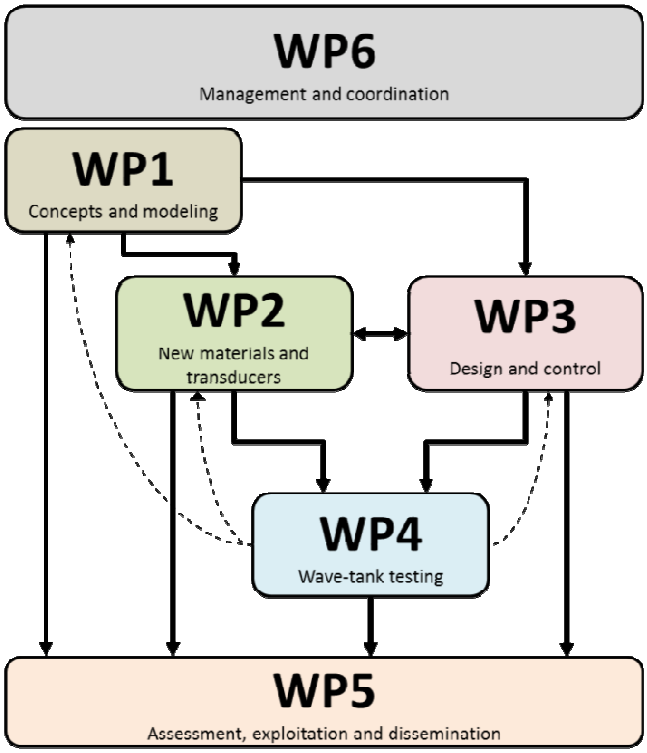

Figure 2-43 - PolyWEC WPs

PolyWEC project started in November 2012. Up to date, its efforts have been concentrated on the numerical simulation of a new concept DE-OWC [83] [84], on the electro-mechanical characterization of some common DEs (acrylics, silicones, natural rubber) and on the modeling and application of a new concept of lozenge-shaped DEG, that is the object of the present thesis [88].

Chapter 3

Dielectric Elastomer Wave Surge Energy Converter

3-1 Modeling of the DE-OWSEC

3-1.1 Introduction

In this chapter, a practical application of the LS-DEG studied in the previous chapter is presented. The generator is exploited as PTO system for a flap hinged to the sea bed. The system has one degree of freedom only, corresponding to the pitch angle formed by the flap with the vertical equilibrium position. This type of WEC belongs to a category of devices defined in the first chapter with the name of Oscillating Wave Surge Energy Converters (OWSECs). This class of devices includes several pre-commercial or model scale prototypes (Oyster, EB Frond, WaveRoller, Bio Wave), that usually exploit a hydraulic PTO system.
These systems are generally thought to work in shallow water conditions (with depth of 10 m about) and, depending on the specific design, are totally or partially submerged.

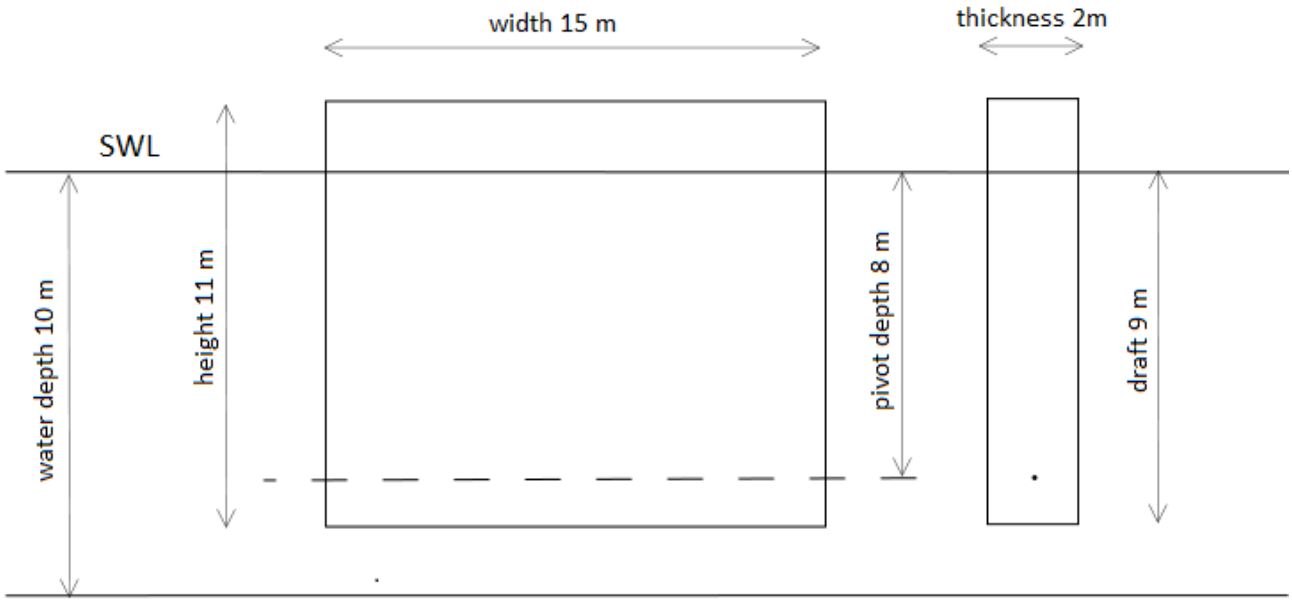

Figure 3-1 – Device geometry

We consider here a particular layout for a bottom hinged wave surge converter: the dimensions and the general features of the system tend to reproduce existing prototype devices (like the Oyster), and were chosen on the advice of the Wave Power Group of Edinburgh University (http://www.mech.ed.ac.uk/research/wavepower).

The layout of the examined device (Figure 3-1) is here briefly described: the flap is a rectangular cuboid of height 11 m, width 15 m and thickness 2m. The draft of the flap is 9 m, so that the flap extends to a height of 2 m above the water surface in equilibrium conditions. The pivot depth of the flap is 8 m, so that there is 1 m of the flap below the pivot.

The flap is taken to be of constant density and to have a mass which is half that of the water it displaces in equilibrium conditions. This means that the flap is subjected to a net buoyancy torque.

Since the sea water density is $\rho = 1030$ kg/m^3 and the displaced volume in equilibrium conditions is $V = 9 \times 2 \times 15$ m^3, the mass of the flap is $m = 0.5 \times \rho \times V = 139050$ kg.

3-1.2 Model description

The mathematic simulation of the considered WEC (regardless the PTO type) can be carried out using the general approach described in chapter one.

Since the introduction of the LS-DEG brings a non-linearity to the model, it is convenient to present a general formulation of the problem in the time domain; linear analyses (in the frequency domain) also will be performed and described later on.

In order to follow this approach, the problem can be implemented in Simulink.

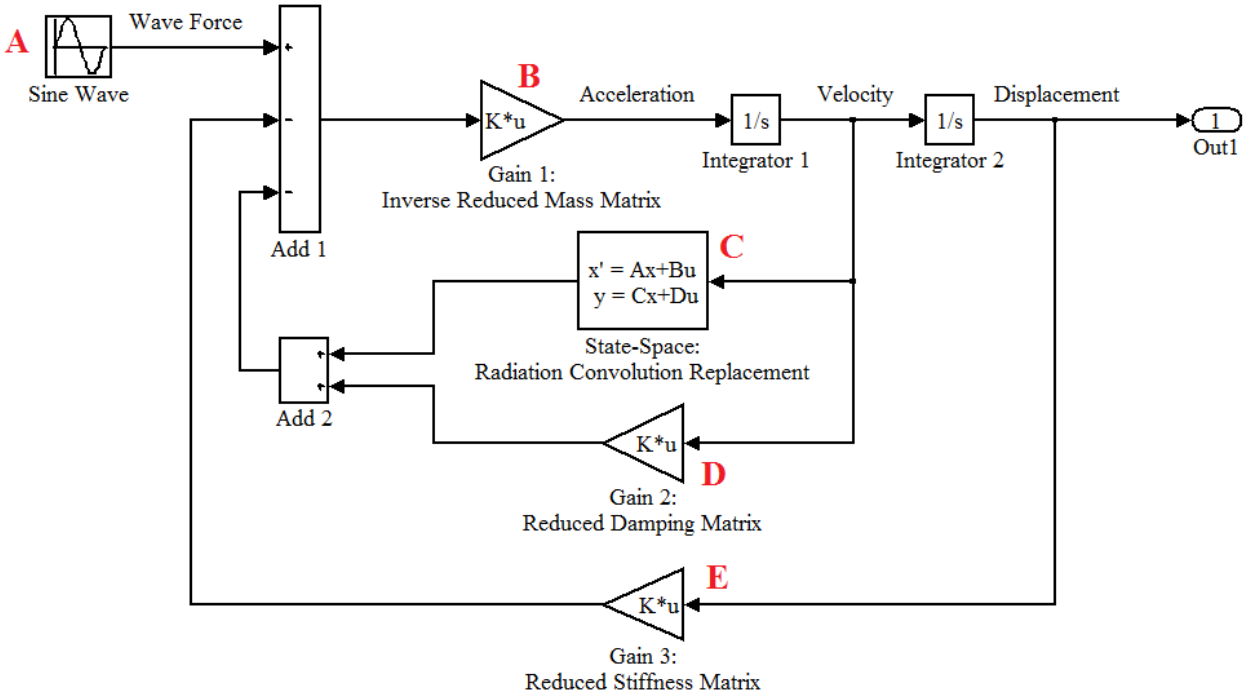

Figure 3-2 - Base Simulink scheme for the problem

A base scheme that can be followed for a first approach of the problem is that shown in Figure 3-2, provided by Edinburgh Wave Power Group.

The main blocks needed to study the problem, can be resumed in:

A. Wave induced torque: it is represented by a Sine-Wave block, the parameters of which are tuned according to the rules for the calculation of wave induced forces on floating bodies implemented in the WAMIT v7 code, that was briefly described in chapter one [50] [89].

   It is assumed here that incident waves are monochromatic, thus, they can be modeled as sine signals in the time domain; deeper analyses should keep into account a wave field spectrum, so that the incident waves appear as a superimposition of a number of different frequencies [19].

   Thanks to the properties of linearity within the linear wave theory, the module of the wave induced torque acting on the flap varies linearly with the wave amplitude. Therefore, it is sufficient to employ the WAMIT code to calculate the wave induced torque for a unitary amplitude wave at different values of frequencies, obtaining a map of the torque as a function of the frequency. With these results, for a generic wave with any value of frequency and amplitude, the effective value of the torque acting on the flap can be calculated interpolating on the frequency and multiplying the results by the value of the wave amplitude.

   It is important to notice that the output of the WAMIT code is calculated with reference to a specific angular position of the flap, that is the vertical equilibrium position. An accurate analysis would require to consider the variability of the wave induced torque with the angular position [90]. The procedure adopted in the present thesis (that uses values of the wave induced torque independent on the pitch position of the flap) guarantees lower computational effort, but is affected by errors in case the pitch oscillation of the flap is large (over ~20° from the vertical position).

B. Inverse reduced mass matrix: more precisely, this block is a Gain block, the gain of which is equal to the reciprocal of the flap moment of inertia around the pivot axis, I. Multiplying the torque by this gain, the value of the angular acceleration of the flap is obtained. Subsequently, with a double integration, the value of the angular position of the flap is obtained.

C. Radiation block: As previously mentioned, in the time domain, the effect of radiation has to be modeled doing the convolution integral between the velocity and the impulse response function [17]. As previously mentioned, this term can be replaced by a state-space model. For this reason, a state-space block simulating the radiation effect has been introduced in the Simulink scheme, the parameters of which were calculated on the basis of WAMIT output results.

D. External damping: an external damping source can be present. This block simulates the presence of a traditional electric (or hydraulic) PTO system, as explained in the

following. The external damping torque is expressed in the form $T_{damp} = B\dot{\theta}$. Even if we are mainly interested in studying a polymeric PTO (that is not well modeled by this block), the external damping block is present for the aim of making comparisons. When the system works with a polymeric PTO, the value of external damping is set to be zero.

E. Stiffness of the system: this block is used to keep into account the combined effect of the buoyancy torque and of eventual external mechanical springs (used, i.e., to bring the system to the resonance condition). In a first approximation, the stiffness can be modeled via a Gain block, since it is assumed proportional to the flap displacement from the vertical position.

If we consider the effect of the buoyancy torque only, however, it must be emphasized that a non-linearity occurs. Buoyancy torque is the result of gravity induced forces: on one side the own weight of the flap F_W, on the other hand the Archimede's force F_A (Figure 3-3).

The buoyancy torque can be expressed as a function of θ in the general form

$$T_{buoy} = -(F_B \cdot r_{buoy} - F_W \cdot r_{weight})$$

where F_B and F_W are the Archimede's force and the weight respectively, and r_{buoy} and r_{weight} are the respective lever arms.

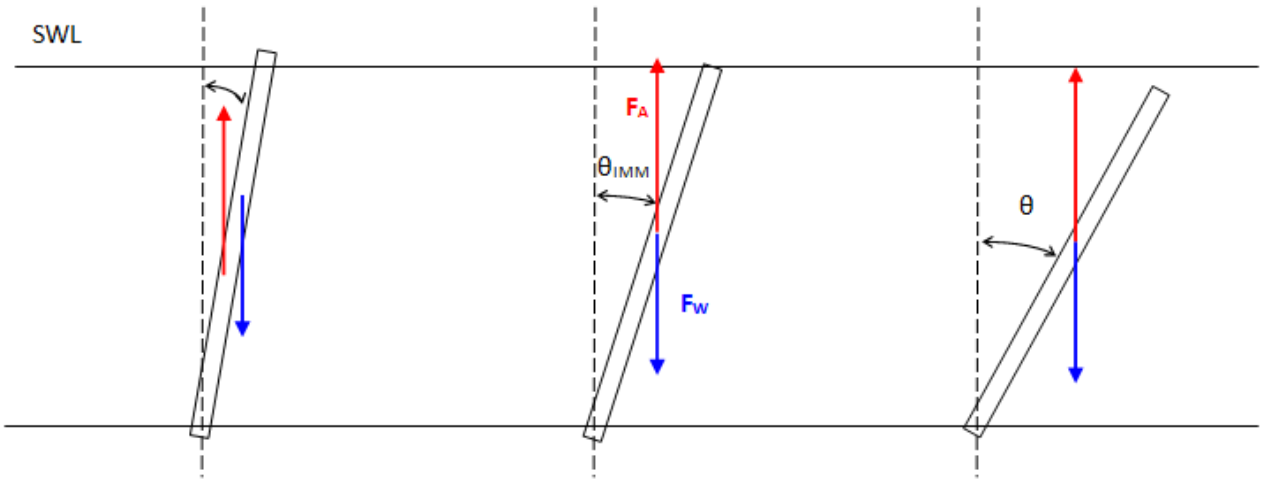

Figure 3-3 - Buoyancy torque explanation

Two sub-cases can be identified: we indicate with $\theta_{IMM} = \text{acos}(h/L)$ the limit angle: h is the water depth (above the pivot) and L is the flap height (above the pivot). For $\theta < \theta_{IMM}$ the flap partially emerges from the water (using as a reference, for simplicity the SWL), while for $\theta \geq \theta_{IMM}$ the flap is fully submerged. In both of the cases, the force F_W is equal to the whole weight of the flap and is applied to its center of mass; the Archimede's force F_B is equal to the weight of an amount of water corresponding to the volume of the submerged portion of the flap, and is applied to the

center of mass of the submerged section of flap only. Therefore, for $\theta < \theta_{IMM}$, the points of application of B and W do not coincide, while they are overlaid for $\theta \geq \theta_{IMM}$.

The effect of non-linear buoyancy can be implemented in Simulink by a proper block (exploiting a User defined Function): this solution will be adopted in the following.

This scheme is the start point for any type of analysis of the converter: further elements will be necessary for the study of the case in exam (in particular, for the implementation of the LS-DEG generator, a new proper block will be required).

In the following of the chapter, two cases are considered:

- First of all, the flap is studied in combination with a traditional PTO system, modeled as a viscous damper. For this type of analysis, the assumption of full linearity is done.
- Successively, the system is combined with a polymeric PTO (the LS-DEG): this case is strongly non-linear, and requires proper modifications of the basic scheme discussed above.

3-1.3 Choice of the reference sea states

For dimensioning and energy productivity assessment purposes, plausible sea states have been identified in literature. In particular, the 9 sea states reported by Corsini and Rispoli [28] were chosen.

These conditions refer to waves present on a location off the Azores Islands (where the PICO OWC was situated), in presence of shallow water with 10 m depth about.

The choice of this conditions was suggested by some reasons, in particular

- Pico Island (off the Azores) is of great interest for Wave Energy Conversion, since high energy levels from the waves are present at relatively low depth.
- The conditions (in particular in terms of water depth) are suitable for the considered WEC, that, as previously mentioned, is suitable to work in shallow water.
- Date are available (thanks to previous analysis and measurements for the Pico project). The data are presented in terms of mean significant wave height H_s and mean period T_e: it is assumed that an univocal correspondence exists between the occurrence of a certain wave period and the corresponding wave height.

  A wider analysis would required the knowledge of the relative frequency of a wider set of sea states (the so-called wave-scatter matrix), including combinations between the values of period and height reported here.

Sea state	*#1*	*#2*	*#3*	*#4*	*#5*	*#6*	*#7*	*#8*	*#9*
H_s [m]	0.65	1.2	1.6	2.0	2.4	2.9	3.4	4.0	4.5
T_e [s]	9.0	9.5	10.0	10.5	11.0	11.5	12.0	12.5	13.0
Z [%]	25	20	17.7	14.5	10	7	4.5	0.7	0.6

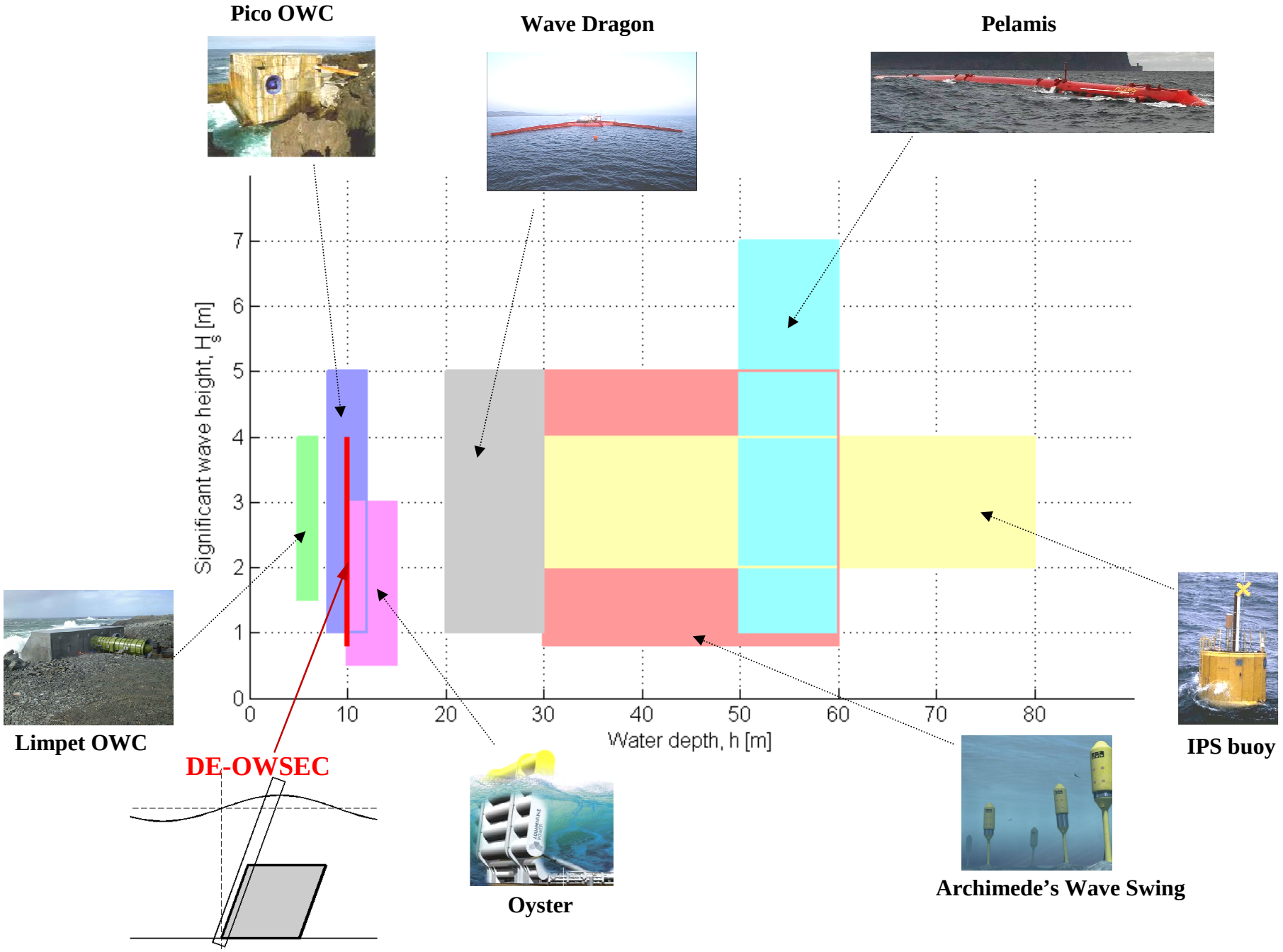
Pico OWC
Wave Dragon
Pelamis
Significant wave height, H_s [m]
Water depth, h [m]
0
1
2
3
4
5
6
7
0
10
20
30
40
50
60
70
80
Limpet OWC
DE-OWSEC
Oyster
Archimede's Wave Swing
IPS buoy

Data are shown in the previous table, where *Z* represents the relative frequency (in percentage) of any sea state.

As explained in chapter one, the significant wave height is a statistical mean parameter calculated from the spectrum for a real sea. With reference to the present case, the significant height for a given wave period is representative of a class of waves with different height having the reference period. In order to make energetic considerations, applying linear waves theory, for each value of period a wave height equal to the significant height divided by $\sqrt{2}$ has to be considered. In this way, the result from the calculation of the power available within the waves using linear theory equation (paragraph 1-1.2.1) and the same result calculated from the significant height (1-1.3) produce consistent results.

Therefore, for the calculations, the adopted values of wave height are calculated accordingly to the equation

$$H = \frac{H_s}{\sqrt{2}}$$

Once the water depth is fixed (10 m), for any sea state (period, height), the equations presented in chapter one allow to calculate the wavelength and the power per unit crest width of the waves.

In the following table, for any sea state, we report the energy available within a wave-front of 15 m width (equal to the flap width). Moreover, considering a reference period of 8760 hours (corresponding to a full-length year), basing on the values of relative frequency, the energy available from each sea state is calculated.

state	H=2a [m]	T_w [s]	Z	hours/yr	P_{wave} [kW]	Available Energy [kWh]
#1	0.46	9	0.25	2190	62	1.35E+05
#2	0.84	9.5	0.2	1752	211	3.69E+05
#3	1.12	10	0.177	1551	383	5.94E+05
#4	1.42	10.5	0.145	1270	628	7.98E+05
#5	1.7	11	0.1	876	915	8.02E+05
#6	2.06	11.5	0.07	613	1364	8.36E+05
#7	2.4	12	0.045	394	1875	7.39E+05
#8	2.82	12.5	0.007	61	2618	1.61E+05
#9	3.2	13	0.006	53	3405	1.79E+05
			tot	8760		4.61E+06

3-1.4 Effect of the damping due to water viscosity

It may be objected that, in the discussed model (Figure 3-2), the effect of water viscosity is not kept into account. According to Babarit [19], a damping torque that depends quadratically on the velocity and takes into account the effect of viscous losses should be considered.

This term would include the effect of shear stress acting on the flap surface and of eventual boundary layer separation due to the water viscosity.

Such an effect could be modeled by using a linear viscous block (like D, with reference to Figure 3-2) [17]: this implies a linearization of the effect of the water viscosity.

A more proper approach consists in the implementation of a wave induced torque in the quadratic form [19]

$$T_{drag} \propto |\dot{\theta}|\dot{\theta}$$

A simplified procedure that allows to obtain a first estimation of the quadratic damping torque on the oscillating flap (and, above all, of its order of magnitude) is presented here.

First of all, we remember that, a rectangular rod moving with uniform velocity U_∞ (or, equivalently, immersed in a stream with velocity U_∞) experiments a drag force given by

$$F_D = C_D \frac{1}{2} \rho {U_\infty}^2 A_f$$

where ρ is the fluid density and A_f is the frontal area of the rod (perpendicular to the flow direction).

The drag coefficient C_D, for high Reynold numbers (Re>10^4), can be assumed equal to 2, basing on the results presented by Cengel et al. [91] (Figure 3-4).

Starting from this assumption, the OWSEC in exam can be thought as divided into slices of infinitesimal height (Figure 3-5).

The drag force on the infinitesimal segment of flap position at a distance r from the pivot is

$$dF_D = C_D \frac{1}{2} \rho r^2 \dot{\theta}^2 dr\, w$$

where w is the width of the flap.

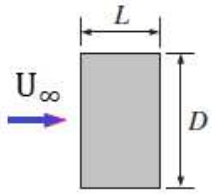

Sharp corners:

L/D	C_D
0.0*	1.9
0.1	1.9
0.5	2.5
1.0	2.2
2.0	1.7
3.0	1.3

*Corresponds to thin plate

Figure 3-4 - Drag coefficient for a rectangular rod

The corresponding torque about the pivot axis is

$$dT_D = C_D \frac{1}{2} \rho r^3 \dot{\theta}^2 dr\, w$$

The consequent total drag torque is

$$T_D = \int_0^{L_{imm}} C_D \frac{1}{2} \rho r^3 \dot{\theta}^2\, w\, dr = \frac{C_D}{8} \rho\, \dot{\theta}^2\, w\, {L_{imm}}^4$$

Where L_{imm} is the submerged height of the flap (that varies with the pitch angle).

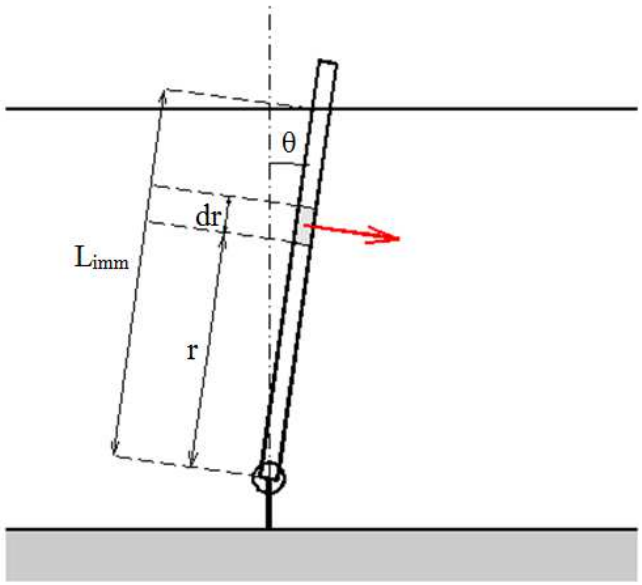

Figure 3-5 - Drag induced torque calculation

The above described calculations are implemented in the Simulink model: the effect of non-linear buoyancy also is accounted, moreover, a user defined function that calculates the height of the submerged part of the flap, L_{imm}, as a function of the angular position is introduced.
External linear damping has been set to zero, so that the only damping effects present are those of the radiation and of the water viscosity.
With reference to different sea states (for e.g those presented in the previous paragraph), the torque due to the radiation and to the quadratic viscous term can be calculated and compared.
We report the results relative to the most intense sea state only (#9):

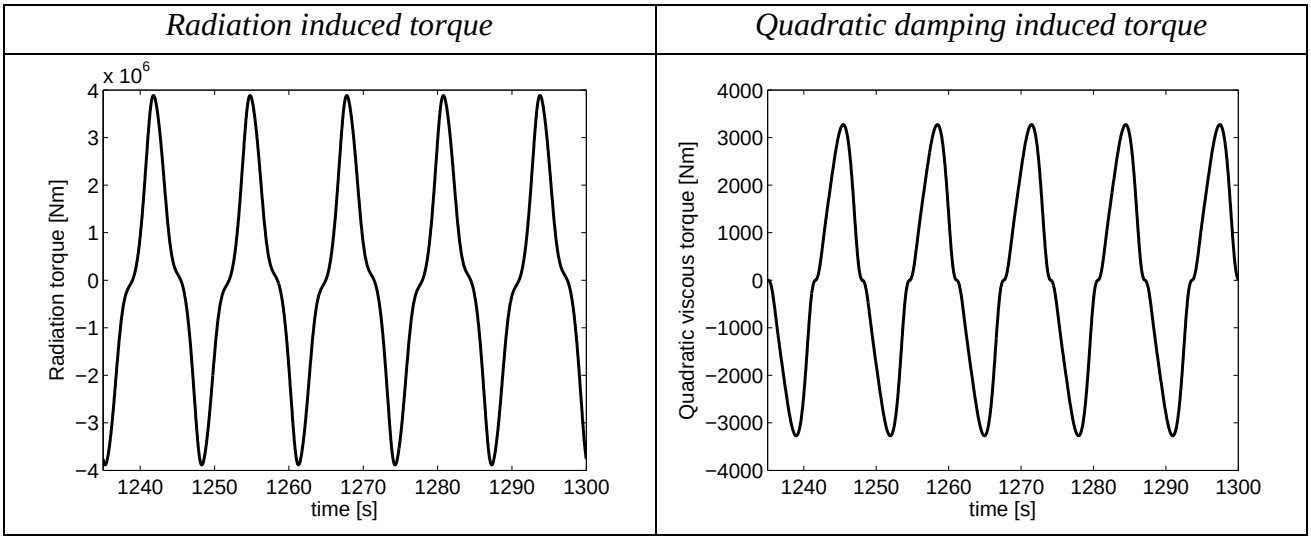

Figure 3-6 - Comparison between damping effects

From the plots of Figure 3-6 it is immediate to notice that the effect of quadratic viscosity is orders of magnitude less relevant than the radiation effect. The same qualitative result is

found for the other sea states. Notice, only for the sake of completeness, that the non-sinusoidal profiles for the torques are a result of the implementation of non-linear buoyancy (and not of the quadratic viscous term).
We can conclude that the effect of the 'drag' quadratic damping is negligible.
A similar result was obtained by Alves [17] in his work on floating buoys.

3-2 Traditional approach: linear analysis of OWSEC with traditional PTO system

In this section, we examine the behavior (in terms of dynamics and of energy productivity) of an OWSEC provided with a traditional PTO system (that is modeled as a viscous damper plus an eventual mechanical spring). This solution represents somehow the 'traditional' approach to the simulation of WECs, therefore, the traditional calculation methodology also is followed [17] [19] [26], and linear theory is exploited. The results from this type of calculation (in terms of power output and energy productivity of the device) represent a sort of 'target' that, as far as possible, would be hopefully to re-produce using the discussed novel concept of polymeric PTO system.

3-2.1 Background

The study of the oscillating behavior of a WEC using the linear theory (thus, the frequency domain approach presented in the first chapter) is the Resonance theory for oscillating systems.
We report here the fundamental results, that can be easily derived from simply equations and are presented in any Mechanics textbook.
Let consider an oscillating system (e.g a mass M connected to a spring with constant K, like in Figure 3-7) subjected to

- A viscous damping effect, producing a resistive force in the form $F_c(t) = f_v \dot{x}(t)$
- An external sinusoidal force in the form $F(t) = \Xi \sin(\omega t)$

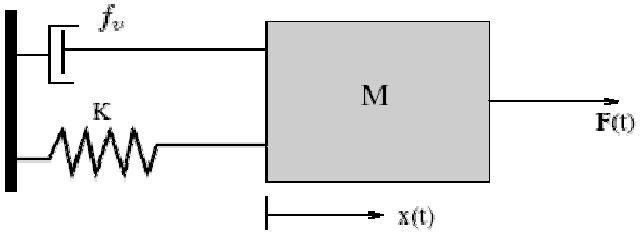

Figure 3-7 - Generic oscillating system with external forcing

When no external force is present, if the system is displaced from its equilibrium position, it keeps oscillate with angular frequency given by

$$\omega_n = \sqrt{K/M}$$

This value of frequency is called 'natural frequency' or 'resonance frequency' of the system.

When the system is subjected to the external sinusoidal force *F(t)*, it oscillates at a frequency that is equal to that of the external force itself (ω).

After a transient phase, the oscillations of the system have constant amplitude and the law of motion of the system takes the form

$$x(t) = X\sin(\omega t + \varphi)$$

This equation describes the 'steady oscillations' of the system.

Supposing to keep the amplitude Ξ of the external force constant, varying the frequency ω only, the amplitude of the oscillations of the body is a function of the normalized frequency ω/ω_n:

$$X = \frac{\Xi}{K\sqrt{(1-(\omega/\omega_n)^2)^2 + {f_v}^2/(MK)\,(\omega/\omega_n)^2}}$$

and the result is shown in Figure 3-8.

It is easy to notice that

- When no damping is present ($f_v = 0$), the oscillations tend to have infinite amplitude for $\omega = \omega_n$ (resonance condition)
- When damping is present ($f_v > 0$), the oscillations have finite amplitude, with maximum value in correspondence of the resonance frequency.

WECs are usually designed to work in resonance with the incident nominal wave, and they are subjected to damping effects provided by both the radiated waves produced by the body itself and by the PTO system that converts mechanical energy from the waves to electric energy.

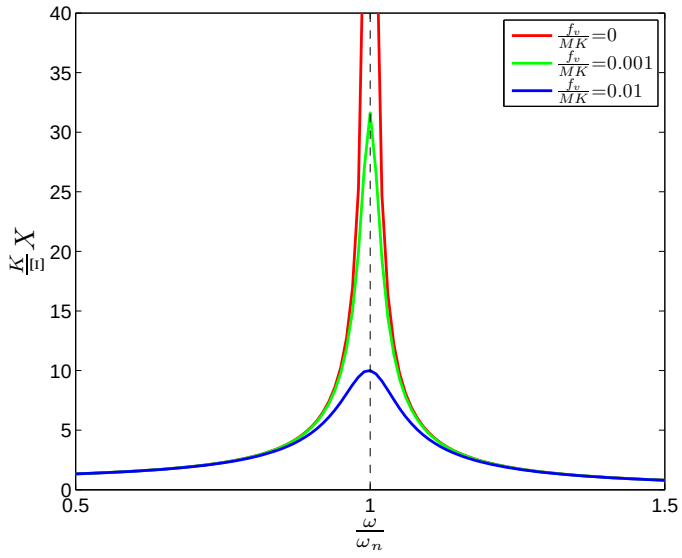

Figure 3-8 - Frequency response of the system

3-2.2 Case study

We use the linear theory to model a wave surge converter (OWSEC) provided with a traditional electric PTO, the effect of which is generally modeled as a viscous damper (that

provides a resistive torque proportional to the instantaneous angular velocity of the device) plus a mechanical spring, that affects the overall stiffness of the system.
Folley et al. [30] examine the problem of a top hinged OWSEC using as PTO a coulomb friction brake, that provides a constant torque the module of which can be adjusted to adjust the level of applied damping, but he states that, according to linear theory, the optimum damping torque is proportional to the flap rotational velocity, with the constant of proportionality depending on the frequency. This effect can be achieved using a variable displacement hydraulic machine or direct drive electric generators.

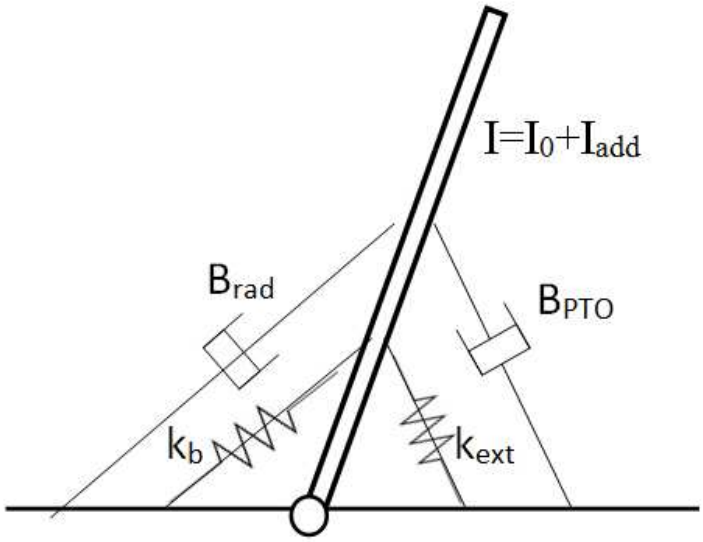

Figure 3-9 - Schematic of the system

According to linear theory (see Chapter 1), a complete schematization of the system (Figure 3-9) includes:

- A pitching body having overall moment of inertia $I = I_0 + I_{add}$, where I_0 is the own moment of inertia of the flap and I_{add} is the hydrodynamic added inertia.
- A torsional spring, with constant k_b, representing the linearization of the buoyancy torque acting on the flap, accordingly to the previous considerations.
- A viscous damper with constant B_{rad} representing the dissipative effect of the radiated waves, generated by the body motion.
- An external spring-like component with constant k_{ext}. This element can be thought as part of the PTO system or as an independent mechanical component. Two different assumptions can be taken on the value of k_{ext}. The first possibility is that the value of k_{ext} is not a constant, but is tuned by the control system and is adjusted in order to guarantee resonance with different incident waves. The second possibility is that k_{ext} is a traditional mechanical spring the value of which is a constant, chosen in order to maximize the energy productivity over the considered range of sea states.

With reference to the above mentioned general scheme, the effect of the radiation block, that in time domain is simulated in general as a state space model, due to the hypothesis of linearity, is simply modeled as the sum of an added mass term and of a damping term.

We recall in fact that, under the hypothesis of linear theory, the radiation force, in the frequency domain, is given by

$$\widehat{\boldsymbol{F}}_r = -i\omega \boldsymbol{B}_{rad}\widehat{\boldsymbol{\xi}} + \omega^2 \boldsymbol{A}\widehat{\boldsymbol{\xi}}$$

This expression is valid in the hypothesis of fully linear system only, and corresponds, in the time domain, to

$$\boldsymbol{F}_r = \boldsymbol{B}_{rad}\frac{d\boldsymbol{\xi}}{dt} - \boldsymbol{A}\frac{d^2\boldsymbol{\xi}}{dt^2}$$

In the case of the oscillating surge, with one degree of freedom only, $\boldsymbol{\xi}$ is the scalar value of the pitch angle θ of the flap, the matrices $\boldsymbol{B}_{rad}$ and $\boldsymbol{A}$ are scalars, corresponding respectively to B_{rad} and I_{add}.

Notice that the added inertia and the radiation damping are functions of the excitation frequency of the system (but not of the amplitude of the incident wave). A characterization has been preliminary done, using the output data of the WAMIT code, provided by the University of Edinburgh.

The profiles of added moment of inertia and radiation damping as a function of the frequency is reported in Figure 3-10.

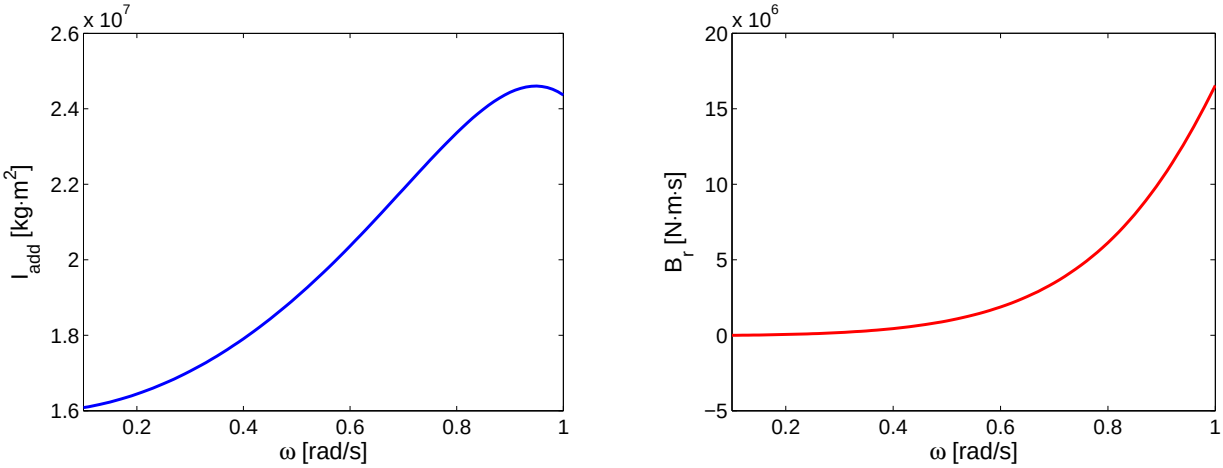

Figure 3-10 - Added inertia (left) and radiation damping (right) as function of frequency

The schematization of the system presented in Figure 3-9 can be further simplified as in Figure 3-11, with the following definitions for the symbols:

$B = B_{rad} + B_{PTO}$ is the overall damping level, due to both radiation and PTO system

$k = k_b + k_{ext}$ is the overall stiffness of the system, including both the effect of buoyancy and external torsional spring.

This schematization is more generic than that of Figure 3-9, because it does not require the buoyancy effect to be linear: it can be thought that only the overall stiffness of the system is constant with varying pitching angles. This effect can be achieved, even in presence of a non-

linear buoyancy, by using a non-linear external spring that, combined with the own buoyancy of the system, creates a compensation producing a constant overall stiffness.

We remember that, in general, the expression 'constant stiffness' means that, at a given frequency, the stiffness of the system does not vary with the pitching angle. Anyway, at different frequencies, different constant stiffness values may be realized.

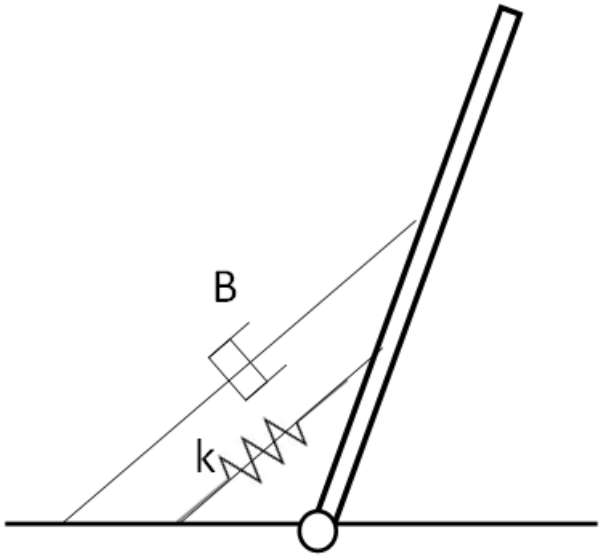

Figure 3-11 – Simplified scheme of the system

We study here the dynamic of the system, by writing its equation of motion:

$$I\ddot{\theta} + k\theta + B\dot{\theta} = T_w$$

where θ is the angle between the flap and the vertical equilibrium position and T_w is the wave induced torque on the flap.

In the hypothesis of linear wave, the external torque is in the form

$$T_w = \Gamma \cos(\omega t + \varphi)$$

with Γ and φ generic amplitude of the sinusoidal torque and phase angle.

Neglecting the eventual transient phase, a solution in the form $\theta = Re\{\Theta e^{-i(\omega t+\varphi)}\}$, with $\Theta \in \mathbb{C}$, can be found.

Calculating the derivatives of $\theta = \Theta e^{-i(\omega t+\varphi)}$ and replacing them in the equation above, a solution can be found for Θ:

$$\Theta = \frac{\Gamma(-I\omega^2 + k - iB\omega)}{(-I\omega^2 + k)^2 + B^2\omega^2}$$

From this equation, the modulus of Θ simply results in

$$|\Theta| = \frac{\Gamma}{\sqrt{(-I\omega^2 + k)^2 + (B_{rad} + B_{PTO})^2\omega^2}}$$

We recall that, if the damping coefficient of the generator is indicated with B_{PTO}, the mean power output is given by

$$P_{dev} = \frac{B_{PTO}}{T}\int_0^T \dot{\theta}^2 dt = \omega^2 B_{PTO}\frac{|\Theta|^2}{2}$$

where T is the wave period, $T = \omega/2\pi$.

Replacing in the expression for P_{dev} the expression for the modulus of Θ, the expression for the device power output is obtained:

$$P_{dev} = \frac{B_{PTO}}{2}\omega^2 \frac{\Gamma^2}{(-I\omega^2 + k)^2 + (B_{rad} + B_{PTO})^2\omega^2}$$

A simple analysis of the expression above shows that the optimum power capture is obtained when

- Resonance is met: $-I\omega^2 + k = 0$
- The damping due to the PTO equals the damping due to the radiation: $B_{PTO} = B_{rad} = B/2$.

Under these hypotheses, the expression for $|\Theta|$ gets simplified to

$$|\Theta| = \frac{\Gamma}{2\omega B_{rad}}$$

Notice that, when resonance occurs, the oscillation amplitude does not depend on the inertia and on the stiffness of the system, while it depends, of course, on the total damping level.

The relative expression for the maximum power output is

$$P_{dev} = \frac{\Gamma^2}{8B_{rad}}$$

Starting from the present considerations, the study of a traditional OWSEC has been carried out.

Two cases are here examined: in the first one, it is supposed that the PTO is able to tune both the external applied damping B_{PTO} and the overall stiffness k in correspondence of different sea states; in the second approach, it is assumed that k represents a constant term (resulting from the combination of the flap buoyancy and of an external mechanical spring), and the PTO is a direct driven electric generator described by the only parameter B_{PTO} (that is assumed tunable).

With respect to the previous dissertation, a further constraint is introduced: it has been required to the flap to make oscillations with a maximum allowed displacement from the vertical position (chosen equal to 45°). Upper limiting the pitch oscillations of the flap represents both an action to safeguard the device and a way to produce a reasonable comparison with the same WEC operating with a polymeric generator which, due to the intrinsic limit of the elastomer mechanical rupture, must cover oscillations within a limited allowed range.

The introduction of such a constraint creates some differences in the optimization procedure with respect to the results derived in the precedent lines. The analytical procedure and the results, relative to the two mentioned cases, are described in the following.

3-2.2.1 Optimal linear PTO system

With reference to Figure 3-9, we assume here that the external stiffness k_{ext} is a mechanical component within the PTO system.

The PTO performs in this case both an active and a reactive behavior. The active component is clearly represented by the external applied damping B_{PTO}; the reactive component is k_{ext}, that combined with the flap buoyancy k_b produces the overall stiffness k. We assume here that the PTO is such that both B_{PTO} and k are adjustable with the frequency, in order to maximize the power output of the device in correspondence of any incident wave.

Such a PTO represents a strong idealization of practical PTOs. Effectively, electric generators (or variable displacement hydraulic machines) produce a controlled damping effect only, behaving as viscous dampers, but they do not allow the control of the reactive energy.

The results discussed in this section (in terms of energy productivity) represent thus an upper limit that is not touched by any of the existing technologies.

The optimization problem for the case in exam has to be solved for each of the considered sea conditions (paragraph …) takes the following form:

$$\max_{k,\, B_{PTO}} \left\{ P_{dev} = \frac{B_{PTO}}{2} \omega^2 \frac{\Gamma^2}{(-I\omega^2 + k)^2 + (B_{rad} + B_{PTO})^2 \omega^2} \right\}$$

with a constraint on the angular displacement from the equilibrium position

$$|\Theta| = \frac{\Gamma}{\sqrt{(-I\omega^2 + k)^2 + (B_{rad} + B_{PTO})^2 \omega^2}} \leq \theta_{LIM} = \frac{\pi}{4}$$

A simple mathematical analysis of the constrained optimization problem above brings to the following results.

The system must be resonating with each incident wave:

$$k = I\omega^2$$

The value of the PTO induced damping is

$$B_{PTO} = B_{rad}, \qquad \text{if} \qquad \frac{\Gamma}{2\omega B_{rad}} \leq \theta_{LIM}$$

$$B_{PTO} = \frac{\Gamma}{\omega \theta_{LIM}} - B_{rad}, \qquad \text{if} \qquad \frac{\Gamma}{2\omega B_{rad}} > \theta_{LIM}$$

In other words, the ideal control of the PTO system is such that the WEC resonates with each of the incident waves (assumed as monochromatic) and the damping level is chosen in order to maximize the power output (according to general result of linear theory) or to keep the oscillation amplitude of the flap below the limit allowed value.

The analytical results are applied to the reference sea states. Numerical results are presented in term of maximum pitch angle from vertical position θ, power output P, capture width ratio ϵ, and the energy productivity [kWh] over a period of 8760 hours. Moreover, for any state, the values of the damping coefficient due to the PTO (that produces the above mentioned conditions) is reported.

state	B_{PTO} [Nms]	θ	P [W]	ϵ	Productivity [kWh]
#1	3.43E+06	0.256	5.47E+04	1.777	1.20E+05
#2	2.75E+06	0.575	1.99E+05	1.890	3.49E+05
#3	3.08E+06	0.785	3.74E+05	1.954	5.81E+05
#4	4.82E+06	0.785	5.33E+05	1.696	6.77E+05
#5	6.37E+06	0.785	6.41E+05	1.401	5.62E+05
#6	8.22E+06	0.785	7.57E+05	1.109	4.64E+05
#7	9.91E+06	0.785	8.38E+05	0.894	3.30E+05
#8	1.19E+07	0.785	9.28E+05	0.709	5.69E+04
#9	1.37E+07	0.785	9.87E+05	0.580	5.19E+04

Yearly productivity: 3.19E+06 kWh

Mean capture ratio: 1.38

This result is of course an upper limit, realized with a totally ideal PTO system exploiting a fully optimal control strategy, operating on both the active and reactive component of the incident energy.

With reference to the case in exam, in Figure 3-12 is a representation of the power output of the OWSEC as a function of the wave height: notice that each value of the height represents a different sea state, thus, the plot may be more properly read as a representation of the power output of the device as a function of the rising sea conditions.

An exam of the results shows that, with increasing sea states, the power output of the devices increases progressively, even if , at most intense sea conditions a saturation tends to occur due to the constraint on the maximum oscillation amplitude.

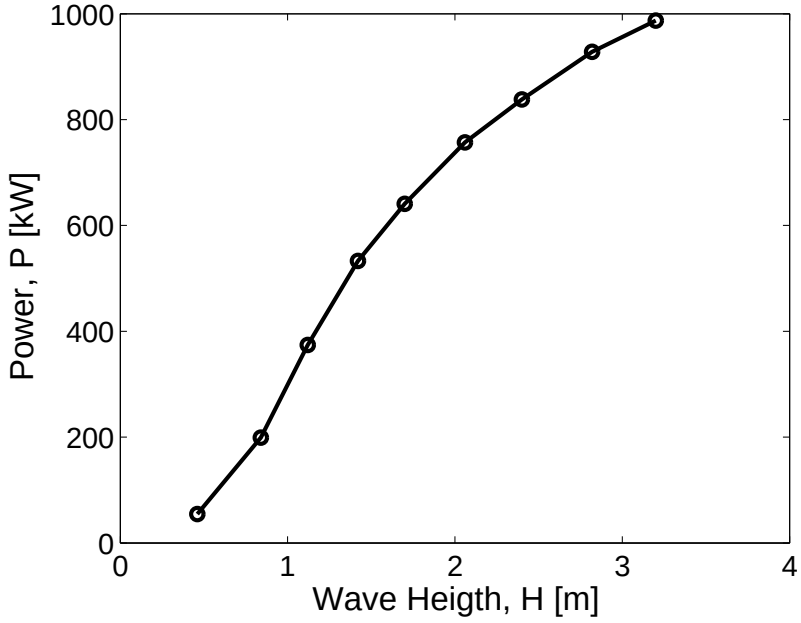

Figure 3-12 - OWSEC power output as a functions of the sea states

Some remarks are necessary, in order to clarify the confidence level within the reported results.

First of all, we remember that monochromatic waves only have been considered. It is then supposed that each of the considered sea states is featured by a precise value of incident frequency: as a consequence, for each sea condition, optimality is simply achieved by exploiting the resonance condition.

Considering a real polychromatic sea would introduce a complication in the resonance condition definition, since the device would be resonating with one harmonic only among those featuring the considered sea state. This would bring, among other, to a reduction in the system performances.

The hypothesis of monochromatic waves also explains the high assessed values of capture width ratio, that in many cases exceeds the unitary value. As already discussed, values of capture width ratio higher than 1 are possible for three-dimensional devices (like the one in exam): the Pelamis WEC, according to the information provided by Pelamis Wave Power, experiments capture width ratios up to 5. Anyway, this result is strongly related to the hypothesis of monochromatic incident wave and, thus, of linear ideal control.

The derived result is consistent with previous literature works. Folley et al. [26] show that, under the hypothesis of fully linear theory, capture width factors higher than 2 may be obtained for a seabed-mounted bottom-hinged flap; a study by Babarit et al. [19] carried out using a linear PTO (like that considered in the present example), but under the hypothesis of polychromatic incident waves assesses a mean yearly capture width of 70% about. Babarit et al. [19] state that linear theory, in general, leads to an overestimation of the dynamic response of the system and of the energy absorption.

Notice that, in the case in exam, due to the presence of a constraint on the oscillation amplitude, the capture width ratio ϵ visibly decreases in correspondence of the most intense sea states. Effectively, capturing a large amount of energy from highest waves would be possible only by exploiting large pitch oscillations.

Another remark on the procedure and on the results presented above is finally necessary. The procedure adopted in the above described problem, is, strictly speaking, valid in a small range of device motion, around the equilibrium position. This is due to the fact that the hydrodynamic parameters, such

- the wave induced damping torque amplitude Γ
- the added inertia due to radiation I_{add}
- the damping due to radiation B_{rad}

are calculated by mean of the WAMIT code with reference to a flap standing in vertical equilibrium position and are therefore reliable and accurate only for small displacement of the system from the vertical position itself. When the flap is off the equilibrium position, strong non-linearities may occur in the hydrodynamic of the system, producing different results with respect to those presented in here.

3-2.2.2 Traditional active PTO system

In the example of the previous paragraph, an optimal control strategy for the OWSEC was assumed, able to tune both the external applied damping and stiffness in order to realize an optimal matching with the incident monochromatic wave.

We consider here the more realistic situation where the overall stiffness *k* of the system is a constant, and it is not related to the PTO system control, so that B_{PTO} is the only control variable.

In other words, it is assumed here that the stiffness of the system is determined by the combination of the flap buoyancy and of an external mechanical spring. Since the flap buoyancy is non-linear, it can be assumed that the mechanical torsional spring also is non-linear, in order to compensate the buoyancy providing a constant overall stiffness *k*.

The PTO system is able to perform a control of the active component only of the incident energy, behaving as a viscous damper. This behavior is obtained by employing an electric generator with speed control.

With these assumptions and regarding the reference sea states, the system has to be optimized in order to maximize the energy productivity over a target period (8760 hours).

In order to optimize the system, the following parameters must be chosen:

- The value of the overall stiffness *k* of the system. This value does not represent a control parameter and is thus kept constant during the operation of the system and in correspondence of different sea states.
- The control parameter B_{PTO}. The velocity control of a traditional electric generator has the effect of varying the level of PTO applied damping. As a consequence, in correspondence of different sea-states, different values of B_{PTO} are adopted in order to both maximize the device power output and to meet the constraint $|\Theta| \leq \theta_{LIM}$.

Considering that the value of the external stiffness is fixed and independent on the incident wave frequency, we preliminarily concentrate on the calculation of the optimal value of B_{PTO} for each reference sea state. The following problem has to be solved:

$$\max_{B_{PTO}} \left\{ P_{dev} = \frac{B_{PTO}}{2} \frac{\Gamma^2}{C^2 + (B_{rad} + B_{PTO})^2} \right\}$$

where $C^2 = (-I\omega^2 + k)/\omega^2$ is constant for the considered sea state, with the constraint

$$|\Theta| = \frac{\Gamma/\omega}{\sqrt{C^2 + (B_{rad} + B_{PTO})^2}} \leq \theta_{LIM} = \frac{\pi}{4}$$

The mathematical solution for the problem allows to calculate B_{PTO} for the considered sea condition:

$$B_{PTO} = \sqrt{C^2 + {B_{rad}}^2}, \qquad \text{if} \qquad \frac{\Gamma/\omega}{\sqrt{C^2 + \left(B_{rad} + \left(C^2 + {B_{rad}}^2\right)^{1/2}\right)^2}} \leq \theta_{LIM}$$

$$B_{PTO} = \sqrt{\frac{\Gamma^2}{{\theta_{LIM}}^2 \omega^2} - C^2}, \qquad \text{if} \qquad \frac{\Gamma/\omega}{\sqrt{C^2 + \left(B_{rad} + \left(C^2 + {B_{rad}}^2\right)^{1/2}\right)^2}} > \theta_{LIM}$$

Thus, once the overall stiffness of the system is known, an analytical solution for the damping coefficient B_{PTO} is determined.

The optimal value of k (and, thus, of C^2) has to be determined. This parameter is chosen in order to bring the system in resonance with a precise frequency ω_{res}:

$$k = I{\omega_{res}}^2$$

The choice of ω_{res} must be carried out in order to maximize the overall annual energy productivity.

It is intuitive that the optimal frequency has to be researched in the range of frequencies of the reference sea states. Thus, indicating with $T_i,\ i = 1,2,\dots 9$ the wave periods for the reference sea conditions, an optimal value for the natural resonance frequency of the OWSEC has to be found in the interval

$$\omega_{res} \in [2\pi/T_9; 2\pi/T_1]$$

The optimization is carried out considering a finite number of values for ω_{res} chosen in the mentioned interval. For each possible choice of ω_{res}, the optimal value of B_{PTO} is calculated for each of the nine reference states, and the resulting yearly productivity is obtained.

The results in term of assessed energy productivity vs. ω_{res} are reported in Figure 3-13.

It results that the optimum choice for the resonance frequency is

$$\omega_{res} = 0.60\ rad/s$$

that corresponds to a resonance time period of $T_{res} = 2\pi/\omega_{res} = 10.48\ s$ that means that the system must be resonating with the fourth sea state. This represent a tradeoff between the energy available from the waves (sea states with larger period and wave-amplitude are associated to larger amounts of power per unit crest width) and the relative frequency of the different states (states with larger wave heights, even being more 'energetic', are much more improbable).

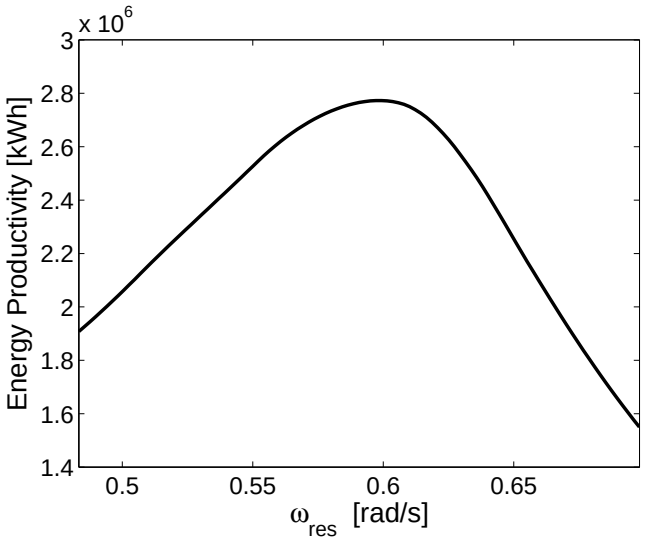

Figure 3-13 - Yearly productivity for different choices of the resonance frequency

The overall external stiffness required to meet the resonance condition at $\omega_{res} = 0.60\ rad/s$ is k=1.23E+07 Nm.

This results gives an information about the mechanical spring component that has to be applied to the flap in order to achieve the condition of maximum energy productivity.

The overall stiffness of the system results from the combination of the own stiffness of the flap and the stiffness provided by mechanical spring-like components. The own stiffness of the system can be calculated considering the resultant torque acting on the flap due to the combined effect of Achimede's force and weight force, as previously discussed.

The resulting 'buoyancy torque' can be easily expressed as a function of the position of the flap (thus, of the angle formed by the flap with the vertical position): the plot in Figure 3-14 shows the profile of buoyancy torque vs. angular position of the device, for the considered angular range $\theta \in [-45°; 45°]$.

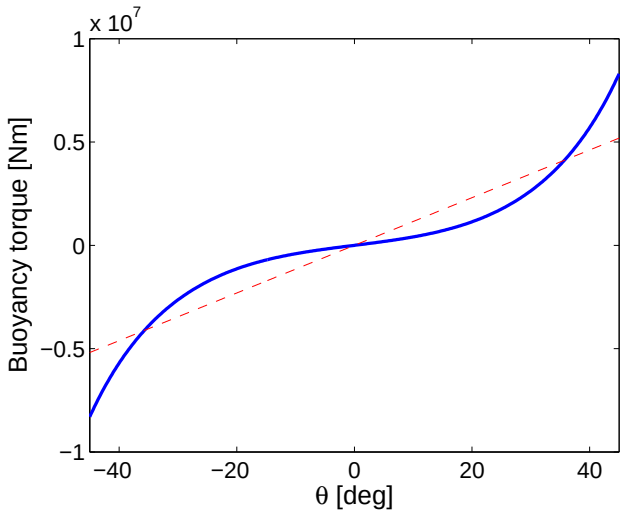

Figure 3-14 - Buoyancy torque vs. angle (blue) and its linearization (red)

Considering a linearization of the above mentioned torque (red line in Figure 3-14), the linearized value of the stiffness due to buoyancy is k_b=6.6E+06 Nm. To reach the desired stiffness it is necessary to apply an external mechanical spring component with stiffness k_{ext}=5.7E+06 Nm.

More precisely, since the effect of buoyancy is visibly non linear (Figure 3-14), the mechanical torsional spring required to achieve the mentioned condition has to be non linear and provide a constant overall stiffness when combined with the buoyancy effect of the flap.

Assuming $\omega_{res} = 0.60\ rad/s$, the results for the nine Azores sea states are reported in the next table.

The yearly productivity results in 2.77E+06 kWh and the mean capture width ratio is 1.20.

Notice that, with the optimal control discussed in the previous paragraph, a reduction in the expected productivity of 13% only has been assessed.

state	B_{PTO} [Nms]	θ	P [W]	ϵ	Productivity [kWh]
#1	8.09E+06	0.129	3.26E+04	1.059	7.14E+04
#2	5.41E+06	0.337	1.34E+05	1.274	2.35E+05
#3	3.15E+06	0.717	3.20E+05	1.667	4.95E+05
#4	4.82E+06	0.785	5.33E+05	1.696	6.77E+05
#5	6.06E+06	0.785	6.10E+05	1.333	5.34E+05
#6	7.24E+06	0.785	6.67E+05	0.978	4.09E+05
#7	8.07E+06	0.785	6.82E+05	0.728	2.69E+05
#8	9.20E+06	0.785	7.17E+05	0.548	4.40E+04
#9	1.00E+07	0.785	7.24E+05	0.425	3.80E+04

With reference to the case in exam, in Figure 3-15 is a representation of the power output of the OWSEC as a function of the wave height.

The saturation of the power output in correspondence of intense sea states, already mentioned for the case in Figure 3-12, is here accentuated and is the result of the limitation present on $|\Theta|$.

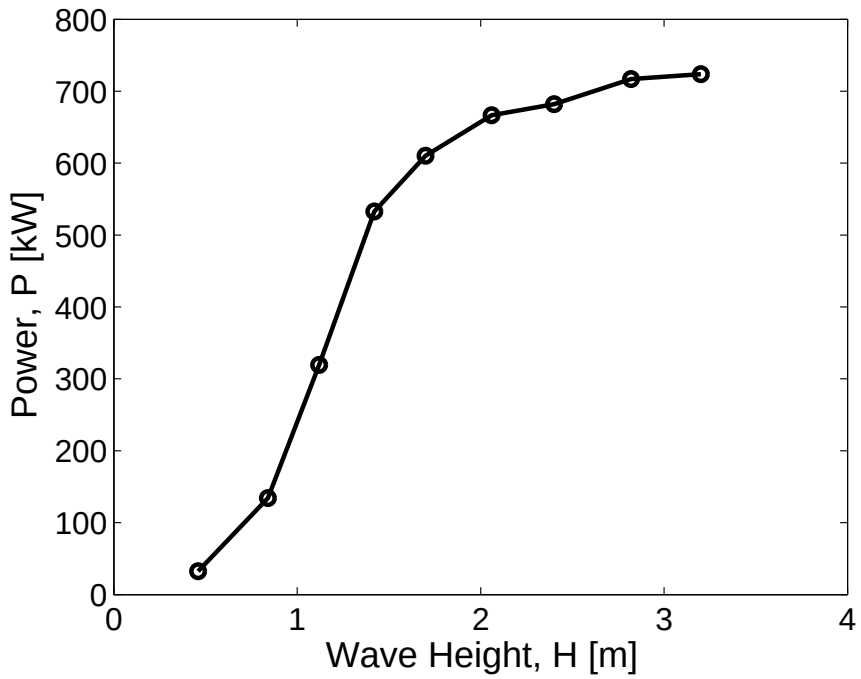

Figure 3-15 - OWSEC power output as a functions of the sea states

This result is not new in the field of Wave Energy: the nominal power output curve for the Pelamis WEC, shown in a previous chapter, has a comparable profile.

The concept that, for a given design of the energy conversion device, the power output is upper limited even with increasing input resources (carrying higher amounts of available energy), is observed also in the field of wind energy generation [92]: typical wind turbines are controlled (varying the rotor angular speed or the pitch angle of the blades) in order to keep the power output constant with stronger wind than the nominal one.

3-3 Application of a LS-DEG PTO

In the present section we consider the application of the LS-DEG, analyzed in chapter two, to the OWSEC.

In paragraph 3-2.2.1 an ideal PTO has been considered, capable of both tuning the applied damping level and the external applied stiffness. This ideal generator does not correspond to any real existing PTO system, and allows energy performances that represent an upper bound for the technology.

In paragraph 3-2.2.2, conversely, the coupled behavior of an OWSEC and a traditional electric generator has been carried out. It has been assumed that the electric PTO is modeled as a viscous damper. This model for the electric generator is quite optimistic, since it does not keep into account intrinsic limitations within the device, but simply assumes that the generator is able to produce any desired value of the applied damping B_{PTO}, without limitations.

For this reason, it can be assumed that a reasonably good target, for the novel polymeric PTO concept investigated here, is reproducing energy performances comparable with those obtained with the traditional electric system.

An approach that allows to dimension the LS-DEG in order to obtain the expected result has been here followed. Two steps are considered:

- In a first preliminary analysis, a volume of polymeric material is fixed that, even without any further mechanical spring component, allows a productivity comparable with that of the electric generator
- Successively, with the assessed volume of polymeric material, an optimization is carried out, and a more generic dimensioning strategy is presented.

Of course, complete and complex models of the problem should include some further fundamental aspects like

- The hydrodynamic of the OWSEC should be studied with models having wider range of validity (since the flap is assumed to move in a large range of pitch angle positions).
- The effect of visco-elasticity and hysteresis of the material should be kept into account.
- Different geometric configurations for the transducer mechanism can be hypothesized.

3-3.1 Layout of the system

A specific configuration has been here adopted for the coupling of the DEG and of the WEC.

The LS-DEG is mounted in a way that, when the flap is in vertical position, the surface of the DE is maximum and has square shape.

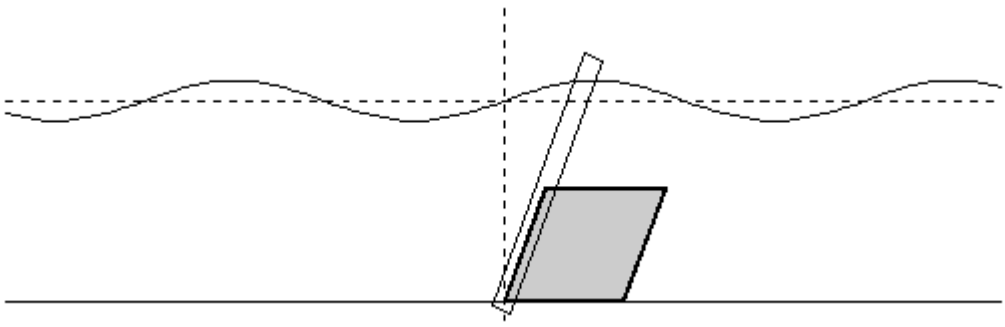

Figure 3-16 - OWSEC with LS-DEG on one side

Let refer for simplicity to a case where the flap has a LS-DEG on one side only (Figure 3-16). The LS-DEG has one side in-built with the flap and another side in-built with the plane housing the pivot axis of the device.

The polymer is shaped in several membranes. As it will be demonstrated later on, large polymer volumes are required. These large amounts of materials can be collocated in the space using a side dimension for the lozenge comparable with the flap length, and using a set of several films, each provided with a couple of compliant electrodes, arranged consecutively along the flap width.

The usage of a set of distinct DE membranes instead of a monolithic volume is a necessity in order to guarantee a homogeneous exploitation of the material and facility in the maintenance operations.

The safeguard of the active material and of the conductive paste of the electrodes must be guaranteed by insulating the generator from marine water. This goal can be achieved by realizing a compliant deformable case, housing the generator components, or by upholstering the generator with a layer of non-stretched polymeric material that plays the only role of decoupling the active part from the water, without introducing any further stiffness.

It is clear that, for an arrangement of the LS-DEG like that considered in Figure 3-16, pitch angular of displacement of the flap must be kept below a security value, in order to escape the mechanical rupture of the polymeric membranes. For this reason, in accordance with the constraint adopted for the traditional linear PTOs also, a limitation on the oscillation amplitude of the device will be considered. In presence of storms, with unusual intense waves, the device has to be brought to a security position, in order to protect both the oscillating part and the generator. It is then necessary a mechanical system that allows the disconnection of the LS-DEG from the flap in presence of critical sea conditions.

The pre-stretches λ_{1p} and λ_{2p} are equal, so that the behavior of the device is symmetric with respect to oscillations occurring in opposite directions. When the generator passes through the vertical position, it is electrically activated: while the flap leaves the vertical position, the surface of the activated membrane reduces and, thus, the charges on the resulting condenser are brought ‘closer’ and electric energy is generated. When the flap reaches the point of maximum angular displacement from the vertical configuration, the membrane gets

deactivated: during the return phase to the vertical position, no charge is present on the membrane faces.

Notice that, for this layout, in the configuration of maximum surface (that corresponds to maximum capacity of the resulting condenser), the elastomer reaches square shape.

In chapter two we demonstrated that, in order to maximize the energy per unit polymer volume that the generator is able to convert, it would be convenient to operate in a range of positions that are far from the square configuration: good values of the energy per unit volume are achieved if, in its operation range, one diagonal of the LS-DEG maintains its length much lower than the other diagonal. Nevertheless, it must be noticed that, with the configuration described above, during a wave period, two active strokes (and 2 inactive strokes) are present, thus, two generation cycles per period are carried out. Using an asymmetric configuration, only one stroke per period would be realized.

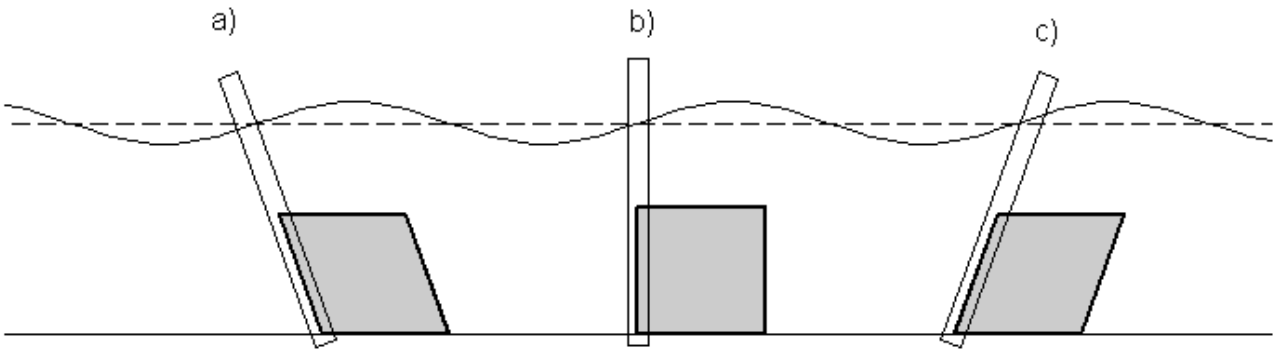

Figure 3-17 - Minimum surface configurations a), c) and maximum surface configuration b)

The calculation of the torque acting on the flap due to the LS-DEG is made using the mathematical models described in the second chapter for both the electric and mechanical response of the DE. The mechanical behavior of the material is described using Gent model.

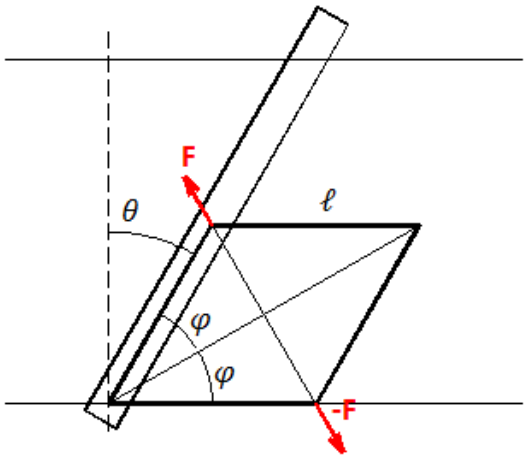

Figure 3-18 - Geometric descriptive parameters of the LS-DEG

With reference to Figure 3-18, indicating with *F* the equivalent force acting on the joint of the lozenge frame connected to the flap (calculated accordingly to the procedure previously illustrated and described by Vertechy et al. [60]), the PTO torque acting on the flap is

$$T_{PTO} = F\ell\cos\varphi$$

where φ is simply given by $\varphi = (\pi/2 - \theta)/2$.

An important consideration is that the LS-DEG induced torque depends on the volume of employed polymer only: once the volume is fixed, the side of the lozenge itself does not affect the resulting torque. This fact guarantees that, for a fixed value of polymer volume, the lozenge side (and thus the membrane thickness) can be arbitrarily varied without affecting the result.

We remember that the membrane volume *Vol* is (the symbols are those in the previous chapter, except for the polymer volume, that is indicated with *Vol* instead that *B* to avoid confusion with the damping coefficient defined in this chapter):

$$Vol = A_0 t_0 = \frac{x_0 y_0}{2} t_0 = \frac{x_p y_p}{2\lambda_{1p}\lambda_{2p}} t_0 = \frac{{x_p}^* {y_p}^*}{2\lambda_{1p}\lambda_{2p}} t_0 \ell^2$$

The overall force *F* acting on the LS-DEG can be split into two addenda [60]: a mechanical addendum F_{off} and an electrostatic addendum F_{em}.

$$F_{off} = \frac{t_0}{2}\left(\frac{\sqrt{4\ell^2 - {x_p}^2}}{\lambda_{2p}}\frac{\partial\psi}{\partial\lambda_1} - \frac{x x_p}{\lambda_{1p}\sqrt{4\ell^2 - x^2}}\frac{\partial\psi}{\partial\lambda_2}\right)$$

$$= \frac{t_0\ell}{2}\left(\frac{\sqrt{4 - {x_p}^{*2}}}{\lambda_{2p}}\frac{\partial\psi}{\partial\lambda_1} - \frac{x^* {x_p}^*}{\lambda_{1p}\sqrt{4 - x^{*2}}}\frac{\partial\psi}{\partial\lambda_2}\right)$$

$$F_{em} = -\frac{\varepsilon {E_{BD}}^2 t_0}{\lambda_1\lambda_2}\frac{2\ell^2 - x^2}{\sqrt{4\ell^2 - x^2}} = -\frac{\varepsilon {E_{BD}}^2 t_0\ell}{\lambda_1\lambda_2}\frac{2 - x^{*2}}{\sqrt{4 - x^{*2}}}$$

The torque acting on the flap is $T_{PTO} = F\ell\cos\varphi \propto t_0\ell^2 \propto Vol$. Thus, once the pre-stretches are given, the torque depends on the overall volume and not on its distribution (side-thickness ratio).

With reference to this observation, let consider the layout in Figure 3-19.

The system consists of two twin LS-DEGs. At any angular position of the flap, the surfaces of the two generators are identical: both the generators apply to the flap the same torque (that tends to bring the flap back to the vertical position).

Since the overall torque depends on the total volume of polymer only, it is immediate to understand that the system of Figure 3-16 can be split into two identical LS-DEGs having the same side of the original generator but with overall occupancy width (parallel to flap width) that is half of that for the single generator.

Thus, splitting the LS-DEG into two twin generators, located on opposites sides of the flap, would simplify the arrangement of the elastomer films along the flap width. Notice,

furthermore, that, since for any position of the flap the surfaces of the twin generators are identical, the ECCs of the two generators are perfectly ‘in phase’, thus, no drawback would occur in the control system of the equipment.

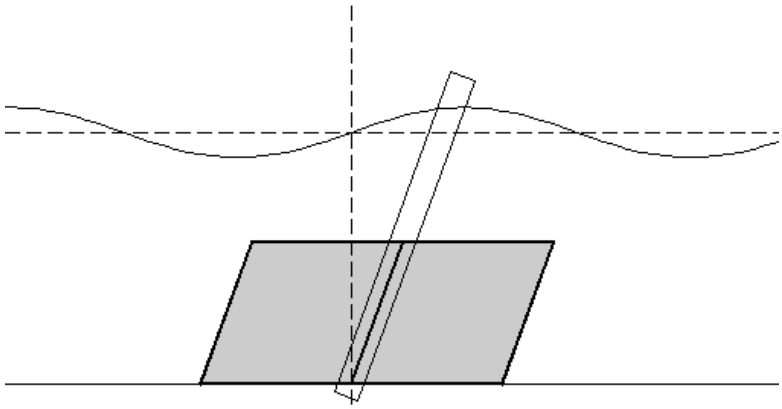

Figure 3-19 - OWSEC with LS-DEG on both sides

3-3.2 General Simulink model

In order to implement the novel concept of polymeric PTO to the OWSEC model, in the most general way, the Simulink scheme of Figure 3-2 has been edited and adapted.
The new scheme is shown in Figure 3-20.
With respect to the blocks described above, some new components have been added:

F. Variable buoyancy: Together with block E, representing the effect of buoyancy and of eventual external torsional springs, a User-defined Function implementing non linear buoyancy (according to the previous considerations) has been realized. The presence of both block E and F allows to choose, case by case, if implementing the buoyancy effect as a constant stiffness effect or as a non-linear effect.

G. PTO block: This block calculates the torque provided by the LS-DEG as a function of the input pitch position of the flap.
   The block is based on a User Defined Function that implements the ideal Energy Extraction Cycles, discussed in chapter two, taking into account the failure conditions for the device.

H. Generator dynamics: the LS-DEG is alternately activated and deactivated. The deposition of the charge on the membrane faces is theoretically instantaneous, nevertheless, since the activation provokes a visible change in the torque applied by the PTO to the membrane, in order to guarantee the numerical stability of the solution, discontinuities on the torque must be avoided.

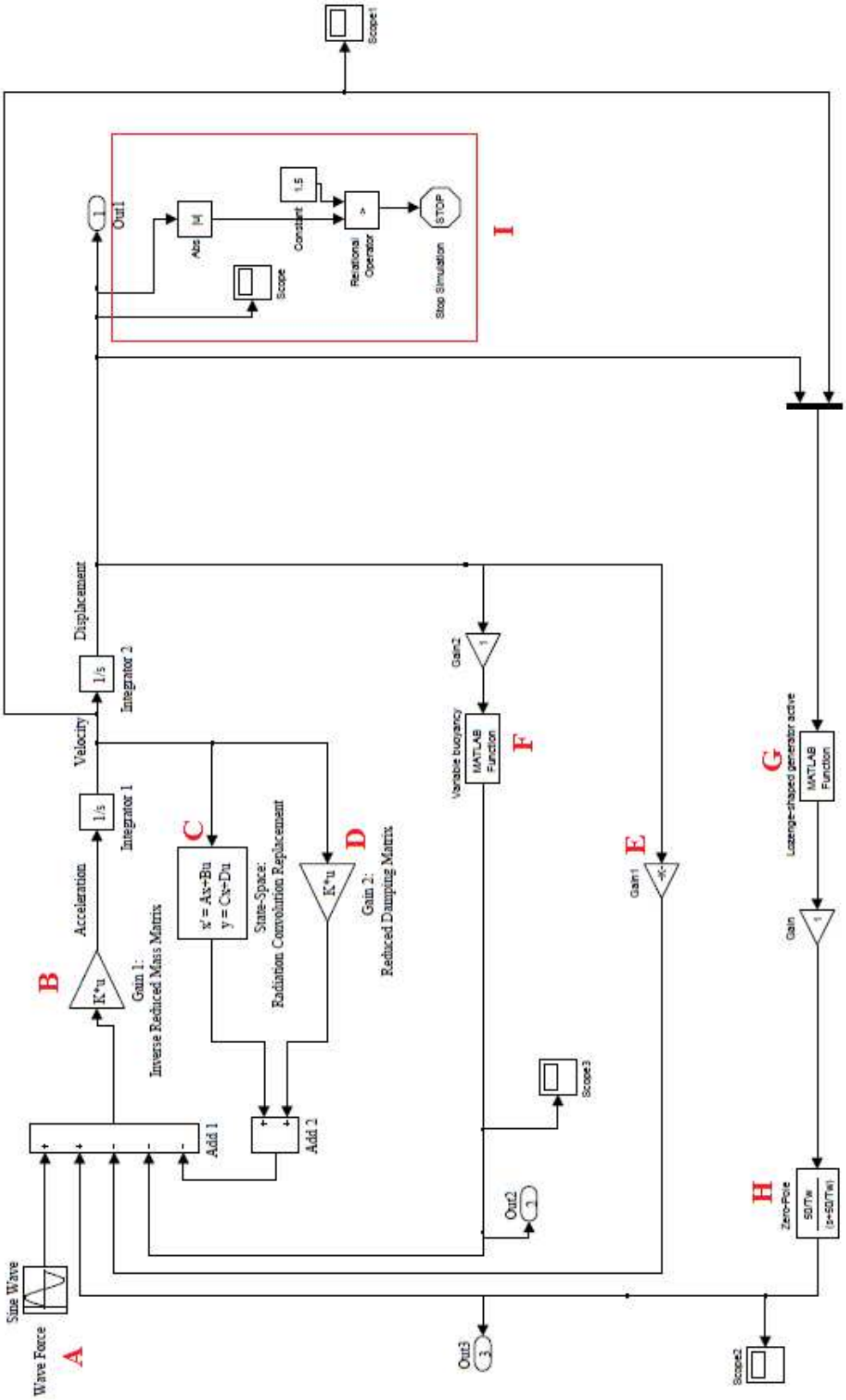

Figure 3-20 - Simulink scheme for the system OWSEC + LS-DEG

For these reasons, a certain dynamic has be assigned to the system, simulated by a transfer function block in the form

$$F(s) = \frac{1}{1 + \tau s}$$

where τ has been fixed equal to $T_w/50$: this assumption is totally arbitrary, since the real dynamics of the system depends on the capacity of the resulting condenser and on the resistivity of the electrodes and of the connected circuitry, anyway, this assumption is only functional to guarantee the numerical stability of the solution.

I. This set of blocks is functional to detect eventual non-physical solutions. The system, modeled accordingly to the previous indications, does not take into account the boundary condition given by the sea-bed, therefore, pitch angles higher than 90° could occur: this would represent a non-physical solution.

Moreover, no end-stops are present within the system, in order to avoid excessive mechanical loads in presence of intense sea states.

The present set of blocks simply stops the simulation when the pitch angle exceeds the value of 90° that would represent a physical non-sense.

It is important to precise that, in the previous analysis, two important phenomena are neglected:

- the inertial effect of the polymeric material and of its frame is not considered: the only inertia is that of the flap WEC (own inertia plus added inertia)
- The effects on the fluid-dynamics due to the presence of the LS-DEG are not examined.

The calculation of the power output of the system is carried out in Matlab, by mean of a routine that controls the running of the Simulink scheme exploiting the *sim* command.

From the results produced by the Simulink model, the oscillation angle of the flap is known, thus, the operative range of the LS-DEG also is known (since the oscillation amplitude defines a value of the maximum/minimum length assumed by the lozenge diagonals during the operation). Using this information, since the control strategy of the generator is given (and defined by the ECC described in chapter two), the energy per unit volume converted by the generator in one stroke, $En_{,st}$, can be calculated. Since the system has two active strokes per period, the mean power produced by the system over one wave period, T_w, is

$$\bar{P} = En_{st}/T_w$$

3-3.3 Preliminary study: approximate dimensioning of sub-optimal LS-DEG PTO

In this section, we present a preliminary dimensioning of a polymeric PTO, capable of energy productivities comparable with those of the electric solution. The procedure presented in here is far from being a general design methodology, and is rather a case-related example that

shows that, even without specific optimizations (like the addition of external mechanical spring-like components), the DE-OWSEC system is capable of relevant energy performances. The dimensioning is carried out using the following approach:

- An approximate value of the necessary polymeric volume is chosen. A first assessment of the order of magnitude of such volume can be produced by exploiting the following consideration.

  Assuming a break-down field E_{BD}=70 MV/m, a maximum convertible energy of ~200 kJ/m^3 is expectable. Thus, in order to produce a mean power output of about 700 kW (like for the electrical PTO) in correspondence of sea state #9 (T_w=13 s) with a LS-DEG that performs two strokes per period, a polymeric volume of at least 30 m^3 is necessary.

  This raw optimistic calculation provides an order of magnitude only of the necessary amount of DE material. A better assessment of the needed volume is determined by repeating a series of simulations with different polymers volumes.
- As for the case examined in paragraph 3-2.2, a maximum value (θ_{LIM}) of the angle formed by the flap with the vertical line during the oscillation is fixed. Again, we use the value of 45°.

  The choice of the maximum allowed angular displacement of the system is crucial in order to dimension the polymeric generator. We assume indeed that the pre-stretches $\lambda_{1,p}$ and $\lambda_{2,p}$ (that have the same value for symmetry reasons) are such that the material reaches the rupture condition (calculated with reference to the conservative value of 5.5 for the rupture stretch λ_u) in the configuration where the flap forms an angle equal to the maximum allowed pitch displacement (45°) with the vertical.
- An example of EEC is shown in Figure 3-21. The filled surface represents the operation range of the device. We assume that the ideal cycle, delimited by the lines representing the various failure condition, is followed, therefore, the energy converted per cycle is proportional to the colored area.

The electric control system of the generator must implement the following operations:

1. Charge introduction at constant stretch (black line): when the flap passes through the vertical position, a certain amount of charge is deposited on the membrane faces. This operations is theoretically instant, since it should be carried out when the flap passes through the vertical position. Anyway, as already mentioned, a dynamic of the generator has been implemented in order to avoid discontinuities.
2. Charge removal at constant electric field (blue line): while the flap moves off the vertical position, charge is progressively removed from the faces of the elastomer sheets. In order to avoid break-down, charge is initially removed keeping the electric field constant and equal to the break-down electric field E_{BD}.

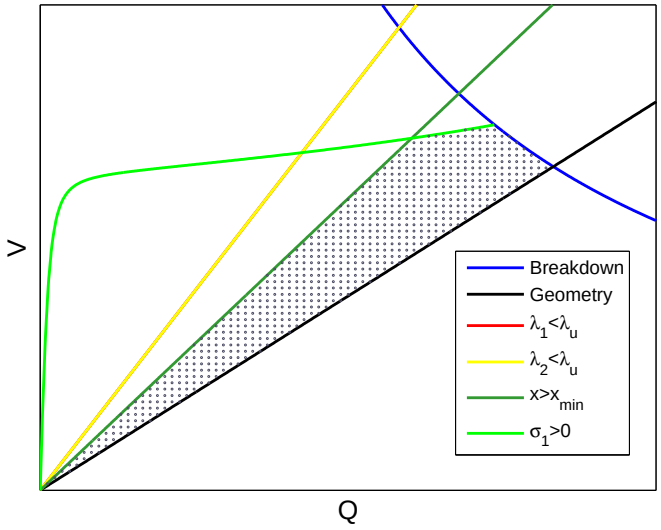

Figure 3-21 - Example of ECC for the LS-DEG connected to the system

3. Charge removal at constant mechanical stress (green line): when the flap approaches to the extreme pitch angles off the equilibrium position, the material tends to loss mechanical tension along the shorter diagonal. The electric control must be tuned in order to avoid material wrinkling.
4. Residual charge removal at constant stretch (dark green): when the generator reaches the condition with minimum surface (when the flap is at the end of its oscillation), charge is completely removed. Also this operation is theoretically instant.

In order to optimize the coupled behavior of the system OWSEC + LS-DEG, it could be useful to follow a slightly different control strategy.

The ECC of the generator affects the dynamic of the system, influencing the value of the oscillation amplitude of the flap. Large oscillations allow to obtain a wider operative range for the generator.

A possible approach consists in the use of a lower value of the electric field (with respect to E_{BD}) during the constant-electric field transformation.

In the example of Figure 3-22, an alternative cycle is carried out, with lower value of the field (we call this value ‘control electric field’).

This operation, at a first sight, appears to reduce the area enclosed by the cycle (in the Q-V plane), since the iso-field line (in blue on the Figures) moves towards the origin of the axes. Nevertheless, if the new value of the electric field allows larger oscillations of the flap, the slope of the line representing the final phase of discharging of the LS-DEG (dark green line) increases, and this could compensate the reduction of the electric field.

Controlling the value of the electric field allows, in a certain sense, to control the stiffness provided by the generator to the system.

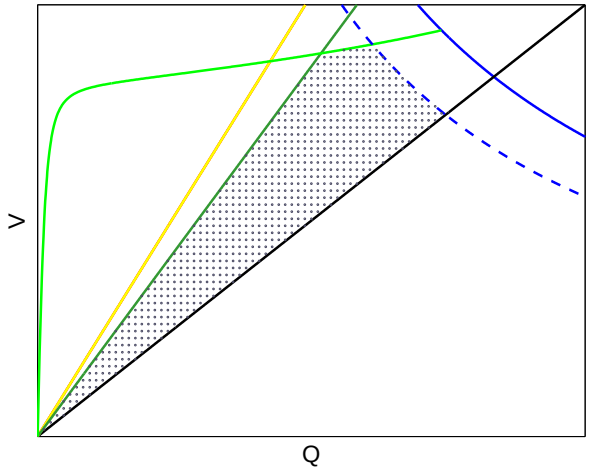

Figure 3-22 - Modified ECC

In the present analysis, the control electric-field value is modified, case by case (that is, for any of the examined sea states) in order to both maximize the power output of the WEC and to respect the constraint on the oscillation amplitude.

Results from the simulations are presented in the following.
After a series of analyses, with different amount of the overall volume of polymer, a value of about 90 m^3 has been identified as appropriate for the aim of the present dimensioning.
Starting from this consideration, a more precise assessment of the employed volume and a definition of the arrangement of the material can be done.
Let consider the layout of Figure 3-16 (LS-DEG on one side of the flap). We assume a value for the lozenge side length of ℓ=4 m. This value is a tradeoff between the necessity of using large lozenge sides, in order to reduce the width of the generator and that of avoiding excessive side lengths that would strongly affect the fluid-dynamics of the system.
While the system moves, the stretches within the material change and, thus, the overall width of the elastomer (given by the sum of the thickness of all the membranes present within the system) varies. The total thickness value is minimum (t_{min}) when the flap is in vertical position and the lozenge has maximum square surface; the thickness is maximum (t_{max}) when the surface of the lozenge is minimum (when the flap forms an angle of 45° with the vertical line). In order to produce a volume of 90 m^3, a total thickness of 8 m is necessary.
Since we demonstrated that the effect of the LS-DEG on the dynamic of the OWSEC depends only on the overall amount of polymer volume, a different side, i.e. of 5 m, could be assumed, that allows a reduction of the total width occupied by the polymer.
In the next table, we report a resume of the geometric features chosen for the generator (for 2 possible values of the side length ℓ):

LS-DEG located on one side of the OWSEC (Figure 3-16); Vol=90.51 m^3	
Side length ℓ= 4 m	Side length ℓ= 5 m
$\lambda_{1,p}= \lambda_{2,p}$=4.21 t_{min}=5.66 m t_{max}=8.0 m	$\lambda_{1,p}= \lambda_{2,p}$=4.21 t_{min}=3.62 m t_{max}=5.12 m

Of course, with the solution shown in Figure 3-19, t_{min} and t_{max} for each of the twin LS-DEG is divided by 2 (assuming the same side lengths).

In the table below, for each of the 9 sea states, we report the resulting power output, the optimal value of the control electric field (accordingly to the previous considerations) and the corresponding energy productivity over a time horizon of 8760 hours.

state	P [kW]	E [MV/m]	ϵ	Energy [kWh]
#1	19	70	0.627	4.23E+04
#2	81	70	0.770	1.42E+05
#3	201	70	1.046	3.11E+05
#4	447	56	1.423	5.68E+05
#5	695	56	1.518	6.09E+05
#6	738	60	1.082	4.53E+05
#7	717	61	0.765	2.83E+05
#8	718	62	0.549	4.40E+04
#9	704	63	0.414	3.70E+04
			tot	2.49E+06

In paragraph 3-2.2, we demonstrated that a maximum yearly energy productivity of 2.77E+06 kWh is possible using a traditional PTO (providing a viscous damping effect) plus a spring that makes the overall stiffness of the system constant (despite the position-dependent buoyancy torque).

In the present case, no external mechanical springs are present and the electric PTO is replaced by a LS-DEG.

With this simple action, for an exemplifying design of the LS-DEG (like that take in exam), a comparable energy productivity (of 2.5E+06 kWh) is obtained.

It must be notice that the power output values presented here are calculated with reference to the LS-DEG only, without considering its dynamics. In other words, the power is calculated extrapolating from the ongoing simulation the motion range of the device and, consequently, by calculating the energy per unit volume converted by the generator implementing the procedure described in chapter 2. With this method, the electrical losses due to Joule effect are neglected. We remember that, assuming a dynamics for the generator (implemented by mean of block H in Figure 3-20) corresponds to hypothesize a resistive component within the generator. Nevertheless, since the dynamic has been set in a quite arbitrary way, in order to guarantee the correct execution of the numerical routine only, we provide here an assessment of the overall electric energy production, including the unavoidable losses due to the dissipative components within the electric circuitry.

The curve that shows the power output of the system as a function of the different sea states for a traditional system (Figure 3-15) can be compared with the corresponding curve relative to the present system (DE-OWSEC). The result for the polymeric system is shown in Figure 3-23.

A qualitative profile similar to that observed for the traditional system (Figure 3-15) is obtained for the polymeric system also.

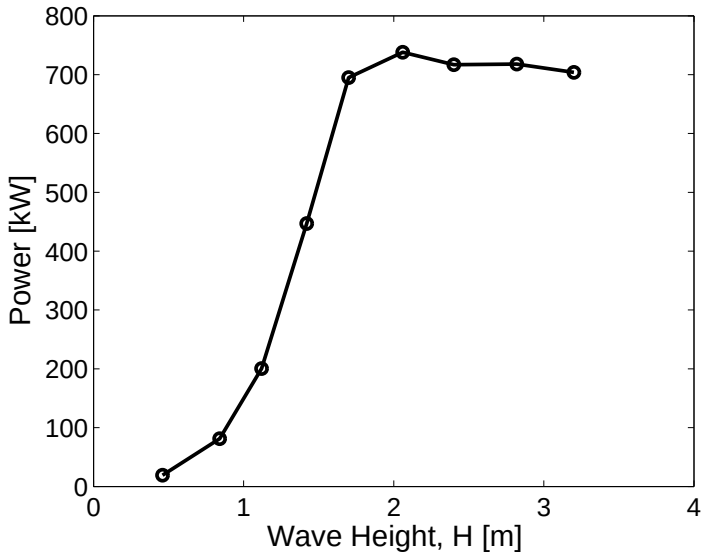

Figure 3-23 - DE-OWSEC power output as a function of the sea states

Like in the above analyzed case, a the power output of the WEC experiments a saturation with increasing sea states. Also in the present case, this behavior is explained remembering that a limitation has been put on the maximum angular displacement of the flap from the equilibrium position.

It is possible to conclude that the DE-OWSC is able to provide performances comparable to those of a traditional system, even without particular optimization measures.

Wider analyses, intended to optimize the system, are carried out in next paragraph.

3-3.4 Definition of a procedure for the design and optimization of DE-OWSECs

3-3.4.1 Simplification of the model

Starting from the results coming from the LS-DEG dimensioning of the previous paragraph, a more general procedure is here illustrated to dimension and optimize DE-OWSECs.

The calculations presented herein refer to a volume of polymer equal to that used in the example of paragraph 3-3.3, and we assume that the same specifics on the pre-stretches are used:

$$Vol=90.51\ m^3 \quad ; \quad \lambda_{1,p}=\lambda_{2,p}=4.21$$

Differently from the previous case, we suppose that the stiffness of the WEC is compensated by an external torsional non-linear spring that, combined with the buoyancy of the flap, provides constant overall stiffness (as in the examples of section 3-2.2).

The aim of the following analysis is providing a general methodology that, with relative modest computational effort, allows the optimization of the DE-OWSEC, that consists in:

- determination of the overall stiffness of the system, *k*.
- for each of the considered sea states, determination of the optimal iso-electric field transformation of the ECC (see previous paragraph).

The analysis starts from an open-loop characterization of block G in Figure 3-20. The block allows to calculate the LS-DEG induced torque on the WEC (with given descriptive parameters of the generator) as a function of the angular position and angular velocity of the flap.

In order to carry out an open-loop analysis of the LS-DEG response, let suppose that the input signals of the block (physically representing the pitch position and the angular velocity of the flap) are Sine Waves. The characterization is carried out using the simple scheme in Figure 3-24.

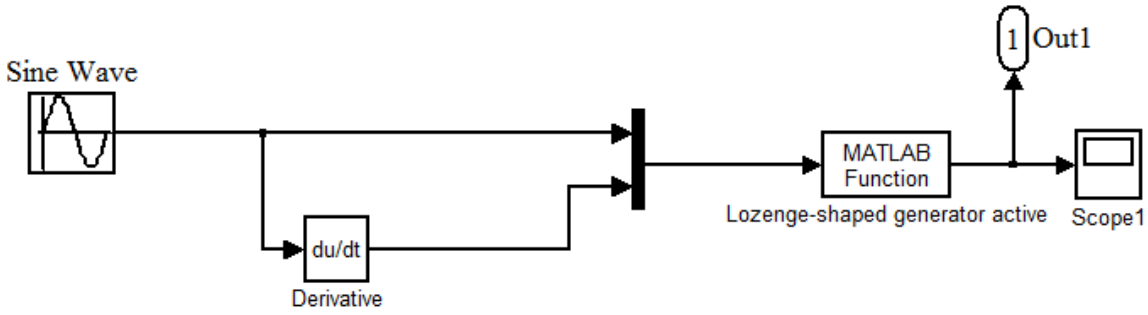

Figure 3-24 – Open-loop analysis of LS-DEG block.

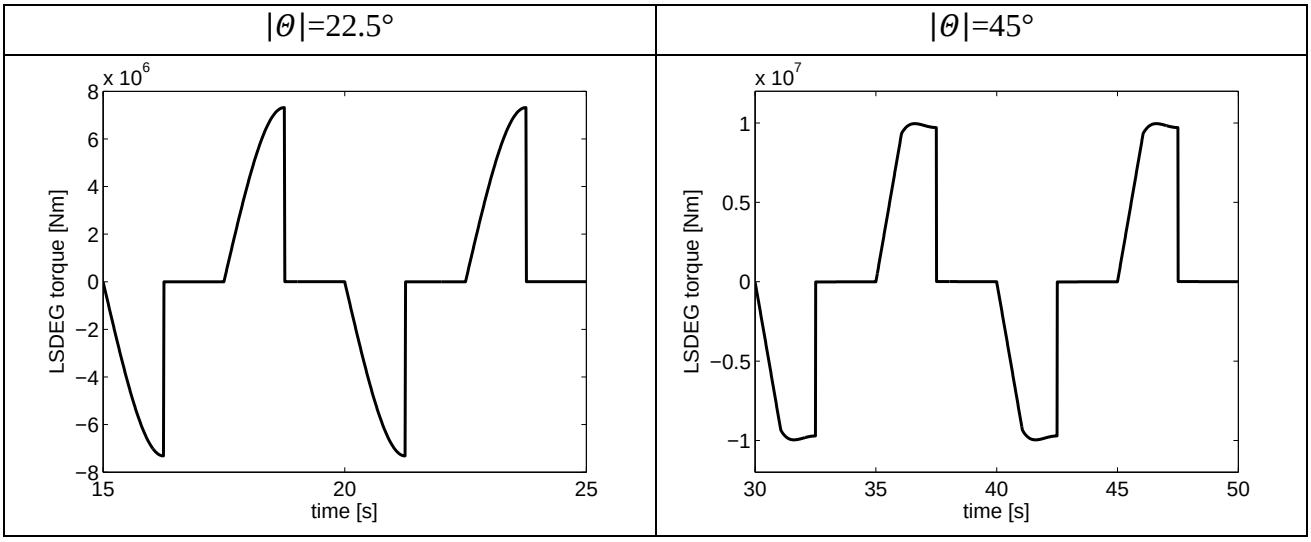

Figure 3-25 - Open-loop response of LS-DEG

Notice that, in the present analysis, the generator only is considered, disregarding its dynamics.

Using the specifics of the LS-DEG of paragraph 3-3.3, assuming a control electric field $E=E_{BD}$=70 MV/m, the following response (Figure 3-25) is obtained for two different amplitudes $|\Theta|$ of the sinusoidal excitation signal.

The plots of Figure 3-25 are slightly different, since for small oscillation amplitude the profile of the LS-DEG torque is 'sharper' than for oscillation amplitude of 45°. This is simply explained by noticing that, when the flap covers small angular ranges, the slope of the dark green line in Figure 3-22 (representing the minimum transducer length during the cyclic operation) decreases, and the constant-stress transformation tends to be drawn from the ECC. With large oscillations, on the contrary, the presence of an iso-stress transformation (corresponding to the condition σ_1=0) generates smooth profile of the induced torque.

Beyond this marginal aspect, the important result is that during inactive phases (when no charge is present on the membranes), the overall torque due to the LS-DEG is negligible. This means that the restoring force due to the material elasticity is negligible with respect to the electric induced torque.

Supposing to multiply the shear modulus of the material by 10 (that is representative of different materials, like natural rubber), the result is the same, with the only difference that, also with large oscillations, the torque profile is quite sharp, since the LoT curve (in the Q-V plane) tends to rise.

The mentioned result leads to the conclusion that the polymeric generator behaves as an on-off component, that produces non-zero torque only during a portion of the WEC oscillation.

Another fundamental aspect that allows a simplification in the modeling of the generator comes from analysis of the LS-DEG as a function of the flap pitch position θ.

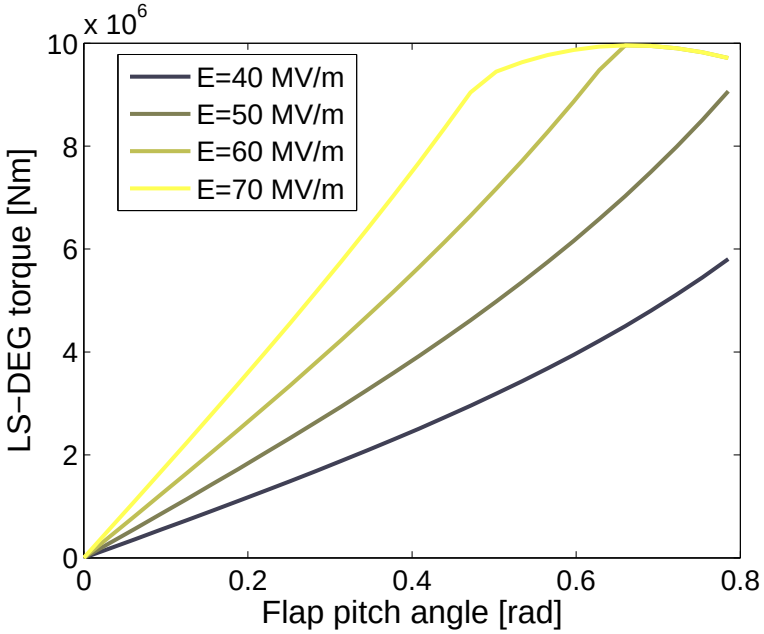

Figure 3-26- LS-DEG torque vs. flap angle for different values of the control field

In Figure 3-26, for different values of the control electric field, the profile of generated torque (during the active phase) vs. pitch angle of the flap is shown. A range of 45° is used for the pitch angle. The specifics for the LS-DEG are those presented in paragraph 3-3.3.

From Figure 3-26 it is possible to notice that the torque profile is, in a very good approximation, linear (except eventually for large pitch angles, where the LoT condition provokes a fall in the value of the torque).

Thus, considering an interval where the torque profiles are practically linear, i.e. [0°,30°], the response of the LS-DEG during the active phase is approximated by that of a torsional spring, with stiffness depending on the control electric field value.

In Figure 3-27, basing on a linearization of the curves of Figure 3-26 made on the angular range [0°,30°], we report the value of the stiffness constant, k_{PTO}, of the equivalent spring as a function of the control electric field.

For the considered amount of polymer volume, the maximum possible value for k_{PTO} is 1.8E+07 Nm, obtained with E=E_{BD}=70 MV/m.

In conclusion, since the polymeric PTO provides negligible torque during the inactive phases, and a torque almost proportional to the pitch angle when the generator is active, the mechanical response of the PTO can be approximately written in the form

$$T_{PTO} = 0 \quad , \quad \text{if } \theta \cdot \dot{\theta} < 0$$

$$T_{PTO} = -k_{PTO}\theta \quad , \quad \text{if } \theta \cdot \dot{\theta} \geq 0$$

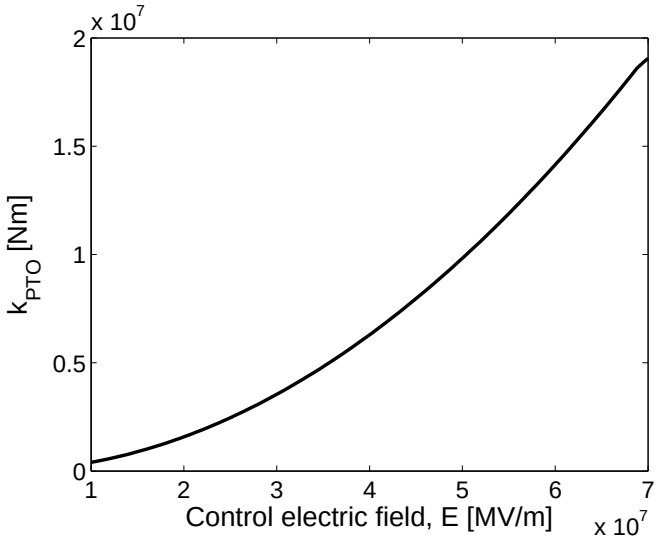

Figure 3-27 - Equivalent stiffness of the active LS-DEG as a function of the control electric field

In other words, the dynamics of the LS-DEG is approximated by that of an on-off torsional spring, that provides a restoring torque proportional to the flap pitch angle only for half of the oscillation time.

This result suggests an optimization methodology for the DE-OWSEC system, that can be also extended to the design problem.

Since the simulation of a system like the on-off spring discussed above is much smarter and less time consuming than the full simulation of the LS-DEG (with the model presented in chapter 2), the Simulink scheme of Figure 3-20 can be edited, by replacing block G (that contains the model of LS-DEG) with a block performing the simplified approximated dynamics. The overall system can be then simulated, and the power output of the new PTO block can be calculated as the mean (over a wave period) of the product of the PTO induced torque times the flap angular velocity.
Notice that, with this simplification, the PTO system is described by a parameter only that is k_{PTO}.
In the following, we consider the application of this simplification to both the optimization of a DE-OWSEC (the specifications of which are already known) and to the design of a polymeric PTO for an OWSEC. We will design the first approach (optimization) as 'direct problem', and the design problem as 'inverse problem'.

3-3.4.2 The direct problem: optimization of a DE-OWSEC

With 'direct problem', we mean the analysis, with a simplified polymeric PTO represented by an on-off spring, of a configuration of LS-DEG, coupled with an OWSEC, the specifications of which (volume, stretches) are known.
We refer, as already mentioned, to the LS-DEG outlined in paragraph 3-3.3. The reference generator has been dimensioned in a relative rough way, by simply assessing the amount of required volume to gain a productivity comparable with that of an electric generator. The aim of the present analysis is the identification of eventual margins of improvement for the energy productivity of the system.
Differently from the previous analysis, it is supposed here that the stiffness of the system, k, is linear, since the buoyancy is compensated by an external mechanical spring.
The optimization of the system is based on two parameters only:

- The stiffness k
- The PTO equivalent constant, k_{PTO}.

It has been already shown that, in correspondence of the considered specifications for the PTO, the constant k_{PTO} can reach a maximum value of 1.8E+07 Nm.
The optimization procedure has the aim of identifying an optimal value of k (that is of course supposed constant since it does not represent a control variable), and an optimal value of k_{PTO} for each of the reference sea states (since k_{PTO} is a control variable) in order to maximize the yearly energy productivity.
The ranges of variability of k_{PTO} and k are sampled. As a consequence, a matrix of states (each featured by a single value of k_{PTO} and k) is obtained. Of course, enlarging the number of samples will improve the accuracy of the calculation but will require long computation time.

Subsequently, for each of the considered sea states, the overall dynamic is solved in correspondence of any possible state (k_{PTO}, k): the output of the calculation provides the power produced by the WEC and the oscillation amplitude of the flap.

Using the results of the mentioned calculations, the determination of the optimum value for k and the control strategy for the system is determined as follows:

- A value of k considered
- For each of the sea states, the value of k_{PTO} is identified that maximize the power output without violating the constraint $|\Theta| \leq \theta_{LIM}$
- With this result, the corresponding energy productivity over a target period of 8760 hours is identified, for the chosen value of k.
- The procedure is repeated for each of the considered samples of k.
- A value of k that maximizes energy productivity is identified. Correspondingly, each sea state is associate to a precise value of k_{PTO} accordingly to the previous points.

The optimal value of k provides an information about the mechanical torsional spring that has to be integrated in the system. The values of k_{PTO} corresponding to each sea state allow to determine the optimal value of the control electric field, thanks to the univocal relationship shown in Figure 3-27.

For the reference design, with the mentioned constraint on the maximum value of k_{PTO}, the application of the mentioned formalism has produced the following optimal conditions (optimal value of k and optimal values of k_{PTO} for each sea state, with corresponding value of the control electric field).

k=6.6E+06 Nm	
k_{PTO} [Nm]	E [MV/m]
1.8E+07	70.0
1.7E+07	67.3
1.4E+07	61.1
1.1E+07	54.2
1.2E+07	56.6
1.3E+07	58.9
1.4E+07	61.1
1.4E+07	61.1
1.5E+07	63.3

Of course, since the simplified model represents an approximation only of the physics of the real system, a verification of the energy productivity with the optimal conditions deduced above has to be carried out exploiting the full model of Figure 3-20, with the non-linear buoyancy (block F) set to 0 and the overall linear stiffness (block E) set to the assessed optimal value. Results are in the following table.

state	P [kW]	E [MV/m]	ϵ	Energy [kWh]
#1	35	70.0	1.149	7.75E+04
#2	141	67.3	1.333	2.46E+05
#3	288	61.1	1.504	4.47E+05
#4	520	54.2	1.655	6.60E+05
#5	651	56.6	1.422	5.70E+05
#6	705	58.9	1.034	4.32E+05
#7	655	61.1	0.699	2.58E+05
#8	724	62.0	0.543	4.37E+04
#9	655	63.3	0.385	3.44E+04

The control field for sea state #8 has be incremented with respect to that forecasted by the optimization algorithm in order to respect the constraint on the oscillation amplitude.

With this choice of the system stiffness and of the electric field control, an annual productivity of 2.77E+06 kWh is forecasted. This level of productivity equals that expected for a linear electric PTO (paragraph 3-2.2.2).

The productivity curve for the case in exam is in Figure 3-28

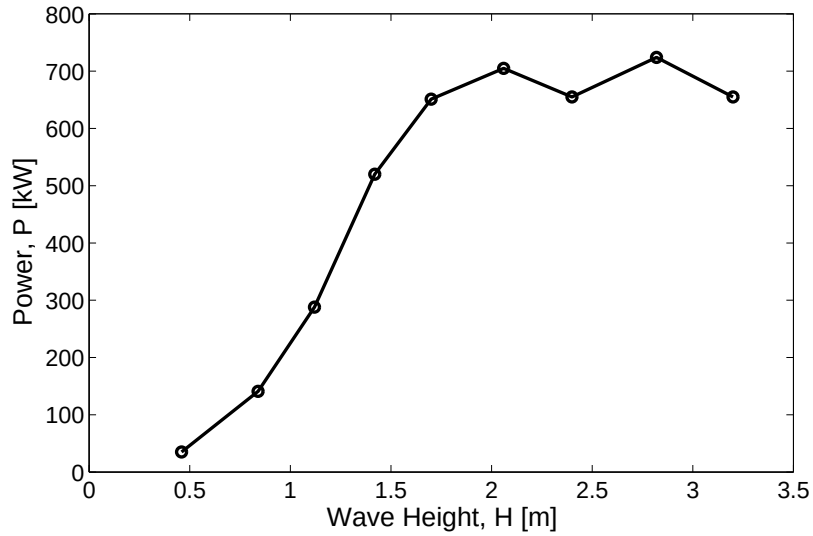

Figure 3-28 - OWSEC power output as a functions of the sea states

We remember, once again, that the power output values reported here include a percentage of electric energy that is lost due to the resistivity of the electrodes of the LS-DEG.

For comparison purposes, in Figure 3-29 we report on the same plot the H-P curves of Figure 3-15 and of Figure 3-28.

Apart from the numerical oscillation of the power curve for the LS-DEG, the output of the two generators are extremely similar.

This analysis leads then to the conclusion that polymeric LS-DEGs in combination with OWSEC systems are capable of power outputs comparable with those of an electric generator.

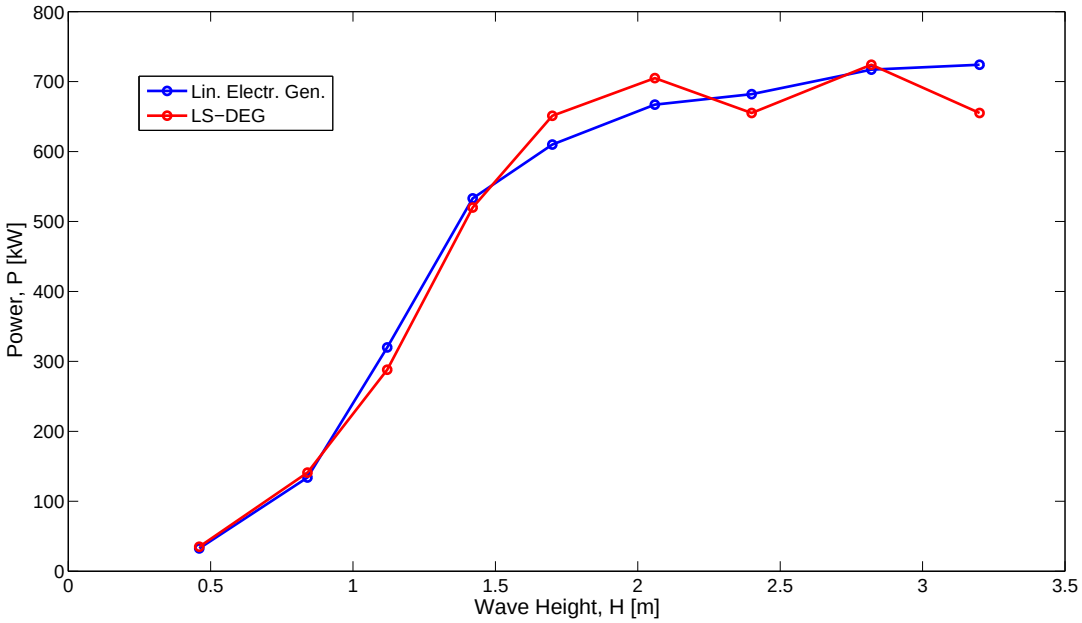

Figure 3-29 - Performance comparison for electric and polymeric generators

As a counterpart, large amounts of polymeric volumes are required, and a complex control strategy of the generator has to be implemented.

The analysis carried out in the previous sections on DE-OWSEC is quite elementary, since it disregards numerous aspects, like the effect on the fluid-dynamics of the massive polymeric generator and the electric losses due to the non-instantaneous charging-discharging dynamics of the LS-DEG. Moreover, all of the present analyses have been carried out with reference to monochromatic sea-states, that is an assumption that tends to produce sensitive overestimations of the WEC productivity.

The numeric results obtained here (for both electric and polymeric PTO) have then to be intended as a first estimation of the order of magnitude of the energy performances of the system, with the aim of comparing different PTO technologies, in order to assess the feasibility of the new polymeric PTO concept. Realistic forecasts about the power output of the surge WEC require indeed a deeper investigation and non-elementary calculation tools.

3-3.4.3 The inverse problem: design of a DE-WSEC

This paragraph has the aim of providing some synthetic indication for the employment of the simplified PTO model to the design problem.

The design starts from the assumption that a set of boundary conditions has been fixed for the WEC, thus, a set of sea states (with known relative frequency) are give and taken onto account for the project. Moreover, for the reference installation location, a design of the flap itself (dimensions, density) is give and, consequently, the fluid-dynamic parameters describing the wave-body interaction are known. We concentrate, thus, on the design of the PTO system only.

The formalism described in paragraph 3-3.4.1 states that a polymeric LS-DEG behaves, in good approximation, as a torsional on-off spring that provides negligible torque during the inactive phases and non-zero torque in the active phases.

Regardless the specifications of the LS-DEG (that are the unknowns of the problems), if the dimensions of the flap are fixed, the polymeric PTO can be thought, in a first approximation, as an on-off spring the constant k_{PTO} of which has to be determined.

The overall system can be then simulated, for a substantial number of values for k_{PTO}, in accordance to the procedure used in paragraph 3-3.4.2 for the optimization problem.

Two projectual choices can be considered:

- External mechanical spring-like components may be introduced. In this case, a multi-variable optimization has to be carried out. For a considerable number of samples of k, for each of the reference sea states, a number of values of k_{PTO} is considered, and the resulting energy productivity is calculated.
- No external stiffness is introduced, and the only stiffness is that provided by the flap buoyancy. In this case, the optimization procedure must concentrate on the choice of the optimum value of k_{PTO} for each of the reference sea states.

The maximization of the energy productivity over a target time horizon allows to determine

- the optimal value of k, if the surge converter is provided with an external mechanical spring
- the optimal value of k_{PTO} for each reference sea condition

Notice that, up to now, the PTO system has been generically described by mean of the variable k_{PTO}.

Once the set of desirable values of k_{PTO} is know, the design parameters of the LS-DEG can be chosen in order to provide the generator with a stiffness (in the active phase) that is within the desired interval (known form the just described optimization procedure).

We remember that the design variables that have to be fixed are

- the overall polymer volume
- the pre-stretches of the polymeric membrane, λ_{1p} and λ_{2p}.
- the space arrangement of the selected volume: lozenge side and overall thickness of the set of polymeric membranes.

With this choice of the geometric parameters, using a set of values for the control electric field, below the break-down value E_{BD}, the LS-DEG (in the active strokes) must be able to provide a stiffness in the assessed range for k_{PTO}.

Notice that the optimization of the parameter k_{PTO} in correspondence of different sea states does not provide any information about the determination of the projectual and control parameters of the LS-DEG. It is sufficient for the projectual choice to meet the requirements on the equivalent PTO stiffness.

The first consequence is that several different designs, that respect the above mentioned conditions, may be found: a further analysis may then indicate which design is preferable (as long as it allows, for example, lower expense of polymeric material).

In conclusion, the fundamental outcome of the present procedure is that the optimization of the design for the OWSEC polymeric PTO is based on one macro-variable only, k_{PTO}, rather than on a series of scattered specific variables describing the geometry and the control of the generator.

Such a result allows flexibility in the design procedure. Since the only requisite for the energetic optimization of the system is the attainment of the required range of values for k_{PTO}, many different (but equivalent) control strategies may be browsed.

As a practical example, let consider the control strategy considered so far. It has been assumed that in correspondence of different sea conditions the generator can be tuned by varying the value of the control electric field. Since the PTO is implemented as a series of multiple membranes, that may be controlled independently, an equivalent way to obtain such a result is using a constant value for the control electric field (i.e. E_{BD}) activating a different number of layers (thus, a different amount of polymeric volume) in correspondence of different sea conditions.

The choice of one control strategy rather than the other one (that is energetically equivalent) may be done on the base of considerations concerning the architecture of the control system only.

Conclusions and Future Work

The present thesis goes through the analysis of Wave Energy Converters (WECs), with a special focus on the study and optimization of a Lozenge-Shaped Dielectric Elastomer Generator (LS-DEG) which can be applied as Power-Take Off (PTO) system in a number of heaving and pitching WECs. A mathematical model of the generator is built and applied to the investigation of an Oscillating Wave Surge Energy Converter (OWSEC) which exploits the novel concept generator as PTO.

The work has been carried out in cooperation with PERCRO SEES laboratory (Scuola Sant'Anna, Pisa) within the PolyWEC project, a FET-Energy project with the aim of investigating the feasibility of new concepts of polymeric generators for Wave Energy Conversion. The research has the aim of understanding the effectiveness of Dielectric Elastomers and Electroactive polymers applied to WECs, starting from the presupposition that these materials present a series of interesting features like simple-manufacturing, low weight, low cost and promising high-efficiency in the particular operating conditions of wave energy conversion.

The fundamentals achievements of this thesis are here briefly synthesized.

General overview on Wave Energy Conversion: a survey of the technologies and of their application has been sketched. Some of the relevant criticalities of the existing technology have been outlined, and a review on the state of the art has been traced.

In the last ten years, a spread of technical solutions, inventions and patents on WECs has taken place. Most of these solutions are of technical interest, are conceptually effective and promising, but are often presented and described, in literary works, on the base of their physical operation principle only, regardless their specific operation framework, the working conditions suitable to their employment and survivability, the sea states that are better adaptable to their proper working. A particular care has thus been addressed to these specific aspects. The existing prototypes have been described with particular attention to the significant data providing useful information on the physical size, the rated power and the operative conditions of the devices, in order to provide a precise order of magnitude of the engineering variables describing the existing prototypes. For a selection of commercial or pre-commercial devices, a table has been realized that clarifies the operation range of the different devices in terms of water depth and wave height.

Moreover, on the basis of the (even simplistic) linear waves theory, some mathematical models of specific WECs have been selected, proposed or re-elaborated. The models allow a

preliminary raw approach to the study of the devices and to the assessment of their performance.

Finally, the general mathematical approach, adopted in great part of literature to the study of WECs, is presented and described. The model bases on a limited number of fluid-dynamics parameters (added mass, radiation damping, wave induced force parameters) and can be mathematically formalized both in time and frequency domain (for non-linear and fully-linear analyses respectively). This model is based on potential-flow theory and provides a relatively simple model that allows approximate but significant predictions that could not be achieved with sophisticated tools (like CFD) due to their excessive computation cost.

Modeling of Lozenge-Shaped Dielectric Elastomer Generator. An overview on Dielectric Elastomers (DEs) is outlined, and their application as Actuators, Sensors and Generators is described. Some relevant literary works, introducing novel concept transducers, are referenced. Attention is of course focused on Generators, looking forward to investigate their application to Wave Energy Conversion. The operative principle of DEGs is explained with examples and mathematical calculations.

Subsequently, a novel prototype of LS-DEG is modeled.

A preliminary experimental work has been carried out on a VHB acrylic elastomer, the mechanical properties of which have been tested on a test rig frame. The fitting of the experimental data has permitted the interpolation of several hyperelastic models describing the mechanical behavior of the material. Three of these models (Ogden, Yeoh and Gent) have been selected and employed for the successive calculations.

A mathematical model for LS-DEGs is proposed and described. In order to build a predictive model - capable of assessing the energy per unit volume that the generator is able to convert - a specific formalism (similar to that used in thermodynamics) has been adopted, exploiting the Charge-Volume plane to trace an Energy Conversion Cycle (ECC), that encloses an area proportional to the converted energy. Theoretical ECCs have been identified by bounding the operation range of the generator with a number of failure conditions (Loss of Tension, Electric Break-Down, Mechanical Rupture). An optimization of the geometric parameters describing the generator (specifically, the pre-stretches of the membranes) has allowed an assessment of the maximum energy productivity per unit polymeric volume. Different hypotheses have been used on the break-down electric field and on the constitutive hyperelastic model for the elastomeric material. Results from the calculations have shown that, although the results of the fitting procedures are alike, the different hyperelastic models produce appreciable differences in term of energy conversion estimative. A maximum amount of convertible energy equal to 0.3 J/g has been obtained in the hypothesis of variable dielectric strength and using a hyper-elastic model in the Gent form.

Previous literature works based on equi-biaxial state of deformation have assessed numerical values up to 10 times higher. The reasons for this result has to be mainly researched in the particular strain field generated by the lozenge-shaped mechanism, that generates a relaxation

of the material along one direction when the membrane is stretched in the perpendicular direction. Due to the particular geometric arrangement, the energy productivity of LS-DEGs is upper bounded by the loss of tensions conditions, that represent a serious limitation for this class of generators. Nonetheless, it is a matter of fact that LS-DEGs are of interest for practical applications, thanks to their simplicity and easy adaptation in existing devices featuring reciprocating motion (like heaving or pitching WECs).

Simulation of a Dielectric Elastomer OWSEC. The above mentioned model of LS-DEG has been applied, in simulation, to a pitching wave surge converter, hinged to the sea bed and free to oscillate around the pivot hinge.

The aim of the analysis was the assessment of the performances of the generator, with respect to traditional PTO systems.

Some boundary conditions have been fixed for the system: it has been chosen that the system is controlled in order to prevent the oscillations to exceed a limit value of 45° off the vertical position; a water depth of 10 m has been chosen for the installation; for what concerns the operative conditions, some significant sea states relative to a similar depth in the sea off Azores Islands have been taken into account, with maximum wave height of 3 m about a maximum period of 13 s. In order to produce a preliminary estimative of the energetic performances of the plant, it has been assumed that all of the reference sea states are featured by monochromatic waves, described by linear theory.

The analysis of the dynamics of the system has been carried out accordingly to the above mentioned approach in the frequency/time domain: a series of fluid-dynamic parameters (wave induced torque parameters, radiation parameters) have been calculated for a flap assumed in vertical position (by mean of the WAMIT code); the dynamics of the system is then simulated in the frequency or time domain keeping into account the overall inertia of the system, the stiffness provided by both buoyancy torque and eventual external mechanical spring-like components, the damping provided by the radiated waves.

The dynamics of the system has been calculated with different hypothesis on the PTO system.

In a first analysis, a linear PTO system has been considered, providing a restoring torque consisting of two addenda: one proportional to the pitch angle of the flap (reactive term) one proportional to its velocity (active viscous term); both the components can be adjusted, in correspondence of different sea states, in order to provide the maximum power output. The simulation is carried out in frequency domain; a maximum power output of almost 1 MW (for the most intense sea state) and an yearly productivity of 3.2 GWh (over 8760 hours) have been assessed. Such a result represents an upper limit that exceeds the real potential of any practical existing PTO.

Successively, a linear PTO providing an active viscous effect only has been simulated: such a model is representative of a class of direct driven electric generators. An external spring-like component has been added in order to tune the natural frequency of the system to an optimal value. With this simplification, a power output larger than 700 kW is expected (for

monochromatic waves) for the largest sea states, and a productivity of about 2.8 GWh is assessed.

Finally, a model of a wave surge WEC with polymeric PTO has been built. Due to non-linearity induced by the specific PTO, the simulation has been carried out in time domain and implemented in Simulink. It has been shown that, for a proper choice of the design parameters, a power output and an energy productivity absolutely comparable with those of the electric generator are obtained.

In order to generalize the dissertation and to provide a pragmatic tool for the design and optimization of LS-DEG for wave surge converters, a simplified model has been proposed, that approximates the polymeric generator to a spring-like component that is alternately put on and off during the different phases of the flap oscillation. Such a simplification allows to reduce the preliminary study and design of this type of system to a simple numeric optimization problem.

The calculations of this section are obtained under strong hypotheses, in particular a) the fluid-dynamic parameters are calculated with reference to a flap in vertical position, but are then used in the entire range of oscillation of the device, although they are rigorously valid in the neighborhood of the equilibrium position only; b) monochromatic waves are hypothesized. This assumption led to an overestimation of the productivity of the system. Anyway, the results are of interest in relative terms since they allow comparisons with the traditional technology, demonstrating that the technology of polymeric PTO is worth of further investigation. In any case, the present results provide important indications about the design and control strategy of Dielectric Elastomer Oscillating Wave Surge Energy Converters (DE-OWSEC).

Of course, since the present thesis has been conceived and carried out within a new just begun project (the PolyWEC program), a large amount of work is still ongoing and several future development are scheduled. Some relevant possible improvements are schematically presented.

Implementation of visco-elastic models for elastomeric materials. It has been assumed here that the reference VHB elastomer has a mechanical behavior that is purely elastic (even if non-linear). As a consequence, the mechanical characterization and the mathematical model of the generator have been carried out regardless the hysteretic dissipative phenomena. Of course, hysteresis is a crucial parameter in the determination of the maximum amount of convertible energy for a polymeric generator. The electro-mechanical model presented so far must thus be integrated with a proper description of the dissipative phenomena. In order to achieve this goal, an extension of the experimental mechanical model for the material has to be carried out, and specific experiments at different deformation speeds have to be performed.

Electric tests. Mechanical characterizations only have been carried out within the present work. An assessment of the proposed model for the LS-DEG requires further experiments concerning the electric behavior of the generator.

Targeting experiments must be carried out in order to experimentally determine the value of break-down electric field for the considered elastomers (and its eventual dependence on the stretch level).

Another important mechanism affecting DEs, that requires experimental investigation, is current leakage through the polymeric membrane. Even being an order of magnitude lower than the currents circulating in the circuit of the film capacitor, these currents provoke a gradual loss of energy by slowly discharging the capacitor.

Another class of electric tests should be addressed to the effective measurement of the converted energy. A control scheme must be designed in order to achieve a series of electric operations on the membranes (charge/discharge at constant voltage/constant electric field, discharge at constant mechanic tension level etc.): these operations must then be gathered to realize ECCs. The measured converted energy must be then compared with the theoretical predictions.

Study of the effect of compliant electrodes. The work carried out so far (both theoretically and experimentally) does not keep into account the presence of the compliant conductive electrodes about the polymeric sheets constituting the Dielectric Elastomer Generator (DEG). Compliant electrodes are usually realized by mean of a conductive paste (with dispersed metallic particles), that is rubbed on opposite faces of the membranes constituting the DEG. The electrodes affect both the mechanical and electrical response of the generator. In particular, the deposition of a viscous paste may modify the mechanical strain-stress characteristic of the elastomeric material, specifically by introducing an ulterior hysteretic behavior. Under the electrical point of view, compliant electrodes represent quite a crucial component, that is responsible for a large portion of the leakage currents and that adds a resistive addendum to the circuitry of the polymeric capacitor, influencing its dynamics. Electric and mechanical tests are thus required in order to clarify these aspects.

Investigation of alternative elastomeric materials. The VHB elastomer considered here has been selected for its easy handling (being an adhesive) more than for its effective properties. Investigations should be done on different DEs, in particular on natural rubber (NR). NR elastomers have larger shear modulus with respect to acrylics and present lower hysteretic losses. Their application to electricity generation is thus of interest since it would allow greater efficiency (thanks to the lower dissipation) and, perhaps, larger amount of convertible energy per unit volume, since the loss-of-tension condition, that is a severe limitation to the performance of LS-DEGs, allows larger margins thank to the high stiffness of the material. For these reasons, the characterization procedure described so far must be extended to the selected elastomers, and the assessment of the energy productivity has to be replied with the new data.

Improvement of the fluid-dynamic model of OWSEC. The fluid-dynamic simulation of the oscillating flap converter presented so far is based on some rough assumptions, that compromise the reliability of the numeric results with respect to a real operating context.
The first simplification, as already mentioned, is the assumption of a series of monochromatic sea states describing the wave climate of the reference location. This hypothesis is responsible, in most cases, of an overestimation of the power output of WECs, therefore a different model for the incident waves has to be adopted that, basing on the significant wave height and mean wave period for each given sea condition, allows the reconstruction of the corresponding wave spectrum.
Another improvement may be addressed to the calculation of the relevant fluid-dynamic parameters describing the wave-body interaction. Instead of using a set of parameters calculated at one specific position of the WEC, an accurate model can be built that keeps into account the modification of the fluid-dynamics parameters as a function of the position of the floating body.
For what concerns the specific layout of DE-OWSEC considered here, specific improvements may concern:

- The implementation of an inertial model of generator. Since the overall volume of polymeric material required to reach a power output of ~700 kW is very large (about 90 m^3), the influence of the inertia of the generator is non-negligible, and represents a further inertial term with respect to the inertia of the pitching body.
- Effect on the fluid-dynamic fields of the LS-DEG. With the assessed dimensions, the polymeric generator represents a rather bulky body, that, positioned in the neighborhood of the flap, affects the interaction of the WEC with waves.

Of course, the considered layout for the coupling WEC-generator is not necessarily the best technical solutions. Many layout can be though, for i.e. polymeric generators housed directly inside the flap rather than positioned outside along its side.
Experimental pool tests. On a long term perspective, a series of targeting pool tests may be realized on wave surge prototypes. These experiments would provide precious information about the real fluid-dynamic interaction between waves and converters, allowing a validation of the numerical model exploited so far. Moreover, pool tests would represent a necessary and desirable confirmation of the eventual effectiveness of the system, downstream a complete and detailed theoretical investigation.

Beyond the aim and the achievements of the present thesis, Wave Energy Conversion (and, more specifically, the employment of DEGs on WECs) remains a still young subject, and a structured and systematic research effort is required primarily to understand the role that the wave resource can play in the framework of Renewable Energies and, in the second instance, to select, optimize and promote a number of specific technologies that are arguably suitable to operate in specific well-defined energetic and environmental contexts.

Appendix A

Incompressible Hyperelastic Materials

Non-linear rubber-like materials are usually designed as 'hyperelastic solids' and their stress-strain behavior is described by a strain-energy density function (or Helmoltz free energy function) ψ [55].

The function ψ is a measure of the elastic potential energy per unit volume present within the material in a given configuration, when mechanical loads and deformation gradients are present.

Let refer, for simplicity, to the elastomeric membrane in Figure A.

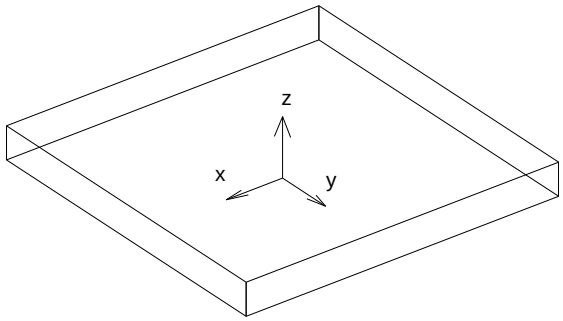

Figure A - DE membrane with reference system

Indicating with λ_1, λ_2 and λ_3 the stretch of the material in *x*, *y* and *z* direction respectively, the strain-energy function takes the general form

$$\psi = \psi(\lambda_1, \lambda_2, \lambda_3)$$

and the corresponding stresses in the principal directions are

$$\sigma_1 = \lambda_1 \frac{\partial \psi}{\partial \lambda_1} \quad ; \quad \sigma_2 = \lambda_2 \frac{\partial \psi}{\partial \lambda_2} \quad ; \quad \sigma_3 = \lambda_3 \frac{\partial \psi}{\partial \lambda_3}$$

Materials which keep the volume constant throughout deformation are characterized by the incompressibility constraint, and their strain energy function can be written in the form

$$\psi' = \psi(\lambda_1, \lambda_2, \lambda_3) - \alpha \cdot (\lambda_1 \lambda_2 \lambda_3 - 1)$$

where ψ is the unconstrained strain energy function and α is an indeterminate Lagrange multiplier which can be identified as a hydrostatic pressure.

As a consequence, for incompressible materials, the stresses are expressed in the form

$$\sigma_i = \lambda_i \frac{\partial \psi'}{\partial \lambda_i}$$

thus, for the case in exam

$$\sigma_i = \lambda_i \frac{\partial \psi}{\partial \lambda_i} - \alpha \cdot \lambda_1 \lambda_2 \lambda_3$$

We remember now that for an incompressible sample of material $\lambda_1 \lambda_2 \lambda_3 = 1$, then

$$\sigma_i = \lambda_i \frac{\partial \psi}{\partial \lambda_i} - \alpha$$

It is possible to conclude that, due to the constrain provoked by incompressibility, the material is subjected to a hydrostatic field of pressure α.

Let now consider the common case where the material is free to expand in one direction. This situation can be reproduced, i.e., considering that the sheet of Figure A is mounted on a frame lying on the *xy* plane and is free to expand in *z* direction (plane stress condition). In this situation, it is clear that

$$\sigma_3 = 0$$

thus

$$\alpha = \lambda_3 \frac{\partial \psi}{\partial \lambda_3}$$

and the stress in the constrained directions is

$$\sigma_1 = \lambda_1 \frac{\partial \psi}{\partial \lambda_1} - \lambda_3 \frac{\partial \psi}{\partial \lambda_3} \quad ; \quad \sigma_2 = \lambda_2 \frac{\partial \psi}{\partial \lambda_2} - \lambda_3 \frac{\partial \psi}{\partial \lambda_3}$$

The explicit dependence of ψ on λ_3 can be eliminated by replacing

$$\lambda_3 = \frac{1}{\lambda_1 \lambda_2}$$

in the expression of ψ, that becomes

$$\psi = \psi(\lambda_1, \lambda_2, 1/\lambda_1 \lambda_2)$$

It is immediate to notice that, if $\lambda_1 \lambda_2 \lambda_3 = 1$,

$$\lambda_1 \frac{\partial \psi(\lambda_1, \lambda_2, \lambda_3)}{\partial \lambda_1} - \lambda_3 \frac{\partial \psi(\lambda_1, \lambda_2, \lambda_3)}{\partial \lambda_3} = \lambda_1 \frac{\partial \psi(\lambda_1, \lambda_2, 1/\lambda_1 \lambda_2)}{\partial \lambda_1}$$

and

$$\lambda_2 \frac{\partial \psi(\lambda_1, \lambda_2, \lambda_3)}{\partial \lambda_2} - \lambda_3 \frac{\partial \psi(\lambda_1, \lambda_2, \lambda_3)}{\partial \lambda_3} = \lambda_2 \frac{\partial \psi(\lambda_1, \lambda_2, 1/\lambda_1 \lambda_2)}{\partial \lambda_2}$$

In the hypothesis of incompressible material, therefore, it is convenient to express the strain-energy function as a function of 2 stretches only:

$$\psi = \psi(\lambda_1, \lambda_2, 1/\lambda_1 \lambda_2) = \hat{\psi}(\lambda_1, \lambda_2)$$

so that the stresses in the principal directions are again written as

$$\sigma_1 = \lambda_1 \frac{\partial \hat{\psi}}{\partial \lambda_1} \quad ; \quad \sigma_2 = \lambda_2 \frac{\partial \hat{\psi}}{\partial \lambda_2}$$

Let suppose now that the membrane is electrically activated by mean of the deposition of a charge on the faces perpendicular to the *z* axis.
Due to electric activation, an electrostatic induced pressure *p* acts on the thickness direction *z*, thus

$$\sigma_3 = -p$$

Using the incompressibility constraint,

$$\alpha = \lambda_3 \frac{\partial \psi}{\partial \lambda_3} + p$$

and the other 2 principal stresses results in

$$\sigma_1 = \lambda_1 \frac{\partial \psi}{\partial \lambda_1} - \lambda_3 \frac{\partial \psi}{\partial \lambda_3} - p = \lambda_1 \frac{\partial \hat{\psi}}{\partial \lambda_1} - p$$

$$\sigma_2 = \lambda_2 \frac{\partial \psi}{\partial \lambda_2} - \lambda_3 \frac{\partial \psi}{\partial \lambda_3} - p = \lambda_2 \frac{\partial \hat{\psi}}{\partial \lambda_2} - p$$

where, we remember, the difference between ψ and $\hat{\psi}$ is that the first one depends on λ_1, λ_2 and λ_3, the second one on λ_1 and λ_2 only.
It can be noticed that the electrostatic induced pressure behaves as a hydrostatic term, inducing an equal pressure along each of the principal directions.

References

[1] Salter S. H.; *Wave Power*; Nature, 249 (5459), 720-724; 1974.

[2] Brooke J.; *Wave Energy Conversion*; ECOR, Editors R. Bhattacharyya & M.E. McCormick; 2003.

[3] Gunnar M., Barstow S., Kabuth A., Pontes M.T.; *Assessing the global Wave Energy Potential*; Proceedings of 29th OMAE Conference; 2010.

[4] Masuda Y., Saitamaken K.; *Ocean Wave Electric Generator*; US Patent 3200255; 1965.

[5] Salter S. H.; *Apparatus and Method for Extracting Wave Energy*; US Patent 3928967; 1975.

[6] McCormick M.E.; *Ocean Wave Energy Conversion*; Dover Publications; 2007.

[7] Baker C.; *Tidal power*; Energy Policy vol. 19 issue 8 792-297; 1991.

[8] Garrett C., Cummins P.; *Generating Power from Tidal Currents*; J. Waterway, Port, Coastal, Ocean Eng., 130(3), 114–118; 2004.

[9] Rodrigues L.; *Wave power conversion systems for electrical energy production*; Nova University of Lisbon; 2008.

[10] Cornett A.; *A Global Wave Energy Resource Assessment*; Proceedings of the 18th International Offshore and Polar Engineering Conference, Vancouver, Canada; 2008.

[11] Arinaga R., Cheung K.F.; *Atlas of Global Eave Energy from 10 years of Reanalysis and Hindcast Data*; Renewable Energy, volume 39 issue 1, 49-64; 2012.

[12] Vicinanza D., Cappietti L., Ferrante V., Contestabile P.; *Estimation of the Wave Energy in the Italian Offshore*; Journal of Coastal Research, SI64, 613-617; 2011.

[13] McCormick M.E.; Ocean Engineering Wave Mechanics; John Wiley and Sons; 1973.

[14] World Meteorological Organization; *Guide to Wave Analysis and Forecasting*; Secretariat of the World Meteorological Organization – Geneva – Switzerland; 1998.

[15] Falcão A.F.; *Wave Energy Utilization: A Review of the Technologies*; Renewable and Sustainable Energy Reviews 14; 2010.

[16] Carter R.W.; *Wave Energy Converters and a Submerged Horizontal Plate*; Master of Science thesis in Ocean and Resources Engineering, University of Hawaii; 2005.

[17] de Araujo Alves M.A.; *Numerical Simulation of the dynamics of point absorber Wave Energy Converters Using Frequency and Time Domain Approaches*; Universidade Tecnica de Lisboa, Instituto Superior Tecnico, PhD thesis in Mechanical Engineering; 2012.

[18] Cruz J.; *Ocean Wave Energy. Current Status and Future Perspectives*; Springer; 2008.

[19] Babarit A., Hals J., Muliawan M.J., Kurniawan A., Moan T., Krokstad J.; *Numerical benchmarking study of a selection of wave energy converters*; Renewable Energy 41, 44-63; 2012.

[20] Muetze A., Vining J.G.; *Ocean Wave Energy Conversion - a Survey*; Proceedings of the IEEE IAS'06, Tampa (USA), vol 3, pp 1410-1417; 2006.

[21] Ben Elghali S.E., Benbouzid M.E.H., Charpentier J.F.; *Marine Tidal Current Electric Power Generation Technology: State of the Art and Current Status*; Electric Machines and Drives conference, IEMDC'07 IEEE international vol. 2; 2007.

[22] Hiroisa T.; *Sea trial of a Heaving Buoy Wave Power Absorber*; Proceedings of 2nd International Symposion on Wave Energy Utilization, Trondheim, Norway; 1982.

[23] Nielsen K, Smed P.F.; *Point Absorber—Optimization and Survival Testing*; Proceedings of 3rd European Wave Energy Conference; 1998.

[24] Waters R., Stalberg M., Danielsson O., Svensson O., Gustafsson S., Stromstedt E.; *Experimental Results from Sea Trials of an Offshore Wave Energy System*; Applied Physics Letters 90(3); 2007.

[25] Nurick A.; *Dynamics of a Heaving Point Buoy for Extracting Sea Wave Energy*; 8th South African Conference on Computational and Applied Mechanics, Johannesburg, South Africa; 2012.

[26] Folley M., Whittaker T., van't Hoff J.; *The Design of Small Seabed-Mounted Bottom-Hinged Wave Energy Converters*; Proceedings of the 7th European Wave and Tidal Energy Conference, Porto, Portugal; 2007.

[27] Haren P., Mei C.; *Wave Power Extraction by a Train of Rafts: Hydro-Dynamic Theory and Optimum Design*; Applied Ocean Research, vol. 1 no. 3; 1979.

[28] Corsini A., Rispoli F.; *Modeling of Wave Energy Conversion with an Oscillating Water Column Device*; Dipartimento di Meccanica e Aeronautica, Università di Roma "La Sapienza".

[29] Carmichael A.D.; *An Experimental Study and Enigneering Evaluation of the Salter Cam Wave Energy Converter*; Massachussets Institut of Technology, Cambridge, Massachussets; 1978.

[30] Folley M., Whittaker T., Osterried M.; *The Oscillating Wave Surge Converter*; Fourteenth International Offshore and Polar Engineering Conference, (ISOPE 2004), Toulon; 2004.

[31] Peiffer A., Roddier D.; *Design of an Oscillating Wave Surge Converter on the WindFloat Structure*; 4th international Conference on Ocean Engineering, Dublin; 2012.

[32] Renzi E., Dias F.; *Resonant Behavior of an Oscillating Wave Energy Converter in a Channel*; Journal of Fluid Mechanics, Volume 701, pp 482-510; 2012.

[33] Kondo H., Watabe T., Yano K.; *Wave Power Extraction at Coastal Structure by Means of Moving Body in the Chambre*; Proceedings of 19th Conference on Coastal Engineering, Houston, Texas; 1984.

[34] Engineering Business Ltd.; *EB Frond Wave Energy Converter*; V/06/0024/00/REP URN 05/865; 2005.

[35] Whittaker T., Collier D., Folley M., Osterried M., Henry A., Crowley M.; *The Development of Oyster – A Shallow Water Surging Wave Energy Converter*; 7th European Wave and Tidal Energy Conference, Aporto, Portugal; 2007.

[36] Henry A., Doherty K., Cameron L., Whittaker T., Doherty R.; *Advances in the Design of the Oyster Wave Energy Converter*; RINA Marine & Offshore Renewable Energy, London; 2010.

[37] Thorpe T.W.; *A Brief Review of Wave Energy*; UK Department of Trande and Industry. ETSU-R120; 1999.

[38] Kofoed J.P.; *Wave Overtopping of Marine Structures - Utilization of Wave Energy; Aalborg University*; ISSN 0909-4296; series paper no. 24; 2002.

[39] Parmeggiani S., Kofoed J.P., Friis-Madsen E.; *Experimental Update of the Overtopping Model Used for the Wave Dragon Wave Energy Converter*; Energies 6 1961-1992; 2013.

[40] Knapp W., Böhm C., Keller J., Rohne W., Schilling R., Holmén E.; *Turbine Development for the Wave Dragon Wave Energy Converter*; Hydro 2003 Conference, Croatia; 2003.

[41] Kofoed J.P., Frigaard P., Friis-Madsen E., Shorensen H.C.; *Prototype Testing of the Wave Energy Converter Wave Dragon*; World Renewable Energy Congress VIII; 2004.

[42] Falnes J.; *A review of Wave-Energy extraction*; Marine Structures (20) 185-201, 2007

[43] Falcão A., Candido J., Justino P., Henriques J.; *Hydrodynamics of the IPS buoy wave energy converter including the effect of non-uniform acceleration tube cross section*; Renewable Energy 41, 105-114, 2012.

[44] Brito-Melo A., Neumann F., Sarmento A.; *Full-scale Data Assessment in OWC Pico Plant*; International Journal of Offshore and Polar Engineering (ISSN 1053-5381), Vol. 18, No. 1, pp. 27–34; 2008.

[45] Le Crom I., Cabrera Bermejo H., Pecher A., Brito Azevedo E., Reis F. V.; *Incident wave climate at the OWC Pico plant: Validation of a feed-forward based propagation method (ANN) and a numerical simulation (SWAN) with measured data*; of the 9th European Wave and Tidal Energy Conference, Southampton, UK; 2011.

[46] Boake C., Trevor J., Whittaker T., Folley M.; *Overview and Initial Operational Experience of the LIMPET Wave Energy Plant*; Proceedings of The 12th International Offshore and Polar Engineering Conference; Kitakyushu, Japan; 2002.

[47] Retzler, C. H.; Pizer, D. J.; *The hydrodynamics of the PELAMIS wave energy device: experimental and numerical results*; Proceedings of 20th International Conference on Offshore Mechanics and Arctic Engineering, 2001.

[48] Collier D., Whittaker T., Crowley M.; *The Construction of Oyster – A Nearshore Surging Wave Energy Converter*; Aquamarine Power, 2008.

[49] Cameron, L., Doherty, R., Henry, A., Doherty, K., Hoff, J. V., Kaye, D., Whittaker, T.; *Design of the next generation of the Oyster Wave Energy Converter*; Proceedings of the 3rd International Conference on Ocean Energy; 2010.

[50] *WAMIT User Manual Version 7*; WAMIT INC., Chestnut Hill, MA (USA); 2013.

[51] Yu Z., Falnes J.; *State-Space Modelling of a Vertical Cylinder in Heave*; Applied Ocean Research 17 265-275; 1995.

[52] Murray R.; *Economic Wave Energy Resource Assessment Methodology & European Assessment*; University of Strathclyde in Glasgow; 2004.

[53] Carpi F., De Rossi D., Kornbluh R.,Pelrine R.E., Sommer-Larsen P.; *Dielectric Elastomers as Elecromechanical Transducers*; Elsevier Ltd.; 2008.

[54] Pelrine R.E., Kornbluh R., Jospeh J.; *Electrostriction of Polymer Dielectrics with Compliant Electrodes as a Means of Actuation*; Sensors and Actuators A 64 77-85; 1998.

[55] Holzapfel G.; *Nonlinear Solid Mechanics: a Continuum Approach for Engineering*; Willey & Sons, New York; 2001.

[56] Shankar R., Ghish T., Spontak R.; *Dielectric Elastomers as Next-Generation Polymeric Actuators*; Soft Matter Issue 9; 2007.

[57] *Polypower DEAP material*; Danfoss

[58] Schaefer R.J.; *Harris' Shock and Vibration Handobook* - chap. 33; McGraw-Hill; 2010.

[59] Kim K., Tadokoro S.; *Electroactive Polymers for Robotic Applications*; Springer; 2007.

[60] Vertechy R., Berselli G., Parenti Castelli V., Vassura G.; *Optimal Design of Lozenge-Shaped Dielectric Elastomer Linear Actuator: Mathematical procedure and Experimental Validation*; Journal of Intelligent Material Structures, vol 21, 503-515; 2010.

[61] Kofod G., Wirges W., Paajanen M., Bauer S.; *Energy Minimization for Self-Organized Structure Formation and Actuation*; Applied Physics Letters 90, 081916; 2007.

[62] Sarban R., Jones R.W., Mace B.R., Rustighi E.; A Tubular Dielectric Elastomer Actuator: Fabrication, Characterization, and Active Vibration Isolation; Mechanical Systems and Signal Processing 25 2879-2891; 2011.

[63] Plante J.S., Devita L.M., Dubowsky S.; *A Road to Practical Electric Elastomer Actuators Based Robotics and Mechatronics: Discrete Actuation*; EAPAD proceedings; 2007.

[64] Wang H., Zhu Y., Zhao D., Luan Y.; *Performance Investigation of Cone Dielectric Elastomer Actuator Using Taguchi Method*; Chinese Journal of Mechanical Engineering Vol. 24; 2011.

[65] Choi H.R., Jung K.M., Kwak J.W., Lee S.W., Kim H.M., Jeon J.W., Nam J.D.; *Multiple Degree-of-Freedom Digital Soft Actuator for Robotic Applications*; Proceedings of SPIE, 5051:262; 2003.

[66] Bar-Choen Y.; *Electroactive polymer (EAP) Actuators as Artificial Muscles: reality, potential and Challenges*; SPIE press; 2004.

[67] Brochu P.; *Dielectric Elastomers for Actuation and Energy Harvesting*; University of California, Los Angeles; 2012.

[68] Wang H., Zhu Y., Wang L., Zhao J.; *Experimental Investigation on Energy Conversion for Dielectric Electroactive Polymer Generator*; Journal of Intelligent Material Systems and Structures 23(8) 885-895; 2012.

[69] Liu Y., Ren K.L., Hofmann H., Zhang Q.; *Investigation of Electrostrictive Polymers for Energy Harvesting*; IEEE transactions on ultrasonics, ferroelectrics, and frequency control, vol. 52, no. 12; 2005.

[70] Pelrine, R., Kornbluh, R., Eckerle, J., Jeuck, P., Oh, S., Pei, Q., Stanford, S.; *Dielectric Elastomers: Generator Mode Fundamentals and Applications*; In Proc. SPIE (Vol. 4329, pp. 148-156); 2001.

[71] Koh, S.J.A., Zhao, X., Suo, Z.; *Maximal Energy that can be Converted by a Dielectric Elastomer Generator*; Applied Physics Letters 94, 262902; 2009.

[72] Koh S., Keplinger C., Li T., Bauer S., Suo Z.; *Dielectric Elastomer Generators: how much Energy can be converted?*; IEEE Transactions on Mechatronics, 16(1): 33-41; 2011.

[73] Jean-Mistral C., Basrour S., Chaillout J-J.; *Modelling of Dielectric Polymers for Energy Scavenging Applications*; Smart Mater. Struct. 19, 105006; 2010.

[74] Yang E., Frecker M., Mockensturm E.; *Viscoelastic Model of Dielectric Elastomer Membranes*; Smart Structures and Materials (pp. 82-93). International Society for Optics and Photonics; 2005.

[75] Morman K.N.; *Why it is Necessary to use Data from more than one Strain Field in determining the Helmoltz Free-Energy (Strain-Energy) Density Function*; ANSOL Corporation; 2005.

[76] Steinmann P., Hossain M., Possart G.; *Hyperelastic Models for Rubber-like Materials: Consistent Tangent Operators and Suitability for Treolar's Data*; Archive of Applied Mechanics, Volume 82, Issue 9, pp 1183-1217; 2012.

[77] Treloar, L. R. G.; *The Physics of Rubber Elasticity*; Oxford University Press; 1975.

[78] Benjeddou A., Jankovich E., Hadhri T.; *Determination of the Parameters of Ogden's Law Using Biaxial Data and Levenberg-Marquardt- Fletcher Algorithm*; Journal of Elastomers and Plastics, Vol. 25; 1993.

[79] Caroll M.M.; A *Strain Energy Function for Vulcanized Rubbers*; Journal of Elasticity, 103(2), 173-187; 2011.

[80] Kofod G., Sommer-Larsen P., Kornbluh R., Pelrine R.; *Actuation Response of Polyacrilate Dielectric Elastomers; Journal of Intelligent Meterial Systems*, 14: 787-793; 2003.

[81] Woo C. S., Park H. S., Kim W. D.; *The Effect of Maximum Strain on Fatigue Life Prediction for Natural Rubber Material*; World Academy of Science, Engineering and Technology; 2013.

[82] PolyWEC Group; *New Mechanisms and Concepts for exploiting Electroactive Polymers for Wave Energy Conversion – Annex 1: description of Work*; 7th Framework Programme, Grant agreement no: 309139; 2012.

[83] Vertechy R., Fontana M., Papini G. R., Bergamasco M.; *Oscillating-Water-Column Wave-Energy-Converter Based on Dielectric Elastomer Generator*; in SPIE (pp. 86870I-86870I). International Society for Optics and Photonics; 2013.

[84] Rosati Papini G.P., Vertechy R., Fontana M.; *Dynamic Model of Dielectric Elastomer Diaphragm Generators for Oscillating Water Column Wave Energy Converters*; ASME Conference on Smart Materials, Adaptive Structures and Intelligent Systems; 2013.

[85] Chiba S., Waki M., Kornbluh R., Pelrine R.; *Innovative Power Generators for Energy Harvesting Using Electroactive Polymer Artificial Muscles*; Proc. SPIE,Vol. 6927, pp. 692715–692719; 2008.

[86] Jean P., Wattez A., Ardoise G., Melis C., Van Kessel R., Fourmon A., Barrabino E., Heemskerk J., Queau J. P.; *Standing Wave Tube Electro Active Polymer Wave Energy Converter*; Proc. of SPIE Vol. 8340, p. 83400C–1; 2012.

[87] Neidlein G., Hentschel C., Scharmann N., Langenstein C., Voss M., Hagemann, B.; *Wellenenergietransformer mit elektroaktiver Polymerfolie*; 2011.

[88] Moretti G., Fontana M., Vertechy R.; *Modeling and control of Lozenge-Shaped Dielectric Elastomer Generators*; ASME Conference on Smart Materials, Adaptive Structures and Intelligent Systems; 2013.

[89] Kornev N.; *Ship dynamics in Waves*; Universitat Rostock; 2011.

[90] McCabe A.P., Aggidis G.A., Stallard T.J.; *A Time-Varying Parameter Model of a Body Oscillating in Pitch*; Applied Ocean Research 28, 359–370; 2006.

[91] Cengel Y., Turner R., Cimbala J.; *Fundamentals of Thermal-Fluid Sciences - 4th edition*; McGraw-Hill; 2011.

[92] Burton T., Jenkins N., Sharpe D., Bossanyi E.; *Wind Energy Handbook*; John Wiley & Sons; 2011.